GEOLOGICA ULTRAECTINA

Mededelingen van de
Faculteit Aardwetenschappen
Universiteit Utrecht

No. 150

Thermodynamic characterisation and modelling of coal liquids

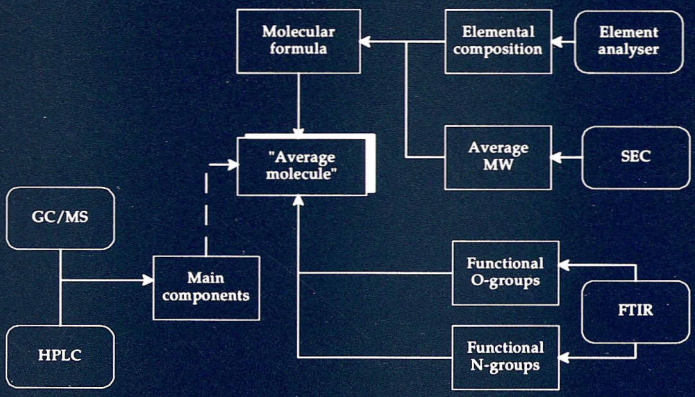

Adriaan M.H. van der Veen

GEOLOGICA ULTRAECTINA

Mededelingen van de
Faculteit Aardwetenschappen
Universiteit Utrecht

No. 150

Thermodynamic characterisation and modelling of coal liquids

ISBN 90-5744-008-3

Thermodynamic characterisation and modelling of coal liquids

Thermodynamische karakterisering en modellering van kolenolie

(met een samenvatting in het Nederlands)

PROEFSCHRIFT

TER VERKRIJGING VAN DE GRAAD VAN DOCTOR AAN DE UNIVERSITEIT UTRECHT, OP GEZAG VAN DE RECTOR MAGNIFICUS PROF. DR. J.A. VAN GINKEL, INGEVOLGE HET BESLUIT VAN HET COLLEGE VAN DEKANEN IN HET OPENBAAR TE VERDEDIGEN OP WOENSDAG 4 JUNI 1997 DES NAMIDDAGS OM 12.30 UUR

DOOR

ADRIAAN MARTEN HEINE VAN DER VEEN

Geboren op 1 augustus 1967 te Breda

Promotor: Prof. Dr. H.A.J. Oonk

Co-promotor: Dr.Ir. K.A. Nater

Samenvatting

Teneinde het temperatuur-druk gedrag van kolenolie te kunnen beschrijven, is een model nodig dat als invoer alleen gegevens van analytisch chemische methoden vereist. Kolenolie wordt verkregen door steenkool om te zetten in vloeistof. De verkregen vloeistof wijkt qua eigenschappen af van aardolie doordat kolenolie een hoger gehalte aan aromatische koolwaterstoffen bevat. Aangezien aromatische koolwaterstoffen sterke interacties hebben dan alifatische, is de modellering van de eigenschappen van deze vloeistoffen moeilijker.

De thermodynamische karakterisering en modellering van deze olieën speelt een belangrijke rol in the ontwerpen van chemische reactoren. Voordat een reactor kan worden gebouwd ten behoeve van destillatie of kraken, moet de benodigdge energie-toevoer kunnen worden geschat. De technologie van het omzetten van steenkool in olie kan ook worden toegepast op andere grondstoffen, zoals bijvoorbeeld bio massa en GFT-afval (groente-, fruit-, en tuinafval).

De basis voor het modelleerwerk is de toestandsvergelijking van Van Laar. Deze vergelijking werd in 1924 gepubliceerd als één van de eerste modificaties van de toestandsvergelijking van Van der Waals. Het gebruik van een toestandsvergelijking het beschrijven van het temperatuur-drukgedrag van organische vloeistoffen is al menigmaal beschreven in de literatuur. Toestandsvergelijkingen zijn daarbij vaak gebruikt om berekeningen bij hoge temperaturen en drukken uit te voeren, waar weinig of geen experimentele gegevens beschikbaar zijn.

Het modelleerwerk vergt een stapsgewijze aanpak. Op verschillende niveaus zijn hiervoor experimentele gegevens noodzakelijk. Op de eerste plaats betreft het de gegevens die gewoonlijk door de industrie worden verzameld. Deze gegevens karakteriseren de olie in termen van hoofd- en nevencomponenten, molecular gewichtsverdeling, of relative concentraties van bepaalde functionele groepen. Voor het verhandelen van dit soort produkten zijn deze gegevens onontbeerlijk.

Een tweede bron van gegevens zijn thermodynamische gegevens van zuivere stoffen. Aangezien voor gesubstitueerde naftalenen slechts weinig gegevens in de lteratuur voorhanden waren, maakte het meten van dampdrukken van een aantal voor kolenolie relevante verbindingen deel uit van dit werk.

Na het verifiëren van de capaciteiten van de toestandsvergelijking aan de hand van zuivere stof gegevens werd gebruik gemaakt van gegevens van binaire mengsels om de invloed van empirische correcties in de toestandsvergelijking te onderzoeken. Voorts levert het onderzoek van binaire mengsels relevante gegevens op voor de interpretatie van de experimentele gegevens van de onderzochte olieën.

Het laatste stadium van de modelontwikkeling is het uitvoeren van een regressie op de coëfficiënten van de toestandsvergelijking, waarbij de afhankelijkheid van de zuivere stof gegevens wordt vervangen door één van de gemiddelde samenstelling van het mengsel (olie). Deze regressie is uitgevoerd aan de hand van een databank van koolwaterstoffen. Vervolgens zijn de resultaten van de regressie geëvalueerd

aan de hand van een reeks van 7 fracties (kooktraject van 30 K) en een olie van Point of Ayr (Wales).

Het eerste deel van het onderzoek diende ter verificatie van de mogelijkheden van Van Laar's toestandsvergelijking. Deze vergelijking ziet er als volgt uit:

$$P = \frac{RT}{V}\frac{V + b_g - b_0'}{V - b_0'} - \frac{a_g}{V(V+c)}$$

waarbij T de temperatuur, P de druk, R de gasconstante en V het volume is. De overige symbolen zijn de coëfficiënten van de vergelijking. Op basis van dit werk is gebleken dat Van Laar's vergelijking door het ontbreken van enkele termen niet in staat was het gehele gebied van vloeistof-damp evenwichten te kunnen beschrijven. Op deelgebieden voldoet de vergelijking echter wel. De Cubic Chain-of-Rotators toestandsvergelijking (CCOR) is vervolgens gekozen als model om mee verder te gaan, aangezien deze vergelijking grote overeenkomsten vertoont met die van Van Laar:

$$P = \frac{RT(1+0.77b/v)}{v-0.42b} + c^R\frac{0.055RTb/v}{v-0.42b} - \frac{a}{v(v+c)} - \frac{bd}{v(v+c)(v-0.42b)}$$

Dampdrukmetingen aan zuivere stoffen is uitgevoerd aan de volgende naftalenen: 1-methylnaftaleen, 2-methylnaftaleen, 1-ethylnaftaleen, 2-ethylnaftaleen, tetralin, 2-methoxynaftaleen, 2-naftol, 2-naftaleencarbonzuur en 2-naftaldehyde over een temperatuurgebied van 40 tot 150 C. De afgeleide thermodynamische functies zijn weergegeven in tabel 1.

Tabel 1 : Samenvatting van afgeleide thermodynamische functies

Substance	**Θ (K)**	**$\Delta G^0(\Theta)$ (J mol^{-1})**	**$\Delta H^0(\Theta)$ (J mol^{-1})**	**ΔC_p^0 (J K^{-1} mol^{-1})**
1-methylnaftaleen	370.00	-20509 ± 150	56360 ± 190	< 2s
2-methylnaftaleen	370.00	-20991 ± 24	54460 ± 170	-49 ± 11
1-ethylnaftaleen	370.00	-18651 ± 14	60940 ± 80	-118 ± 10
2-ethylnaftaleen	370.00	-18832 ± 22	59820 ± 70	-105 ± 14
tetralin	370.00	-24680 ± 14	48910 ± 140	-51 ± 9
2-naftaleencarbonzuur	370.00	22497 ± 46	112950 ± 560	< 2s
2-naftol (vast)	370.00	-13719 ± 44	83975 ± 470	< 2s
2-naftol (vloeibaar)	420.00	-25430 ± 14	59650 ± 540	< 2s
2-methoxynaftaleen	370.00	-14734 ± 46	74654 ± 920	< 2s
2-naftaldehyde	370.00	-17144 ± 22	42884 ± 264	< 2s

Voor een aantal verbindingen konden de waarden voor ΔC_p^0 niet kwantitatief worden bepaald, omdat de residuele standaardafwijking van de regressie te groot is.

Twee binaire systemen werden experimenteel onderzocht: tolueen - 1-ethylnaftaleen en tolueen 2-methoxynaftaleen. De experimentele gegevens tonen aan dat de samenstelling van de damp hoofdzakelijk wordt bepaald door de lichte component. Dit geldt in mindere mate ook voor de dampdruk. Deze vaststellingen zijn nuttig gebleken bij het interpreteren van de gegevens van de monsters van Point of Ayr.

De CCOR blijkt in de klassieke vorm matig geschikt voor zware aromaten. Voor een goede modellering van deze verbindingen is een modificatie van het model vereist, die rekening houdt met de associërende eigenschappen van deze verbindingen. Ook voor binaire mengsels blijkt dit op te gaan. Verder is gebleken dat het model ook sterk afhankelijk is van empirische correcties, die rekening houden met de asymmetrie van het mengsel.

De thermische stabiliteit van de gedestilleerde oliemonsters bleek in alle gevallen voldoende te zijn voor de andere metingen. De dampdrukmetingen aan een olie van Exxon geven aan dat met een zorgvuldig ontwikkelde meetprocedure de werkelijke dampdruk van een mengsel met zeer uiteenlopende componenten goedkan worden benaderd. Een zeker verlies van zeer vluchte verbindingen blijkt echter onontkoombaar.

De moleculair gewichtsverdeling bepalingen met MALDI-MS (*matrix-assisted laser-desorption ionisation mass spectrometry*) en SEC (*size exclusion chromatography*) zijn gecompliceerd gebleken. De Exxon olie bevatte een zeer brede verdeling in moleculair gewichten, wat de bepaling erg moeilijk maakte. Het gemiddelde moleculairgewicht is niet alleen wegens experimentele moeilijkheden van twijfelachtige waarde, maar men mag zich ook afvragen of een gemiddelde van een bereik tussen 1000 en 200 000 u iets zegt over de eigenschappen van de vloeistof.

De moleculairgewichtsbepalingen van de monsters van Point of Ayr geven aan dat goede resultaten met SEC kunnen worden bereikt. Problemen deden zich hier echter voor ten gevolge van verschillen in polariteit van de monsters. Uiteindelijk zijn de gegevens van SEC gebruikt ter ondersteuning van gemiddelde moleculairgewichten afgeleid van GC-MS en HPLC analyses.

De ontwikkeling van een toestandsvergelijking door regressie van de coëfficiënten bleek niet tot een bruikbaar model te leiden. Echter, regressie van de kritische temperatuur, kritische druk, en de acentrische factor (ω) bleek wel succesvol. De vergelijkingen die verkregen zijn zien er als volgt uit:

$$T_{cr} = \alpha_1 + \frac{\alpha_2}{\sqrt{C_{tot}}} + \alpha_3 H_{al} + \alpha_4 H_{ar} + \frac{\alpha_5 H_{al} + \alpha_6 H_{ar}}{C_{tot}} + \alpha_7 \left(C_{ar} + C_{ar,al} \right)$$

$$G_P = \alpha_1 C_{al} + \alpha_2 C_{ar} + \alpha_3 C_{ar,al} + \alpha_4$$

$$\omega = \alpha_1 C_{al} + \alpha_2 C_{al}^2 + \alpha_3 \left(C_{ar} + C_{ar,al} \right)^2 + \alpha_4 C_{ar} + \alpha_5 C_{ar,al} + \alpha_6 H_{al}^2 + \alpha_7 H_{ar}^2 + \alpha_8$$

waarbij opgemerkt moet worden dat in plaats van de kritische druk de parameter G_P is gebruikt. Deze parameter is een functie van de kritische druk (P_{cr}) en het moleculairgewicht. De waarden van de coëfficiënten zijn weergegeven in tabel 2.

Tabel 2 : Coëfficiënts van de regressie-vergelijkingen

Coëff.	α_1	α_2	α_3	α_4	α_5	α_6	α_7	α_8
T_{cr}	1007.406	-684.955	4.201066	2.999799	-122.344	-175.31	0.026036	
G_P	0.022342	0.015411	0.016299	0.033814				
ω	0.044761	-0.00157	0.006305	0.015054	0.000389	0.000381	-0.00211	-0.03828

De resultaten verkregen door vergelijking van de experimentele dampdrukken van de monsters van Point of Ayr geven aan dat het model goede resultaten oplevert, daarbij in aanmerking nemend de problemen met de bepaling van de gemiddelde moleculairgewichten. De enige uitzondering is de olie, waarvan de voorspelde waarden aanzienlijk slechte waren dan die van de fracties. Het mag daarom geconcludeerd worden dat het model voldoet voor gefractioneerde olieën, aangezien voor niet-gefractioneerde olieën het gemiddelde moleculairgewicht geen bruikbare informatie oplevert omtrent de te verwachten dampdruk.

Summary

For the description of the temperature-pressure relationship of coal oils, a model is required that requires as input only data from analytical chemical techniques. Coal oils are obtained during liquefaction and differ in properties from crude oils in their contents of aromatic hydrocarbons. As aromatic hydrocarbons have stronger interactions, the modelling of fluids with high contents of aromatic hydrocarbons is more difficult than that of aliphatic fluids.

The thermodynamic characterisation and modelling of these liquids plays an important role in reactor design. Before a chemical reactor for upgrading and/or cracking of these fluids can be constructed, the energy required by these separation and conversion processes should be estimated. The technology of coal liquefaction, that is the production of coal oils from coal, is not limited to coal: other solid feedstocks, such as municipal waste and biomass may serve as a feedstock as well.

The basis for the modelling was Van Laar's equation of state. This equation of state was developed in 1924 as one of the first modifications of the Van der Waals equation of state. The use of an equation of state as a tool for the modelling of the temperature-pressure relationship of organic fluids has been reported earlier in literature. Equations of state are usually used for calculations at high temperatures and/or pressures, where little or no experimental data are available.

The thermodynamic modelling work requires a stepwise process. At various levels, data are required to support the model development. Firstly, the data commonly available for these liquids should be obtained. These data may characterise the fluid in terms of major and minor components, elemental composition, molecular weight distribution, or relative concentrations of functional groups. For the trade in these fluids, these data are required anyway.

A second source of data is the literature, where from many pure substances experimental thermodynamic data are available. As for substituted naphthalenes data were lacking, vapour pressure measurements o several substituted naphthalenes have been carried out.

After verification of the capabilities of the equation of state with pure substances, binary mixture data were used in order to investigate the influence of empirical corrections on the performance of the equation of state. Furthermore, experimental work on binary systems provides useful information on the dependency of the vapour pressure on the composition of the mixture.

The final stage of the model development is the regression of the coefficients of the equation of state to parameters that can be obtained for coal oils as well. This regression is carried out on a database of pure substance data, and then the regression formulae can be tested with experimental data on coal oils. In this work, an oil of the Point of Ayr facility and 7 of its fractions, each with a boiling range of about 30 K, have been used for this purpose.

The first part of this work was an investigation of the capabilities of Van Laar's equation of state. It reads as

$$P = \frac{RT}{V}\frac{V + b_g - b_0'}{V - b_0'} - \frac{a_g}{V(V+c)}$$

where T is the temperature, P is the pressure, R is the gas constant, V is the volume. The other letters are coefficients, specific to the substance or mixture. From this work it was concluded that this equation of state was not capable of representing the whole vapour-liquid equilibrium area. The Cubic Chain-of-Rotators equation of state was selected as model to be developed further. This selection was based on the fact that both equations of state have a similar mathematical shape, although their background is different. This equation of state reads as

$$P = \frac{RT(1+0.77b/v)}{v-0.42b} + c^R\frac{0.055RTb/v}{v-0.42b} - \frac{a}{v(v+c)} - \frac{bd}{v(v+c)(v-0.42b)}$$

In this work, vapour pressure measurements were carried out on the following substituted naphthalenes: 1-methylnaphthalene, 2-methylnaphthalene, 1-ethylnaphthalene, 2-ethylnaphthalene, tetralin, 2-methoxynaphthalene, 2-naphthol, naphthalene-2-carboxylic acid , and 2-naphthaldehyde in the temperature range 40 C to about 150 C. The thermodynamic properties derived from these measurements are shown in table 1.

Table 1 : Summary of derived thermodynamic properties

Substance	Θ (K)	$\Delta G^0(\Theta)$ (J mol^{-1})	$\Delta H^0(\Theta)$ (J mol^{-1})	ΔC_p^0 (J K^{-1} mol^{-1})
1-methyl naphthalene	370.00	-20509 ± 150	56360 ± 190	< 2s
2-methyl naphthalene	370.00	-20991 ± 24	54460 ± 170	-49 ± 11
1-ethyl naphthalene	370.00	-18651 ± 14	60940 ± 80	-118 ± 10
2-ethyl naphthalene	370.00	-18832 ± 22	59820 ± 70	-105 ± 14
tetralin	370.00	-24680 ± 14	48910 ± 140	-51 ± 9
naphthalene-2-carboxylic acid	370.00	22497 ± 46	112950 ± 560	< 2s
2-naphthol (solid)	370.00	-13719 ± 44	83975 ± 470	< 2s
2-naphthol (liquid)	420.00	-25430 ± 14	59650 ± 540	< 2s
2-methoxy naphthalene	370.00	-14734 ± 46	74654 ± 920	< 2s
2-naphthaldehyde	370.00	-17144 ± 22	42884 ± 264	< 2s

For several substances, the ΔC_p^0 values could not be determined quantitatively, due to the fact that this parameter contains also some of the residual standard error from the regression analysis.

Two binary systems were investigated experimentally: toluene - 1-ethylnaphthalene and toluene - 2-methoxynaphthalene. The experimental data show that the vapour phase composition is determined almost completely by the light component (toluene). To a lesser extent, this holds also for the vapour pressure. These observations have proved to be very useful in interpreting the modelling results of the Point of Ayr fractions.

The CCOR performs in its classical form not too well on heavy aromatic substances. For a good modelling of these substances, a modification is required to account for association of molecules in the fluid. The results on the binary mixtures are not too

well either. Except for the reason already mentioned, the model requires empirical correction factors to account for the asymmetry in the mixture. These coefficients have been left out in this work, as they cannot be determined for coal oils.

The thermal stability of the (distilled) oils obtained in this project was sufficient for all other experiments. The vapour pressure measurements on the Exxon oil indicate, that with a properly designed experimental procedure, vapour pressure data may be obtained that approximate the real vapour pressure of a coal oil very nicely. However, a certain loss of volatiles, observed as a drop in vapour pressure at the same temperature with increasing run number, is inevitable.

The molecular weight determinations with both MALDI-MS (matrix-assisted laser-desorption ionisation mass spectrometry) and SEC (size exclusion chromatography) proved to be complicated. The Exxon oil was probably a mixture with a very wide variety in molecular weights, resulting in great difficulties in determining them. The average obtained for this oil is not only questionable from an experimental point of view: the range of molecular weights is that large (from below 1000 to over 200 000 u), that an average may be of little value to describe the complete fluid.

The molecular weight determinations of Point of Ayr oil and its fractions indicate that reasonable results with SEC with respect to molecular weight estimation can be obtained. However, problems arose due to differences in polarity of the samples. Finally SEC was used as "backup" and estimates were generated from GC-MS and HPLC data.

The development of an equation of state, capable of modelling the temperature-pressure relationship of coal oils and other ill-defined mixtures was found to be not successful when modelling the coefficients of the equation of state. Regression of the critical pressure, critical temperature, and the acentric factor provided a better basis. The equations read respectively

$$T_{cr} = \alpha_1 + \frac{\alpha_2}{\sqrt{C_{tot}}} + \alpha_3 H_{al} + \alpha_4 H_{ar} + \frac{\alpha_5 H_{al} + \alpha_6 H_{ar}}{C_{tot}} + \alpha_7 \left(C_{ar} + C_{ar,al}\right)$$

$$G_P = \alpha_1 C_{al} + \alpha_2 C_{ar} + \alpha_3 C_{ar,al} + \alpha_4$$

$$\omega = \alpha_1 C_{al} + \alpha_2 C_{al}^2 + \alpha_3 \left(C_{ar} + C_{ar,al}\right)^2 + \alpha_4 C_{ar} + \alpha_5 C_{ar,al} + \alpha_6 H_{al}^2 + \alpha_7 H_{ar}^2 + \alpha_8$$

where the regression of G_P (a function of the critical pressure and molecular weight) appeared to be more convenient. The values of the coefficients of the equations are given in table 2.

Table 2 : Coefficients for the regression equations

Coeff.	α_1	α_2	α_3	α_4	α_5	α_6	α_7	α_8
T_{cr}	1007.406	-684.955	4.201066	2.999799	-122.344	-175.31	0.026036	
G_P	0.022342	0.015411	0.016299	0.033814				
ω	0.044761	-0.00157	0.006305	0.015054	0.000389	0.000381	-0.00211	-0.03828

The results obtained for the Point of Ayr fractions are quite good, taking into account the difficulties in obtaining estimates for the average molecular weight. The only exception is the oil, for which the predicted values are poor. From these results, it can be concluded that the model is not suitable for unfractionated oils, because in that case the average molecular weight provides little information about the content of the lightest components.

Voorwoord

Het in dit proefschrift gepresenteerde onderzoek is uitgevoerd in twee projecten die gedeeltelijk door de Europese Gemeenschap voor Kolen en Staal (EGKS) zijn gefinancierd. Het onderzoek is uitgevoerd bij twee werkgevers, namelijk European Centre for Coal Specimens SBN (1 juli 1990 - 28 februari 1994) en Nederlands Meetinstituut (1 maart 1994 - 16 december 1996).

Het eerste project was getiteld "Thermodynamic properties of coal liquids" (ECSC 7220/EC-602) en had tot doelstelling het onderzoeken van de mogelijkheden om met behulp van de toestandsvergelijking van Van Laar de druk als functie van de temperatuur in systemen van pure aromatische stoffen te beschrijven. Deze stoffen komen voor in olie verkregen uit steenkool.

Nadat uit het eerste project gebleken was dat er in de vergelijking van Van Laar een aantal onvolkomenheden zaten, is een andere vergelijking gekozen, die wat betreft vorm overeenkomst heeft met die van Van Laar. Deze toestandsvergelijking is in de literatuur al regelmatig onderzocht, zodat de eigenschappen van dit model voor stoffen en mengsels van stoffen waarvoor dampdruk gegevens beschikbaar zijn bekend zijn.

Het tweede project was getiteld "Thermodynamic basis for coal liquefaction modelling" (ECSC 7220/EC-603) en omvatte naast een voortzetting van de modelleringen uit het eerste project een experimenteel programma. Dit experimentele programma was bedoeld om de thermodynamische modellering te ondersteunen. Tevens had het de doelstelling ook na te gaan, of met de gangbare karakterisaties waaraan kolenolieën worden onderworpen in de insdustrie, het mogelijk is het dampdrukgedrag van deze vloeistoffen te voorspellen als functie van de samenstelling van de vloeistof.

Preface

The research presented in this thesis has been carried out in two projects funded in part by the European Coal and Steel Community (ECSC). The work was carried out at two employers, in fact European Centre for Coal Specimens SBN (1 July 1990 - 28 February 1994) and Nederlands Meetinstituut (1 March 1994 - 16 December 1996).

The first project was titled "Thermodynamic properties of coal liquids" (ECSC 7220/EC-602) and aimed to investigate the modelling capabilities of the Van Laar equation of state in modelling the temperature-pressure relationship for pure aromatic substances. These substances are found in coal liquids.

From the first project, it followed that the Van Laar equation of state contained some imperfections. Another model of similar mathematical shape was selected as basis for the following work. This equation of state had been investigated quite extensively already, so that its features in modelling substances and mixtures for which vapour pressure data exist.

The second project was titled "Thermodynamic basis for coal liquefaction modelling" (ECSC 7220/EC-603) and contained in addition to the continued modelling work an experimental programme. This programme intended to support the thermodynamic modelling work. It also aimed to verify whether the common characterisations of coal liquids as used in industry provide a sufficient basis for the prediction of the behaviour of the vapour pressure of these liquids as a function of temperature.

Dankwoord

Dit onderzoek is tot stand gekomen dankzij de hulp van velen. Op de eerste plaats gaat mijn dank uit naar mijn promotor, Harry Oonk, en mijn co-promotor, Koen Nater. Hun hulp en kritische opmerkingen gedurende het onderzoek hebben aanzienlijk bijgedragen tot het verwezenlijken van de doelstellingen. In dit verband bedank ik ook Huub Chermin, die samen met Koen Nater de basis heeft gelegd voor het onderzoek.

Bij de totstandkoming van de databank en bijbehorende software is de handkracht van Siegfried Broos van groot belang geweest. Het ontwerp en de programmering van een thermodynamische databank is een "vak apart" en wordt nogal eens onderschat of weggestopt in de thermodynamische literatuur. Daarnaast moeten in dit kader ook Manon Cohnen en Romy Lemmens genoemd worden. Zij hebben veel werk gehad aan het invoeren van thermodynamische gegevens en de controle ervan. Met name Romy Lemmens had ook een groot aandeel in de totstandkoming van dit proefschrift. De illustraties (formules, figuren) en tabellen komen voor een belangrijk deel van haar hand. Ik ben hen voor hun bijdragen zeer erkentelijk.

Het experimenteel werk is door verschillende vooraanstaande groepen uitgevoerd. In dit kader wil ik Aad van Genderen en Paul van Ekeren van het Thermodynamisch Centrum Utrecht (TCU) bedanken voor het beschikbaar stellen van hun faciliteiten en het assisteren bij de dampdrukmetingen, en de stabiliteits- en warmtecapaciteitsmetingen aan de coal liquids.

I would like to thank Dr. Veluswamy of Exxon USA for the supply of about 5 dm^3 of coal liquid from the Wilsonville Utility. The amount of material allowed extensive tests for optimising the vapour pressure measurements of such very complex mixtures. I also would like to thank Sam Moore of the Point of Ayr Liquefaction Project for the supply of an oil from this project and a range of fractions. The experimental results of these fractions contribute considerably to the knowledge of the distribution of aromatic species in a coal oil.

I would like to thank the European Coal and Steel Community (ECSC) for funding in part the research. I would like to thank in particular Mr. James Wilkinson for his interest in the work, and his advice and help during the two ECSC-funded projects.

Die Karakterisierung der Kohlenöle und Kohlenölfraktionen ist teilweise vorgenommen worden von RWTÜV in Essen. Ich möchte mich sehr herzlich bedanken bei der Frau Dr. Inge Wieschenkämper und bei dem Herrn Dr. Andeas Kunze für ihre Mitarbeit. Außerdem möchte ich mich bedanken bei dem Herrn Dipl.-Ing. Bernd Strobl von DMT in Essen für seine Beratung im Bereich Karakterisierung von Kohlenölen.

Furhermore, I would like to thank Dr. Rafael Kandiyoti and Dr. Alan Herod from Imperial College in London (UK) for their molecular weight determinations of the coal liquids and coal liquid fractions.

René van Doorn ben ik zeer erkentelijk voor zijn hoofdvakscriptie, die een goed inzicht verschaft in de ontwikkeling van (kubische) toestandsvergelijkingen en de sterkten en zwakten van de bestaande modellen.

Verder bedank ik mijn werkgevers, European Centre for Coal Specimens SBN en NMi Van Swinden Laboratorium B.V. voor de mogelijkheid om dit onderzoek uit te kunnen voeren en hierover een proefschrift te schrijven.

Bij de totstandkoming van dit proefschrift zijn een aantal mensen betrokken die ik hiervoor zeer erkentelijk ben. Op de eerste plaats geldt dit Anton en Jennifer Alink, die de tekst inhoudelijk respectievelijk qua Engels taalgebruik hebben beoordeeld. Verder heb ik het kritisch volgen van de totstandkoming van het proefschrift door Hugo Ent zeer op prijs gesteld. Ook aan alle collega's die meegeleefd hebben, mijn hartelijke dank.

Tenslotte wil ik mijn familie bedanken. Dit geldt op de eerste plaats mijn ouders, Marten en Marijke, en mijn zussen Martine en Nannette. Tevens gaat mijn dank uit naar Frans en Mariëtte Tiggelman en hun dochter Suzanne. Hun medeleven tijdens het onderzoek en de afronding ervan is mij zeer tot steun geweest.

Eygelshoven, April 1997

Adriaan M.H. van der Veen

Curriculum Vitae

Adriaan M.H. van der Veen is geboren te Breda op 1 augustus 1967. Na in 1979 de basisschool St. Alexanderschool (Bennekom) te hebben afgerond, is heeft hij na 6 jaar zijn VWO-diploma gehaald.

In 1985 begon dan zijn Scheikundestudie in Utrecht. Zijn bijvak liep hij bij de vakgroep Heterogene Katalyse van Prof. Ir. J.W. Geus, waar hij de eerste schreden zette op het gebied van numerieke wiskunde en niet-lineaire regressie. Het hoofdvak had als onderwerp het karakteriseren van zeolieten door middel van het meten van luminescentie van zeldzame aarden (met name Gadolinium en Europium). Dit onderzoek werd uitgevoerd onder in de vakgroep Gecondenseerde Materie bij Prof. Dr. G. Blasse. Op 25 juni 1990 werd het doctoraalexamen met succes afgelegd.

Op 1 juli 1990 trad Adriaan in dienst van European Centre for Coal Specimens SBN als promovendus voor een periode van 2 jaar. Na deze periode werd de verbintenis omgezet in een vaste aanstelling als wetenschappelijk medewerker. Met ingang van 1 maart 1994 trad hij bij het Nederlands Meetinstituut in dienst, dat de activiteiten van zowel European Centre for Coal Specimens SBN als van Materialenbank Nederland (MBN) overnam.

Naast het thermodynamische werk ontwikkelde hij diverse dynamisch-statistische modellen (Monte Carlo modellen) om inzicht te verkrijgen in de statistiek van monsterneming, monstervoorbehandeling en sub-bemonstering. De basis voor deze modellering bestaat uit de praktische ervaring opgedaan bij SBN en MBN. Het eerste deel van de modellering is gepubliceerd in 1993, het tweede deel in 1995 en 1996.

Table of contents

Appendices

List of tables

List of figures

1. INTRODUCTION

1.1 Background

Coal liquefaction is he conversion of coal into fluid fuels and/or feedstocks. The primary objective of coal liquefaction is to convert coal into liquids, that can be used in a wide variety of applications, where the use of coal is inappropriate or impossible. One of the best known examples is probably the production of oil from coal as a substitute of crude oil. Several examples exist in history. One of the probably best known examples is Germany before World War II (1933-1945), that had been struck by an oil boycott.

There may be a variety of economical, political, and geographical factors that are in favour of the production of oil from coal on an industrial scale. If a country has large amounts of coal, but little or no crude oil resources, coal liquefaction may be an alternative to the import of crude oil. In the USA for instance, many research has been done on coal liquefaction, and more generally in the preparation of transport fuels from coal. Transport fuels are fuels, either solid, slurry, liquid, or gaseous, that can be transported through pipelines, rather than by train, ship, or lorry. The USA has big coal resources, and it was recognised that the transport of coal by classical transportation techniques was to a certain extent inefficient and costly.

Currently (1997), it seems that the technology of coal liquefaction has lost its significance. There are however several reasons, why this is not the case. Firstly, the coal resources are far greater, than the sum of other hydrocarbons (oil, natural gas, etc.) and uranium together, when expressed in EJ (exa Joules, 1 EJ = 10^{18} J). Bender reported data at the World Energy Conference in 1980 [1]. The data are shown in figure 1.1-1. It should be emphasised [2] that the major part of the hydrocarbon resources and reserves are tar sands and shale oils, rather than crude oil or natural gas. Tar sands and shale oils require a similar kind of conversion and upgrading in order to produce liquid fuels and/or feedstocks.

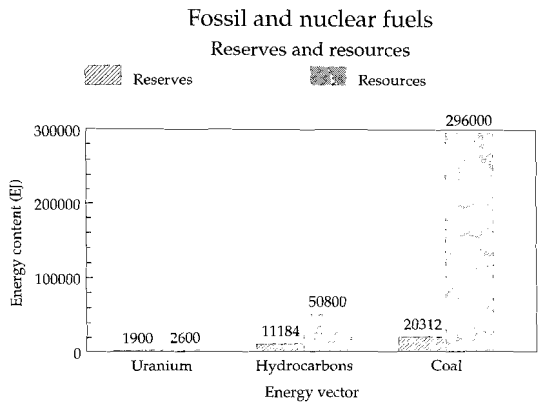

Figure 1.1-1 : Reserves and resources of fossil and nuclear fuels after Bender

Although in the past 15 years there have been developments in discovering new resources in crude oil and natural gas, these discoveries do not lead to a radical change in the picture of Bender. After the second oil crisis in 1979, there was some

pessimism that the crude oil reserves and resources would be sufficient to satisfy the (increasing) need till about 2030. Recent estimates are more optimistic and predict that, apart from economic or political crises, the oil resources would be sufficient till at least beyond the year 2050.

Secondly, the technology of converting organic matrices in liquid fuels and feedstocks can also be used for the conversion of biomass. There may be a wide variety of reasons for the liquefaction of wood, municipal waste, and other biomass. In the developed countries, often the reuse of materials is an issue in order to reduce the amount of waste produced and to save energy resources.

The conversion of coal to a liquid fuel or feedstock is a process, that involves a primary liquefaction step, followed by several upgrading and separation steps. The primary product from liquefaction is usually not very stable. A distillation step is usually implemented in the process to (1) separate the product from the reaction mixture and (2) to stabilise the product. The distilled oil is relatively stable and can be used as a feedstock for further upgrading, refining or separation.

The further processing of the liquid product, as well as the production of coal liquids requires reactors. In reactor design, the process conditions play a key role. The key variables in such a process are temperature (T) and pressure (P). The temperature in the reactor determines mainly the reaction rate, and thus the required residence time of the reaction mixture in the reactor. The pressure of the system is usually set in order to obtain the desired products in the desired time. However, a change in temperature or composition of the reaction mixture has a strong influence on the system pressure.

Therefore, for an efficient reactor design, the relationship between pressure and temperature of the reaction mixture at the temperature and pressure of interest should be known. However, it is no use to determine the behaviour of the reaction mixture for every mixture likely to occur in the reactor. The composition of the mixture is usually a strong function of the feedstock (coal). The properties of coals that are used for liquefaction differ widely, and so do the oils obtained from these coals. A further complication is that the pressures and temperatures in reactors are usually far beyond what can be realised in a laboratory.

For these reasons, a model should be developed that is capable of predicting the relationship between temperature and pressure of these fluids far beyond regions that are experimentally accessible in a laboratory.

1.2 Concepts

The main objective of this work is to develop an equation of state that is capable of predicting the temperature-pressure relationship of liquids produced from coal. An equation of state is a model that provides a relationship between temperature, pressure, and density of fluids. Although there are examples of equations of state for solids, their performance is usually far less than that of equations of state for fluid states. The use of a suitable equation of state is of special interest for extrapolations. Many empirical models that relate pressure to temperature do not provide useful results in extrapolations.

For the modelling of complex fluids with many components, it is no use to take a model only capable of describing the properties of the pure components and simple mixtures. However, such a model may be a suitable basis for the development of a model for coal liquids.

For such a model development, it is crucial to define a set of properties that

1. provide characteristic information about the mixture;
2. form a minimum set;
3. cover the (average) properties of the whole fluid.

It is no option to make an attempt to identify all separate components in this kind of mixtures. Many components may be present in very low concentrations, that cannot be measured by analytical chemical techniques. Several spectroscopic techniques are however capable of identifying and quantifying structure fragments in the fluid. These structural fragments determine in part the properties of the fluid. Another parameter that is very important is the (average) molecular weight. From these data, an "average molecule" can be constructed that incorporates the properties of the fluid. Although there is no such thing as an "average molecule", the concept is useful to define the properties of the fluids.

As a result, the characterisation of a coal liquid will lead to an average composition of the mixture. An equation of state requires usually several pure substance properties in order to determine the values of the coefficients of the model. The model development essentially aims to replace the relationship between the pure substance properties and the coefficients of the equation of state by a relationship between the *average properties of the liquid* and the coefficients of the model.

The success of modelling oils depends on both the need for empirical corrections in binary mixtures relevant to the composition of the oil, and on the representativety of the properties of the "average molecule" for the oil. Another part of the success must come from the characterisation part in terms of composition of the oil. The main objective of this characterisation is to establish concentration levels for all structure fragments that can be distinguished in the mixture. Whether structure fragments should be detected separately does not only depend on the analytical chemical capabilities: the difference in contribution to the physical properties is more important.

Without clever generalisations, the job of modelling of ill-defined mixtures becomes impossible. Many functional groups show overlap with other functional groups, and sometimes these groups even appear at other locations in the spectrum. For simple systems, one could make fine interpretations. For ill-defined mixtures however, this is virtually impossible. An additional question to be answered is to what extent the results of the composition analysis can be correlated to the coefficients of the equation of state. If these correlations are weak, then it is no use to take them into account.

1.3 Implementation of the work

The basis for the modelling work was the equation of state of Van Laar [3]. He published 1924 his equation of state as a modification of the equation of state. The background of this choice was the fact, that the repulsive part of Van Laar's equation of

state is better capable of describing fluids at high densities (liquids, heavily compressed gases) than Van der Waals' equation of state is.

However, it turned out that Van Laar's equation of state contained some mathematical imperfections, that made it impossible to cover the complete ranges of temperature, pressure, and density over which a fluid can exist. Literature research had showed that there was a similar equation of state, the Cubic Chain-of-Rotators equation of state (CCOR) [4-6]. This equation is closely related to the Chain-of-Rotators equation of state (COR). The CCOR has a great advantage over the COR: it is cubic in density, which makes that no iterative calculations are necessary for the calculation of densities. A cubic equation can be solved analytically.

As a result, the Cubic Chain-of-Rotators equation of state has been used as starting point for the model development. A feature of the CCOR is that its representation of the repulsive forces between particles in the fluid are represented better at high densities than by equations of state of the Van der Waals type. It should however been verified whether this leads to an improved representation of especially mixtures, where the quality of the densities predicted by the equation of state is of influence.

The objective of developing a model capable of describing and predicting the properties can only be met if several requirements have been fulfilled. The work programme is a reflection of the verification process necessary to demonstrate the capabilities of the model.

The availability of experimental data is the first requirement. The basic data required for demonstrating the capabilities of the equation of state are vapour pressure data. Vapour pressure data are obtained when measuring the equilibrium pressure of a liquid as a function of temperature. In order to determine the coefficients of a classical equation of state, some pure substance data are required additionally. The equation of state provides then a predicted pressure for a given system temperature. For pure substances, this is visualised in figure 1.3-1.

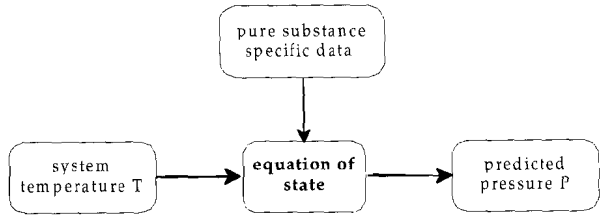

Figure 1.3-1 : Principle of an equation of state for pure substances

The performance of the model can be assessed by comparing the predicted pressure P with the experimental one from a set of vapour pressure data. For several substituted heavy aromatic hydrocarbons, data are lacking. These substances are commonly found in coal liquids, and a proper assessment of the capabilities of the equation of state should include the evaluation of its performance on experimental data of these substances. The results of these measurements are given in chapter 5, the performance of the model is subject of chapter 6 of this work.

For mixtures, the input required by the model increases. For a prediction of the pressure in a system containing two components, pure substance data of both components are required (figure 1.3-2). A further requirement is that the composition of the mixture should be known. For every additional component in the mixture, a box with "substance data" is to be added. The composition of the mixture becomes more complex too. Following this trend, it is easily seen that for a mixture of 10 components, a considerable amount of information is required in order to 'feed' the model.

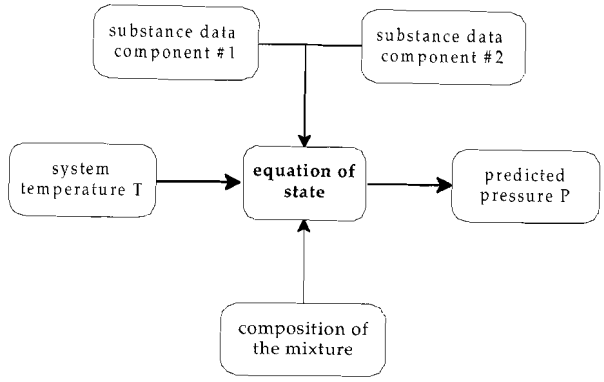

Figure 1.3-2 : Principle of an equation of state for a binary mixture

For the assessment of the performance of the model, again experimental data are required. These data comprise the vapour pressure as a function of the composition of the mixture and temperature. Data from binary mixtures are the basis for this evaluation. As in coal liquids often components of different molecular weight and different side-chains appears, such binary systems are of special interest. In the experimental programme, two systems of this type have been investigated (chapter 7 of this work).

The performance of the model in describing experimental data from binary mixtures is important for two reasons, in fact (1) to demonstrate the capabilities of the model and (2) to find out, what range of components can be handled by the model. The larger the range in molecular weights in the fluid, the worse the performance of an equation of state becomes. Furthermore, it is not very realistic to determine the average properties of a mixture (that is, the artefact "average molecule") if there is a very wide variety of components. In that case, the distribution of components is that wide that the averages can no longer be regarded as being representative for the properties of the mixture.

The final step in the modelling process is to change the required input for the calculation of the coefficients of the equation of state. This conversion can be carried out by fitting the values of the input parameters or the coefficients of the equation of state to a set of parameters that can be obtained from analytical chemical techniques and represent the whole liquid. This has been described as composing the "average molecule", that is an artefact that has the average properties of the fluid.

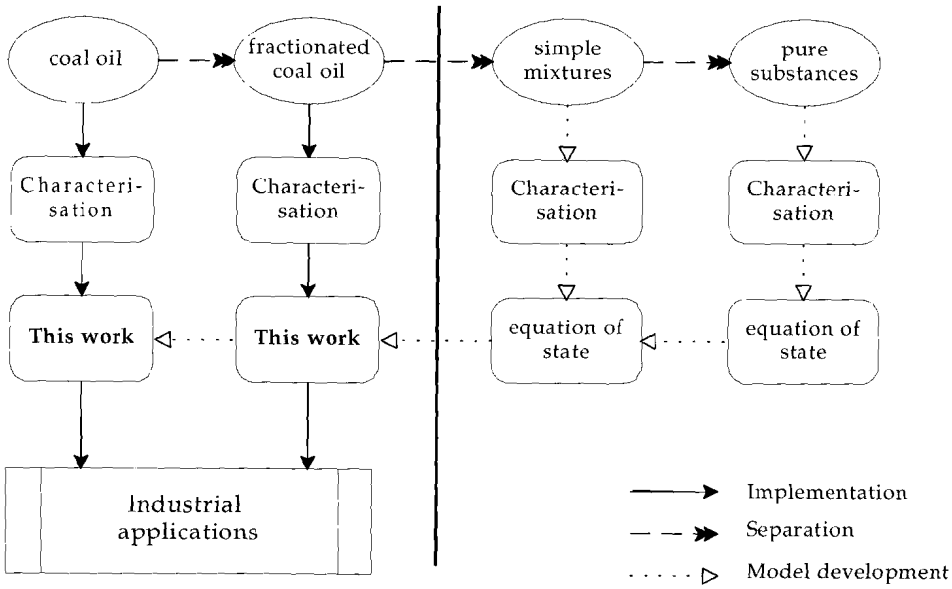

Figure 1.3-3 : Model development and application

The modelling process can be summarised as follows (figure 1.3-3). The double arrows indicate further separation steps. After a separation, the system becomes less complex. Simple mixtures are often obtained by mixing pure substances, rather than by successive separations. So, the arrow from "fractionated coal oil" to "simple mixtures" should be regarded to guide thoughts, rather than representing real-world processing of this kind of oils. The single arrows ("implementation") show how the model will work in practice. The open arrows ("model development") show how the model development proceeds in this work.

As already stated, the open arrows in figure 1.3-3 indicate the process of model development. The process starts right in the figure with pure substances, followed by the extension to simple mixtures with known composition. As stated earlier, the resulting model is unsuitable for application in the left part of the figure. The model to be developed in this work uses other variables, that are based on the "average composition" of the mixture. Obviously, the input parameters for this model can also be obtained for simple mixtures and pure substances. The verification of the model includes the assessment of the performance for simple mixtures and pure substances too.

The most important verification of the capabilities of the model is in the very left column of figure 1.3-3. If the model is sufficiently well established, then it could be possible to predict the behaviour of an oil with a variety of components. A link between coal oil and simple mixtures is a fractionated oil. A coal oil can be separated into fractions by means of distillation. The fractions contain substances of similar boiling point, and for this type of mixtures usually molecules of similar size. The characterisation of oil fractions is not only part of this work, but it is done in practice

frequently too. Oil is usually fractionated in order to obtain different kind of fuels (gasoline, diesel fuel, etc.) or feedstocks.

The resulting model of this work is shown in figure 1.3-4. The model ("this work") is a simple in handling as the model for pure substances (figure 1.3-1). The model is the machinery that allows to predict thermodynamic behaviour of the oil or oil fraction. The input for the machinery are the average properties of the oil, denoted by ('average molecule").

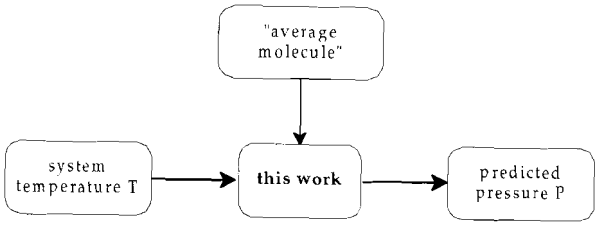

Figure 1.3-4 : Final result of the modelling work

2. COAL LIQUEFACTION

2.1 Coal petrology

Coal is an organic matrix. Its structure resembles that of stone and rocks, in a sense that different phases can be identified in the matrix. The organic part of the matrix can be divided into three groups of *maceral groups*, based on their structure. A *maceral* is the organic analogue of a mineral in stone. The three maceral groups are vitrinite, exinite, and inertinite.

The properties of the coal depend on the concentrations of vitrinite, exinite, and inertinite. A coal can be split into its maceral groups by a combination of grinding or chemical communition, followed by a separation based on density [8,9]. Exinite is the most reactive of the three groups, and contains most volatile matter. Vitrinite reflects often in properties about the average of the coal, whereas intertinite is the least reactive maceral group. It is usually also the maceral group with the lowest volatile matter content.

Coal also contains minerals. During combustion, these minerals are converted into ash. During liquefaction, the mineral matter forms together with char a solid residue. The minerals present in coal influence conversion processes, due to the fact that some minerals show catalytic activity during the conversion process (liquefaction, combustion).

A measure for the reactivity of the coal is the rank. There are various ranking systems, but they all have in common that with increasing rank

- the volatile matter content (corrected for ash content) decreases;
- the reactivity of the coal decreases;
- the gross calorific value (corrected for ash content) increases;
- the hydrogen content (corrected for ash content) decreases;

Anthracites are coals with a high rank, whereas brown coal is the lowest rank coal. Although anthracite has a high calorific value, its reactivity is usually low, so that it is unsuitable as a feedstock for some conversion processes. Blending of anthracites with low rank coals may speed up the conversion process. Low rank coals on the other hand have as disadvantage that their calorific value is usually considerably lower, which results in a higher feed rate in order to produce the same amount of energy per unit of time.

2.2 Coal structure

Before providing a very brief overview over published results and principles on coal liquefaction, some attention should be paid to the structure of coal, and the fundamental mechanisms in liquefaction in absence of vehicle oil and/or reducing agents (such as hydrogen). The primary step is usually pyrolysis, that is the decomposition of the coal due to heating. In a thesis, Tromp [2] investigates pyrolysis under a wide

variety of conditions. In addition to heating rate and temperature, the structure of the coal is a dominant factor.

The structure of coal has been modelled in various ways, and it is not aimed to give an overview here. The molecular structure of coal is very complex, and many aspects of the structure are not known yet. The model, that a coal is constructed from aromatics, aliphatics, and functional groups leads to Shinn's coal model [10] (figure 2.2-1).

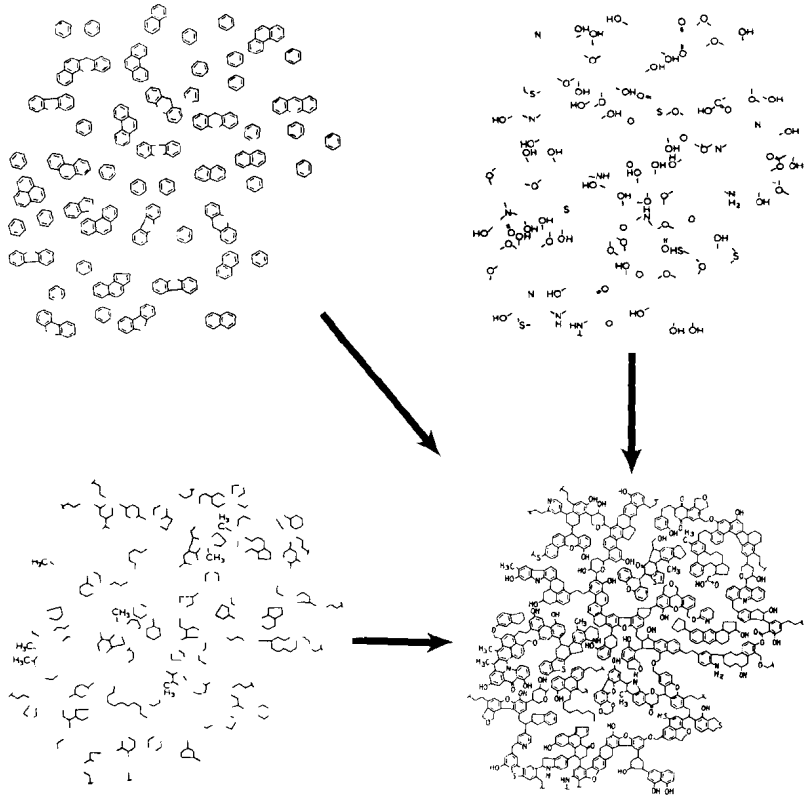

Figure 2.2-1 : Coal model for a bituminous coal after Shinn [10]

The model of Shinn has been developed for bituminous coals. The model structure has an arbitrary molecular weight of about 10 000 g/mol. The functional groups contain the hetero-atoms in a coal structure. The basic structure of the carbon skeleton is the graphite structure. The graphite structure consists of layers of fused aromatic rings. The model of Shinn shows to what extent such a layer is found in bituminous coals. The structure contains lots of gaps and holes when compared to a

perfect graphite lattice. Another major difference is the presence of hetero-atoms, such as oxygen, nitrogen, and sulphur. The aromatics (upper left in figure 2.2-1) and the aliphatics (lower left of figure 2.2-1) contain hydrogen, as do some functional groups (amine, carboxylic acid, mercaptan).

In his thesis, Tromp [2] gives two other models, one for a semi-anthracite (figure 2.2-2, left) and one for a lignite (brown coal).

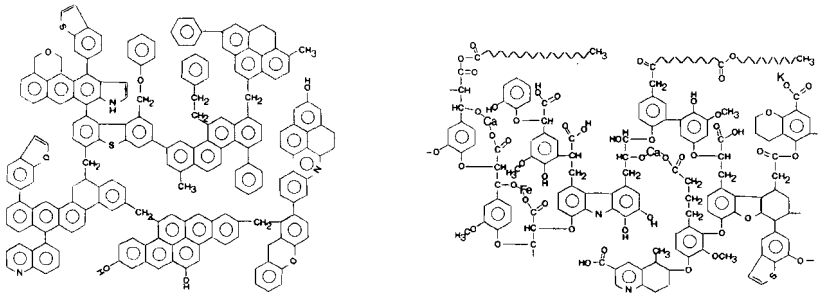

Figure 2.2-2 : Possible structures for a semi-anthracite (left) and a lignite (right) [2]

From figure 2.2-2 it becomes clear that the structure of a lignite is more "open" than that of a semi-anthracite. The aromaticity of the coal increases with rank, which is also seen from figure 2.2-2. However, aromatic structures are relatively stable, so the pyrolysis of a semi-anthracite is more difficult than that of a lignite. In many liquefaction processes, bituminous or sub-bituminous coals are used rather than higher rank coals (hard coal, semi-anthracite, anthracite) because the lower rank coals are less stable and react more rapidly under pyrolysis conditions.

Pyrolysis of coal is a very complex process. The principal processes are visualised in figure 2.2-3. A coal particle undergoes thermal decomposition, that leads to the formation of free radicals. As secondary reaction, two reaction types can be identified, in fact

1. polymerisation reactions, leading to char formation
2. other stabilisation reactions, leading to volatile products

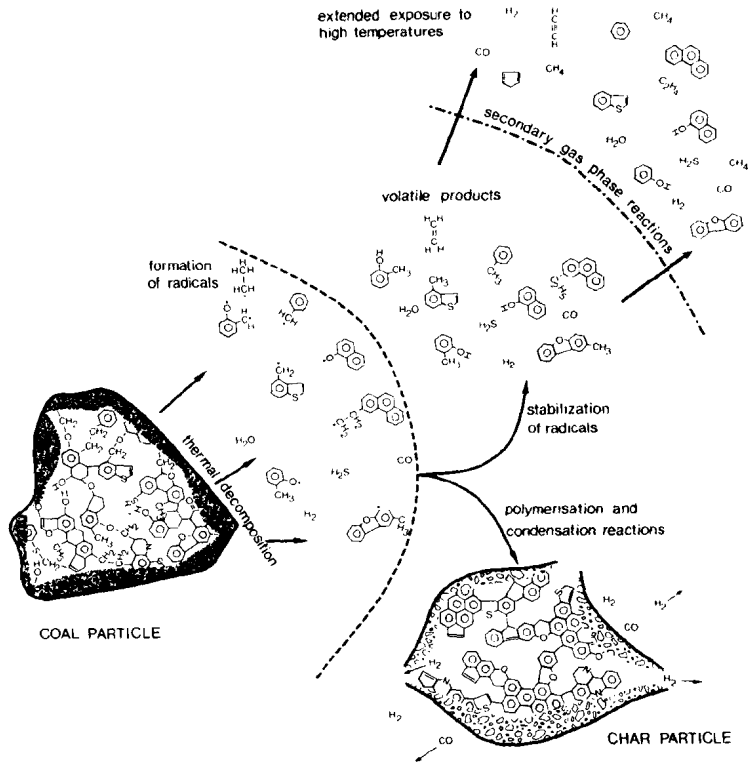

Figure 2.2-3 : Reactions and processes during pyrolysis of coal [2]

The nature of the volatile products depends highly on the coal type, and the contents of hetero-atoms. When coal is pyrolysed in presence of an extracting agent, the volatile species are stabilised more rapidly and usually the conversion yield increases. In the next sections, where several types and processes of liquefaction are presented, several examples are given. Another method to increase the yield of volatiles is to add hydrogen (usually through a vehicle oil and/or a catalyst) to the coal when being pyrolysed.

2.3 Principles of coal liquefaction

There are two principal ways to produce coal liquids, either on laboratory or on industrial scale: direct liquefaction and indirect liquefaction. In the first type of process, the liquid is produced directly from the coal, by means of pyrolysis, extraction, and/or hydrogenation. Indirect liquefaction involves in a first step the total conversion of coal to synthesis gas (a mixture of hydrogen and carbon monoxide), followed by further reactions of the mixture to form to coal liquids (Fischer-Tropsch synthesis). Obviously, the nature of the products differs considerably between the two

types of processes. Within these two groups, the variety of the properties is also considerable.

Most liquefaction processes carried out on a semi-industrial or industrial scale are examples of direct liquefaction processes. Therefore, most of the examples given in this section and the next are examples of direct liquefaction. The products from direct liquefaction differ considerably between the different processing pathways, and they also depend on the feedstock (coal), reaction conditions, such as pressure, temperature, presence of a catalyst and so on.

A typical route for the production of a coal liquid from a medium volatile bituminous coal by means of direct liquefaction is as follows. First the coal is pyrolysed at 600 C, and then a hydrogenation step is carried out. The hydrogenation of coal can be carried in numerous ways, depending on the type coal used. A commonly applied method involves the use of a vehicle oil as recycling solvent, hydrogen at a pressure of 10-13 MPa and a catalyst. An alternative for the use of hydrogen gas is the use of a hydrogen donor solvent, such as tetralin or other partly hydrogenated aromates [12]. In most cases, the process is designed in such a way, that after tetralin has donated its hydrogen, it is re-hydrogenated. This re-hydrogenation can be carried out by means of hydrogen gas and a catalyst. In such a process, tetralin can be considered as a catalyst too.

The presence of a catalyst is essential when using hydrogen gas as source for hydrogen, since hydrogen gas is too unreactive for a direct reaction. Commonly used hydrogenation catalysts are based on nickel- and/or molybdenumchloride, tin(II)chloride [12], or zinkchloride. The catalyst may be dispersed by either mixing of the solid catalyst or by using a molten salt catalyst [13]. In the latter case, potassium chloride is added in order to reduce the melting point temperature of the catalyst [14]. A study on Australian Liddel coal by Collin et.al. [12] showed, that the performance of nickel/molybdenumchloride as a hydrogenation catalyst is low: only 5% of the coal reacted during their experiments. Tin(II)chloride in combination with hydrogen performed better. The product spectrum consists of alkanes, naphthalene, indan derivatives, phenol, cresols (methylphenols), phenanthrene, and carbazole. The use of tetralin as donor solvent in combination with hydrogen and nickel/molybdenumchloride as catalyst yielded much methyl- and dimethyltetralin, but it also increased the overall yield in comparison with the experiment without tetralin.

The vehicle oil plays a very important role in liquefaction. The nature of this type of oil differs considerably, and even commercial vehicle oils differ a lot in chemical composition and properties [12,15]. A vehicle oil may be a coal derived oil, or a donor solvent such as tetralin or a combination of both. The most important properties of the vehicle oil are the ability to extract species from the coal and the ability to solve the liquefied products. Another property of a vehicle oil is its hydrogen-donating capacity. Since most liquefaction processes involve hydrogenation of the coal and/or the products, it is beneficial if the vehicle oil itself can act as hydrogen donor, just as tetralin. Normally, there are enough polyaromatic species present in the oil which can serve as hydrogen donors. More fundamental studies involve the behaviour of hydrogen-donating pure solvents [16-18].

From a study on the hydro-liquefaction of Liddel coal (Australia, rank medium volatile bituminous) using tetralin as vehicle and a commercial catalyst (Cyanamid HDS-3A), it is shown that the reaction conditions determine mainly the types of products obtained [19]. As is to be expected, a longer reaction time allows a further hydrogenation of the species, and therefore it yields smaller molecules. The same holds for a higher hydrogen pressure. With increasing hydrogen pressure and increasing reaction time, the average fused aromatic ring number decreases. The further hydrogenation of the species also leads to a decrease of the overall oxygen content in the liquid products.

A study on the average chemical structure of coal liquids obtained via hydrogenolysis of coal with red-mud and sulphur as catalysts gave similar dependencies on hydrogen pressure and temperature [20]. The experiments were carried out at 400 C and 450 C respectively and with 3 MPa hydrogen, 10 MPa hydrogen, and with 3 MPa hydrogen + 7 MPa nitrogen. The higher hydrogen pressure contributes to the saturation of more aromatic rings and it yields more extract. The higher temperature causes thermal decomposition of the aliphatic structures (mainly found in the oil extract) but it does not change the aromatic structures. When only the pressure is high (in this case by adding 7 MPa nitrogen) the reaction products remain the same, but the reaction itself is accelerated. An explanation for this fact is that the reaction proceeds to a greater extent in the liquid state by suppressing the vaporisation of low-molecular-weight matter under the higher pressure. Thus, the yield increases with temperature and also with pressure. Other investigations confirm this observation [19,21 ,22]. An increase in hydrogen pressure favours the hydrogenation of aromatic rings, and it slows down condensation and dehydrogenation reactions.

The study on the dependency of the yield on several reaction conditions [20] also assumes and shows evidence for the following pathway for the generation of oils according to [23]

coal → asphaltenes → oils

which is found in many references elsewhere. Results from other experiments confirm that asphaltenes are really an intermediate for oil [19]. Some authors wish to include pre-asphaltenes in this scheme as well

coal → pre-asphaltenes → asphaltenes → oils

An alternative for hydrogen gas is the *in situ* production of hydrogen. Mondragon [24,25] has reported in two articles the liquefaction of several coals. The investigated processing parameters included the amount of reducible metal, coal rank, and reaction temperature. Using wash oil as solvent, a maximum benzene conversion of 96 % was obtained.

In the literature, many studies have been published which make attempts to model the conversion of a coal as a function of several coal parameters [26], and studies which cover several coals from one country [26-30]. Coal parameters which are commonly used are the C:H-ratio, the volatile matter content, and the concentration of reactive macerals [31]. Most liquefaction experiments are carried out with low-rank coals, which is easily explained by the fact that as the rank increases, it becomes more difficult to pyrolyse and hydrogenate the coal. Both reactions are fa-

voured by a high number of hetero-atoms and by a low C:H-ratio (see also section 2.3).

Drying of a coal is a commonly used step in various coal conversion processes. Since drying of coal has its influence on the coal properties, it is important to find out to what extent the liquefaction behaviour differs from untreated coal. A study on the influence of drying of a Belle Ayr coal in liquefaction with a heavy distillate SRC-II oil showed that after drying the yield in the liquefaction experiment decreased. This holds for coals dried in nitrogen as well as for coals dried in air. The analysis of the residues showed that a high content of coke was formed [32]. Another study confirmed this fact, but showed also that when further oxidising the coal the liquefaction yield increased again. The first fact is explained by the formation of a network structure in the coal, whereas the second can be explained by assuming ring opening and cleavage of bridges and thus, increasing the number of reactive sites in the coal [33].

Coal cleaning is another treatment that a coal may undergo before further processing. The aim of coal cleaning is to reduce the content of sulphur and ash, which are the main contributors to environmental pollution by coal combustion processes. The presence of sulphur in the coal is also undesired if the liquid products are to be used as a transport fuel. Another aspect is the effect of coal cleaning on the behaviour of coals during liquefaction. The main objective of coal cleaning is to reduce the amounts of ash and sulphur in the coal. From a study on Irish coals during a SRC-II liquefaction process, it has been observed that the cleaning of the coal did not influence the H:C ratio, the O:C ratio, the vitrinite content, the exinite content, and the reactive macerals content.

A third issue on the processing of coals in conversion processes is the use of a blend. A blend of coals is commonly used if the properties of one coal are not suitable for the task. Then, a mixture of coals is used as feedstock. When a blend is liquefied, it is normally believed that the solvation of one coal favours the solvation of the other(s). A study has shown that this is only true when enough hydrogen is available. If not, only the most reactive coals are liquefied, and the others remain unreacted [34]. The additivity law on the extraction yields is therefore only valid when enough hydrogen is available.

For engineering purposes, the viscosity of the reaction mixture during the reaction is very important. Some parameters involved are the type of vehicle oil, coal:oil ratio, particle size of the coal, atmosphere, catalyst, and coal rank. The viscosity of coal paste appears to increase under hydrogen atmosphere, due to the disintegration of the coal under hydrogenation conditions [35].

2.4 Examples of liquefaction in industry

The principles presented in the previous sections have been implemented in various ways on an industrial scale. The examples cover both direct liquefaction and indirect liquefaction processes.

The *Bergius IG-Farben* process was developed before World War II in Germany. The coal is crushed and slurried in recycle oil together with a cheap iron oxide catalyst. The slurry is heated up to 500 C and the coal is destructively hydrogenated at a hy-

drogen pressure of 70 MPa [21]. Ash, spent, and catalyst are then removed and the product is distilled and further hydrogenated to petrol and lighter oils. The process is mechanically difficult and very expensive, but it allowed the Germans during World War II to produce up to 4 Mtonnes of synthetic oil a year.

A second process, which is very popular nowadays is the *solvent refined coal* (SRC) process, which has been developed in the United States of America. Ground coal and recycle oil are hydrogenated at medium pressures (12 MPa) with use of modern fixed bed catalysts [21]. The coal extract is separated by vacuum distillation. The distillate, that is known as SRC, is a relatively clean and sulphur free fuel which can be used in boilers, for instance for power generation. In the literature, the SRC processes are divided into SRC-I and SRC-II processes. The main difference between these two groups are the reaction temperature and pressure. The principles remain however the same.

The SRC-II process uses a tubular reactor, operated at 728-733 K and at a hydrogen pressure of 14 MPa. The catalyst consists of mineral matter from the recycled coal. The product spectrum of an Illinois No.6 bituminous coal consists of 15-20 % gas, 45-50 % distillate and 35-40 % residue. 4.5-5 % hydrogen gas is consumed.

In a series of articles, Singh et.al. give an almost complete description of a new kinetic model, the mass balance, and several other subjects related to plant operation in the SRC-II process [36-39]. The energy balance is reduced to one figure (in fact the heat of reaction per kilogram of hydrogen gas), and so is the heat capacity. It needs hardly explanation that for a successful simulation of the SRC-II process, more thermodynamic data are needed, since the energy effects play an important role in reactor and plant design. The heat capacity of the system is a function of the coal, the vehicle oil, and the vapour phase, and none of them remains constant during the liquefaction process. Especially the modelling of the thermal behaviour of the reactor [38] can be improved by more thermodynamic data.

The *H-coal* process is similar to the SRC process. The main difference is the use of a fluidised bed catalyst ($CoO\text{-}MoO_3/Al_2O_3$ with sulphur). The process operates at 720-735 K and at a pressure of 17 MPa. The vaporised products are further hydrogenated and then distilled. The remaining coke-like solid can be burnt or gasified [21]. It is very ash-rich. A typical product spectrum from an Illinois No.6 coal consists of 10 % C_1-C_3, 53 % distillate, and 37 % residue. 5-5.5 % hydrogen is consumed.

The *Exxon donor solvent* (EDS) process uses a hydrogenated recycle solvent and a fixed bed catalyst. The product vapours are hydrogenated further before they are fractionated by means of distillation.

The *National Coal Board* in the United Kingdom is developing a process for liquefaction of coal in order to obtain liquids usable as chemical feedstock or as transport fuel. Crushed, dried coal is extracted with solvent oil under carefully controlled conditions. No gaseous hydrogen is used. The filtrate is hydrocracked over catalysts to produce naphtha, spirit, diesel oils, and recycle solvent oil.

The only example of an indirect liquefaction process is the *Fischer-Tropsch* synthesis. Over a catalyst, synthesis gas (hydrogen and carbon monoxide) is allowed to react to organic oxygen species, normally to methanol and higher alcohols. Synthesis gas is

obtained by gasifying coal with steam and oxygen. Several studies on kinetics and mechanisms have been published [40,41].

2.5 Mechanisms and catalysis in direct liquefaction

It is generally believed that many reactions of coal are initiated by radical formation. This believe is in agreement with the mechanism assumed for coal pyrolysis (see also section 2.3). These radicals play a central role in various mechanisms. The hydro-liquefaction of coal with a donor solvent for instance can be represented by the formation of a radical site on the coal, which is followed by a reaction between the radical site and a hydrogen donor in the solvent. The dehydrogenated donor becomes then a radical itself, which can create a new radical site on the coal or can form another radical species elsewhere. Such a mechanism is terminated as soon as two radicals combine [42].

The radical mechanism is favoured by the fact that in coal and in coal liquids several species are found which can be classified as hydroaromatic species. The high aromaticity of the liquid is very important: the aromatic rings are able to stabilise the radical. A further effect of the presence of hydroaromatic species is that if they release hydrogen by reducing other sites or species in the reaction mixture, they can form new aromatic rings, which are very stable. The stability of these aromatic rings makes that species such as tetralin relatively easily donate their "excess" hydrogen in order to form the dehydrogenated aromatic species (figure 2.5-1).

Figure 2.5-2 shows a very simplified mechanism for the hydroliquefaction of coal by means of direct hydrogenation with hydrogen. The initiating step is the cleavage of the H-H bond over a suitable catalyst. The formed radicals can either hydrogenate the coal and thus forming a hydrogenated site and a radical site or the radicals may cause a cleave of a bond in the coal and a molecule is released (R-H in figure 2.5-2, where R is some organic structure). The termination of the radical mechanism occurs by recombination of two radicals (R and R' in figure 2.5-2). The groups R and R' may be any type of radical (radical site in the coal, hydrogen, or some organic group).

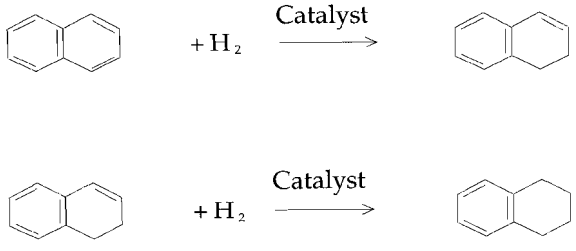

Figure 2.5-1 : Hydrogenation of naphthalene

From an extensive kinetics study of the hydroliquefaction of coal, the following conclusions were drawn [43-48]. First of all, the coal shows a quick break-up to soluble products. The THF[1]-insoluble fraction decreases first to a minimum, followed by an increase if the solvent is "poor". If a better solvent is used, such as tetralin, the increase was less. The increase of THF-insoluble compounds is favoured by higher temperatures.

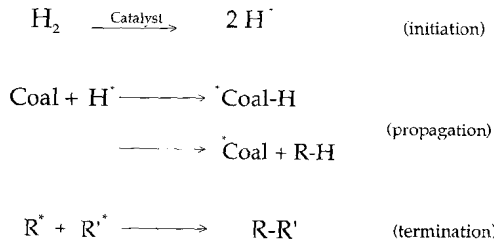

Figure 2.5-2 : Radical mechanism in coal liquefaction

Second, coal breaks up in radicals, which then react with non-radical species. Radical-radical reactions are generally retrogressive. The behaviour of the radical-radical reactions is complex, and it depends on both the solvent and the temperature. Retrogressive reactions predominate with high radical concentrations, whereas progressive liquefaction reactions predominate in a rapid break-up of the coal, not involving radicals [43].

More fundamental work includes the study of the hydrogen-donating abilities of several key-compounds and of several vehicle oils in SRC-II processes [49] and the thermolysis of coal structures such as bibenzyl and naphthols [50].

The use of deuterated reagents has found application in kinetics studies of coal liquefaction [51]. The principle of the use of deuterium is simple: deuterium is found in the products only on those places which are capable in exchanging hydrogen, or at places where a reduction has taken place. It also provides additional information on the mechanisms involved in the hydroliquefaction processes.

2.6 Characterisation of coal liquids

For the analysis of coal liquefaction products, several analysis techniques are used. One of the most commonly used techniques is gas chromatography (GC), sometimes combined with mass spectroscopy (MS) [52]. The GC equipment consists primarily of an injection part, a column, and a detection part. For the analysis of coal liquids the use of a capillary column of fused silica is reported [15,53]. For the quantification of the species in the liquid, several detector types for the GC are available. The most commonly used detector is a flame ionisation detector (FID), whereas for nitrogen compounds the use of a nitrogen-sensitive alkali flame detector has been reported [54]. The results from the two detectors agreed satisfactorily.

Another technique commonly used in the analysis of coal liquids is high performance liquid chromatography (HPLC), sometimes combined with MS. A special form

[1] THF = tetrahydrofuran

of MS, field ionisation mass spectroscopy (FIMS) has been used in order to analyse distillate recycle solvents from the SRC-I process. The HPLC separates the species based on the number of unsaturated bonds. FIMS separates on molecular weight and on "z", which is related to the C:H ratio in the molecule: C_nH_{2n+z} [55]. For benzene for example, z=-6, because there are 6 carbon atoms (n=6) and the number of hydrogen atoms in the benzene molecule is and the number of hydrogen atoms is given by 2n+z, where 2n=12. For benzene, the number of hydrogen atoms is 6, so z = -6.

A technique which gives direct information about the types of hydrogen in the molecules is ^{1}H-NMR (proton nuclear magnetic resonance). This technique is very useful for determining the number of a specific group of hydrogen atoms, such as aromatic or aliphatic hydrocarbons [56]. The technique has found wide application in characterisation of industrial liquefaction products, such as products obtained from SRC-I and SRC-II plants [57]. A list of proton shifts is listed in table 2.6-1.

Table 2.6-1 : NMR-shifts (ppm) for protons [51]

Chemical Shift	Type of Hydrogen
6.2-9.2	Aromatic hydrogen
1.7-4.4	H_αO-CH_3
	α-CH_3
	α-CH_2
	β-CH_2 tetralins
	β-CH_2 indans
1.0-1.7	β-CH_3
	Remote CH_2
	β-CH_2
0.0-1.0	H_γ Remote CH_3

A similar technique is available for the determination of the surroundings of carbon atoms in a molecule, in fact ^{13}C-NMR. ^{13}C-NMR allows the identification of carbons typical for methyl- and methylene-groups, alkanes, naphthalenes, benzenes, phenanthrenes, and fluorenes. The technique also detects the presence of hetero-atoms as neighbours of carbon in the molecule. Together with ^{1}H-NMR it is possible to obtain much information about the components in the mixture [15,19].

Infrared spectroscopy (IR) is also an analysis tool used by many organic chemists. Since IR spectra from organic compounds are normally very complex, the direct technique is of little interest for the analysis of coal liquids. In order to improve the performance of the technique, the signal from the apparatus is treated by means of a fourier transform, which is normally integrated in the equipment. This fourier transformed infrared spectroscopy (FTIR) is a very powerful tool in the analysis of coal liquids. Just as in the case of ^{1}H-NMR and ^{13}C-NMR, the technique provides information about the structure of all molecules in the sample [57].

Another problem in dealing with very complex mixtures is the determination of the molecular weight (MW). As in the case with polymers, it is impossible to give an exact molecular weight. For many applications, a MW value which characterises the liquid is more valuable. The MW can be determined by vapour pressure osmometry (VPO). The osmotic pressure is a function of the number of molecules in a solution, and via the numerical concentration the average molecular weight may be calculated. The theory has been outlined by Chung et.al. [58]. Just as in the case of poly-

mers, the molecular weight can be calculated as number average or weight average [59].

3. VAPOUR PRESSURE OF COAL CHEMICALS

3.1 Experimental data

For a wide range of substances relevant to coal liquefaction, vapour pressure data exist. The quality of data is very different, ranging from pure experimental data to the reporting of coefficients of one of the vapour pressure equations discussed in this chapter. For modelling work, the availability of consistent experimental data is a must. The quality of data is mainly determined by the experimental equipment used, and possibly methods for data processing afterwards. Data processing is a useful tool for finding gross errors or suspicious data points, as the results of the measurement of the vapour pressure as a function of temperature can be evaluated by means of empirical models.

However, the use of the coefficients of a vapour pressure equation is not recommended for the assessment of the capabilities of a model. The use of a model may introduce a bias, which influences the results of the evaluation of the performance of the model of interest. When it comes to modelling, such a bias is unacceptable.

Data from a single source may also be biased. There are two options to deal with this bias due to measurement. Firstly, one may use a suitable standard for the calibration of the equipment. The calibration procedure may lead to adjusting the equipment in order to perform the measurement with less bias. Otherwise, one could correct for this bias. In the measurements presented in this work, always the first possibility was used. A second solution to the problem of bias due to measurement is to use data from different sources. For some substances, this could be done, but for the majority of substances of interest only one data set was found in literature.

An extensive review of experimental data on "coal chemicals" by Chao [60] gives an indication on developments in the measurement of vapour pressures of these substances. For most monocyclic aromatics (derivates of benzene), sufficient data were available for modelling work. For substituted naphthalenes, data were scare, except for naphthalene itself. For 1- and 2-methylnaphthalene, 1- and 2-naphthol data existed already. For modelling coal fluids, it is not sufficient to look only at benzene derivates. From literature data on coal liquids and coal liquid modelling, as well as from the results from PAH[1]- and GC/MS[2]-analysis of the coal oils used in this study, it is clear that polycyclic aromatic hydrocarbons have a great influence on the physical and chemical properties of coal oils. Therefore, the experimental programme on pure substances aimed to extend the data on substituted naphthalenes. Naphthalene was used as reference. The experimental results obtained are the subject of chapter 5.

[1] PAH = polycyclic aromatic hydrocarbons
[2] GC/MS = gas chromatography/mass spectrometry

3.2 Database development

A database system was developed in order to maintain reported data and to support calculation applications. The database system developed is a simplified prototype, that can be further developed into a full-blown database management system that provides a user-friendly interface and extensive capabilities of exportation and plotting of data. This second step however was beyond the scope of the work. The database system should at least be able to keep key properties of the substances of interest, but also maintaining key results of calculations.

When developing a database system, it is aimed to store a minimum amount of data. Any result, that follows directly from other data already stored is usually left out. This would also apply to the coefficients of models applied in this study. It has been decided to store temporary results as well, as they may be of interest when performing further calculations. It is no use to recalculate the coefficients of a vapour pressure equation (see sections 3.4 and 3.5 of this chapter) every time these coefficients are needed for interpolation purposes. Vapour pressure equations provide a convenient way for modelling the relationship between the vapour pressure at saturation of a fluid and the temperature. After the model parameters have been computed and the goodness-of-fit has been verified, these coefficients can be used to calculate the vapour pressure at a temperature not given in the data sets available from literature or experiment.

In the design of the database system, the properties of a pure substance at its critical point are of special interest. The critical point plays a key role in correlating the parameters of an equation of state to the properties of the fluid. These correlations are subject of chapter 4. The properties at the critical point can be measured, but they can also be estimated. For many coal chemicals, it is unlikely that the substance will not decompose before the critical point has been reached. For many benzene derivates, experimental values for critical pressure, volume, and temperature exist, as well as for some naphthalene derivates. In absence of experimental data, an estimation method, such as the method of Joback-Lydersen [61] or the method of the Texas Research Centre [62] has to be applied. The application of these methods will be discussed in more detail, when modelling pure coal chemicals with the use of equations of state.

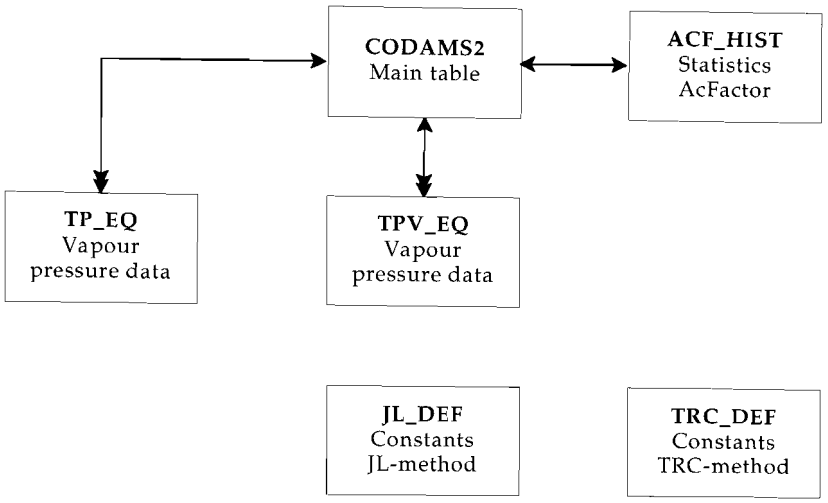

Figure 3.2-1 : Database structure

The database structure of the thermodynamic database CoDaMS II is given in figure 3.2-1. The main table is linked to a table holding statistics from calculations of vapour pressure correlations (ACF_HIST) in a 1:1-relationship, and to two tables containing vapour pressure data (TP_EQ and TPV_EQ) in 1:n-relationships. TP_EQ contains only temperature, pressure, and substance code, whereas the table TPV_EQ contains several other properties of the coexisting phases, such as densities, energy, enthalpy, etc..

The tables JL_DEF and TRC_DEF hold the data for the estimation methods of Joback and Lydersen [61] and that of the Texas Research Centre [62] respectively. They have no direct link to the main table.

The main table of the database system has been designed in such a way, that all key properties can be stored. These key properties are

- substance code (primary key)
- name, molecular formula, Chemical Abstracts Sequence number (CAS)
- melting temperature, boiling temperature, triple point temperature
- critical point properties: pressure, volume, temperature, compressibility factor
- coefficients of vapour pressure equations
- coefficients of equations of state

At the beginning of the study, it could not be foreseen whether the coefficients of the equation of state could be computed from other data (critical pressure, critical temperature, and acentric factor for instance) that were already stored, or that these coefficients would be the result of an optimisation procedure. In the latter case, it was required to reserve fields in the database for storing these properties.

Apart from the main table, several other tables were defined, that keep vapour pressure data. These tables are linked to the main table by means of the relational database model. In appendix C, the specifications of the database system are given.

The software framework is visualised in figure 3.2-2.

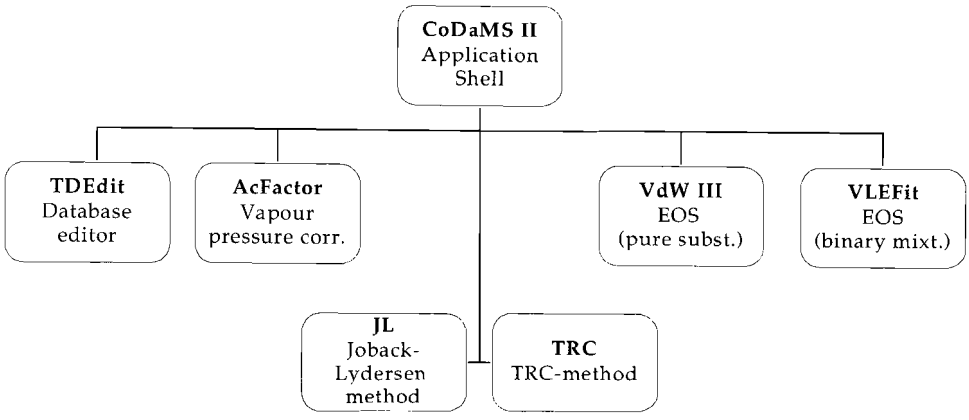

Figure 3.2-2 : Application framework

The applications JL and TRC implement estimation methods for the properties of pure fluids at the critical point. VdW III and VLEFit implement calculations with equations of state for pure substances and binary mixtures respectively. CoDaMS II is the application shell.

The vapour pressure equations have been implemented in AcFactor and are discussed in the remainder of this chapter. TDEdit is the database editor, used for manual alterations in the database.

3.3 General aspects of modelling vapour pressure data

In the modelling and prediction of the thermodynamic properties of pure fluids, the relationship between the saturated vapour pressure and the temperature plays a key role. These vapour pressure data can be correlated either (1) with empirical equations as discussed in this chapter or (2) by means of equations of state as discussed in the next chapters. The objective of the two types of models is different.

Empirical vapour pressure equations aim to give a description of the saturated vapour pressure as a function of the temperature for fluid phase equilibrium only, whereas equations of state aim to present the relationship between pressure, temperature, and volume in general. The accuracy in representing the saturation line differs considerably between the two types of models. Most vapour pressure equations are very well capable in representing the saturation line at a level well below the experimental uncertainty.

The basis for the modelling of the saturation line follows from corresponding states theory and the Clausius-Clapeyron equation [63]. This equation follows from the

conditions for vapour-liquid equilibrium that the pressure, temperature, and chemical potential in both phases are equal. It reads as

$$\frac{dP^{sat}}{dT} = \frac{\Delta H_v}{T\Delta V_v} \qquad 3.3\text{-}1$$

where P is the vapour pressure, T is the absolute temperature, ΔH_v is the latent heat of vaporisation, ΔV_v is the difference in (molar) volumes of the vapour and the liquid phases at vaporisation. It can also be expressed as

$$\frac{dP^{sat}}{dT} = \frac{\Delta H_v}{\left(RT^2/P\right)\Delta Z_v} \qquad 3.3\text{-}2$$

where ΔZ_v is the difference in compressibility factors of the vapour and the liquid phase. This equation can be rearranged to

$$\frac{d\ln P^{sat}}{d\left(1/T\right)} = -\frac{\Delta H_v}{R\Delta Z_v} \qquad 3.3\text{-}3$$

Most vapour pressure equations stem from the integration of equation 3.3-3. Before doing this, an assumption has to be made about the behaviour of the quotient $\Delta H_v/\Delta Z_v$ as a function of the temperature. The simplest approach is to assume this quotient to be constant, leading to the equation

$$\ln P^{sat} = A - \frac{B}{T} \qquad 3.3\text{-}4$$

which provides a reasonable approximation over small temperature ranges. The coefficient B is directly related to the quotient $\Delta H_v/\Delta Z_v$, in fact B equals $\Delta H_v/R\Delta Z_v$.

Over longer temperature ranges, the performance of equation 3.3-4 is poor. Antoine proposed a simple correction to this equation, resulting in

$$\ln P^{sat} = A - \frac{B}{T+C} \qquad 3.3\text{-}5$$

This equation is widely used for correlating vapour pressure data. The only way to obtain the coefficients is to use regression techniques. The Antoine equation has one disadvantage: it is unreliable in extrapolating to higher temperatures. As sometimes experimental data may be not available at the temperature desired, this failure makes it difficult to apply the Antoine for estimation outside the temperature range where data are available.

Several more complex vapour pressure equations have been tested in their capacity of representing the saturation line in an accurate way, in order to have a reliable method of interpolating and limited extrapolating of vapour pressure data. As these equations are to a high degree empirical, any extrapolation should be dealt with with great care.

The models tested are divided into two groups, where the first group of equations require the saturation pressure as a function of the temperature only, whereas the second group requires some kind of reference point too. For two equations, the coefficients for many fluids relevant to this study are presented at the end of the chapter.

In chapter 5, where experiments on naphthalenic coal chemicals discussed, the set of coefficients is expanded.

3.4 Vapres-2 and related equations

In a preceding study, the "European Coal Database II" project, the Vapres-2 equation was used to represent the saturation curve of heavy aromatic substances [64].The Vapres-2 equation reads as follows

$$\ln P^{sat} = A + \frac{B}{T} + CT + DT^2 + E \ln T \qquad 3.4\text{-}1$$

The equation has 5 coefficients and is linear in its coefficients. The relative high number of coefficients allow to represent the saturation line in a very accurate way. Especially for aromatic substances, it is to be expected that this equation provides better estimates than more simple models do.

As stated in the preface, the work started with studying the experiments and theory of Van Laar. In his work, he proposed a very simple equation to describe the saturation line. The Van Laar equation reads as [3]

$$\ln P^{sat} = A + \frac{B}{T} + CT + D \ln T \qquad 3.4\text{-}2$$

Apart from the T^2-term, this equation is identical to the Vapres-2 equation.

The Riedel equation is of the same type as the Van Laar equation. The only difference is the T^6-term instead of the T-term [65]

$$\ln P = A + \frac{B}{T} + CT^6 + D \ln T \qquad 3.4\text{-}3$$

This equation has also been part of the study, in order to see whether the T^6-term contributes to a better representation of the saturation line. Another equation of the same type as the previous one is the Miller equation [65]

$$\ln P = A + \frac{B}{T} + CT + DT^2 \qquad 3.4\text{-}4$$

that differs from the Vapres-2 equation by missing the ln T-term.

For the calculation of thermodynamical properties from experimental data, a vapour pressure equation after Clarke and Glew has been implemented. The model reads as [66]

$$\ln P^{sat} = A + \frac{B}{T} + C \ln T \qquad 3.4\text{-}5$$

or alternatively

$$R \ln \frac{P}{Pa} = \frac{-\Delta G^\circ(\Theta)}{\Theta} + \Delta H^\circ(\Theta)\left(\frac{1}{\Theta} - \frac{1}{T}\right) + \Delta C_P^\circ \left\{\left(\frac{\Theta}{T}\right) - 1 + \ln\left(\frac{T}{\Theta}\right)\right\} \qquad 3.4\text{-}6$$

where R is the ideal gas constant and Θ is a reference temperature. The coefficients A, B, and C are related to the thermodynamic properties as follows

$$A = \frac{1}{R}\left(-\frac{\Delta G^0(\Theta)}{\Theta} + \frac{\Delta H^0(\Theta)}{\Theta} - \Delta C_p^0 \ln\Theta - \Delta C_p^0\right)$$

$$B = \frac{1}{R}\left(-\Delta H^0(\Theta) + \Theta\Delta C_p^0\right) \qquad 3.4\text{-}7$$

$$C = \frac{\Delta C_p^0}{R}$$

where $\Delta G^0(\Theta)$ and $\Delta H^0(\Theta)$ are the Gibbs free energy and enthalpy differences between the vapour and the liquid phases at a given temperature Θ. ΔC_P^0 is the difference in heat capacity between the two phases.

The coefficients of the equations are obtained by either general linear least squares (GLS) or by GLS followed by fitting the relationship P versus T with the Marquardt-Levenberg algorithm [67]. As Θ is a temperature that can be selected, the calculation of the properties $\Delta G^0(\Theta)$, $\Delta H^0(\Theta)$, and ΔC_P^0 follows directly from the equations 3.4-7, starting with coefficient *C*.

3.5 Equations requiring a reference point

The introduction of a reference point that is specific to the substance leads to a reduction in the differences of saturation curves, if the data are related to this reference. The vapour pressure equations presented in this section use such a reference point. Most commonly, the critical point is selected as reference point, as the critical properties play an important role in modelling vapour-liquid equilibria. The significance of the critical point for this kind of modelling follows from the fact that at the critical point, the differences between the vapour and the liquid phases vanish.

The equations presented in this section use $\ln P/P_{cr}$ as dependent variable, and T/T_{cr} as independent value. The Cox equation uses an arbitrary reference point for the relationship between T and P [68]

$$\ln\frac{P}{P_{ref}} = \left\{1 - \frac{T_{ref}}{T}\right\}\exp\left[A + BT + CT^2\right] \qquad 3.5\text{-}1$$

When both sides are divided by the pre-exponential factor, a second logarithm can be taken on both sides to provide the linear relationship between an expression of P and the coefficients

$$\ln\left\{\frac{\ln\left\{\frac{P}{P_{ref}}\right\}}{1 - \frac{T_{ref}}{T}}\right\} = A + BT + CT^2 \qquad 3.5\text{-}2$$

The reference point may be the critical point, but any other selection of (T_{ref}, P_{ref}) would be valid too.

Wagner has selected a different approach for accurate modelling of vapour pressure data. He has developed a method for calculating the best vapour pressure equation for a given compound. For most compounds, four terms with exponents ranging

from 1 to 6 will perform well. The Wagner equation reads (P_{cr} and T_{cr} are the pressure and the temperature at the critical point) [65,69]

$$\ln\frac{P}{P_{cr}} = \frac{T_{cr}}{T}\left\{A\left[1-\frac{T}{T_{cr}}\right] + B\left[1-\frac{T}{T_{cr}}\right]^{1.5} + C\left[1-\frac{T}{T_{cr}}\right]^{3.0} + D\left[1-\frac{T}{T_{cr}}\right]^{6.0}\right\} \qquad 3.5\text{-}3$$

There are however, two other equations with other exponents, which are the best suitable for methane and propene respectively. The Wagner equation for methane reads [65,69]

$$\ln\frac{P}{P_{cr}} = \frac{T_{cr}}{T}\left\{A\left[1-\frac{T}{T_{cr}}\right] + B\left[1-\frac{T}{T_{cr}}\right]^{1.5} + C\left[1-\frac{T}{T_{cr}}\right]^{2.5} + D\left[1-\frac{T}{T_{cr}}\right]^{5.0}\right\} \qquad 3.5\text{-}4$$

and the Wagner equation for propene reads [65]

$$\ln\frac{P}{P_{cr}} = \frac{T_{cr}}{T}\left\{A\left[1-\frac{T}{T_{cr}}\right] + B\left[1-\frac{T}{T_{cr}}\right]^{1.5} + C\left[1-\frac{T}{T_{cr}}\right]^{4.0} + D\left[1-\frac{T}{T_{cr}}\right]^{4.5}\right\} \qquad 3.5\text{-}5$$

Wagner has proposed a method for estimating the exponents in these equations. This method is not of great importance in this study, as the first form of it provides good results for virtually all substances of interest.

3.6 Calculation of the acentric factor

The acentric factor (ω) appears in several empirical expressions for coefficients of equations of state. It is a measure for the difference between the actual shape of the molecule of a substance and that of a spherical molecule. For molecules that are (almost) spherical, such as argon or methane, the value of the acentric factor is close to 0. For a spherical molecule, its value is exactly 0. For many simple organic compounds, literature values of ω are known. Unfortunately, for more complex and for aromatic hydrocarbons, these values are less often found in the literature. Therefore, a program has been written to calculate the acentric factor, using the vapour pressure as a function of the temperature and the critical point values of T and P. The acentric factor can be calculated from the saturated vapour pressure at a reduced temperature of 0.700.

The relationship between the acentric factor (ω) and the reduced saturated vapour pressure at T_r=0.700 is as follows [71]

$$\omega = -\log P_r(T_r = 0.700) - 1.000 \qquad 3.6\text{-}1$$

where P_r is the reduced vapour pressure (P/P_{cr}). The calculation of ω requires the vapour pressure at T_r=0.700. Since this value has been measured is only a few cases, the vapour pressure at this temperature should be calculated by interpolation of VLE data. This calculation is quite straightforward, although some precautions should be taken, especially when pure empirical data are used.

Experimental data have one great advantage: one is absolutely sure that no error is introduced by smoothing the values of the measurement using some correlation formula. The disadvantage of the use of this kind of data is that the data might contain serious errors due to experimental circumstances. If such an error happens to be

in the direct neighbourhood of T_r=0.700, the value of ω may be very unreliable. Therefore, another method has been chosen to calculate the vapour pressure at that point. The points around the temperature $0.7T_{cr}$ are correlated by an empirical equation and subsequently the value of P at T_r=0.700 may be calculated. This method is far more safe than direct interpolations, since a part of the random error of measurement may be eliminated by the correlation.

In this work, the Wagner-1 equation was used for the computation of acentric factors in absence of experimental data. In a recent paper [73], Twu et.al. demonstrate the capabilities of this vapour pressure equation in calculating the acentric factor. There is a good agreement between calculated and experimental acentric factors.

4. INTRODUCTION TO EQUATIONS OF STATE

4.1 Thermodynamic framework

The modelling of the pressure-temperature-volume behaviour of fluids plays a key role in engineering calculations. Thermodynamics provides many conditions that are to be satisfied by an equation of state. Many conditions follow from well known relationships between internal energy (U), enthalpy (H), entropy (S), free energy (A), and free enthalpy (G) on one hand, and the pressure (P), volume (V), and temperature (T) on the other.

In this section, the relationship between the thermodynamic functions U, H, S, A, and G and the variables of an equation of state (P, V, and T) are given. An equation of state can be either pressure-explicit [74]

$$P = f(T,V) \qquad 4.1\text{-}1$$

or volume-explicit

$$V = f(P,T) \qquad 4.1\text{-}2$$

Many equations of state are pressure-explicit, as in that form it is possible to describe co-existing phases with a single formula. The simplest form capable of describing two phases by means of a pressure-explicit equation of state is an equation that is cubic in volume.

In addition to thermodynamic conditions, there is a second type of conditions that are to be satisfied. These conditions follow from extreme states for a fluid: a compressed liquid ($P \rightarrow \infty$), or a gas or vapour at infinite dilution ($P \rightarrow 0$). From a theoretical point of view, the "correctness" of a model is not only determined by meeting the requirements as stated by the laws of thermodynamics, but also by how an equation of state behaves in extreme cases. Another boundary condition is the critical point, where the difference between the liquid and vapour phases vanishes. The critical point conditions can be expressed as [75]

$$\left(\frac{\partial P}{\partial V}\right)_{T=T_c} = 0 \qquad 4.1\text{-}3$$

and

$$\left(\frac{\partial^2 P}{\partial V^2}\right)_{T=T_c} = 0 \qquad 4.1\text{-}4$$

These conditions play a key role in the development of relationships between the coefficients of an equation of state and the critical point values of P, V, and T for a given substance.

The derivation of the relationships between the thermodynamic functions and an equation of state can be carried out in several ways. Prausnitz [74] gives the relationships following from the derivation of Beattie [75,76]. At constant temperature and composition, one of Maxwell's relations can be used to give the effect of volume on energy and entropy

$$dU = \left[T\left(\frac{\partial P}{\partial T}\right)_{V,n_T} - P \right] dV \qquad 4.1\text{-}5$$

$$dS = \left(\frac{\partial P}{\partial T}\right)_{V,n_T} dV. \qquad 4.1\text{-}6$$

These two equations form the basis of the derivation for the desired equations. First, expressions are found for the energy and entropy. The other properties are then calculated from their definitions. By definition, the following relationships exist between the thermodynamic functions

$$H = U + PV \qquad 4.1\text{-}7$$

$$A = U - TS \qquad 4.1\text{-}8$$

$$G = U + PV - TS \qquad 4.1\text{-}9$$

$$\mu_i = \left(\frac{\partial A}{\partial n_i}\right)_{T,V,n_j} \qquad 4.1\text{-}10$$

$$RT \ln \frac{f_i}{f_i^0} = \mu_i - \mu_i^0. \qquad 4.1\text{-}11$$

where μ_i is the chemical potential of component i. f_i is the fugacity of component i, whereas f^0 is the fugacity at a reference state. With use of these definitions, the thermodynamic functions can be expressed in terms of P, V, T, and several constants.

$$U = \int_V^\infty \left[P - T\left(\frac{\partial P}{\partial T}\right)_{V,n_T} \right] dV + \sum_i n_i u_i^0 \qquad 4.1\text{-}12$$

$$H = \int_V^\infty \left[P - T\left(\frac{\partial P}{\partial T}\right)_{V,n_T} \right] dV + PV + \sum_i n_i u_i^0 \qquad 4.1\text{-}13$$

$$S = \int_V^\infty \left[\frac{n_T R}{V} - \left(\frac{\partial P}{\partial T}\right)_{V,n_T} \right] dV + R\sum_i n_i \ln \frac{V}{n_i RT} + \sum_i n_i s_i^0 \qquad 4.1\text{-}14$$

$$A = \int_V^\infty \left[P - \frac{n_T RT}{V} \right] dV - RT\sum_i n_i \ln \frac{V}{n_i RT} + \sum_i n_i \left(u_i^0 - Ts_i^0\right) \qquad 4.1\text{-}15$$

$$G = \int_V^\infty \left[P - \frac{n_T RT}{V} \right] dV - RT\sum_i n_i \ln \frac{V}{n_i RT} + PV + \sum_i n_i \left(u_i^0 - Ts_i^0\right) \qquad 4.1\text{-}16$$

$$\mu_i = \int_V^\infty \left[\left(\frac{\partial P}{\partial n_i} \right)_{T,V,n_j} - \frac{RT}{V} \right] dV - RT \ln \frac{V}{n_i RT} + RT + u_i^0 - Ts_i^0 \qquad 4.1\text{-}17$$

and finally,

$$RT \ln \varphi_i = RT \ln \frac{f_i}{y_i P} = \int_V^\infty \left[\left(\frac{\partial P}{\partial n_i} \right)_{T,V,n_j} - \frac{RT}{V} \right] dV - RT \ln z \qquad 4.1\text{-}18$$

where

$$Z = \frac{PV}{RT} \qquad 4.1\text{-}19$$

is the compressibility factor of the mixture. For a pure component equation 4.1-18 becomes

$$RT \ln \left(\frac{f}{P} \right)_{\text{pure } i} = \int_V^\infty \left[\frac{P}{n_i} - \frac{RT}{V} \right] dV - RT \ln z + RT(z - 1) \qquad 4.1\text{-}20$$

The symbols in the equations given here have the following meaning

h_i^0 = molar enthalpy of pure i as an ideal gas at temperature T

s_i^o = molar entropy of pure i as an ideal gas at temperature T and 1 bar

$\mu_i^0 = h_i^0 - Ts_i^0$, and f_i^0 = 1 bar

n_i = number of moles of i

n_T = total numbers of moles

y_i = mole fraction of $i = n_i / n_T$

The difference between capitals and lower case symbols for the properties V, U, H, S, A, and G should be noted. All extensive properties denoted by capital letters (V, U, H, S, A, and G) represent the total property for n_T moles and therefore are *not* on a molar basis. Extensive properties on a molar basis are denoted by lowercase letters (v, u, h, s, a, and g). In equations (4.1-11) to (4.1-14), the pressure P is in bar (1 bar = 10^5 Pa).

A similar set of equations can be derived for a volume-explicit equation of state [74].

4.2 Equations of state of the Van der Waals type

The first equation of state ever developed is the ideal gas law, that goes back to the laws of Boyle and Gay-Lussac. The ideal gas law reads as follows

$$P = \frac{nRT}{V} \qquad 4.2\text{-}1$$

where the symbols have their usual meanings. The ideal gas law can also be represented by stating Z = 1, see equation 4.1-17.

It was Van der Waals [77] who developed in 1873 the first equation of state capable of representing both the liquid and vapour phase of a fluid simultaneously. Van der Waals' equation of state reads as follows

$$P = \frac{RT}{V-b} - \frac{a}{V^2} \qquad 4.2\text{-}2$$

where a and b are the coefficients of the equation of state. These coefficients are specific for every substance.

The first part on the right-hand side of equation 4.2-2 represents the repulsive forces in the fluid. The "Van der Waals type" equations of state have this term in common, that is

$$Z_{rep} = \frac{V}{V-b} \qquad 4.2\text{-}3$$

Van der Waals reported in his thesis, that the coefficient b should not be a constant, but a function of temperature and volume in order to represent wider ranges of liquid and vapour volumes. However, in the literature equation 4.2-2 is cited as Van der Waals' equation of state, with constant a and b. If a and b are taken as constants, then they take up at any temperature the values at the critical point (denoted as a_c and b_c respectively). The expressions for the coefficients of Van der Waals' equation of state at the critical point read as follows

$$b_c = \frac{RT_c}{8P_c}$$
$$a_c = \frac{27}{64}\frac{R^2T_c^2}{P_c} \qquad 4.2\text{-}4$$

Both Van der Waals as well one of his co-workers, Van Laar have attempted to improve the capabilities of equation 4.2-2. In section 4.3 of this chapter, a short summary of the work of Van Laar [3] (1924) is given, as it is provides an experimental basis for the Cubic Chain-of-Rotators equation of state, which is the simplest of the two models covered in this study.

Several modifications have been proposed in order to improve the capabilities of Van der Waals equation of state. The first major contribution is made by Redlich and Kwong (1949) [78], who proposed the following equation

$$P = \frac{RT}{V-b} - \frac{a(T)}{V(V+b)} \qquad 4.2\text{-}5$$

where b is still a constant, but a is a function of the temperature. Equation 4.2-5 is known as the Redlich-Kwong equation of state. The equation of state uses a repulsive term very similar to that of Van der Waals (only the value of b differs, as will be shown shortly), and an empirical correction to account for attractive forces. The expressions for a and b read as

$$b = 0.08664\frac{RT_c}{P_c}$$

$$a(T) = \frac{0.42748R^2T_c^2}{P_c}\sqrt{\frac{T_c}{T}} \qquad 4.2\text{-}6$$

From equation 4.2-6, it follows that a is proportional to $T^{-½}$. The Redlich-Kwong equation of state represents vapour-liquid equilibrium properties of fluids considerably better than Van der Waals' equation does. However, the representation of PVT-behaviour of fluids not in an equilibrium state is only slightly improved.

A modification to the equation of Redlich and Kwong was made by introducing Pitzer's acentric factor (see chapter 3) in the representation of the temperature dependency of a. The expression for a(T) for the Soave-Redlich-Kwong equation of state (SRK) reads as follows [79]

$$a(T) = \frac{0.42748R^2T_{cr}^2}{P_{cr}}\left[1 + f(\omega)\left(1 - \sqrt{T_R}\right)\right]^2 \qquad 4.2\text{-}7$$

where

$$f(\omega) = 0.48 + 1.574\omega - 0.176\omega^2 \qquad 4.2\text{-}8$$

ω is the acentric factor, as defined by Pitzer [71]. Graboski and Daubert [80] have made a further modification on Soave's temperature function. Instead of 4.2-8, they use the formula

$$f(\omega) = 0.48508 + 1.55171\omega - 0.15613\omega^2 \qquad 4.2\text{-}9$$

that is based on a larger set of substances. Again, this improvement has an empirical basis.

In 1979, Soave published an alternative to equation 4.2-7 [81]. The new temperature function reads as follows

$$a(T) = \frac{0.42748R^2T_{cr}^2}{P_{cr}}\left[1 + \left(1 - T_R\right)\left(m + \frac{n}{T_R}\right)\right] \qquad 4.2\text{-}10$$

where m and n are substance-specific constants.

Another modification to the Van der Waals equation of state has been proposed by Peng and Robinson. Their equation of state reads as [82]

$$P = \frac{RT}{V - b} - \frac{a(T)}{V^2 + 2Vb - b^2} \qquad 4.2\text{-}11$$

The major difference with the SRK is the attractive term. The expressions for a (a function of the temperature) and b (constant) for the Peng-Robinson equation of state (PR) read as

$$a = \frac{0.45724R^2T_c^2}{P_c}\left[1 + f(\omega)\sqrt{1 - T_r}\right]^2$$

$$b = 0.07780\frac{RT_c}{P_c} \qquad 4.2\text{-}12$$

where

$$f(\omega) = 0.37464 + 1.54226\omega - 0.26993\omega^2 \qquad 4.2\text{-}13$$

The PR is a further improvement over the SRK and RK. It provides a better description of the liquid phase, and it is better capable of handling non-associating polar liquids.

In addition to these very well known modifications, numerous others have been proposed on the Van der Waals equation of state. Many of them are very well capable in accounting for vapour and gas phase imperfections, and are also capable in representing the thermodynamic properties of fluids at vapour-liquid equilibrium.

4.3 Van Laar's work revisited

In the project "Thermodynamic properties of coal liquids" (ECSC 7220/EC-602), Van Laar's work has been investigated. Van Laar was a Dutch Physicist who has published numerous contributions to thermodynamics and physical chemistry. He also published 1924 a book entitled "Die Zustandsgleichung von Gasen und Flüssigkeiten" [3], that contains a recollection of his articles in the Proceedings of the Dutch Royal Academy of Sciences. This work may be regarded as one of the first attempts to improve the work of Van der Waals. As explained in section 4.1, Van der Waals introduced the first equation of state capable of dealing with more than a single fluid state.

Van Laar recognised the significance of Van der Waals' work, but he disagreed about the constants a and b in the Van der Waals equation of state. It is interesting to see how the experimental results of Van Laar compare to the Cubic Chain-of Rotators equation of state (section 4.5). Before making this comparison, the work of Van Laar will be summarised. A more extensive presentation of this work is given in the final report of the above mentioned project [7].

Van Laar states that Van der Waals' equation of state is valid, if it is accepted that both a and b are functions of temperature and volume, in other words

$$a = a_{cr} f(T,V) \qquad 4.3\text{-}1$$

and

$$b = b_{cr} g(T,V) \qquad 4.3\text{-}2$$

Van Laar starts his theory with stating that

$$\left(b_g\right)_{cr} = \varphi_1 b_{cr} \qquad 4.3\text{-}3$$

$$\left(a_g\right)_{cr} = \varphi_2 a_{cr} \qquad 4.3\text{-}4$$

where the subscript "g" denotes for very large volumes ($V \to \infty$). Furthermore, according to Van Laar, $\varphi_1 > 1$, $\varphi_2 > 1$, and $\varphi > 1$ where

$$\varphi = \frac{\varphi_1}{\varphi_2} \qquad 4.3\text{-}5$$

This would mean that the volume dependency of b is greater than that of a. For gases at low to moderate pressures, the volume dependencies of a and b appear to be about equal. This kind of inconsistencies in observations is typical for the approach of that time. At the beginning of this century, data were scarce, and usually data were only available over limited ranges of temperature, pressure, and/or density (volume). The work of Van Laar and others from that time shows a good compromise between empirical observations and theory building.

In the time of Van Laar, thermodynamic calculations were in many cases tedious, so in his derivation of the volume functions for a and b, he proceeds by first assuming that the volume dependency of a may be neglected in the VLE-area. To a certain extent, this assumption can be made, as in the VLE-area the volume dependency of b is far more important than that of a.

For the derivation of the volume dependency of b, Van Laar uses the *empirical fact* that the mean of the reduced densities of the coexisting phases at VLE can be approximated very well by a straight line. The relationship reads as follows

$$\frac{1}{2}\left\{\rho_{liq}+\rho_{gas}\right\}-1=\gamma'\left\{T_{cr}-T\right\} \qquad 4.3\text{-}6$$

In reduced form, the relationship reads

$$\frac{1}{2}\left\{\rho_{r,liq}+\rho_{r,gas}\right\}-1=\gamma\left\{1-T_{r}\right\} \qquad 4.3\text{-}7$$

where

$$\gamma'=\gamma\frac{\rho_{cr}}{T_{cr}} \qquad 4.3\text{-}8$$

If a and b were independent of the volume, then γ would be exactly ½. However, in practice the line of equation 4.3-7 shows always some curvature. This can be brought into account by introducing a factor V_{liq}:b_{liq}, where the latter expresses the value of b at the volume V_{liq}.

$$\frac{1}{2}\left\{\rho_{0}-\rho_{liq}\right\}=\gamma'T\bullet\frac{V_{liq}}{b_{liq}} \qquad 4.3\text{-}9$$

Recalling, b is a function of the volume, so for the vapour and the liquid, two values of b exist. One of the best features of Van der Waals' equation of state was the capacity of representing two phases in equilibrium with a single mathematical expression. In order to maintain this capacity, the volume dependency of b should be expressed as a function of the volume with several constants. The derivation of this volume function is given below.

In equation 4.3-9, ρ_0 is the extrapolated liquid density at 0 Kelvin. In this equation, γ' is the slope of the line at 0 Kelvin, which may differ from the mean slope of equation 4.3-7. At low temperatures, the pressure is much smaller than the attractive part of the Van der Waals equation of state ($P << a/V^2$), so that the equation of state of Van der Waals can be simplified to

$$V_{liq} - b_{liq} = RT\frac{V^2_{liq}}{a_{liq}} \qquad 4.3\text{-}10$$

In equation 4.3-9, ρ can be substituted by 1/V. After this substitution and combination with equation 4.3-10, the following expression is obtained

$$\frac{V_{liq} - b_{liq}}{V_{liq} - V_0} = \frac{R}{2\gamma' a_{liq}}\frac{b_{liq}}{V_0} \qquad 4.3\text{-}11$$

This equation is the key equation in Van Laar's derivation of the volume function for *b*. If it is assumed that at 0 K, V_0 equals b_0, then the following equation can be obtained

$$\frac{V - b}{V - b_0} = \beta\frac{b}{b_0} \qquad 4.3\text{-}12$$

where

$$\beta = \frac{R}{2\gamma' a} \qquad 4.3\text{-}13$$

The subscripts "liq" have been removed in equation 4.3-12. Since g' is the reduced slope of the line of mean densities, equation 4.3-13 can be expressed as

$$\beta = \frac{RT_{cr}V_{cr}}{2\gamma a} \qquad 4.3\text{-}14$$

which becomes invalid if *a* is a volume function too[1].

For the critical point, the following equation can be derived

$$RT_{cr} = \frac{8}{27}\lambda\frac{a_{cr}}{b_{cr}} \qquad 4.3\text{-}15$$

where λ is a constant close to unity [3]. The derivation follows from the application of the conditions of the critical point (equations 4.1-3 and 4.1-4). As this derivation does not provide relevant information in this context, it has been left out here. It has been documented elsewhere [7].

Equation 4.3-14 can be written as

$$\frac{1}{\beta} = \frac{(\gamma_0 + 1)(8\gamma_0 - 1)}{4}\frac{\gamma}{\gamma_0}\frac{a}{a_{cr}} \qquad 4.3\text{-}16$$

where γ_0 is the reduced slope of the straight line represented by equation 4.3-7 extrapolated to T = 0 K. g is the actual value of the slope of this line, which is a weak function of the temperature. According to Van Laar, γ is always somewhat smaller than γ_0, which implies that if γ is replaced by γ_0, β is slightly underestimated.

The parameter *b* is now a function of *V* and β

[1] This problem is associated with the approach followed by Van Laar. However, with the resources available in that time, this approach is certainly useful and it leads to reasonable results, even when compared to the requirements of equations of state of today.

$$b = f(V,\beta) = f(V,T) \qquad 4.3\text{-}17$$

Since β depends on *a*, equation 4.3-12 describes both the temperature and volume dependency of *b*, as long as *a* is assumed to be temperature function only. It can be shown that equation 4.3-12 is not only valid along the liquid border of the VLE-area. In fact, the equation is valid for the entire liquid border and along isotherms, as long as *a* is not a function of the volume.

In addition to this observation, two more limiting cases should be taken into account. When deriving equation 4.3-12, an extrapolation was made when $T \rightarrow 0$ for liquids. The second limiting case is for T and P tending to ∞. In that case, b will approach a minimum value too (b_0'), which will differ in value from b_0.

Finally, the third limiting case is where V tends to ∞. In that case, *b* will have a maximum value, which can be obtained from equation 4.3-12. Introduction of this maximum value for *b*, symbolised by b_g, allows the elimination of β in equation 4.3-12. The expression for b reads as

$$1 = \beta \frac{b_g}{b_0} \qquad 4.3\text{-}18$$

and the volume function for *b* reads as

$$b = \frac{b_g}{1 + \dfrac{b_g - b_0'}{V}} \qquad 4.3\text{-}19$$

where b_0 is replaced by b_0'.[1] Substitution of this equation in Van der Waals' equation of state leads to

$$P = \frac{RT}{V}\frac{V + b_g - b_0}{V - b_0} - \frac{a}{V^2} \qquad 4.3\text{-}20$$

This equation of state differs considerably from that of Van der Waals, because equation 4.3-20 is far better in predicting liquid densities. The volume function of *b* is correct in a sense that the volume function provides still valid results for limiting cases.

However, there are some notes to be made. Firstly, the derivation is not valid if *a* is a function of the volume too, as certain equations become invalid. However, when moving along the liquid border, the effect of the volume dependency of *a* is small, as the change in V is small too. From the Cubic Chain-of-Rotators equation of state (see next section) it is known that for a good description of the VLE-area, the volume dependency of *a* may not be neglected at all. The reason that this derivation works is likely to be

1. the volume dependency of *b* is indeed of greater importance than that of coefficient *a* in Van der Waals equation of state

[1] As a consequence of this substitution, equation 4.3-19 becomes exact for the gas phase rather than for the liquid phase.

2. the derivation is carried out in a region where the volume function of b plays a dominant role in representing the fluid properties accurately, and then extrapolated to other regions of interest

A second objection against the volume function as given in equation 4.3-19 is that this equation is only correct if b_0 equals b_0'. Although the difference between b_0 and b_0' may not be too large, for real fluids it will be present. According to Van Laar, the ratio V_{cr}:b_0 would be about 3.8, whereas the ratio V_{cr}:b_0' would equal about 4.0.

The expression for β becomes now

$$\frac{b_g}{b_0'} = \frac{1}{\beta} \qquad 4.3\text{-}21$$

which is in agreement with equation 4.3-19.

Van Laar's formula for the volume dependency of a reads as

$$a = \frac{a_g}{1 + c/V} \qquad 4.3\text{-}22$$

where

$$c = \frac{a_g - a_0}{a_o} b_o' \qquad 4.3\text{-}23$$

The subscripts "g" and "0" have the same meaning as for the volume function of b. Equation 4.3-23 follows from the fact, that for $V = V_0 = b_0'$, a should equal a_0. Substitution of both volume functions into the equation of state of Van der Waals yields the following expression

$$P = \frac{RT}{V}\frac{V + b_g - b_0'}{V - b_0'} - \frac{a_g}{V(V + c)} \qquad 4.3\text{-}24$$

This equation of state resembles the Cubic Chain-of-Rotators equation of state (CCOR), that is subject of section 4.4. The only major difference is that the CCOR has an additional attractive term, which is a mathematical necessity [5]. Calculations with Van Laar's equation of state (equation 4.3-24) have verified this.

Van Laar developed, based on the critical point conditions a calculation procedure for the parameters involved [3]. This procedure will not be repeated here. The significance of the work of Van Laar is that in addition to the method used by the developers of the CCOR, there is an alternative pathway for obtaining this equation of state. Nowadays, it is recognised that the repulsive term of equation 4.3-24 is superior in predicting liquid densities in comparison to that of Van der Waals (equation 4.2-2).

4.4 Cubic chain-of-rotators equation of state

The Cubic Chain-of-Rotators equation of state [4-6] has been derived from the Chain-of-Rotators equation of state [83], that in turn is a further development of the hard spheres equation of state of Carnahan and Starling (CS) [84]. This equation of state describes the behaviour of an artificial fluid of hard spheres. The CS is superior

in predicting liquid densities of real fluids when compared to the Van der Waals equation of state. The reason for this is that the prediction of the density of hard spheres fluid remains correct up to the maximum density, i.e. the closest random packing of spheres.

However, in real fluids not only the repulsive forces are of interest, but also the attractive forces have an influence on the properties of a fluid. The concept of developing equations of state has moved from a highly (or entirely) empirical approach to an approach where a model for the repulsive forces is selected, and a perturbation term is being developed. This perturbation term, which may be regarded as a "disturbtion" of the force field created by repulsive forces, may be based on various approaches [85].

The Cubic Chain-of-Rotators equation of state (CCOR) has been derived from the Chain-of-Rotators equation of state by means of fitting the reference term of Carnahan and Starling, resulting in a simpler reference term. The equation of state is cubic in v and reads as

$$P = \frac{RT\left(1+0.77b/v\right)}{v-0.42b} + c^R \frac{0.055RTb/v}{v-0.42b} - \frac{a}{v(v+c)} - \frac{bd}{v(v+c)(v-0.42b)} \qquad 4.4\text{-}1$$

where a, b, c, and d are the coefficients of the equation of state. c^R is a coefficient related to the rotational degrees of freedom. The coefficients of this equation of state have been related to the critical temperature (T_{cr}), critical pressure (P_{cr}) and the acentric factor (ω). The prediction of the critical compressibility factor of the CCOR is a substance-specific constant. In principle, the experimental critical compressibility should be used, but in cases where this property is not known, it may be estimated by

$$Z_{cr} = 0.291 - 0.080\omega \qquad 4.4\text{-}2$$

where Z_{cr} is the critical compressibility.

The coefficients of the equation of state can be expressed as follows

$$a_c = \Omega_a \frac{R^2T_c^2}{P_c} \qquad 4.4\text{-}3$$

$$b_c = \Omega_b \frac{RT_c}{P_c} \qquad 4.4\text{-}4$$

$$c_c = \Omega_c \frac{RT_c}{P_c} \qquad 4.4\text{-}5$$

$$d_c = \Omega_d \frac{R^2T_c^2}{P_c} \qquad 4.4\text{-}6$$

where Ω_a, Ω_b, Ω_c, and Ω_d are substance-specific constants. These constants have been correlated to Z_{cr} and one another according to the scheme given below.

Ω_b depends on Z_{cr} only.

$$\Omega_b = 0.4756 - 3.396Z_{cr} + 8.236Z_{cr}^2 \qquad 4.4\text{-}7$$

Now Ω_c can be calculated, as it has been expressed in terms of Ω_b and Z_{cr}

$$\Omega_c = 0.42\Omega_b + 1.0 - 3.0Z_{cr} \qquad 4.4\text{-}8$$

The next coefficient to be computed is c^R; it is a function of the acentric factor (ω) only

$$c^R = 24.863\omega - 33.368\omega^2 + 57.266\omega^3 \qquad 4.4\text{-}9$$

for any $\omega>0$. If the acentric factor is negative, then c^R equals 0. Now Ω_a can be expressed as a function of Ω_b, Ω_c, and c^R

$$\Omega_a = 0.42\Omega_b\Omega_c + \Omega_c + (0.77 + 0.055c^R)\Omega_b + 3.0Z_{cr}^2 \qquad 4.4\text{-}10$$

and finally

$$\Omega_d = \frac{1}{\Omega_b}\left\{(0.77 + 0.055c^R)\Omega_b\Omega_c + 0.42\Omega_a\Omega_b - Z_{cr}^3\right\} \qquad 4.4\text{-}11$$

Both coefficients *a* and *c* are functions of the temperature. The respective temperature functions read as (for $T_R<1$)

$$\alpha = \left\{1.0 + a_1\left(T_R^{-0.25} - 1\right) - a_2\left(1 - T_R^2\right)\right\}^2 \qquad 4.4\text{-}12$$

and for $T_R>1$

$$\alpha = \exp\left[a_3\left(T_R - 1\right) - a_4\left(T_R^{0.5} - 1\right)\right]$$

for coefficient *a* and

$$\gamma = \exp\left[c_1\left(1 - T_R^{c_2}\right)\right] \qquad 4.4\text{-}13$$

for coefficient *c*. The constants a_1, a_2, a_3, a_4, c_1 and c_2 are substance specific. They have been correlated to the acentric factor (ω) as follows

$$a_1 = 2.66709 + 5.51328\omega - 2.65333\omega^2 \qquad 4.4\text{-}14$$

$$a_2 = 0.18471 + 0.38357\omega - 0.32706\omega^2 \qquad 4.4\text{-}15$$

$$a_3 = 0.38349 + 4.88359\omega + 14.2113\omega^2 \qquad 4.4\text{-}16$$

$$a_4 = 1.17543 + 14.3109\omega + 30.5032\omega^2 \qquad 4.4\text{-}17$$

$$c_1 = 7.04333 - 5.00422\omega + 1.88597\omega^2 \qquad 4.4\text{-}18$$

and

$$c_2 = 0.23177 + 0.16896\omega + 0.03179\omega^2 \qquad 4.4\text{-}19$$

For a given temperature *T*, the coefficients *a* and *c* of the Cubic Chain-of-Rotators equation of state are given by

$$a(T) = \alpha a_c \qquad 4.4\text{-}20$$

$$c(T) = \gamma c_c \qquad 4.4\text{-}21$$

For a pure fluid, the fugacity coefficient is given by

$$\ln\frac{f}{P}=\left[\frac{d}{0.42(c+0.42b)RT}-\frac{1.19+0.055c^{R}}{0.42}\right]\ln\frac{v-0.42b}{v}+\ldots$$
$$\ldots+\frac{a(c+0.42b)-bd}{c(c+0.42b)RT}\ln\frac{v}{v+c}+z-1.0-\ln z \qquad 4.4\text{-}22$$

In several publications [4-6,86-87], the CCOR has been tested, both when modelling pure fluids and when modelling mixtures. The model has been selected in this study in order to test the capabilities on heavy aromatic substances, and to find out whether the model is capable of handling coal oils and other ill-defined mixtures.

Before discussing a second candidate-model for modelling coal fluids, it should be noted that there is a close resemblance between the CCOR and the work of Van Laar. In the previous section, a summary of the work of Van Laar was given. It can be shown easily, that the repulsive terms developed by Van Laar and that of the CCOR have the same mathematical form, in fact

$$P_{rep}=\frac{RT}{V}\frac{V+b_1}{V-b_0} \qquad 4.4\text{-}23$$

It is also interesting to note, that this fact has not been observed by others. The attractive part of the equations of state differs in one term: the last term of equation 4.4-1. It has already been noted that this term is required in order to cover the complete VLE-area.

4.5 Algorithm for equilibrium calculations

For the calculation of the equilibrium properties of a pure substance at vapour-liquid equilibrium, many methods exist. Two principal routes have been used in this project. The first method is based on the fact, that at vapour-liquid equilibrium

$$P\Delta V=\int_{V_1}^{V_2}PdV \qquad 4.5\text{-}1$$

where

$$\Delta V=V_2-V_1 \qquad 4.5\text{-}2$$

V_2 is the molar volume of the vapour phase, V_1 is the molar volume of the liquid. Equation 6-2 is to be applied under the condition of constant temperature. So, the function P to be integrated may be regarded as a function of V only.

The equations of state, as represented by equation 4.5-1 can also be expressed as a polynomial in V. In the most simple case, this polynomial is of degree 3 and typically of the form

$$V^3+z_1V^2+z_2V+z_3=0 \qquad 4.5\text{-}3$$

With use of Laguerre's method [88] this polynomial can be solved. The coefficients z_i (i = 1, 2, 3) are functions of the coefficients of the equation of state, and the pressure and temperature.

In principle, with use of equations 4.5-3, 4.5-2, and 4.5-1 it is possible to calculate P, V_1, and V_2 at a given temperature T if the coefficients of the equation of state are known. Usually, these coefficients are of the form

$$a = f(T_{cr}, P_{cr}, \omega)\, g(T) \qquad 4.5\text{-}4$$

where the function $f(T_{cr}, P_{cr}, \omega)$ defines the value of a at the critical point (usually denoted as a_{cr}), and the function g(T) corrects the value of a for the temperature T. In the most simple case,

$$g(T) = 1 \qquad 4.5\text{-}5$$

for any value of T. Most equations of state have one or more temperature-dependent coefficients. The functions g_i for these coefficients a_i are usually expressed in terms of T_{cr}, T, and ω.

This algorithm has been used during the screening of equations of state suitable for modelling the thermodynamical properties of coal chemicals. Except for the equations of state shown in this chapter, several other ones have been verified as possible candidates. Therefore, the integral in equation 7.1-1 has been implemented as a numerical procedure using the algorithm of Romberg [89].

In a later stage, a quicker implementation became necessary in order to finalise the calculations. The results of these calculations are presented in chapter 6 of this report. The second implementation is based on the use of fugacity coefficients. Based on the definition given in equation 4.1-20, the fugacity coefficients for a pure substance in the liquid phase (L) and the vapour phase (V) can be calculated. The algorithm for obtaining the equilibrium molar volumes and vapour pressure (at saturation) is as follows [90]

1. Guess the saturation pressure P
2. Calculate the vapour and liquid molar volumes using the equation of state
3. Calculate ϕ^L and ϕ^V
4. Calculate $P_{new} = P_{old}\, \phi^L / \phi^V$
5. Go to 2. As long as $\phi^L \neq \phi^V$

Both algorithms provide the same results, as it should. The second one is less easy to implement, especially for complicated equations of state, but the calculations are faster. The first algorithm could have been speed up by replacing the numerical integration method by the analytical form of the integral of equation 7.1-1. However, as expressions for the fugacity coefficients were available for all relevant equations of state, the second algorithm has been used.

5. VAPOUR PRESSURE MEASUREMENTS

5.1 Experimental

The vapour pressure measurements have been carried out at the Utrecht University, Thermodynamics Centre (TCU). Figure 5.1-1 shows an outline of the equipment for measuring vapour pressures. The pressure sensor is a differential pressure device (MKS Baratron) of type capacity manometer. The valves are coated with plastic, suitable for temperatures up to 200 C.[1] The entire equipment, except for the sample container, is in an air-thermostat, in which the temperature can be kept constant within 2-3 K. The sample container retains its temperature by means of a aluminium block, winded with thermocoax wire. In this aluminium block, two platinum resistance thermometers are located. One is used by the thermostat, the other is used for the actual temperature measurement. The measurement thermometer has been calibrated by NMi (Nederlands Meetinstituut) against a precision resistance thermometer. The temperatures can be measured with an uncertainty (2 times standard deviation) of 0.006 K. The error in the temperatures of the aluminium block are estimated to be 0.02 K. The temperature of the sample container is controlled within 0.01 K, so the uncertainty in the sample temperatures is 0.02 K.

A measurement runs as follows. With valve #1 closed and valve 2 opened, both sides of the differential pressure sensor are brought under high vacuum (better than 10^{-4} Pa). During 5 minutes, the system is pumped. After that, the manometer is read (zero pressure). Then, valve #2 is closed and valve #1 is opened. With intervals of 6 seconds, the pressure of the sample is recorded for 30 minutes.

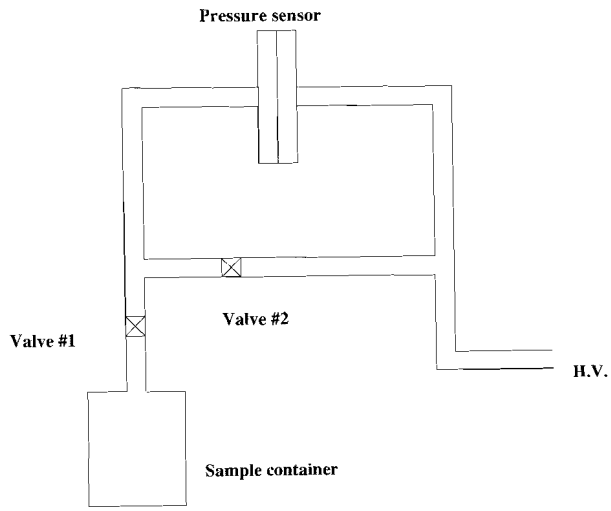

Figure 5.1-1 : Experimental set-up for vapour pressure measurements

During the final 10 to 20 minutes, the pressure increase approaches a low, constant value: the pressure of the sample is now determined by extrapolating back the linear part of the pressure versus time to the moment when valve #1 was

[1] Temperatures expressed in degrees Celcius (symbol: C) are derived from the thermodynamic temperature (in Kelvin, symbol K) by T/C = T/K - 273.15. According to the SI-system, the notation should be C rather than °C.

opened. The measured pressure is then corrected for the zero pressure determined earlier. Since the pressure difference is being measured against high vacuum, the pressure difference may be regarded as being the absolute vapour pressure of the sample.

During a complete run, series of 6 measurements are carried out, where the sample is stirred by means of a magnetic stirrer. The temperature increase between two sets is about 10 K.

Before the start of the first measurement, the equipment was tested by measuring naphthalene. The pressures matched the values of De Kruif et. al. [91] within 1%.

5.2 Programme

In the literature, some data on substituted naphthalenes was found. In order to establish a connection to existing data, several substances have been included in the experimental programme. In coal liquids, substituted aromatic substances are more common than ring systems without side-chains. Common side-chains are methyl, ethyl, hydroxyl, carboxylic acid, and under reducing conditions aldehyde could be formed, although this functional group is not very stable under reaction conditions. However, as a key substance, it is useful to include naphthaldehyde to the suite of substances. The selected substances may be regarded as key-substances for naphthalenic substances in oils from coal.

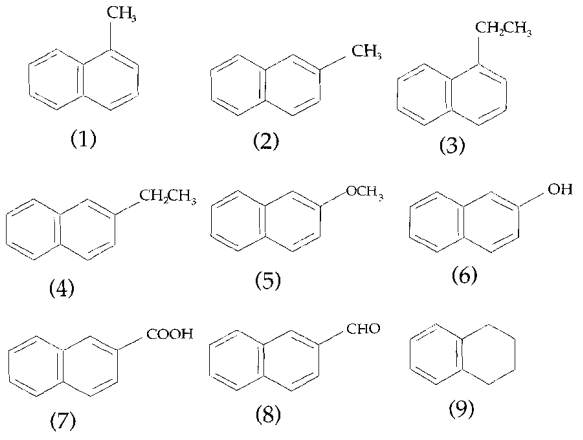

Figure 5.2-1 : Chemical structure of selected naphthalenes and tetralin

The selected key substances are shown in figure 5.2-1: 1-methylnaphthalene (1), 2-methylnaphthalene (2), 1-ethylnaphthalene (3), 2-ethylnaphthalene (4), tetralin (9), 2-methoxynaphthalene (5), 2-naphthol (6), naphthalene-2-carboxylic acid (7), and 2-naphthaldehyde (8). The selection of tetralin has another reason. In many reactors where hydrogen is used as a reductor, naphthalene is used as hydrogen carrier by reducing it to tetrahydronaphthalene, also known as tetralin.

In this section, the experimental results from vapour pressure measurements are presented. The model of Clarke and Glew [66] has been used to calculate the heat of vaporisation and some other basic thermodynamic properties. Recalling from chapter 3, the equation reads as follows

$$R\ln\frac{P}{Pa}=\frac{-\Delta G^{\circ}(\Theta)}{\Theta}+\Delta H^{\circ}(\Theta)\left(\frac{1}{\Theta}-\frac{1}{T}\right)+\Delta C_P^{\circ}\left\{\left(\frac{\Theta}{T}\right)-1+\ln\left(\frac{T}{\Theta}\right)\right\} \qquad 5.2\text{-}1$$

where R is the gas constant (8.31451 J K^{-1} mol^{-1}), P is the vapour pressure, T is the absolute temperature and Θ is a reference temperature. $\Delta G^0(\Theta)$ and $\Delta H^0(\Theta)$ are the free enthalpy and enthalpy differences between the vapour and the liquid phases at a given temperature Θ. ΔC_P^0 is the difference in heat capacity between the two phases. The coefficients of the equation are directly related to thermodynamic properties.

5.3 Results

1-Methylnaphthalene was obtained from Merck, purity > 97%. After placement of a 5 ml sample in the equipment, the sample was evacuated at room temperature for about 30 minutes in order to remove air and volatile contaminants (if present) in the sample.

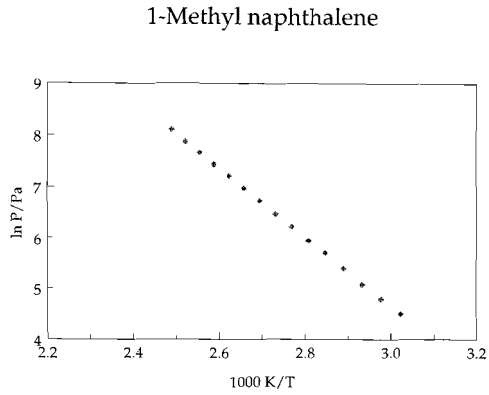

Figure 5.3-1 : Experimental vapour pressure of 1-methyl naphthalene

The results of the vapour pressure measurements of 1-methylnaphthalene are shown in table 5.3-1. The melting point is 242.55 K, the boiling point is 517.75 K, the molar weight is 142.20 g mol^{-1} [92]. Vapour pressures have been measured between about 57.65 and 128.45 C. The experimental results given in the second column are the averages of the two measurement series. The differences between the measurements were well below experimental uncertainty for all data points.

In the third column, the calculated pressure is given. The vapour pressure is calculated after fitting the experimental results to the model of Clarke and Glew. From the fit, the following values for the thermodynamic properties were obtained (Θ = 370.00 K)

$\Delta H^0(\Theta)$ = 56360 ± 190 J/mol

$\Delta G^0(\Theta)$ = -20590 ± 150 J/mol

$\Delta C_P^0 < 2s$

The difference in standard heat capacity of both phases is smaller than two times its standard deviation.

Table 5.3-1 : Experimental and calculated vapour pressure of 1-methylnaphthalene

T (C)	P (Pa) (measured)	P (Pa) (calculated)	$100\frac{P_{meas} - P_{calc}}{P_{meas}}$
57.65	90	89	1.01
62.75	120	122	-1.38
67.75	160	164	-2.28
72.85	220	219	0.24
77.95	300	292	2.72
82.95	380	383	-0.75
88.05	500	501	-0.22
93.05	650	648	0.35
98.05	840	831	1.02
103.15	1070	1065	0.44
108.15	1360	1350	0.76
113.25	1700	1707	-0.42
118.35	2130	2146	-0.76
123.35	2640	2671	-1.16
128.45	3330	3319	0.32

The relative difference between measured and calculated vapour pressure never exceeded 3%.

In the literature, vapour pressure data of 1-methylnaphthalene were already reported in the temperature range 150-320 C by Wieczorek et.al. [93] and in the temperature range 5-39 C by Macknick et.al [94]. The results obtained in this work agree well with both data sets. The data sets were combined and added to the thermodynamic database developed (CoDaMS II).

2-Methylnaphthalene was obtained from Merck with a purity stated of more than 98%. The pre-treatment of a sample of 5 ml was the same as for 1-methylnaphthalene. The vapour pressure was measured as a function of the temperature from about 40 C up to over 150 C in two runs. The averaged results of both runs are shown in table 5.3-2. The differences between both runs were within experimental uncertainty. A plot of ln P versus 1000/T is given in figure 5.3-2. The following results were derived from the vapour pressure measurement by fitting the results to the equation of Clarke and Glew (Θ = 370.00 K)

$\Delta H^0(\Theta) = 54460 \pm 170$ J/mol

$\Delta G^0(\Theta) = -20991 \pm 24$ J/mol

$\Delta C_P^0 = -49 \pm 11$ J/(mol K)

The difference in calculated and measured vapour pressure never exceeded 2%.

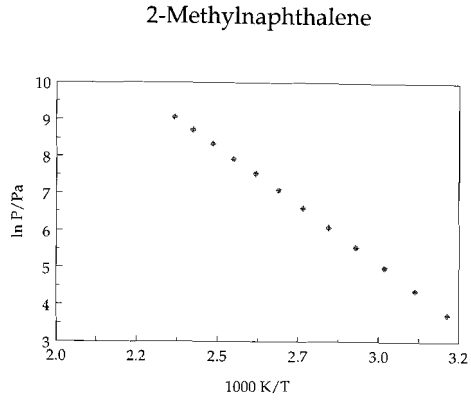

Figure 5.3-2 : Experimental vapour pressure of 2-methylnaphthalene

Table 5.3-2 : Experimental and calculated vapour pressure of 2-methyl naphthalene

T (C)	P (Pa) (measured)	P (Pa) (calculated)	$100\frac{P_{meas} - P_{calc}}{P_{meas}}$
42.84	41.2	41.2	0.00
52.73	79.2	79.6	-0.51
62.68	147	147	0.00
72.62	263	262	0.38
82.56	450	449	0.22
92.55	747	746	0.13
102.50	1200	1199	0.08
112.46	1860	1872	-0.65
122.40	2800	2847	-1.68
132.37	4250	4229	0.49
142.30	6180	6135	0.73
152.15	8700	8692	0.09

In the same paper where Wieczorek reports his experimental vapour pressure data of 1-methylnaphthalene, he reports data of 2-methylnaphthalene as well [93]. The temperature range of his work (150-365 C) is complementary to the results of this work. Again, there is a good agreement between the measurement results. This result is more or less to be expected for 1-methylnaphthalene, 2-methylnaphthalene, and 2-ethylnaphthalene (to be discussed shortly), as the equipment was calibrated with naphthalene. The chemical natures of naphthalene and the alkyl naphthalenes are very similar. However, it should always be verified whether the actual measurement matches data reported earlier.

About 5 ml 1-ethylnaphthalene (FLUKA, >98%) was placed into the sample container. In order to remove volatile impurities, the sample container was evacuated at room temperature. No other purification was carried out.

After evacuation, a complete run was carried out from 40 C to over 150 C. A second run followed in order to test the reproducibility of the measurement. The results of the two runs were within experimental uncertainty in agreement. Table 5.3-3 shows the experimental data obtained by averaging the results of the two runs.

In figure 5.3-3, a plot of the experimental data is shown. From the fit of the experimental data to the equation of Clarke and Glew, the following values for thermodynamic properties have been derived (Θ = 370.00 K)

$\Delta H^0(\Theta)$ = 60940 ± 80 J/mol

$\Delta G^0(\Theta)$ = -18651 ± 14 J/mol

ΔC_P^0 = -118 ± 10 J/(mol K)

The absolute differences between measured and calculated vapour pressures were all well below 2%. The computed vapour pressures are given in table 5.3-3.

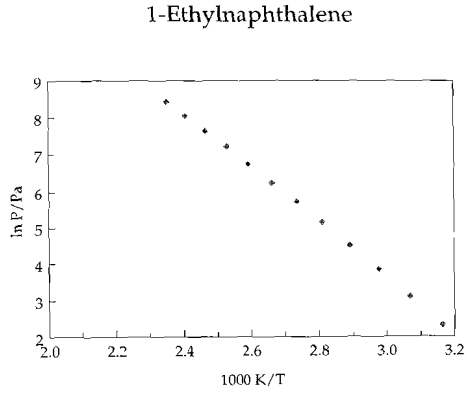

Figure 5.3-3 : Experimental vapour pressure of 1-ethylnaphthalene

Table 5.3-3 : Experimental and calculated vapour pressure of 1-ethylnaphthalene

T (C)	P (Pa) (measured)	P (Pa) (calculated)	$100\frac{P_{meas}-P_{calc}}{P_{meas}}$
40.78	10.1	10.2	-0.99
50.73	22.4	22.4	0.00
60.70	47	46.5	1.06
70.65	92	91	1.09
80.60	170	170	0.00
90.55	305	304	0.33
100.50	520	521	-0.19
110.43	850	858	-0.94
120.40	1360	1369	-0.66
130.35	2100	2112	-0.57
140.31	3170	3167	0.09
150.20	4650	4609	0.88

2-Ethylnaphthalene was obtained from FLUKA, purity > 99.5%. The sample (about 5 ml) was evacuated at room temperature prior to the first run.

Vapour pressures were measured from about 40 to 150 C. The results of the vapour pressure measurement are plotted in figure 5.3-4. The experimental results, accompanied by the calculated vapour pressures are shown in table 5.3-4. The following values for the thermodynamic properties were derived (Θ = 370.00 K)

$\Delta H^0(\Theta)$ = 59820 ± 70 J/mol

$\Delta G^0(\Theta)$ = -18832 ± 22 J/mol

ΔC_P^0 = -105 ± 14 J/(mol K)

In the paper of Macknick cited earlier [94], data on 2-ethylnaphthalene vapour pressure data in the temperature range 13-45 C is reported. The data of this work agree well with these results.

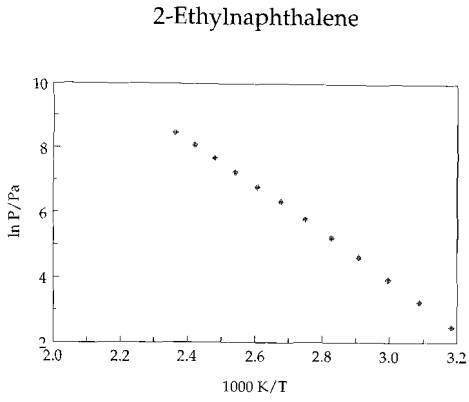

Figure 5.3-4 : Experimental vapour pressure of 2-ethylnaphthalene

Table 5.3-4 : Experimental and calculated vapour pressure of 2-ethylnaphthalene

T (C)	P (Pa) (measured)	P (Pa) (calculated)	$100\frac{P_{meas} - P_{calc}}{P_{meas}}$
40.75	11.8	11.8	0.00
50.72	25.5	25.4	0.39
60.69	51.3	51.8	-0.97
70.66	99	100	-1.01
80.58	185	184	0.54
90.51	330	325	1.52
100.46	560	550	1.79
110.42	885	899	-1.58
120.38	1400	1424	-1.71
130.29	2170	2185	-0.69
140.17	3260	3262	-0.06
150.20	4770	4731	0.82

Tetralin, or 1,2,3,4-tetrahydronaphthalene has been investigated earlier. As already stated in chapter 2, the substance plays an important role as hydrogen donor in coal liquefaction processes.

There are several publications reporting results of vapour pressure measurements and coefficients of vapour pressure equations, such as the Antoine equation. In this work, the vapour pressure of tetralin was determined from about 40 C to 150 C. Tetralin was obtained from Merck, stated purity >98%. Apart from evacuating the sample prior to measurement, no further purification was carried out.

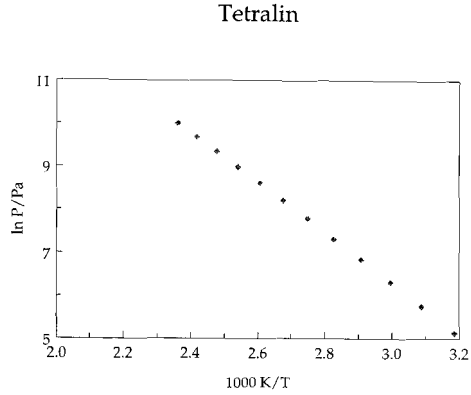

Figure 5.3-5 : Experimental vapour pressure of tetralin

The experimental results, plotted as ln P/Pa versus 1000 K/T are shown in figure 5.3-5. The measurement procedure was adopted from the alkylnaphthalenes. The following thermodynamic properties were derived by fitting the vapour pressure data to the equation of Clarke and Glew (Θ = 370.00 K)

$\Delta H^0(\Theta)$ = 48910 ± 140 J/mol

$\Delta G^0(\Theta)$ = -24680 ± 18 J/mol

ΔC_P^0 = -51 ± 9 J/(mol K)

The calculated and measured vapour pressures are tabulated in table 5.3-5. The absolute difference between measured and calculated pressure was well below 2%.

Table 5.3-5 : Experimental and calculated vapour pressure of tetralin

T (C)	P (Pa) (measured)	P (Pa) (calculated)	$100\frac{P_{meas} - P_{calc}}{P_{meas}}$
41.55	170	172	-1.18
51.50	315	315	0.00
61.46	550	552	-0.36
71.43	940	932	0.85
81.37	1500	1517	-1.13
91.35	2400	2396	0.17
101.32	3680	3679	0.03
111.28	5500	5500	0.00
121.24	8000	8033	-0.41
131.20	11500	11481	0.17
141.16	16000	16088	-0.55
151.08	22100	22111	-0.05

The second part of the experimental programme was carried out with naphthalenes that have oxygen in a functional group. Although it is usually aimed to reduce the contents of oxygen, nitrogen, sulphur, and other elements in the production of coal liquids, usually some oxygen and nitrogen are found. Oxygen can be present as carboxylic acid (-COOH), hydroxyl (-OH), or alkoxy (-OR). The shortest alkoxy group is methoxy (-OCH_3). The fourth substance selected is an aldehyde. If a carboxylic

acid group is partly reduced, it is converted into an aldehyde. However, aldehydes are not very stable and readily reduced to form an alcohol.

Data on 2-Naphthol have been measured earlier by Vargaftik [95]. The pure substance melts at 122 C. The vapour pressure of 2-naphthol has been measured from about 40 C up to 160 C. The experimental data, both of solid and liquid 2-naphthol are shown in figure 5.3-6.

From the experimental data, the following thermodynamic properties have been derived for the vapour-solid equilibrium (VSE) (Θ = 370.00 K)

$\Delta H^0(\Theta)$ = 83975 ± 470 J/mol

$\Delta G^0(\Theta)$ = -13719 ±44 J/mol

$\Delta C_P^0 < 2s$

where s is the standard deviation in the parameter. The heat capacity difference is smaller than two times the standard deviation. For the vapour-liquid equilibrium, the following results were obtained (Θ = 420.00 K)

$\Delta H^0(\Theta)$ = 59650 ± 540 J/mol

$\Delta G^0(\Theta)$ = -25420 ± 14 J/mol

$\Delta C_P^0 < 2s$

Again, the difference in heat capacity of the vapour and condensed phase (in this case the liquid phase) is smaller than two times standard deviation.

2-Naphthol

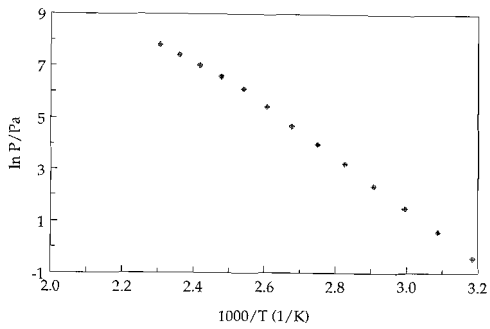

Figure 5.3-6 : Experimental and calculated vapour pressure of 2-naphthol

Table 5.3-6 : Experimental and calculated vapour pressure of 2-naphthol

T (C)	P (Pa) (measured)	P (Pa) (calculated)	$100\frac{P_{meas}-P_{calc}}{P_{meas}}$
40.72	0.65	0.66	-1.54
50.68	1.80	1.76	2.22
60.65	4.5	4.48	0.44
70.64	10.6	10.8	-1.89
80.59	25	24.6	1.60
90.51	54	53.7	0.56
100.48	110	112.7	-2.45
110.44	230	227.4	1.13
120.40	445	442.8	0.49
130.31	720	722	-0.28
140.25	1110	1107	0.27
150.20	1670	1665	0.30
160.16	2450	2458	-0.33

The calculated pressures for both parts of the vapour pressure curve are shown in table 5.3-6. The difference between measured and calculated vapour pressure is smaller than 3% for all measurements.

Naphthalene-2-carboxylic acid was obtained from Janssen Chimica (99%). The substance melts at 185 C. The vapour pressure measurements were carried out from about 40 C to 150 C. The results are plotted as ln P versus 1/T in figure 5.3-7.

The following thermodynamic properties were obtained for the vapour-solid equilibrium (Θ = 370.00 K)

$\Delta H^0(\Theta)$ = 112950 ± 560 J/mol

$\Delta G^0(\Theta)$ = 22497 ± 46 J/mol

$\Delta C_P^0 < 2s$

The difference in standard enthalpy is the heat of sublimation. The agreement between calculated and measured vapour pressures is good. The calculated data fit within 2% of the experimental data (see table 5.3-7).

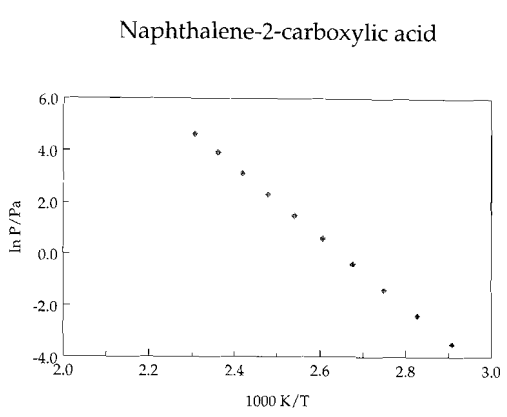

Figure 5.3-7 : Experimental vapour pressure of naphthalene-2-carboxylic acid

Table 5.3-7 : Experimental and calculated vapour pressure of naphthalene-2-carboxylic acid

T (C)	P (Pa) (measured)	P (Pa) (calculated)	$100\frac{P_{meas} - P_{calc}}{P_{meas}}$
70.65	0.03	0.029	3.33
80.60	0.09	0.089	1.11
90.52	0.25	0.25	0.00
100.48	0.68	0.69	-1.47
110.44	1.8	1.77	1.67
120.40	4.4	4.33	1.59
130.32	10	10.1	-1.00
140.25	23	22.7	1.30
150.21	50	49.2	1.60
160.16	103	102.9	0.10

The methoxy-group is quite frequently observed as a side chain. The coal models shown in chapter 2 confirm this. Depending on the treatment of the coal, the oil may contain smaller or larger contents of oxygen. Most of the oxygen in the coal is present in -OH (hydroxyl) groups, or in -O- bridges between hydrocarbon fragments. The methoxy-group is found in mass spectra from pyrolysis experiments [2]. If no complete removal of the oxygen by means of (catalysed) reduction has taken place during the production of the oil, methoxy-substituted aromatic molcules may be expected.

From a thermodynamic point of view, including 2-methoxynaphthalene and 2-naphthaldehyde can provide information on the influence of the presence of oxygen in weak polar groups on the thermodynamic properties of coal chemicals and coal fluids.

2-Methoxynaphthalene

2-Methoxynaphthalene obtained from Janssen Chimica (98%). The measurement procedure was adopted from the measurement of the methylnaphthalenes. The vapour pressure measurement was run from about 75 to 155 C. The melting point of 2-methoxynaphthalene is 73 C. Figure 5.3-8 shows the experimental vapour pressure as a function of the temperature.

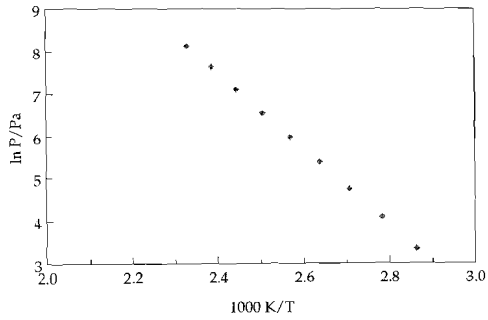

Figure 5.3-8 : Experimental vapour pressure of 2-methoxynaphthalene

From the experimental data, the following thermodynamic properties for the vapour-liquid equilibrium have been derived (Θ = 370.00 K)

$\Delta H^0(\Theta)$ = 74654 ± 920 J/mol

$\Delta G^0(\Theta)$ = -14734 ± 46J/mol

$\Delta C_P^0 < 2s$

Table 5.3-8 : Experimental and calculated vapour pressure of 2-methoxynaphthalene

T (C)	P (Pa) (measured)	P (Pa) (calculated)	$100\frac{P_{meas} - P_{calc}}{P_{meas}}$
76.19	28	29	-3.57
86.17	60	58	3.33
96.16	115	115	0.00
106.14	220	217	1.36
116.12	395	398	-0.76
126.10	700	707	-1.00
136.10	1220	1223	-0.25
146.08	2060	2061	-0.05
156.06	3400	3390	0.29

The experimental and calculated results are summarised in table 5.3-8. The difference between calculated and measured vapour pressure is over 3% for the first two data points, and for the remaining points in the data set well below 2%. A possible explanation for the larger deviation in the first two data points is that the pressure is recorded as

pressure difference (measured pressure, corrected for zero pressure). For very low vapour pressures, a small fluctuation in either the measured pressure or the zero pressure may lead to a considerable difference in the measured vapour pressure.

2-Naphthaldehyde was obtained from Janssen Chimica (98%). About 5 ml of sample was put in the sample container and evacuated for purification. After that, the vapour pressure was measured as a function of the temperature.

The experimental results have been fitted to the equation of Clarke and Glew in order to obtain at 370.00 K (Θ) the thermodynamic properties of the substance at vapour-liquid equilibrium. The results read as follows

$\Delta H^0(\Theta) = 42884 \pm 264$ J/mol

$\Delta G^0(\Theta) = -17144 \pm 22$ J/mol

$\Delta C_P^0 < 2s$

Again, the ΔC_P^0 is smaller than two times its standard deviation.

The agreement between calculated and measured vapour pressure is good: all differences are below 2% of the measured vapour pressure. The results are shown in table 5.3-9.

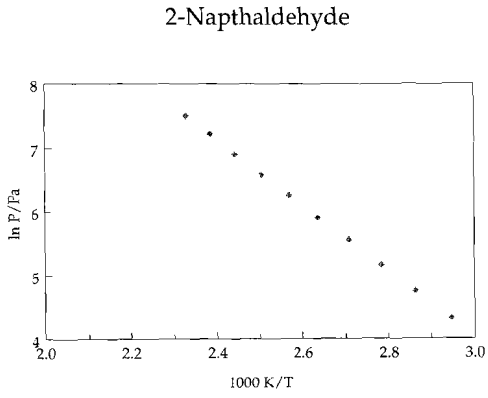

Figure 5.3-9 : Experimental and vapour pressure of 2- naphthaldehyde versus reciprocal temperature

Table 5.3-9 : Experimental and calculated vapour pressure of 2-napthaldehyde

T (C)	P (Pa) (measured)	P (Pa) (calculated)	$100\frac{P_{meas.} - P_{calc.}}{P_{meas}}$
66.20	75	74.7	0.40
76.19	115	115.4	-0.35
86.17	175	174	0.57
96.15	260	256	1.54
106.14	365	370	-1.37
116.13	520	525	-0.96
126.12	725	731	-0.83
136.10	1000	1002	-0.20
146.09	1360	1353	0.51
156.07	1820	1801	1.04

The derived thermodynamic properties have been summarised in table 5.3-10 (see next page). There are a few remarks to be made.

First a general remark on the difference in heat capacity. This third coefficient of the equation of Clarke and Glew is more sensitive to measurement uncertainty than the other two parameters (difference in free enthalpy (ΔG^0) and difference in enthalpy (ΔH^0). Therefore, the difference in heat capacity can only be obtained if the measurement uncertainty is low. If the difference between measured and calculated vapour pressure increases, then the difference in standard heat capacity becomes smaller than 2 times its standard deviation. In that case, it is of little use to report the value, because effects of the fitting procedure contribute considerably to the value of this property.

The heat of vaporisation of the 1- and 2-methylnaphthalenes are smaller than those of 1- and 2-ethylnaphthalenes. Furthermore, the heat of vaporisation of the 2-alkylnaphthalenes is smaller than their 1-substituted isomers.

By far the greatest heat of vaporisation (sublimation) shows naphthalene-2-carboxylic acid. The next substances are 2-naphthol (solid, 370 K) and 2-methoxynaphthalene (liquid, 370 K). Despite of the fact, that the -OH functional group in 2-naphthol is able to form H-bonds, the heats of vaporisation are relatively close to one another.

Table 5.3-10 : Summary of derived thermodynamic properties

Substance	**Θ (K)**	**$\Delta G^0(\Theta)$ (J mol^{-1})**	**$\Delta H^0(\Theta)$ (J mol^{-1})**	**ΔC_p^0 (J K^{-1} mol^{-1})**
1-methylnaphthalene	370.00	-20509 ± 150	56360 ± 190	< 2s
2-methylnaphthalene	370.00	-20991 ± 24	54460 ± 170	-49 ± 11
1-ethylnaphthalene	370.00	-18651 ± 14	60940 ± 80	-118 ± 10
2-ethylnaphthalene	370.00	-18832 ± 22	59820 ± 70	-105 ± 14
tetralin	370.00	-24680 ± 14	48910 ± 140	-51 ± 9
naphthalene-2-carboxylic acid	370.00	22497 ± 46	112950 ± 560	< 2s
2-naphthol (solid)	370.00	-13719 ± 44	83975 ± 470	< 2s
2-naphthol (liquid)	420.00	-25430 ± 14	59650 ± 540	< 2s
2-methoxynaphthalene	370.00	-14734 ± 46	74654 ± 920	< 2s
2-naphthaldehyde	370.00	-17144 ± 22	42884 ± 264	< 2s

6. CORRELATION OF PURE SUBSTANCE DATA

6.1 Introduction

The objectives of the modelling of pure substance data are twofold in this work. First, insight should be gained in how existing correlation and prediction techniques perform on heavy hydrocarbons. The main focus of the modelling is put on polycyclic substances, such as naphthalenes, indans, and tetralin. These substances are commonly produced during coal liquefaction and therefore are suitable key substances.

The second objective of the correlation of pure substance data is to fill gaps in the database. For many of the substances selected in this work, no critical point data are available. The same holds for the acentric factor (section 3.6), that is commonly used as third parameter in the correlation of coefficients of an equation of state to pure substance properties.

6.2 Selection of key substances

The models used in this project have already been investigated at several occasions. The modelling of pure substance data focuses therefore mainly on polycyclic aromatic hydrocarbons. A part of the vapour pressure data used for the modelling work are from the experimental work discussed in chapter 5, whereas the rest is found in recent literature.

In order to enable a comparison between this work and that of previous studies, several benzene derivates have been included too, including benzene and toluene. From these substances, reference data are available from the National Bureau of Standards (NBS, nowadays NIST, National Institute of Standards and Technology) for the whole vapour-liquid equilibrium-range [97,98].

Table 6.2-1 : Selected aromatic hydrocarbons

Name	T_{min} (K)	T_{max} (K)	P_{min} (kPa)	P_{max} (kPa)	n
Benzene	280.000	562.600	5.300	4924.000	48
Toluene	220.000	593.950	0.010	4236.500	79
Ethyl benzene	329.739	410.274	6.357	103.912	20
o-Xylene	336.610	418.517	6.355	103.915	20
m-Xylene	332.353	413.191	6.356	103.915	20
p-Xylene	286.435	452.380	0.582	270.044	45
1,8-Dimethylnaphtalene	338.150	413.150	0.034	1.803	16
2,3-Dimethylnaphtalene	378.150	408.150	0.459	1.761	7
2,6-Dimethylnaphtalene	384.150	418.150	0.805	3.442	7
2,7-Dimethylnaphtalene	369.150	398.150	0.375	1.504	7
Indan	374.274	465.558	9.585	143.240	19
1,1-Dimethylindan	313.150	467.221	0.258	101.325	23
4,6-Dimethylindan	313.150	467.220	0.057	47.375	18
4,7-Dimethylindan	313.150	469.966	0.050	47.375	17
1,1,4,6-Tetramethylindan	313.150	468.638	0.032	38.565	18

Name	T_{min} (K)	T_{max} (K)	P_{min} (kPa)	P_{max} (kPa)	n
1,1,4,7-Tetramethylindan	313.150	468.799	0.025	31.177	18
Naphthalene	356.030	452.660	1.140	38.787	31
1-Methylnaphthalene	330.800	518.476	0.090	102.765	44
2-Methylnaphthalene	315.990	520.050	0.041	114.875	44
Tetralin	314.700	479.350	0.170	98.667	18
1-Ethylnaphthalene	313.930	423.350	0.010	4.650	12
2-Ethylnaphthalene	313.900	423.350	0.012	4.770	12
1-Naphthol	414.650	555.650	1.333	101.333	19
2-Naphthol	417.150	561.150	1.333	101.333	19
2-Naphthaldehyde	339.350	429.220	0.075	1.820	10
2-Methoxynaphthalene	349.340	429.210	0.028	3.400	9

Data were obtained from Osborn et.al. [101] for 1,8-dimethylnapthalene, 2,3-dimethylnapthalene, 2,6-dimethylnapthalene, and 2,7-dimethylnapthalene. The data for indan, 1,1-dimethylindan, 4,6-dimethylindan, 4,7-dimethylindan, 1,1,4,6-tetramethylindan, and 1,1,4,7-tetramethylindan were obtained from Osborn and Scott [102]. For benzene and toluene, the NBS-data have been used, as already stated. The data of the alkylbenzenes were taken from the data collection of Vargaftik [95]. The data of 1- and 2-naphthol were taken from the data collection of Boublik et.al. [96]. The data were combined with the experimental data obtained from the experiments described in chapter 5.

6.3 Estimation of the critical point properties

For several polycyclic aromatics, the critical point data are not known. In order to enable the calculation of the coefficients of equations of state, an estimation procedure has been applied. In this work, two estimation methods have been tested. The first one is that of Joback and Lydersen [61], and a verification for light aromatics showed that the estimates provided by this method were reasonable. The second one tested was a method from the Texas Research Centre (TRC) [62]. This method is more complex, but it has been tested on a wider range of substances. This method has shown to provide good estimates for naphthalene. Therefore, the method of TRC is used for the estimation of the critical point.

For some substances, critical data were available. For tetralin, the critical data from Reid [90] were used. For naphthalene, 1-methylnapthalene, and 2-methylnaphthalene, the experimental data from the paper of Somayajulu [62] were taken.

Table 6.3-1 : Critical constants of several polycyclic hydrocarbons

Substance	NBP[1] (K)	MW (g/mol)	T_{cr} (K)	P_{cr} (bar)	V_{cr} (ml/mol)
1-methylnaphthalene	517.75	142.20	772.00	35.40	462.5
2-methylnaphthalene	514.25	142.20	761.00	35.40	462.5
1-ethylnaphthalene	531.82	156.23	775.17	31.41	516.5

[1] The normal boiling points printed in italic have been estimated with use of the Joback-Lydersen method.

Substance	NBP[1] (K)	MW (g/mol)	T_{cr} (K)	P_{cr} (bar)	V_{cr} (ml/mol)
2-ethylnaphthalene	525.15	156.23	765.45	31.41	516.5
tetralin	480.17	132.20	716.42	30.03	509.5
naphthalene-2-carboxylic acid	*647.23*	172.20	910.19	35.15	482.3
1-naphthol	552.15	144.17	812.54	46.78	405.7
2-naphthol	558.65	144.17	821.54	46.78	405.7
2-methoxynaphthalene	547.15	158.40	799.59	33.81	481.40
2-naphthaldehyde	*550.38*	156.20	814.75	38.03	465.3
1,8-dimethylnaphthalene	543.15	156.23	791.69	31.41	515.4
2,3-dimethylnaphthalene	541.15	156.23	788.77	31.41	515.4
2,6-dimethylnaphthalene	534.65	156.23	779.30	31.41	515.4
2,7-dimethylnaphthalene	535.15	156.23	780.03	31.41	515.4
1,1-dimethylindan	467.22	146.23	685.20	32.16	498.6
4,6-dimethylindan	*531.26*	146.23	775.66	32.16	497.5
4,7-dimethylindan	*531.26*	146.23	775.66	32.16	497.5
1,1,4,6-tetramethylindan	*572.59*	174.29	809.25	26.18	607.5
1,1,4,7-tetramethylindan	*572.59*	174.29	809.25	26.18	607.5

For some substances, even the normal boiling point was not known. Although vapour pressure data exists, extrapolations far beyond the range of temperatures and pressures measured is tricky, and usually not recommended. This fact will be shown in section 6.4, where the correlation of vapour pressure data to empirical equations of state is discussed. For those substances, where no normal boiling point was known, the estimation method of Joback and Lydersen (appendix V.3 of this work) was used. Based on these estimated boiling points, the estimate for the critical point temperature (T_{cr}) was computed.

The significance of the critical properties thus estimated is as follows. For some substances, such as 1- and 2-ethylnaphthalene, it is likely that experimental values could be obtained. For a substance like naphthalene-2-carboxylic acid, it may be expected that the substance decomposes before reaching critical conditions. However, even if a substance is not stable at its critical point, the critical data are not without significance.

The concepts of modelling vapour-liquid equilibria all include the point, where the density of the co-existing phases becomes equal. This is the end of the boiling curve. Both vapour pressure equations and equation of state include the end of the boiling curve. For most cubic equations of state, the coefficients at the critical point have been correlated to the critical properties (temperature, pressure, and sometimes volume or compressibility factor). If a substance decomposes below the critical point, which will be the case for many heavy polycyclic aromatic hydrocarbons, then the predictions of the model are valid up to the point where decomposition occurs. However, in order to implement the model, knowledge about the (hypothetical) critical point properties is necessary.

6.4 Correlation of data to empirical vapour pressure equations

In chapter 3, several empirical models have been introduced that describe the relationship between the pressure at saturation as a function of the temperature at va-

pour-liquid equilibrium. These equations provide a way for data reduction. Given a set of coefficients of a given substance of for example the Vapres-2 equation and the temperature interval for which they are valid would allow to calculate the vapour pressure of that substance for any temperature T within that interval. The quality of this computed vapour pressure depends heavily on the quality of the model at that given temperature T. Fitting results of benzene and toluene show, that the difference between the calculated and measured vapour pressure is a function of the temperature too. This will be shown shortly for selected models.

The use of benzene and toluene for the purpose of assessing the quality of the models follows from the fact that reference data are available [97,98]. These reference data cover the complete VLE-area and have been compiled from various sources and tested for their consistency.

The models Vapres-2, Van Laar, Miller, Riedel, Cox, and Wagner-1 have been selected. The Antoine equation has not been included in the comparison of the models, as it has been reported that this model does not perform well in extrapolations.

The models have been tested on several key-compounds. The most interesting one for the project from that series is benzene. The data are from the National Bureau of Standards (NBS). The fitting results are given in the form of scatter plots below.

The Vapres-2 equation is a five-parameter equation, and it may be expected that the fitting results of this model will be the best. Figure 6.4-1 indicates that there is a small systematic difference between calculated and measured pressure, The difference seems to increase with increasing temperature, but it should be recalled that ln P is about proportional to 1/T, so the increase in pressure is far greater than that in temperature. So, on a relative basis, the difference is smaller than for low temperatures, even near the critical point. For interpolations and estimation of the vapour pressure, the fitting is good.

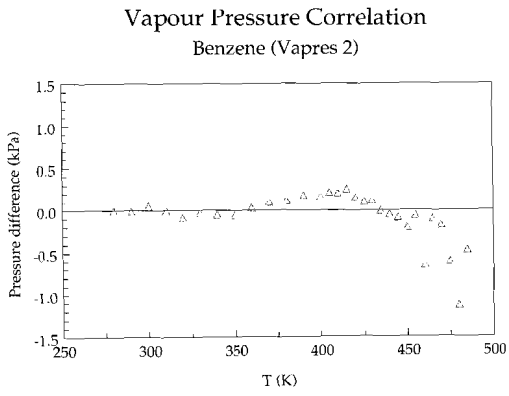

Figure 6.4-1 : Fitting results of benzene with the Vapres-2 equation

The empirical vapour pressure equation of Van Laar misses the DT^2-term of the Vapres-2 equation. The fitting results of this equation are shown in figure 6.4-2. The fitting of the vapour pressure data of benzene is poorer than with the Vapres-2 equation. This result was obtained for other fluids from which data is available from the triple point up to the critical point too.

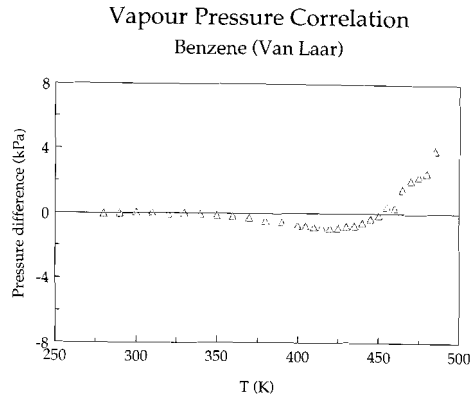

Figure 6.4-2 : Fitting results of benzene with the Van Laar equation

The fitting results of the NBS data of benzene to the Miller equation are shown in figure 6.4-3. This equation performs better than the Van Laar equation. In comparison to the Vapres-2 equation,. the term E ln T is missing. The results are poorer than those of the Vapres-2 equation. It should however be realised that the Vapres-2 equation is a five-parameter equation, which has greater flexibility than four parameter equations, such as the Miller or Van Laar equations.

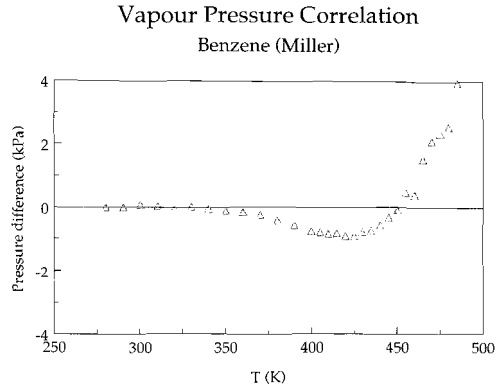

Figure 6.4-3 : Fitting results of benzene with the Miller equation

The fitting of the Riedel equation (figure 6.4-4) is the best of the set of four-parameter equations. The fitting results are comparable with those of the Vapres-2 equation, that has 5 parameters. The difference between calculated and measured pressure is less than in the case of the case of the Miller and Van Laar equations.

The Riedel equation (section 3.3) differs from the Van Laar equation in the third term. Van Laar uses the term CT, whereas Riedel proposes the term CT^6. This exponent is also found in the last term of the Wagner-1 equation (section 3.3).

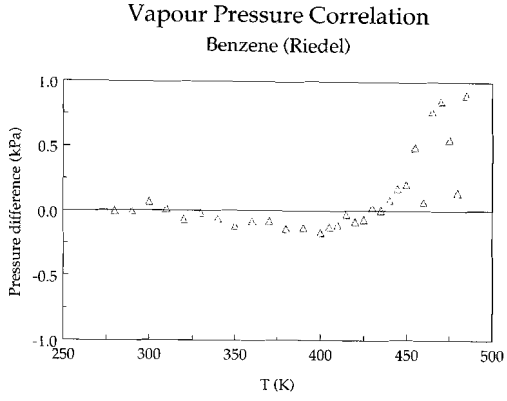

Figure 6.4-4 : Fitting results of benzene with the Riedel equation

The Cox equation is a three-parameter equation with as reference point the critical point. The fitting results are comparable to those from the Miller equation. The Cox equation does not require the critical point to be the reference point. Any other well-established pair of temperature and saturated vapour pressure will do too. For the use in coal liquefaction engineering, this is a great advantage, as for many substances and mixtures, the (pseudo)critical properties are difficult to obtain, whereas a boiling point at a given pressure can be obtained relatively easily.

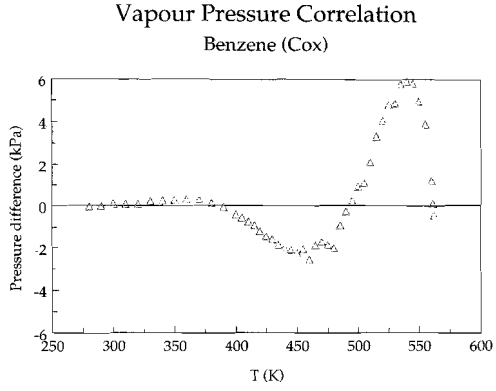

Figure 6.4-5 : Fitting results of benzene with the Cox equation

The fitting results for benzene with the Cox equation are shown in figure 6.4-5. A principal difference in the implementation of the Cox equation and the equations of Riedel, Vapres-2, Miller, and Van Laar is that the fitting of the Cox equation by means of the Marquardt-Levenberg algorithm still involves ln P, rather than P. it is however not likely that this is the reason for the poorer fitting (when compared to the Vapres-2 results of figure 6.4-1 for instance). The fact that the Cox equation has only three adjustable constants if the reference pressure is kept constant (and not included as fitting parameter).

The fitting results of the Wagner-1 equation (figure 6.4-6) are the poorest of the models presented here to fit the data of benzene. It is a four-parameter equation with the critical point as reference. Although the performance may seem to be poor, it should be realised that the critical pressure of benzene is 4898 kPa. So, the relative pressure difference is small, even for the temperature range 530-560 K.

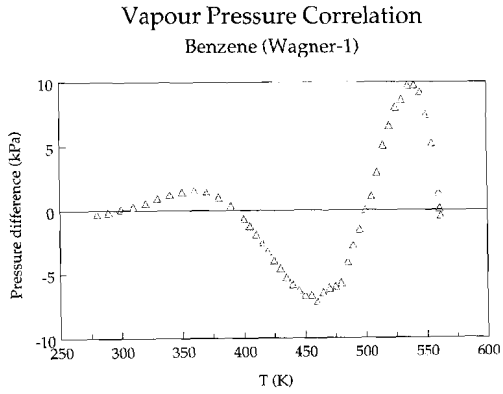

Figure 6.4-6 : Fitting results of benzene with the Wagner-1 equation

The results for benzene are representative for fitting the vapour-liquid area with empirical models. The models perform better on smaller temperature ranges, but they are only suitable for interpolation purposes.

For the modelling of the substances measured here, two equations were selected, in fact the Vapres-2 and the equation of Clarke and Glew. The performance of the equations is shown in table 6.4-1.

From many substances, the average absolute deviation, defined as

$$AAD = \frac{100}{n}\sum_{i=1}^{n}\frac{|P_m - P_c|}{P_c}$$

is given for the selected group of substances. From these results, it may be concluded that the use of a vapour pressure correlation does not contribute too much to the measurement uncertainty. From chapter 5, it is known that the experimental uncertainty is of the order of about 0.01 (relative toe the measured pressure P_m). Thus the difference of the calculated pressure (P_c) and the measured pressure is for many engineering applications of little interest.

Table 6.4-1 : Performance of Vapres-2 and Clarke and Glew equations on selected key substances

Substance	Vapres-2 AAD	Clarke-Glew AAD
benzene	0.04	1.32
toluene	0.69	4.05
ethylbenzene	0.01	0.03
1,2-dimethylbenzene	0.01	0.04
1,3-dimethylbenzene	0.01	0.03
1,4-dimethylbenzene	0.02	0.21
propylbenzene	0.07	0.08
(2-propyl)benzene	0.00	0.04
phenanthrene	0.35	0.34
1,8-dimethylnaphthalene	0.16	0.18
2,3-dimethylnaphthalene	0.34	1.71
2,6-dimethylnaphthalene	0.06	0.04
2,7-dimethylnaphthalene	0.04	0.04
indan	0.00	0.00
1,1-dimethylindan	0.03	0.25
4,6-dimethylindan	0.05	0.28
4,7-dimethylindan	0.10	0.39
1,1,4,6-tetramethylindan	0.13	0.29
1,1,4,7-tetramethylindan	0.04	0.23
diphenylmethane	0.46	0.48
naphthalene	0.16	0.16
1-methylnaphthalene	0.54	0.65
2-methylnaphthalene	0.17	0.15
1,2,3-trimethylbenzene	0.02	0.03
1,2,4-trimethylbenzene	0.24	0.26
1,3,5-trimethylbenzene	0.02	0.03
tetralin	0.76	1.14
1-ethylnaphthalene	0.44	0.99
2-ethylnaphthalene	1.71	2.01
2,3-dimethylphenol	2.21	2.43
2,4-dimethylphenol	0.00	0.02
2,6-dimethylphenol	0.02	0.01
3,5-dimethylphenol	0.01	0.01
1-naphthol	0.98	1.06
2-naphthol	1.51	1.48
naphthalene-2-carboxylic acid[1]	2.05	4.93
2-naphthaldehyde	0.48	0.63
2-methoxynaphthalene	0.50	1.02

In addition to the critical point properties, the acentric factor has to be computed. From its definition (section 3.6), it can be computed directly from the reduced vapour pressure at a reduced temperature of 0.700. From the coefficients obtained for the substances in table 6.4-1, this was only possible for a few substances. For many substances of interest, acentric factors were not available, and vapour pressure data

[1] Solid

were limited. The only exceptions were 1- and 2-methylnaphthalene, tetralin, indan, and 1,1-dimethylindan.

In order to establish good estimates for the acentric factor, a different technique has been used. In a recent paper, Twu et.al. [73] express the reduced vapour pressure as follows

$$\ln P_r = \ln P_r^{(0)} + \omega \ln P_r^{(1)} \qquad 6.4\text{-}1$$

where ω is the acentric factor (see equation 3.6-1, chapter 3). The two terms have been related to the Wagner-1 equation

$$\ln P_r^{(0)} = \frac{1}{T_r}\left\{-5.96346\left[1-T_r\right]+1.17639\left[1-T_r\right]^{1.5}-0.59607\left[1-T_r\right]^{3.0}-1.31901\left[1-T_r\right]^{6.0}\right\} \qquad 6.4\text{-}2$$

$$\ln P_r^{(1)} = \frac{1}{T_r}\left\{-4.78522\left[1-T_r\right]+0.413999\left[1-T_r\right]^{1.5}-8.9239\left[1-T_r\right]^{3.0}-4.9662\left[1-T_r\right]^{6.0}\right\} \qquad 6.4\text{-}3$$

These equations implement not only the critical point correctly ($T_r = 1$, $P_r = 1$), but they are also in agreement with the definition of the acentric factor. In their paper, Twu et.al. demonstrate the capabilities of equations 6.4-1 through 6.4-3 in predicting acentric factors for n-alkanes and several other fluids. The results obtained for benzene and toluene agree well.

Based on this method the following acentric factors were obtained (table 6.4-2). The critical point properties for indan and naphthalene were taken from the database of Texas Research Centre [62].

Table 6.4-2 : Critical properties and acentric factors for selected substances

Substance	T_{cr} (K)	P_{cr} (bar)	ω
naphthalene	748.40	40.51	0.2723
1-methylnaphthalene	772.00	35.40	0.3025
2-methylnaphthalene	761.00	35.40	0.3093
1-ethylnaphthalene	775.17	31.41	0.3553
2-ethylnaphthalene	765.45	31.41	0.3651
tetralin	716.42	30.03	0.2806
1-naphthol	812.54	46.78	0.3642
2-naphthol	821.54	46.78	0.3604
2-methoxynaphthalene	799.59	33.81	0.3857
2-naphthaldehyde	814.75	38.03	0.3379
1,8-dimethylnaphthalene	791.69	31.41	0.3624
2,3-dimethylnaphthalene	788.77	31.41	0.3409
2,6-dimethylnaphthalene	779.30	31.41	0.3329
2,7-dimethylnaphthalene	780.03	31.41	0.3397
indan	684.90	39.50	0.2570
1,1-dimethylindan	685.20	32.16	0.3109
4,6-dimethylindan	775.66	32.16	0.2388
4,7-dimethylindan	775.66	32.16	0.2486
1,1,4,6-tetramethylindan	809.25	26.18	0.1946
1,1,4,7-tetramethylindan	809.25	26.18	0.2197

The results obtained by the method of Twu et.al. provided more consistency than the results that would have been obtained from extrapolations by either the Wagner-1, Vapres-2, or Clarke-Glew equations. For substances where vapour pressure data are available up to the normal boiling point, the estimates for the acentric factors were reasonable. However, regression of vapour pressure data in the low reduced pressure range is usually less stable due to

the fact that more scattering is observed in experimental data than at higher reduced pressures.

In a recent paper, Aly et.al. [103] publish some acentric factors for substituted naphthalenes. For 2,3-dimethylnaphthalene, Aly reports an acentric factor of 0.500, whereas in this work a value of 0.3409 is obtained. The same holds for 2,6-dimethylnaphthalene, where a value of 0.510 is reported. The agreement between the results for 1-methylnaphthalene is better. Aly reports 0.310, in this work a value of 0.3025 is obtained. The agreement for naphthalene is less good. The value find in this work is lower (0.2723) when compared of that of Aly et.al. (0.303). The differences in critical properties for these substances are below the uncertainty in the estimation of the critical point properties.

The estimates found are in fair agreement with what can be observed from studying acentric factors of benzene derivates. The acentric factor for toluene (0.2607) is greater than that of benzene (0.2092). The same is true for ethylbenzene (0.3123). This pattern is also found in naphthalene, the methylnaphthalenes, and the ethylnaphthalenes. The acentric factors of the dimethylnaphthalenes are about equal to those of the ethylnaphthalenes, which is also found when comparing ethylbenzene with the xylenes (ortho: 0.3123; meta: 0.3263; para: 0.3215) [65]. This agreement in results may be an indication for the validity of the estimation technique of Twu et.al., as applied here.

6.5 Calculations with equations of state

Based on the acentric factors of section 6.4, and the critical properties thus obtained, two equations of state were tested. The Soave-Redlich-Kwong equation of state (SRK) is often used in coal liquefaction modelling, as already stated. Therefore, this equation of state is chosen to be the "reference equation of state". The results of the Cubic Chain-of-Rotators equation of state (CCOR) are compared to the results of the SRK.

Table 6.5-1 : Performance of the SRK and CCOR on selected heavy aromatic substances

Substance	SRK		CCOR	
	AAD (%)	Bias (%)	AAD (%)	Bias (%)
naphthalene	18.59	-18.59	12.11	-12.11
1-methylnaphthalene	26.85	-26.85	19.34	-19.34
2-methylnaphthalene	32.36	-32.36	25.29	-25.29
1-ethylnaphthalene	56.59	-56.59	36.16	-36.16
2-ethylnaphthalene	69.50	-69.50	48.30	-48.30
tetralin	16.10	-16.06	9.51	-9.18
1-naphthol	74.23	-74.23	68.05	-68.05
2-naphthol	71.77	-71.77	65.67	-65.67
2-methoxynaphthalene	104.68	-104.68	79.51	-79.51
2-naphthaldehyde	65.16	-60.27	56.24	-44.14
1,8-dimethylnaphthalene	69.86	-69.86	49.53	-49.53
2,3-dimethylnaphthalene	56.38	-56.38	43.41	-43.41
2,6-dimethylnaphthalene	52.45	-52.45	41.92	-41.92
2,7-dimethylnaphthalene	53.73	-53.73	40.09	-40.09
indan	21.43	-21.43	17.25	-17.25

Substance	SRK		CCOR	
	AAD (%)	Bias (%)	AAD (%)	Bias (%)
1,1-dimethylindan	33.92	-33.92	26.51	-26.51
4,6-dimethylindan	15.58	4.19	14.81	10.06
4,7-dimethylindan	15.84	1.87	14.06	8.26
1,1,4,6-tetramethylindan	27.03	18.08	27.55	21.73
1,1,4,7-tetramethylindan	21.78	13.82	22.47	19.12

A few notes have to made about these results. In section 6.4, the estimation of the acentric factor with the Wagner-1 equation was described. As already stated, the acentric factors for the naphthalenes are low when compared to acentric factors published elsewhere. The method of Twu [73] provides good estimates for heavy alkanes.

From table 6.5-1, it can be seen that the results are better for the lighter aromatic substances and the indans, than they are for naphthalenic substances. This may probably be due to the fact that the π-π interactions of the aromatic systems of naphthalenic substances are stronger. There are probably two reasons for these stronger interactions between molecules. The aromatic systems are greater in naphthalenic substances, than they are in monocyclic aromatic substances, including the indans. Second, if an aromatic ring is substituted steric hindrance in the formation of dimers may be observed. However, for naphthalenes this steric effect is usually of less importance, as with one substitution, there is still a "free" aromatic ring to enable dimerisation.

Another indication that dimerisation may be a sensible explanation is the difference in results between relatively a-polar substances like methoxynaphthalene, and the results of the naphthols.

In various publications, acentric factors can be found that are suitable for several purposes. For the Soave-Redlich-Kwong equation of state for instance, Reid et.al. [90] report an extensive lists of acentric factors that minimise the difference between the temperature function of coefficient a of the SRK, and the experimental temperature function as can be calculated from the equation of state and experimental vapour pressure data. In that case, the difference between the vapour pressure at saturation predicted by the equation of state and the experimental value is minimised.

This approach could lead to an improvement of the results of the Cubic Chain-of-Rotators equation of state as given in table 6.5-1, but there are two serious problems. First, the link with Pitzer's definition [71,72] is lost, which may seem to be unimportant. However, in this work it was attempted to determine values of the acentric factor that are consistent with Pitzer's definition by means of the method of Twu et.al., that in turn is based on Wagner's vapour pressure equation. The method of Twu et.al. provides an independent way of obtaining acentric factors in agreement with the definition of Pitzer. This option would be unavailable if the link between the definition and the value of the acentric factor would be lost if the acentric factor would be re-estimated in order to minimise the difference between the temperature function for coefficient a of the equation of state and the experimental temperature function.

For the Cubic Chain-of-Rotators equation of state, the recipe that is used for the Soave-Redlich-Kwong equation of state does not work. This is due to the fact, that a series of coefficients depends on the acentric factor. From the formulas given in section 4.4, it may be seen that the following coefficients of the CCOR depend on ω: Ω_a, Ω_b, Ω_c, Ω_d, c^R, a_1, a_2, a_3, a_4, c_1, and c_2. Although not listed, the coefficients a_{cr}, b_{cr}, c_{cr}, and d_{cr} are functions of w too, as the coefficients Ω_a, Ω_b, Ω_c, and Ω_d depend on ω.

So, changing the value of the acentric factor would cause a series of coefficients to be changed. As already stated, the problems in modelling heavy aromatic substances are likely to be due to dimerisation. There are several approaches possible to model substances that form dimers. Probably one of the best is the pseudo-chemical approach, where the dimerisation equilibrium is part of the model. Examples of this approach can be found in numerous references, like in a publication and a review of Anderko [104,105].

In order to test whether the correlation results of the CCOR and SRK improve if other values for the acentric factor are used than computed here, for four substances, the correlation has been carried out with the acentric factors given by Reid et.al. [90]. The results are shown in table 6.5-2.

Table 6.5-2 : Performance of the SRK and CCOR on selected heavy aromatic substances with acentric factors from Reid et.al. [90]

Substance	SRK		CCOR	
	AAD (%)	Bias (%)	AAD (%)	Bias (%)
1-ethylnaphthalene	6.17	-0.61	14.04	14.04
tetralin	3.66	-3.66	3.14	3.14

These results indicate for the SRK a clear improvement of the results by modifying the SRK. For the CCOR, the improvement is less. For several other substances, such as 1- and 2-methylnaphthalene, 2-ethylnaphthalene, no clear improvement of the results of the CCOR could be found by replacing the acentric factor obtained in this work by acentric factors reported by Aly et.al. [103], or Reid et.al. [90].

6.6 Concluding remarks

The results presented here may indicate that for heavy aromatic species, the acentric factor system does not suffice in the same manner as it does for many other organic substances, especially saturated hydrocarbons. The substances without hetero-atoms used here are qua size comparable with saturated hydrocarbons of size C_8-C_{14}. The agreement between the results reported on these substances [73] is far better than that for the substances presented here.

An improvement of the CCOR is not as easy as it is for the SRK. Modification of the value of the acentric factor leads to a change of the values of all coefficients of the CCOR, which is in contrast to the SRK, where only the temperature function of the coefficient *a* depends on the acentric factor. For the CCOR, two options are open: regression of all coefficients to a modified acentric factor, or the implementation of a mechanism in the CCOR that accounts for dimerisation equilibria. In order to main-

tain the sound theoretical basis for the CCOR, the second option should be preferred.

7. BINARY MIXTURES

7.1 Principles

The description of mixtures plays a key role in engineering thermodynamics. Almost any design of a chemical process includes the design of separation operations. These include in turn distillation, absorption, and extraction. A rational design can only be established if the phase equilibria involved are known. For separation processes, the so-called K-value is very important. The K-value of component *i* is the ratio of the mole fraction of *i* in the vapour and the mole fraction of *i* in the liquid [106],

$$K_i = \frac{y_i}{x_i} \qquad 7.1\text{-}1$$

where y_i is the mole fraction of component *i* in the vapour phase, and x_i denotes the mole fraction of *i* in the liquid phase. For an efficient separation process, the value of K_i should be either far greater than unity, or far smaller.

In this study, the modelling of mixtures aims to test the validity of the Cubic Chain-of-Rotators equation of state and its modification. The calculation of K-factors is not a primary objective, but they are used in modelling mixtures with equations of state. This topic is covered in more detail in section 7.3.

A second objective of the modelling of binary mixtures is to complete the set of data from experiments. Two binary mixtures have been investigated in this work. The total pressure has been measured as a function of temperature (T) and liquid composition (x). From the data, the vapour phase composition has to be calculated.

For a vapour-liquid equilibrium (VLE) in a mixture, the following relationship has to be satisfied

$$f_i^L = f_i^V \qquad 7.1\text{-}2$$

where f_i denotes the fugacity of component *i* in the mixture, *L* denotes the liquid phase, and *V* denotes the vapour phase. The main principle of the calculations involved is to compute the variables that are hard to obtain experimentally from the variables that have been measured or set. A mixture is characterised by T, P, x_i, y_i for any component i = 1..m. Table 7.1-1 provides an overview over all possible problems [106].

Table 7.1-1 : Calculation procedures for the system properties of mixtures as a function of the variables given

given	find	Calculation procedure[1]
P, x_1, x_2, ..., x_m	T, y_1, y_2, ...,y_m	bubble point T
T, x_1, x_2, ..., x_m	P, y_1, y_2, ..., y_m	bubble point P
P, y_1, y_2, ..., y_m	T, x_1, x_2, ..., x_m	dew point T
T, y_1, y_2, ..., y_m	P, x_1, x_2, ..., x_m	dew point P

where x_i is the mole fraction of component *i* in the liquid phase (L) and y_i denotes the mole fraction of component *i* in the vapour phase. In each of these problems, there are *m* unknowns. It is easily seen why for a real coal liquid, where typically m > 10, it becomes almost impossible to solve all equations simultaneously. This is the reason that for coal oil, fractionated oils and other mixtures with many components a different approach has to be selected.

There are numerous algorithms and procedures for finding the solution of the problems given in table 7.1-1. In this work, Barker's data reduction method [107-111] has been used for the calculation of the vapour phase composition from total pressure data. A binary system is overdetermined if *T*, *x*, and *P* are known. Barker's method does not only provide estimates for the vapour phase composition, and thus the K-factors, but it also provides an estimate of the equilibrium pressure.

The equilibrium pressure of a mixture is from all parameters the most sensitive one. According to Van Ness [109], the vapour phase composition (*y*) is less sensitive to the selection of an equation of state for representing the vapour phase imperfections. Even with the ideal gas law, reasonable estimates for the vapour phase composition can be obtained for a-polar mixtures.

The principles of Barker's method are as follows. Given the equilibrium condition in equation 7.1-2, the fugacity of the vapour phase can be expressed as

$$f_i^V = \phi_i y_i P \qquad 7.1\text{-}3$$

where ϕ_i is the vapour phase fugacity coefficient. *P* is the system pressure. The activity coefficient γ_i relates the liquid phase fugacity to the mole fraction and the standard state fugacity (f^{0L})

$$f_i^L = \gamma_i x_i f_i^{0L} \qquad 7.1\text{-}4$$

There exists a relationship between fugacity of a component in the vapour phase and the volumetric properties of that component. The volumetric properties of a component are represented by an equation of state.

If it is accepted that at low to moderate densities the virial equation of state, truncated after the second terms represents these volumetric properties well, then the fugacity coefficient may be computed. The virial equation of state reads as follows

$$z = \frac{Pv}{RT} = 1 + \frac{BP}{RT} \qquad 7.1\text{-}5$$

[1] All four calculation procedures have specific names in literature. These names are given in this column.

where B is the second virial coefficient. z is the compressibility factor, v is the molar volume, P is the pressure, and T is the temperature. R is the ideal gas constant, and B is the second virial coefficient. Whether this assumption is valid can be verified by assessment of the predicted equilibrium pressure.

The second viral coefficient for a mixture of m components is given by

$$B = \sum_{i=1}^{m}\sum_{j=1}^{m} y_i y_j B_{ij} \qquad 7.1\text{-}6$$

For a binary mixture, equation 7.1-6 becomes

$$B = y_1^2 B_{11} + 2y_1 y_2 B_{12} + y_2^2 B_{22} \qquad 7.1\text{-}7$$

where B_{ij} depends only on the temperature and components i and j. The fugacity coefficient follows from the relationship

$$\ln \phi_i = \int_0^P \frac{z_i - 1}{P} dP \qquad 7.1\text{-}8$$

where

$$z_i = \frac{P v_i}{RT} \qquad 7.1\text{-}9$$

and the partial molar volume (v_i) follows from its definition

$$v_i = \left(\frac{\partial V}{\partial n_i}\right)_{T,P,n_j} \qquad 7.1\text{-}10$$

In this equation V is the total volume, containing n_i moles of component i, n_j moles of component j, etc.. Substitution of equations 7.1-6 and 7.1-7 in equation 7.1-8, it follows

$$\ln \phi_i = \left[2\sum_{j=1}^{m} y_j B_{ij} - B\right]\frac{P}{RT} \qquad 7.1\text{-}11$$

For associating components, the virial equation of state is no longer valid (equation 7.1-5), and another method has to be used for the calculation of the vapour phase imperfection.

For the liquid phase, the activity coefficient has to be computed. In order to do so, an arbitrary choice has to be made about the standard state liquid fugacity.

7.2 Data reduction method of Barker

The complete description of a fluid mixture in vapour-liquid equilibrium provides the equilibrium compositions of all components in the mixture, as well as the equilibrium temperature and pressure. For each of the m components is the mixture, the chemical potential μ should be equal in both the liquid (L) and the vapour phase, that is

$$\mu_i^L = \mu_i^V \qquad 7.2\text{-}1$$

where i denotes component number i. For both fluid phases, the temperature and pressure should be equal too. In a system with m components, there are 2(m-1) mole fractions to be determined (the m^{th} mole fraction follows directly from the fact, that the sum of mole fractions in a single phase should always be unity). From an experimental point of view, even for a binary mixture it is a considerable effort to obtain all variables experimentally. This effort can be reduced by applying the Gibbs-Duhem equation that states (at constant temperature and pressure)

$$\sum_i x_i d\bar{m}_i = 0 \qquad 7.2\text{-}2$$

which is also valid for excess properties. The bar over the m in equation 7.2-2 denotes a molar property. Excess properties are used to describe the properties of mixtures, taking the pure components as reference point. The Gibbs-Duhem equation can also be applied to activity coefficients. In terms of activity coefficients, equation 7.2-2 becomes

$$\sum_i x_i d\ln\gamma_i = 0 \qquad 7.2\text{-}3$$

again at constant T and P. The symbol γ denotes the activity coefficient. The activity coefficient is defined as

$$\gamma_i \equiv \frac{f_i}{x_i f_i^0} \qquad 7.2\text{-}4$$

For a binary mixture with isothermal data available for one component, the Gibbs-Duhem equation can be written as

$$x_1 \frac{d\ln\gamma_1}{dx_1} = x_2 \frac{d\ln\gamma_2}{dx_2} \qquad 7.2\text{-}5$$

Using this result, isothermal total pressure data can be used to calculate the properties of a mixture. For a binary mixture, the total pressure can be written as

$$P = \gamma_1 x_1 P_1^{sat'} + \gamma_2 x_2 P_2^{sat'} \qquad 7.2\text{-}6$$

where $P^{sat'}$ is the "corrected" vapour pressure of a component. This pressure can be calculated with use of the second virial coefficients of components 1 and 2, according to

$$P_1^{sat'} = P_1^{sat} \exp\left[\frac{\left(v_1^L - B_{11}\right)\left(P - P_1^{sat}\right) - P\delta_{12}y_2^2}{RT}\right] \qquad 7.2\text{-}7$$

$$P_2^{sat'} = P_2^{sat} \exp\left[\frac{\left(v_2^L - B_{22}\right)\left(P - P_2^{sat}\right) - P\delta_{12}y_1^2}{RT}\right]$$

where

$$\delta_{12} = 2B_{12} - B_{11} - B_{22} \qquad 7.2\text{-}8$$

where B is the second virial coefficient, and y is the mole fraction of a component in the vapour phase. Equation 7.2-7 is rigorous, as long as it may be assumed that the

vapour phases of the pure components 1 and 2 as well as their mixture are adequately described by the volume-explicit virial equation of state. The reason for implementing the virial equation of state here rather than models like the Cubic Chain-of-Rotators equation, is to have two independent methods for describing mixtures.

At constant temperature, the activity coefficients are functions of the composition only. For the implementation of Barker's data reduction method, the series expansion of Redlich-Kister [112,113] has been used. The model reads as follows [114]

$$g^E = x_1 x_2 \left[A + B(x_1 - x_2) + C(x_1 - x_2)^2 + D(x_1 - x_2)^3 + \ldots \right] \qquad 7.2\text{-}9$$

Using the Gibbs-Duhem equation, the series expansion of Redlich-Kister for the excess-Gibbs energy (g^E) can be converted into two expressions for the activity coefficients. These expressions read as

$$RT \ln \gamma_1 = a^{(1)} x_2^2 + b^{(1)} x_2^3 + c^{(1)} x_2^4 + d^{(2)} x_2^5 + \ldots \qquad 7.2\text{-}10$$

and

$$RT \ln \gamma_2 = a^{(2)} x_1^2 + b^{(2)} x_1^3 + c^{(2)} x_1^4 + d^{(2)} x_1^5 + \ldots \qquad 7.2\text{-}11$$

where the coefficients A through D are to be determined. The relationship between the coefficient in equations 7.2-10 and 7.2-11 read as follows

$$\begin{aligned} a^{(1)} &= A + 3B + 5C + 7D \\ b^{(1)} &= -4(B + 4C + 9D) \\ c^{(1)} &= 12(C + 5D) \\ d^{(1)} &= -32D \end{aligned} \qquad 7.2\text{-}12$$

and

$$\begin{aligned} a^{(2)} &= A - 3B + 5C - 7D \\ b^{(2)} &= 4(B - 4C + 9D) \\ c^{(2)} &= 12(C - 5D) \\ d^{(2)} &= 32D \end{aligned} \qquad 7.2\text{-}13$$

It is assumed that v^L, B, P, and δ_{12} are known. P will be known, as it is assumed that the total pressure of the system is known. For v^L, good estimation procedures exist to calculate this property for any of the substances involved. For B, estimation methods exist too. For the implementation of Barker's method, the estimation method of Tsonopoulos [115-117] has been used.

The steps to obtain the coefficients of the Redlich-Kister equation are as follows

1. First, set $y_1 = y_2 = 0$
2. Calculate A through D in such a way, that the calculated total pressure curve agrees best with the one measured.
3. Calculate y_1 and y_2, using the new values for A through D.
4. Substitute these vapour phase mole fractions and proceed with 2, as long as there is no agreement in subsequent estimates for y_1 and y_2.

Usually, three or four iterations are sufficient [114].

7.3 Phase envelop calculations using equations of state

In many engineering problems, equations of state are used for modelling and predicting fluid phase equilibria. The use of a suitable equation of state has some advantages over methods such as Barker's method [107-111] or other common techniques for modelling equilibria. Probably the most important ones are

1. many equations of state are capable of representing the components in the system in the phases present simultaneously;
2. most cubic and higher-order equations of state produce reasonable estimates, even far beyond regions where experimental data are available.

The calculation procedure for obtaining the system variables of a multicomponent system involves the solution of equations that are strongly non-linear. As a result, an iterative procedure is required.

The basic equations 7.1-1 and 7.1-2 are still valid. The first difference is observed in implementing equation 7.1-2. The equations of state used in this study are all capable of representing more phases simultaneously. So, rather than having two separate expressions for the liquid and vapour phase, there is only one basic relationship between the fugacity coefficient ϕ_i and the fugacity f_i

$$\phi_i^L = \frac{f_i^L}{x_i P}$$
$$\phi_i^V = \frac{f_i^V}{y_i P} \qquad 7.3\text{-}1$$

where the superscript L denotes the liquid phase and the superscript V denotes the vapour phase. Since at vapour-liquid equilibrium the fugacities of both phases, as well as the pressures of both phases are equal, it follows

$$K_i = \frac{\phi_i^L}{\phi_i^V} \qquad 7.3\text{-}2$$

Equation 7.3-2 is the result of substituting equation 7.3-1 into equation 7.1-1. If it is assumed that the equation of state is pressure-explicit, the fugacity coefficients can be calculated from the relationships already given in chapter 4. Recalling (see also equation 4.1-18),

$$RT\ln\phi_i^L = \int_{V^L}^{\infty}\left[\left(\frac{\partial P}{\partial n_i}\right)_{T,V,n_j} - \frac{RT}{V}\right]dV - RT\ln Z^L$$
$$RT\ln\phi_i^V = \int_{V^V}^{\infty}\left[\left(\frac{\partial P}{\partial n_i}\right)_{T,V,n_j} - \frac{RT}{V}\right]dV - RT\ln Z^V \qquad 7.3\text{-}3$$

where the compressibility factor is given by equation 4.1-19 for both phases. The differentiation of P with respect to n_i is quite straight forward.

The algorithm for the calculation of the vapour phase composition (y_i) and system pressure (P) from the liquid phase composition (x_i) and system temperature is outlined in figure 7.3-1. This procedure has been implemented, as it is in agreement with the experimental work done on two binary systems in this work. The vapour pressure was measured as a function of the temperature and composition.

The computational procedure involves some strongly non-linear equations, and so an iterative procedure is required. The second box in figure 7.3-1 calculates the first estimate for the system pressure. For this estimation, the vapour phase composition is set equal to the liquid phase composition, and the pressure is calculated if the mixture would be ideal.

Then, for all components, K_i is set to unity. Now the vapour phase composition can be computed (next step in figure 7.3-1). For the first iteration, y_i equals x_i, as all K_i were set to unity. Then the sum of all mole fractions of the vapour phase is calculated. This sum (denoted by Σy) is used in the next step of the procedure to compute a new estimate for the system pressure. After calculating Σy, all mole fractions of the vapour phase are normalised again to unity.

In the next step, the current value of the system pressure is kept for convergence checking (P_{old}). The new estimate for the system pressure is calculated with use of Σy. If the pressure difference is smaller than 10^{-4} Pa, then the procedure is converged and the final results (y_i and P) have been obtained.

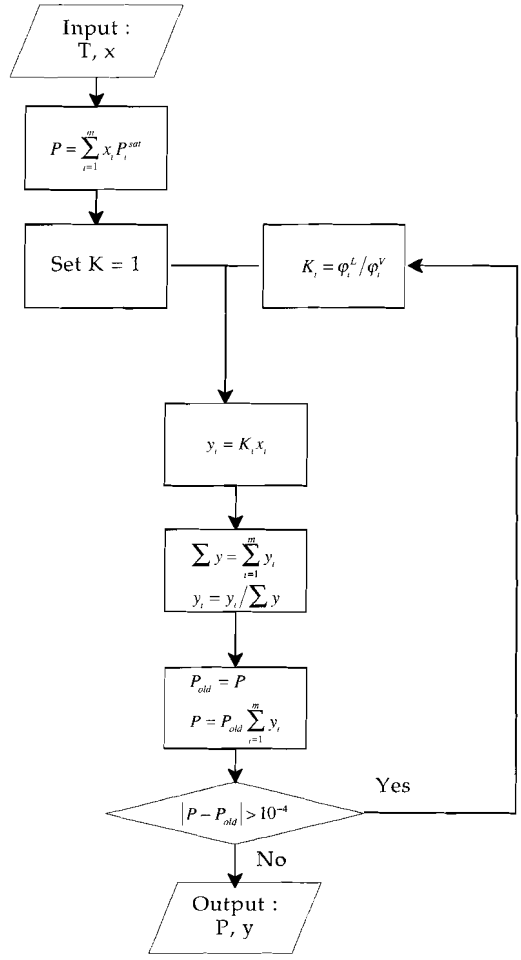

Figure 7.3-1 : Bubble point T-algorithm [118]

If not, then the values of K_i are computed again. For all iterations after the first one, the equation of state is used for this calculation.

7.4 Soave-Redlich-Kwong equation of state

The Soave-Redlich-Kwong equation of state is widely used for representing the properties of fluid mixtures. For coal liquids, even a correlation exists between the parameters of the equation of state and spectroscopic data, as will be discussed

shortly. The Soave-Redlich-Kwong equation of state is based on the perturbation term of Van der Waals. The equation of state reads as follows

$$P = \frac{RT}{V-b} - \frac{a}{V(V+b)} \qquad 7.4\text{-}1$$

For mixtures, usually the following mixing rules are used

$$a_M = \sum_{i=1}^{m}\sum_{j=1}^{m} x_i x_j a_{ij}$$
$$b_M = \sum_{i=1}^{m}\sum_{j=1}^{m} x_i x_j b_{ij} \qquad 7.4\text{-}2$$

where the subscript M denotes the mixture with m components. x_i denotes the mole fraction of component i. The coefficients a_{ij} and b_{ij} represent the coefficients of the components in the mixture. For i = j, these coefficients are the coefficients of the pure component i. For i ≠j, these coefficients account for the interaction between i and j. For the Soave-Redlich-Kwong equation of state, the expressions read as follows

$$a_{ij} = \left(1-k_{ij}^{a}\right)\sqrt{a_{ii}a_{jj}}$$
$$b_{ij} = \left(1-k_{ij}^{b}\right)\frac{b_{ii}+b_{jj}}{2} \qquad 7.4\text{-}3$$

where a_{ii}, a_{jj}, b_{ii}, and b_{jj} represent the coefficients of pure i and pure j respectively. The expressions for the pure substances are given in section 4.2, equations 4.2-6 through 4.2-8.

For the modelling of ill-defined mixtures, the binary interaction coefficients cannot be obtained. These empirical coefficients can only be obtained for simple mixtures. Leaving out the binary interaction coefficients, the expressions for a_{ij} and b_{ij} become

$$a_{ij} = \sqrt{a_{ii}a_{jj}}$$
$$b_{ij} = \frac{b_{ii}+b_{jj}}{2} \qquad 7.4\text{-}4$$

The expression for the fugacity coefficient in a mixture reads as follows [106]

$$\ln\varphi_i = \frac{b_i}{b}(Z-1) - \ln(Z-B) + \frac{A}{B}\left(\frac{b_i}{b} - 2\left(\frac{a_i}{a}\right)^{1/2}\right)\ln\left(\frac{Z+B}{Z}\right) \qquad 7.4\text{-}5$$

where

$$A = \frac{aP}{R^2T^2}$$
$$B = \frac{bP}{RT}$$

With these equations, the algorithm as shown in figure 7.3-1 was implemented.

7.5 Cubic Chain-of-Rotators equation of state

Recalling from section 4.4, the Cubic Chain-of-Rotators equation of state is given by

$$P = \frac{RT(1+0.77b/v)}{v-0.42b} + c^R \frac{0.055RTb/v}{v-0.42b} - \frac{a}{v(v+c)} - \frac{bd}{v(v+c)(v-0.42b)} \qquad 7.5\text{-}1$$

where *a*, *b*, *c*, and *d* are the coefficients of the equation of state. The expressions and temperature functions for the coefficients for pure fluids were given in section 4.4. The coefficients for a mixture have been computed in accordance with the Van der Waals one fluid theory [6]

$$\Theta_{ij} = \sum_{i=1}^{m}\sum_{j=1}^{m} z_i z_j \Theta_{ij} \qquad 7.5\text{-}2$$

where Θ equals either *a*, *b*, *c*, *d*, or c^R. Kim et.al. [6] give the following mixing rules for the coefficients

$$a_{ij} = \left(1-k_{a_{ij}}\right)\sqrt{a_{ii}a_{jj}} \qquad 7.5\text{-}3$$

$$b_{ij} = \left(\frac{b_{ii}^{1/3}+b_{jj}^{1/3}}{2}\right)^3 \qquad 7.5\text{-}4$$

$$c_{ij} = \left(1-k_{c_{ij}}\right)\left[\frac{c_{ii}+c_{jj}}{2}\right] \qquad 7.5\text{-}5$$

$$d_{ij} = \sqrt{d_{ii}d_{jj}} \qquad 7.5\text{-}6$$

$$c_{ij}^R = \frac{c_{ii}^R + c_{jj}^R}{2} \qquad 7.5\text{-}7$$

For i = j, the expressions for pure substances apply. An alternative set was given by Lin et.al. [5], where the coefficients *a* and *b* had interaction parameters. The interaction coefficients have not been used in this work, because they cannot be determined for mixtures with a large number of components. So, equations 7.5-3 and 7.5-6 reduce to

$$a_{ij} = \sqrt{a_{ii}a_{jj}} \qquad 7.5\text{-}8$$

$$c_{ij} = \frac{c_{ii}+c_{jj}}{2} \qquad 7.5\text{-}9$$

The expression for the fugacity coefficient of the Cubic Chain-of-Rotators equation of state is very complex. Without derivation, the expression reads as follows [5]

$$\ln\varphi_i = -\ln Z - \frac{0.11\left(\sum \eta_k c_{ik}^R - c^R\right) + 1.19 + 0.055c^R}{0.42}\ln\frac{v-0.42b}{v} +$$
$$\frac{(1.19+0.055c^R)b_M'}{v-0.42b} + \left[\frac{2\sum \eta_k a_{ik}}{cRT} - \frac{ac_M'}{c^2RT}\right]\ln\frac{v}{v+c} - \frac{ac_M'}{cRT(v+c)} +$$
$$\left[\frac{db_M + 2b\sum \eta_k d_{ik}}{c+0.42b} - bd\frac{c_M + 0.42b_M}{(c+0.42b)^2}\right]\left[\frac{1}{0.42bRT}\ln\frac{v-0.42b}{v} - \frac{1}{cRT}\ln\frac{v}{v+c}\right] +$$
$$\frac{bdc_M'}{c(c+0.42b)RT}\left[\frac{1}{c}\ln\frac{v}{v+c} + \frac{1}{v+c}\right] - \frac{db_M}{(c+0.42b)RT}\left[\frac{1}{0.42b}\ln\frac{v-0.42b}{v} + \frac{1}{v-0.42b}\right] \qquad 7.5\text{-}10$$

where

$$b_M = 2\sum \eta_k b_{ik} - b_M \qquad 7.5\text{-}11$$

$$c_M' = 2\sum \eta_k c_{ik} - c_M \qquad 7.5\text{-}12$$

$$d_M' = 2\sum \eta_k d_{ik} - d_M \qquad 7.5\text{-}13$$

In equations 7.5-10 through 7.5-13, η_i denotes the mole fraction of component *i*. For the vapour phase, η_i equals y_i, whereas for the liquid phase η_i equals x_i.

7.6 Experiments

In the literature, numerous systems relevant to coal liquids are found. Especially systems that are highly asymmetric, such as systems containing hydrogen, have been investigated extensively. The performance of the Cubic Chain-of-Rotators equation of state for many of these systems has also been reported [4-6,86-87].

Therefore, based on the work of pure substances, two moderate asymmetric binary mixtures have been investigated. These model systems are typical for coal fluids, as can be seen from the GC/MS-results of the Point of Ayr oil, that will be discussed in chapter 10.

For the measurement of the total vapour pressure as a function of temperature and liquid composition, the same apparatus was used as for the pure substances. The measurement procedure was as follows. The two components of a mixture were put into the sample container of the vapour pressure measurement apparatus. The composition was calculated from the weights of the two components.

A measurement runs as follows. The sample container is evacuated for a short time in order to remove air. Then the first run was made by the procedure outlined in chapter 5. In order to maintain the composition of the mixture as good as possible, the time for evacuation of the sample between two runs was kept very short (about 20 seconds), after the mixture was cooled down to about room temperature. Then a second run was carried out. In all cases, the results from the first and second runs agreed within experimental error. The sample weight was determined after measurement. Although some material was lost, the contribution of the change in liquid composition was small in comparison to the measurement uncertainty of the vapour pressure measurement.

Two systems were measured. The results of the first system are shown in table 7.6-1.

Table 7.6-1 : Experimental vapour pressures for the system - toluene (1) - 1-ethylnapthalene (2)

x_1	0	0.16	0.41	0.51	0.71	1
T (K)	P (Pa)	P (Pa)	P (Pa)	P (Pa)	P (Pa)	P (Pa)
320	17	1610	4640	5420	6520	10720
325	25	1910	5570	6510	8040	13280
330	35	2255	6650	7780	9860	16330
335	50	2650	7910	9250	12010	19925
340	71	3100	9350	10930	14545	24150
345	98	3600	11000	12865	17520	29070
350	135	4175	12880	15065	20990	34780
355	185	4820	15015	17565	25025	41370
360	245	5540	17430	20330	29685	48925
365	330	6345	20150	23580	35050	57550
370	430	7240	23205	27155	41200	67350
375	560	8230	26620	31160	48220	78430
380	720	9325	30340	35620	56200	90910

The numbers on top of the columns are the liquid compositions of the mixture. Table 7.6-2 shows the results for the system toluene - 2-methoxynaphthalene.

Table 7.6-2 : Experimental vapour pressures for the system - toluene (1) - 2-methoxynapthalene (2)

x_1	0	0.18	0.39	0.52	0.67	0.89	1
T (K)	P (Pa)	P (Pa)	P (Pa)	P (Pa)	P (Pa)	P (Pa)	P (Pa)
310	1	1500	3660	4640	6320	6450	6830
315	1.8	1790	4390	5550	7580	7920	8600
320	2.7	2110	5200	6600	9040	9700	10720
325	4.2	2500	6200	7800	10700	11800	13280
330	6.3	2930	7320	9170	12650	14300	16330
335	10	3420	8600	10750	14850	17200	19925
340	14	4000	10000	12500	17350	20600	24150
345	21	4600	11700	14500	20200	24500	29070
350	30	5300	13500	16800	23400	29000	34780
355	44	6100	15600	19300	27000	34200	41370
360	60	7000	18000	22100	31000	40100	48925
365	85	7930	20500	25300	35500	46900	57550
370	120	9000	53400	28800	40500	54500	67350
375	165	10200	26600	32600	46000	63200	78430
380	230	11500	30100	36900	52000	73000	90910
385	310	21900	34000	41500	58800	83900	105250

7.7 Correlation of the binary systems with equations of state

The experimental results have been correlated to both the Soave-Redlich-Kwong equation of state (SRK) and the Cubic Chain-of-Rotators equation of state (CCOR). The method of Barker was implemented as well, but due to the fact that the system

is very asymmetric, the optimisation procedure did not converge. The implementation of Barker's method was verified by means of the data for the system cyclopentane-benzene, as given by Hermsen and Prausnitz [109]. For this system, the implementation worked well.

Another probable reason why Barker's data reduction method failed was probably the use of the virial equation of state to represent the vapour phase imperfections. The reason for implementing the virial equation of state was to have a method completely independent from cubic equations of state for the determination of the vapour phase composition.

The experimental data as presented in tables 7.6-1 and 7.6-2 were correlated to both the SRK and the CCOR. The results of these correlations are shown in appendix VII. Tables 7.7-1 and 7.7-2 show the correlation results for the system toluene - 1-ethylnaphthalene for both the SRK and the CCOR at 380 K. The compositions of the vapour phase as computed by the equations of state agree well, and so do the K-factors. From the vapour phase composition (y is by definition the concentration of component, in this case toluene), it can be seen that the system is very asymmetric, and therefore not likely to occur in a fractionated oil. The system is however representative for coal oils, with very high contents of aromatic species.

Table 7.7-1 : Toluene - 1-ethylnaphthalene (SRK) at T = 380 K

T (K)	x	y	K	P_{exp} (Pa)	P_{calc} (Pa)	P_{exp}-P_{calc} (Pa)	AAD
380	0.16	0.9445	5.903	9325	15408	-6083	0.652
380	0.41	0.9840	2.400	30340	38214	-7874	0.260
380	0.51	0.9892	1.940	35620	47375	-11755	0.330
380	0.71	0.9953	1.402	56200	65634	-9434	0.168

Table 7.7-2 : Toluene - 1-ethylnaphthalene (CCOR) at T = 380 K

T (K)	x	y	K	P_{exp} (Pa)	P_{calc} (Pa)	P_{exp}-P_{calc} (Pa)	AAD
380	0.16	0.9584	5.990	9325	19137	-9812	1.052
380	0.41	0.9862	2.405	30340	44003	-13663	0.450
380	0.51	0.9899	1.941	35620	52724	-17104	0.480
380	0.71	0.9946	1.401	56200	68256	-12056	0.215

The correlation results of the system toluene - 2-methoxynaphthalene resembles closely those of the system toluene - 1-ethylnaphthalene. The correlation results are shown in tables 7.7-3 and 7.7-4, at a temperature of 310 K. The results at other temperatures are given in appendix VII. Again, the vapour phase compositions and K-factors calculated by the two equations of state agree well.

Table 7.7-3 : Toluene - 2-methoxynaphthalene (SRK) at T = 310 K

T (K)	x	y	K	P_{exp} (Pa)	P_{calc} (Pa)	P_{exp}-P_{calc} (Pa)	AAD
310	0.18	0.9963	5.535	1500	1308	192	0.128
310	0.39	0.9987	2.561	3660	2811	849	0.232
310	0.52	0.9992	1.922	4640	3721	919	0.198
310	0.67	0.9996	1.492	6320	4743	1577	0.250
310	0.89	0.9999	1.123	6450	6201	249	0.039

Table 7.7-4 : Toluene - 2-methoxynaphthalene (CCOR) at T = 310 K

T (K)	x	y	K	P_{exp} (Pa)	P_{calc} (Pa)	P_{exp}-P_{calc} (Pa)	AAD
310	0.18	0.9980	5.544	1500	1719	-219	0.146
310	0.39	0.9992	2.562	3660	3362	298	0.081
310	0.52	0.9995	1.922	4640	4193	447	0.096
310	0.67	0.9996	1.492	6320	4995	1325	0.210
310	0.89	0.9999	1.123	6450	5998	452	0.070

In order to assess the capabilities of the equations of state, the vapour phase composition or the K-factors are unsuitable, for two reasons. First, no experimental K-factors were obtained. The second reason is less obvious. The goodness of correlation of a system is best analysed by using the vapour pressure. This parameter is the most sensitive one towards the model used [106]. The AAD, computed as the absolute difference between the calculated and vapour pressure measured, divided by the experimental vapour pressure is plotted for both systems in figures 7.7-1 and 7.7-2.

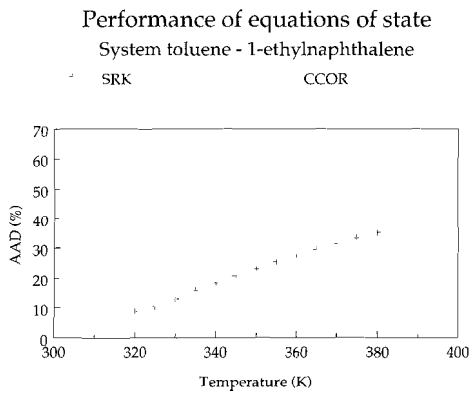

Figure 7.7-1 : Performance of equations of state in modelling toluene - 1-ethylnaphthalene

From figure 7.7-1, it can be seen that the performance of the CCOR is worse than that of the SRK at all temperatures. A possible explanation can be that the repulsive term of the CCOR is not very well suited for mixtures. The repulsive term of the CCOR is a fitting of the hard sphere equation of state of Carnahan and Starling [6]. From this equation of state, it is known that its performance in describing mixtures of hard spheres is not too well. Boublik [119] and Mansoori et.al. [120] have modified the Carnahan-Starling equation of state in order to improve the capabilities of this equation of state in modelling mixtures. This modification has found application in numerous equations of state based on the Carnahan-Starling equation of state, such as the equation of state of Aly et.al. [103] and that of Dohrn and Prausnitz [121].

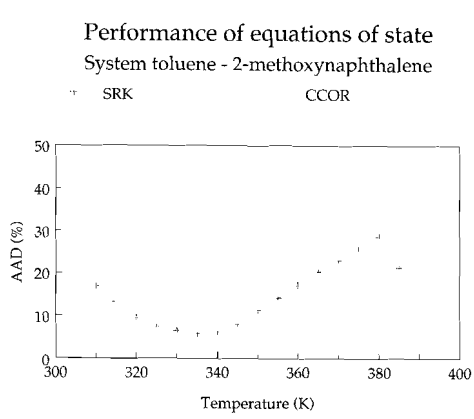

Figure 7.7-2 : Performance of equations of state in modelling toluene - 2-methoxynaphthalene

Probably a modification of the mixing rules in a similar manner as carried out by Boublik and Mansoori for the hard spheres equation of state of Carnahan and Starling would solve this problem. In order to improve the correlation performance, the *k*-coefficients in the mixing rules of the CCOR and SRK, as shown in sections 7.4 and 7.5. These coefficients do however not contribute to the understanding of these mixtures, and they are useless in modelling ill-defined mixtures.

The results of the system toluene 2-methoxynaphthalene have been plotted in figure 7.7-2. The performance of the CCOR is better for the data sets at 310 K and 315 K, about equal at 320 K, and worse for T > 320 K, when compared to the results of the Soave-Redlich-Kwong equation of state.

8. EXPERIMENTS ON AN EXXON COAL LIQUID

8.1 Sample procurement and experimental programme

The Exxon oil was obtained from the liquefaction plant in Wilsonville (USA), and is a recycle oil of that utility. About 5 dm^3 of oil were available for measurements and experiments, which proved to be very useful.

Thermodynamic measurements can only take place when it has been verified that the sample is sufficiently stable. The stability of the coal liquids has been verified by means of differential scanning calorimetry. The thermodynamic measurements comprise the measurement of the vapour pressure and heat capacity as functions of temperature.

In order to determine the average properties of the mixture, the average molecular weight, the elemental composition, and the relative concentration levels of the functional groups should be determined (see also the general introduction in chapter 1).

As a result, the experimental programme involves

1. thermal stability verification
2. vapour pressure measurement
3. heat capacity measurement
4. elemental analysis
5. GC/MS and HPLC-analysis for the determination of main components
6. Infrared spectroscopy
7. ^{1}H-NMR and ^{13}C-NMR spectroscopy

8.2 Thermal stability

The thermal stability of a coal liquid should be verified prior to performing thermodynamic measurements. It is no use measuring the vapour pressure or heat capacity on a material that is not stable. The thermal stability was verified between room temperature and about 350 C by means of differential scanning calorimetry (DSC). The measurements were performed on a DSC from Seiko, type DSC 120.

The DSC-measurement indicated that the oil was sufficiently stable in order to perform other measurements. The results of this measurement were the same as for the heat capacity measurement, shown in section 8.4.

8.3 Vapour pressure measurements

The vapour pressure measurements of the Exxon oil turned out to be rather complicated. Much experimental effort was needed in order to obtain the best estimate of the vapour pressure of the oil. The equipment that was used for the vapour pressure measurements was the same as for the pure substances and binary mixtures.

The first measurement procedure tried was the procedure that lead to acceptable results for pure substances. This procedure involves an evacuation of the sample container between runs and prior to the first run. The sample container was filled under nitrogen in order to prevent reactions with air oxygen, either during filling of the sample container or during measurements. The results of this procedure were unsatisfactory, because the vapour pressure of the oil decreased steadily as a function of the run number.

The first modification made to the procedure was to shorten the time intervals of evacuation, and leaving out the evacuation after placement of the sample container. The results of this measurement procedure are shown in figure 8.3-1. The results for the first run are more or less typical for this measurement procedure. During the first cycle, the pressure drops as a function of the temperature. This is clearly due to the fact that gases are solved in the oil and are released during measurement.

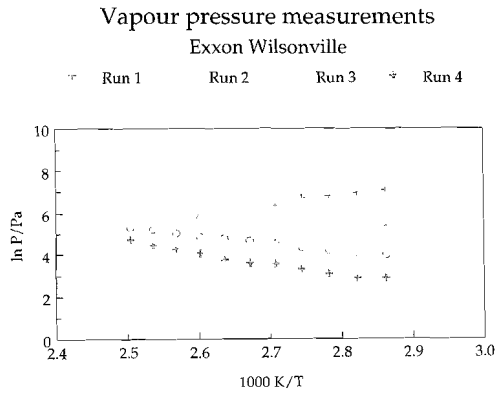

Figure 8.3-1 : Vapour pressure measurement of Exxon oil with measurement procedure for pure substances

Another feature of this procedure is that the vapour pressure steadily decreases between runs. This is shown clearly in figure 8.3-1. The differences in vapour pressure between runs is considerably greater than experimental uncertainty.

With a new sample, and very short intervals of evacuation of the sample container, the results of figure 8.3-2 were obtained. The sample was evacuated for about 15 minutes at room temperature in order to remove solved gases. The results of run 3 and 4 agree within experimental uncertainty. However, there is still a tendency that the vapour pressure decreases as a function of the run number. Furthermore, it was suspected that this procedure caused a serious loss of volatile sub-

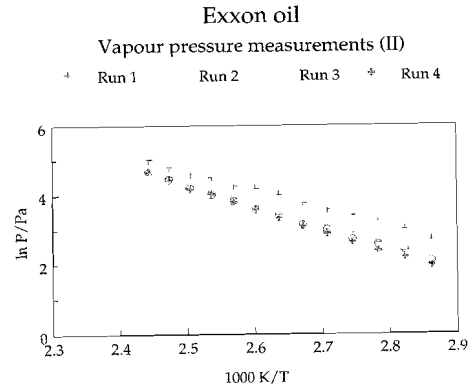

Figure 8.3-2 : Vapour pressure measurement of Exxon oil, second procedure

stances from the mixture.

These two weaknesses in the experimental method had to be removed. A new series of experiments was carried out. The main difference with the procedure used for obtaining the results shown in figure 8.3-2 is that the sample container is exposed to vacuum for about 15 seconds at room temperature in order to remove most of the gases. After that, the first measurement is started. After the first complete run, the sample is cooled down to room temperature and exposed to vacuum for about 15 seconds again. Then 2 more runs follow.

The results of this procedure for the Exxon oil are shown in figure 8.3-3. The results from the first run are not shown. The results from the second and third run agree rather well, although at higher temperatures, the difference in vapour pressure between run 2 and run 3 increases. The measured vapour pressures are given in table 8.3-1.

Table 8.3-1 : Experimental vapour pressure of Exxon oil

T/K	P/Pa Run #2	P/Pa Run #3
315.70	2200	2100
320.75	2980	2750
325.80	3690	3400
330.84	4460	3900
335.88	5280	4700
340.93	6100	5400
345.97	7000	6100
351.02	8000	6700
356.07	8800	7700
361.12	9800	8900
366.15	10900	9700
371.23	12000	10600
376.25	13100	11600
381.33	14200	12600

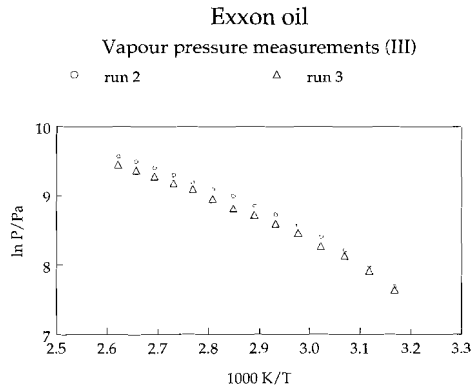

Figure 8.3-3 : Vapour pressure measurement of Exxon oil with optimised measurement method

From the results in table 8.3-1, it can be seen that the vapour pressures measured in run #3 are lower than those of run #2. The relative pressure difference is about 5%. The difference between fitted and measured data for pure substances was typically of the order of 2-3%. The measurement of the vapour pressure of complex mixtures at vapour-liquid equilibrium is more complex than that of pure substances. Therefore, it may be assumed that the vapour pressure of run #2 is the best estimate for the saturation pressure of the Exxon oil as a function of the temperature. The results from run #2 are better estimates than the average of both runs, because between run #2 and run #3, some loss of volatile components is inevitable. Taking this fact into account, the best result for the mixture is that of the run with the lowest run number.

8.4 Heat capacity measurement

For a heat capacity determination using a Differential Scanning Calorimeter (DSC), three experiments must be performed. All experiments are performed using an empty sample container as a reference. The first experiment is performed using an empty sample container; thus this experiment is performed using two empty containers. For the second experiment the same sample container is filled with an amount of sapphire (which is a standard reference material for heat capacity measurements). For the third experiment the sapphire is removed from the sample container, after which it is filled with the sample to be investigated. All experiments are performed under the same experimental conditions and using the same temperature programme.

The result from the experiment which was performed with two empty sample containers is used to correct the other two results for small systematic errors such as asymmetry of the instrument design and small differences between sample and reference sample containers. This is done by subtracting this result from the other two results. The results of this exercise are two corrected DSC-curves, one for sapphire and one for the sample under investigation.

The heat capacity of the sample under investigation may be calculated using the following equation:

$$C_{p,s}(T) = \left(\frac{m_r}{m_s}\right)\left(\frac{\Phi_s(T)}{\Phi_r(T)}\right)C_{p,r}(T) \qquad 8.4\text{-}1$$

where $C_{p,s}(T)$ and $C_{p,r}(T)$ are the sample and sapphire heat capacities at temperature T, m_s and m_r are the sample and sapphire masses and $\Phi_s(T)$ and $\Phi_r(T)$ are the net heat-flow signals at temperature T for the sample and sapphire measurements, respectively. All calculations are performed with the software which was supplied with the instrument.

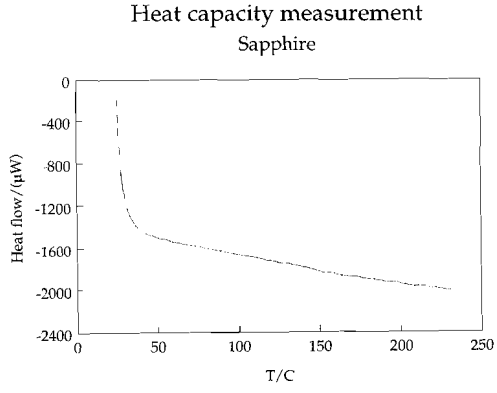

Figure 8.4-1 : Net DSC result of the measurement on synthetic Sapphire

It should be noted that for substances with a non negligible vapour pressure instead of the heat capacity at constant pressure C_p the heat capacity at the saturated vapour pressure C_s is measured. $C_s \geq C_p$, because at a higher temperature the vapour pressure is higher; this implies that part of the substance has evaporated. The heat which is associated with this evaporation is included in C_s. Normally the difference between C_s and C_p is small, because the volume of the hermetically sealed

sample containers is small so that only very small amounts of substance can evaporate.

The experiments were performed using a Seiko DSC-120 instrument. For all experiments an empty Aluminium sample container was used as a reference. This sample container had a mass of 363.95 mg. The sample container which was used for the standard reference material (Sapphire) and for the sample had a mass of 364.62 mg. The internal volume of the sample containers is about 70 µl. As described at the beginning of this section, three experiments were performed: the first with the two empty sample containers, the second with an amount of 117.46 mg Sapphire and the third with an amount of 13.27 mg coal liquid. During each experiment the calorimeter was heated from 25 to 235 C with a rate of 1 C min^{-1}.

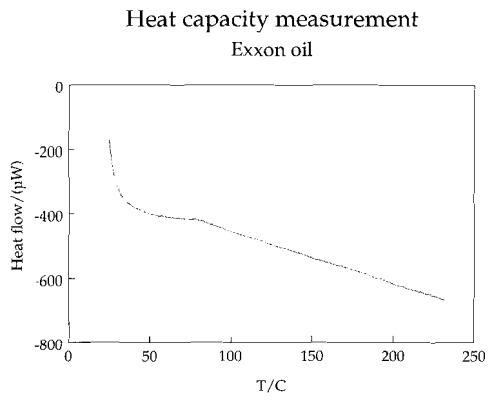

Figure 8.4-3 : Net DSC result of the measurement on the Exxon coal liquid

The DSC-curve which was recorded during the first experiment (with the two empty sample containers) was subtracted from the other two curves to obtain the net results. These net results are plotted in the figures 8.4-1 and 8.4-2.

The net results were used to calculate the heat capacity of the sample as indicated in the previous section. The experimental heat capacities are presented in table 8.4-1 and plotted as a function of temperature in figure 8.4-3.

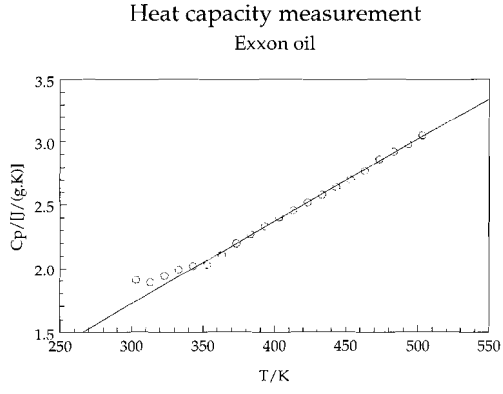

Figure 8.4-2 : Heat capacity of Coal Liquid (Exxon) as a function of Temperature. O : Experimental results; drawn line: best linear fit result.

From figure 8.4-3 it is observed that at temperatures above about 100 C (373 K) the heat capacity linearly depends on temperature. At temperatures lower than 80 C (353 K) probably a small endothermic effect interfered with the measurements. In figure 8.4-3, the linear function which represents the best

fit of the experimental results at temperatures above 100 C (373 K) is also plotted. This function may be described with the following equation

$$\frac{C_P(T)}{J/gK} = -0.225 + 6.492 \cdot 10^{-3}(T/K) \qquad 8.4\text{-}2$$

Table 8.4-1 : Experimental heat capacities of Coal Liquid (Exxon) as a function of temperature

T (K)	C_P (J g^{-1} K^{-1})	T (K)	C_P (J g^{-1} K^{-1})
303.15	1.91	413.15	2.46
313.15	1.89	423.15	2.52
323.15	1.94	433.15	2.58
333.15	1.99	443.15	2.64
343.15	2.02	453.15	2.70
353.15	2.03	463.15	2.77
363.15	2.11	473.15	2.86
373.15	2.20	483.15	2.92
383.15	2.27	493.15	2.98
393.15	2.33	503.15	3.05
403.15	2.40		

8.5 Elemental analysis

The elemental composition was determined at the laboratory of RWTÜV Anlagentechnik GmbH in Essen (Germany). The carbon, nitrogen, and hydrogen contents have been determined by means of an element analyser of Perkin Elmer 2400. The oxygen content is determined with a modified CS-tube oven (Ströhlein) equipped with a CO-NDIR detector from UNOR. For these determinations, Acetanilide p.A. (Merck) was used as measurement standard.

Table 8.5-1 : Elemental composition of Exxon coal liquid

Element	concentration (weight %)
C	88.7
H	9.54
N	0.53
O	1.2
S	0.02
Cl	< 0.02

The chlorine and sulphur contents were determined in accordance with DIN 51577-1 (total chlorine content) and DIN 51400-2 (total sulphur content) respectively. A sample was combusted at a temperature of 1000 C in a flow of oxygen. The detection followed from ion chromatography (IC), type DIONEX IC 2000. Synthetic chloride and sulphate solutions, prepared from standard solutions from Merck, were used for the quantitative determination of the two elements.

The elemental composition of a coal liquid is one of the basic parameters for linking spectroscopic data to an equation of state. The elemental composition of the Exxon oil is given in table 8.5-1.

From the results in table 8.5-1, it follows that the H:C ratio is 1.3 (mole:mole). The oxygen content is relatively high, and the concentration levels of sulphur and chlo-

rine are low. For the properties of a coal liquid, the nitrogen and oxygen contents are of special interest, as they may be present in H-bonding groups, such as amine, acid amine, carboxylic acid, and hydroxyl.

8.6 ^{1}H-NMR and ^{13}C-NMR

The next step in the composition of the "average molecule" in an ill-defined mixture is to determine the fractions of different types of hydrogen and carbon. The thermodynamic properties of a fluid are not only a function of the elemental composition, but they also depend on the aromaticity, the number of olefinic groups, etc..

A convenient way to get information on the different types of hydrogen and carbon in a hydrocarbon is the use of nuclear magnetic resonance spectroscopy (NMR). For the differentiation of carbon, one can use ^{13}C-NMR. For hydrogen, ^{1}H-NMR can be used. The shift in resonance of ^{13}C and ^{1}H is measured against a standard, often TMS (tetramethyl silan, $Si(CH_3)_4$). The ^{1}H-NMR and ^{13}C-NMR spectra were measured using a 300 MHz NMR Spectrometer (Varian). The determinations were carried out with a deuterated solute.

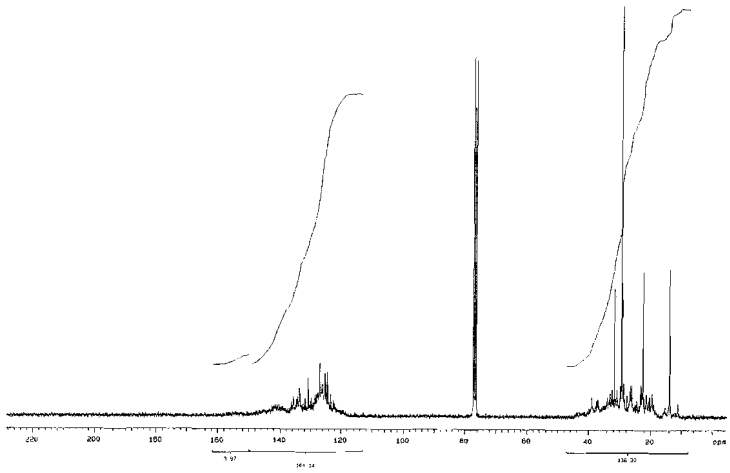

Figure 8.6-1 : ^{13}C-NMR spectrum of Exxon oil

The ^{13}C-NMR-spectrum of the Exxon oil is shown in figure 9.5-1. Two types of carbon can be identified, in fact aromatic carbon (δ = 110-150 ppm), and aliphatic carbon (δ = 10-50 ppm).

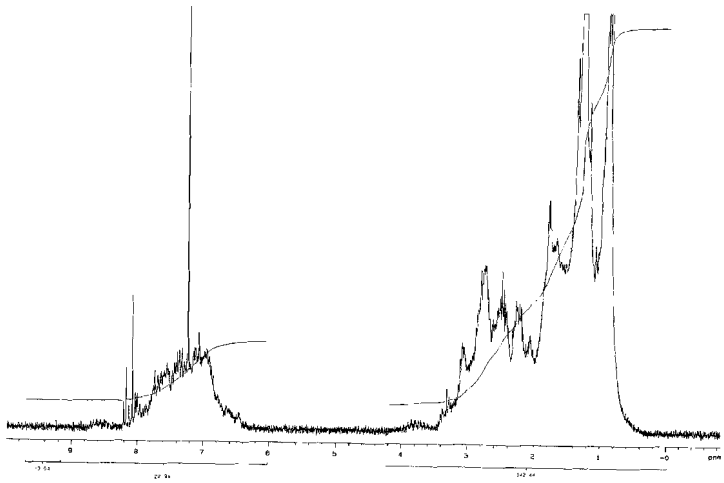

Figure 8.6-2: ^{1}H-NMR spectrum of Exxon oil

From the spectrum of ^{1}H-NMR (figure 8.6-2), it can be seen that only aromatic hydrogen and aliphatic hydrogen are present. From the NMR spectra, the following data have been obtained

- The hydrogen distribution is 13.8% aromatic and 86.2% saturated
- The carbon distribution is 44.3% aromatic (from which 1.6% alkyl-substituted), and 55.7% is saturated
- No olefins are found in the oil

8.7 IR

The IR-spectra have been measured with a FT-IR spectrofotometer (Nicolet, 205 FT-IR) at RWTÜV in Essen (D). IR-spectroscopy is of particular interest for the determination of the amounts of polar groups in the oil, such as hydroxyl, amine, and carboxylic acid.

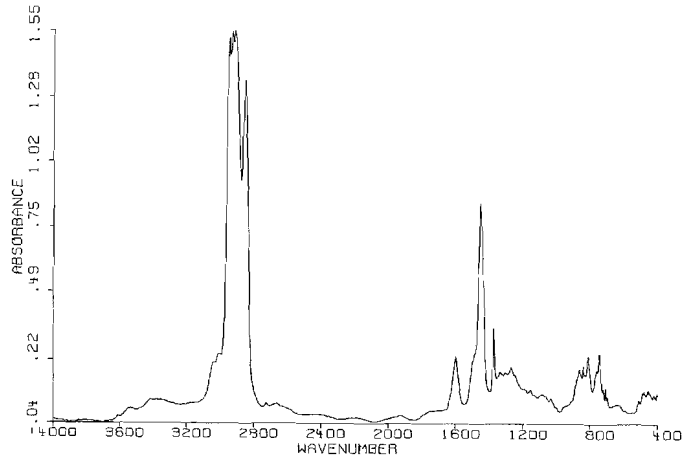

Figure 8.7-1 : IR spectrum of the Exxon oil

From the spectrum, it can be seen that the nitrogen and oxygen present are mainly present in the form of hydroxyl and amine (stretch vibrations > 3200 cm^{-1}). Due to the fact, that there is no peak around 1700 cm^{-1}, it may be concluded that no carbonyl groups are present. This is not surprising, as most liquefaction processes include a hydrocracking or hydrogenation step. In such a step, carbonyl and carboxylic acid groups are readily reduced to alcohols.

8.8 Gas Chromatography and PAH-analysis

The oil was investigated by gas chromatography in order to identify light chlorated hydrocarbons and aromates with a single ring. The gaschromatographic analysis, that was used for the determination of benzene and its derivates, as well as aliphatics C_9-C_{23} were measured on a GC/FID[1] (Hewlett-Packard HP-5890), with a Ultral 2, 25 m capillary column (Hewlett-Packard), with a film thickness of 0.3 µm and a inner diameter of 0.2 mm. The measurement was carried out with toluene-D_8 (Merck) as standard.

Table 8.8-1 : Results from gas chromatography (monocyclic aromates)

Substance	Concentration (mg/kg)
Benzene	< 0.1
Toluene	28
Ethylbenzene	2.6
o+m+p-Xylene	35
1,2,3-Trimethylbenzene	< 0.1
1,2,4-Trimethylbenzene	27
1,3,5-Trimethylbenzene	< 0.1
1,2,3,5-Tetramethylbenzene	57
Pyridine	< 0.1
Isopropylbenzene	< 0.1
n-Alkanes C_9-C_{25}	200 10^3

The light haloginated hydrocarbons have been determined on a GC/ECD[2] (Siemens SiChromat 1), equipped with a capillary column DB 624, 30 meter in length, 1.8 µm film thickness and an inner diameter of 0.325 mm.

No light hydrocarbons were found in concentration levels above the determination limit. For the other hydrocarbons, the following results were obtained (table 8.8-1).

Several heavy aromatic hydrocarbons have been identified by high performance liquid chromatography (HPLC). For the determination of polycyclic aromatic hydrocarbons (PAHs), a high performance liquid chromatography (HPLC) system (Hewlett-Packard HP 1090) equipped with both a DAD[3] and FCD 1046A. The column is from Vydac, type 201 TP 54, with C18 as column packing. A range of measurement standards has been used: naphthalene (Dr. Ehrenstorfer, certified 99.9%), acenaphthylene (Dr. Ehrenstorfer, 95%), fluorene (Dr. Ehrenstorfer, 99%), phenanthrene

Table 8.8-2 : Results from gas chromatography (polycyclic aromates)

Substance	Concentration (mg/kg)
Naphthalene	560
Acenaphthylene	330
Acenaphthene	740
Fluorene	620
Phenanthrene	640
Anthracene	53.6
Fluoranthene	520
Pyrene	5840
Benzo(a)anthracene	1045
Chrysene	490
Benzo(b)fluoranthene	11.1
Benzo(k)fluoranthene	3.5
Benzo(a)pyrene	17.5
Dibenzo(a,h)anthracene	< 10
Benzo(g,h,i)perylene	53.9
Indeno(1,2,3-c,d)pyrene	< 10
Total PAH according to EPA	10.9 10^3

[1] FID = flame ionisation detector
[2] ECD = electric conductivity detector
[3] DAD = Diode Area Detector

(preparation), anthracene (FLUKA, puriss.), fluoranthrene (BCR[1]), pyrene (Dr. Ehrenstorfer, certified 99.3%), benz(a)anthracene (FLUKA, puriss.), chrysene (Dr. Ehrenstorfer, certified 97.9%), benzo(b)fluoranthrene (BCR), benzo(k)fluoranthrene (BCR), benzo(a)pyrene (FLUKA, pract.), dibenz(a,h)anthracene (FLUKA, puriss.), benzo(g,h,i)perylene (BCR), and Indeno(1,2,3-c,d)pyrene (BCR).

This analysis does not involve all components of the oil, but it can provide information over a selected group substances present in the oil. Table 8.4-2 lists polycyclic aromates in the Exxon oil.

8.9 Molecular weight determination

The last parameter necessary for characterisation of the "average molecular compo-

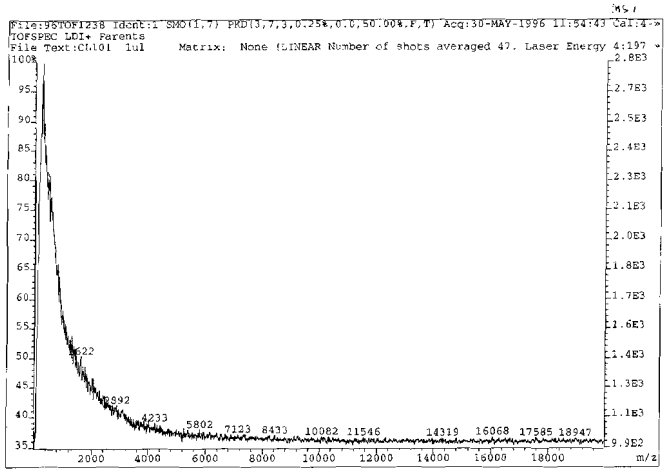

Figure 8.9-1 :MALDI-MS spectrum in absence of a matrix for the Exxon oil

sition of a coal oil is the determination of the average molecular weight. This property can be computed from the molecular weight distribution. There are several experimental techniques for the determination of the molecular weight distribution (MWD). A common technique is vapour pressure osmometry. Other techniques include various forms of mass spectrometry (MS) and size exclusion chromatography (SEC).

For the characterisation of this oil, matrix-assisted laser-desorption ionisation mass spectrometry (MALDI-MS) and size exclusion chromatography have been used. The experiments were carried out at Imperial College of Science, Technology and Medicine at the Chemical Engineering Department (London, UK).

MALDI-MS was carried out with a Fisons VG-TOFSPEC mass spectrometer with a nitrogen laser operating at 337 nm. The data systems is a VAX 4000-based system

[1] BCR = Bureau of Reference Materials of the European Communities

with OPUS software. The sample was applied to the target spot using chloroform/methanol in a 4/1-volume ratio, both in absence of matrix and in the presence of a number of matrices: sinapinic acid, 2-5,dihydrobenzoic acid (DHB), or α-cyano-

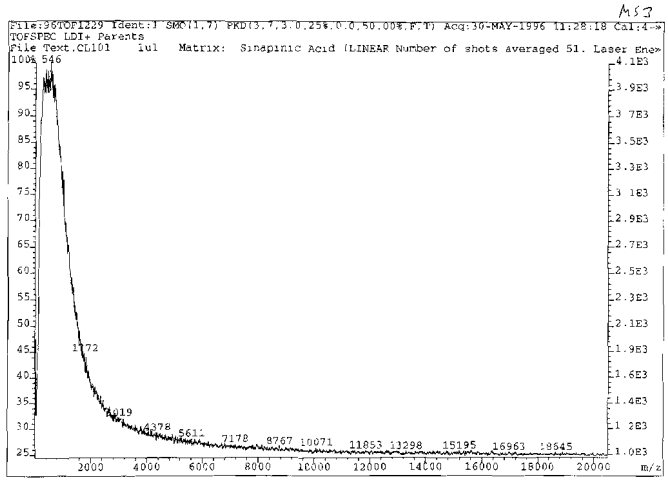

Figure 8.9-2 :MALDI-MS spectrum with sinapinic acid as matrix for the Exxon oil

4-hydroxy cinamic acid (α-cyano). In each case, two sample concentrations (sample thicknesses) were applied to the spot to indicate the effect of concentration and matrix on the spectra. Spectra were summed from approximately 50 separate laser shots [124].

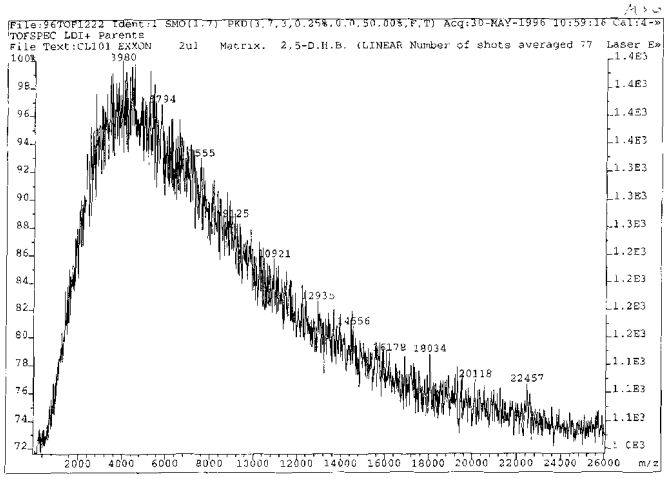

Figure 8.9-3 :MALDI-MS spectrum with 2,5-DBH as matrix for the Exxon oil

Figure 9.8-1 shows the spectrum obtained in absence of a matrix. The spectra obtained with in the presence of matrices are shown in figures 9.8-2 (sinapinic acid), 9.8-3 (2,5-DBH), and 9.8-4 (α-cyano). With MALDI-MS, high mass components in a complex matrix such as a coal oil are difficult to detect quantitatively in the presence of small molecules. These problems arise due to the fact that most of the ionisation goes preferentially to the small molecules.

The spectrum shown in figure 9.8-1 is from the low concentration sample (1 μl), in the absence of the matrix. The spectrum is better than that of the 2 μl (not shown) in a sense that the signal of the diluted sample was better. Except for the difference of relative intensity between 2000 and 6000 u, the spectra agree well. For the spectra with sinapinic acid (figure 9.8-2), the same is true. The mass envelope is broader for these spectra than for those in absence of a matrix (figure 9.8-1).

The spectra in the other two matrices, 2,5-DHB (figure 9.8-3) and α-cyano (figure 9.8-4) were better with the high-concentrated sample (2 µl). The spectrum for 2,5-DBH is extended to higher masses when compared to the 1 µl-spectrum (not shown). In this case, the upper mass exceeds 26000 u, with a continuing fall in intensity, suggesting the presence of molecules with a higher molecular weight (MW). The results obtained with α-cyano (figure 9.8-4) with the 2 µl-sample were better in the higher MW-range than those without or with sinapinic acid as matrix, but not

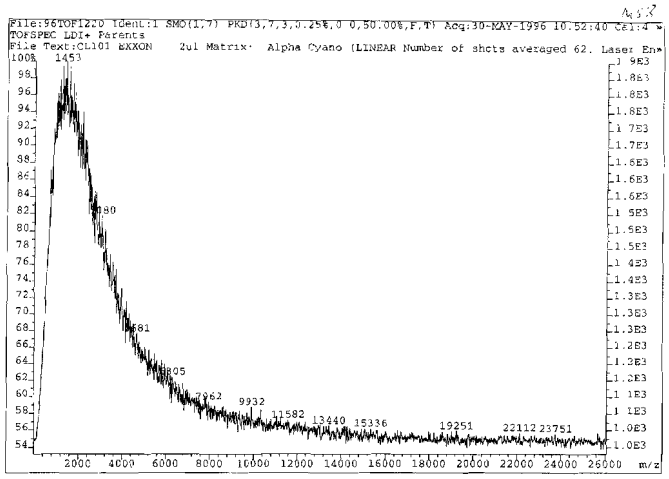

Figure 8.9-4 : MALDI-MS spectrum with α-cyano as matrix for the Exxon oil

better than the results obtained with 2,5-DBH.

It is difficult to derive an average molecular weight from the spectra. Clearly, the use of a matrix influences the properties of the MWD. The spectra obtained with a-cyano and 2,5-DBH indicate clearly that there is a fraction of molecules, that has a MW of over 26000 u. However, the most probable value for the average MW is between 1000 and 2000 u. In this range all maxims are found, and for some spectra the maximum of the MWD is below 1000 u.

The SEC-measurements were performed on two different columns, Mixed D and Mixed E. Both columns were packed with polystyrene/polydivinylbenzene polymers. The columns have different porosity ranges and the use of the Mixed D column allows separate evaluation of the material excluded from the lower mass the Mixed E column. The mass range of operation differs by an order of magnitude of polystyrene standards.

NMP (1-methyl-2-pyrrolidinone) was used as solvent. The Mixed E column was operated at 85 C and a flow rate of 0.45 ml min^{-1}. The Mixed D column was operated at 80 C and a flow rate of 0.5 ml min^{-1}. Detection was carried out at three different wave lengths in the UV-range, in fact 300, 350, and 450 nm.

The results obtained from SEC are shown in figures 9.8-5 (Mixed D) and 9.8-6 (Mixed E) respectively. Using either SEC column, the profiles at 300 and 350 nm are very similar to one another, but the profiles at 450 nm are very different. The bulk of the profile at 450 nm in either column is shifted to shorter elution times, indicating that at this wavelength, a fraction with higher molecular mass is detected than at the other wavelengths.

The porosity of the column Mixed E corresponds to an exclusion of molecules with a molar mass greater than 20 000 u (polystyrene standard), whereas for Mixed D this limit is 200 000 u. These is evidence that at every wavelength, some material is excluded from the column.

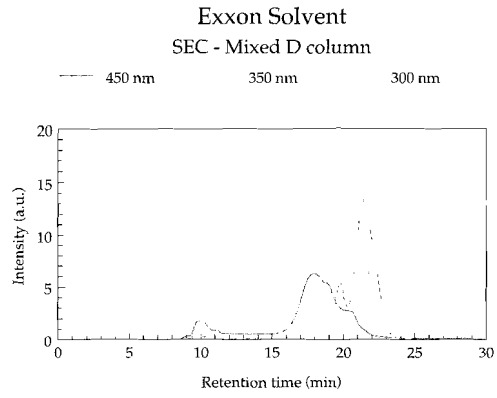

Figure 8.9-5 : SEC-chromatogram of the Exxon Solvent from the Mixed D-column

There is only a weak link between the molar masses from a coal liquid and a polystyrene standard. This is due to the fact, that the matrices are very different from one another. Especially the presence of polar functional groups may influence the elution time considerably, and thus influencing the molar mass that could be obtained from a polystyrene calibration graph. This weakness can only be resolved by preparing suitable standards, that include a certain level of polar functional groups. Another problem are possible steric effects. It may be expected that ortho-substituted benzenes behave differently than the corresponding para-

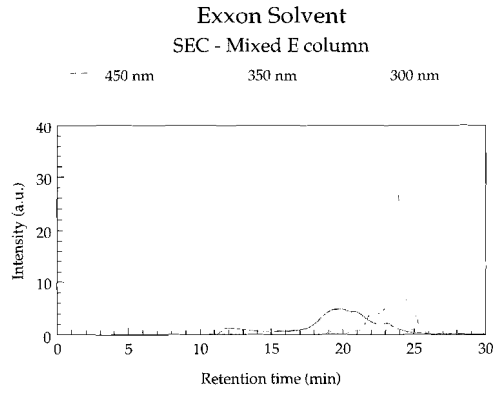

Figure 8.9-6 : SEC-chromatogram of the Exxon Solvent from the Mixed E-column

substituted ones, which would lead to a difference in molar mass (after conversion of the retention time to molar mass).

For species of higher molar mass, often of polycyclic nature, steric effects from side chains may become of less importance, as the influence on the shape of a molecule is greater for a dimethylbenzene than it is for a dimethylnaphthalene.

From the SEC measurements, it follows that there is a very wide range of molecular weights present in the Exxon liquid. The average molecular weight will be a few thousands g/mole, but this average will not be very representative for the fluid as a whole.

9. EXPERIMENTS ON A POINT OF AYR OIL

9.1 Sample procurement

From Coal Technology, Development Division (CTDD) an oil sample with a set of fractions was obtained. The oil is one of the oil samples obtained from the coal liquefier in Clwyd (United Kingdom). It cannot be stated that the oil sample is truly representative for the liquefier, but it may be assumed that the oil obtained is a reasonable approximation [122].

The oil is produced in a two-steps Liquid Solvent Extraction (LSE) process from a Point of Ayr-coal. This coal is a high volatile bituminous coal of about 38% volatile matter content (dry and ash-free basis, daf) and 0.79% vitrinite random reflection. The latter parameter is an indicator for the coal rank. A typical analysis of the coal is given in table 9.1-1.

Table 9.1-1 : Typical analysis of a Point of Ayr coal [122]

Parameter	Content
Moisture content (weight %)	1.5
Ash content (weight %)	13.5
Carbon content (weight %)	71.2
Hydrogen content (weight %)	4.8
Sulphur content (weight %)	1.8
Nitrogen content (weight %)	1.4
Chlorine content (weight %)	0.2
Crushed size range	75% less than 75 μm
	0% greater than 200 μm

The oil was removed from the hydrocracker by continuous on-line distillation. The sample represents a bulk product over a period of at least several hundred hours of operation. Therefore, it is not possible to specify the exact conditions. The oil is produced in a two-steps process. The first step is the digestion step, followed by a hydrocracking step. The approximate conditions are as follows

digestion step	solvent:coal ratio 2:1 as received pressure 15 bar temperature 435 C residence time 75 minutes
hydrocracking step	space velocity 0.8 kg/kg catalyst/hour catalyst: sulphided NiMo on alumina pressure 205 bar temperature 435 C

The digestion step in the LSE process is the conversion (extraction) of the pulverised coal in a solvent that is capable of donating hydrogen. In section 2.5 of this work, the principle of this donation was explained. In order to maintain good extraction yields, it is necessary to transfer about 1 % by weight of hydrogen to the coal. The coal fragments that are produced during the thermal degradation of the coal are stabilised by the donation of hydrogen. The solvent used for the LSE process is a mix-

ture of aromatic and hydroaromatic hydrocarbons. No catalyst of hydrogen gas is used at this stage.

The residual solids, consisting of undissolved coal and mineral matter, are removed by filtration. The filtration is carried out at 300 C. The filter cake can be washed with a light oil (usually called wash oil) to recover coal liquids still present in the cake. The product from filtration is a solids-free liquid filtrate, known as coal solution. This filtrate is the feed for the fractionation and hydrocracking plants. The filtration step is one of the essential differences between the LSE process and other coal liquefaction processes [122].

The filtered coal solution is fractionated in vacuo to recover wash oil. The material can also be treated by thermal cracking to reduce the level of (undesired) saturated components in the solvent. This process is known as satcracking. The concentrated solution is then preheated, hydrogen is added, and it is fed to the hydrocracking reactors. The hydrocracking step must meet the following objectives

1. to hydrocrack the product, in order to produce distillate product and sufficient solvent for recycle
2. to rehydrogenate the solvent fraction
3. to maintain pitch levels in the solvent at acceptable levels

The hydrocracking is carried with use of catalyst which are similar to those used in the oil industry for the desulphurisation of heavy oil residua. The catalyst bed is kept fluidised in the reactor by feeding hydrogen and coal solution at the bottom of the reactor. The necessary velocity is maintained by recycling a high proportion of the reactor effluent to the bottom of the reactor [122].

The product spectrum contains naphtha (boiling below 180 C), middle distillate (boiling between 180 - 300 C). LPG (propane and butane) is recovered from processing off-gases. A by-product pitch stream, nominally boiling above 500 C can be taken off, although most of this material is recycled to the digestion stage as part of the solvent. In the remaining by-product streams, light hydrocarbon gases (methane and ethane mainly), and heterogases such as ammonia and hydrogensulphide are found [122].

The following samples were obtained from CTDD (table 9.1-2). Apart from the fraction VII (boiling range > 300 C), all samples were liquids and contained no visible solids. Fraction VI (270 - 300 C) was coloured deep brown-black, whereas the others were clear liquids, ranging in colour from light yellow to red-brown.

Table 9.1-2 : Samples obtained from CTDD

Fraction identification	Boiling range (C)	Yield (%)
I	< 150	14.3
II	150 - 180	7.9
III	180 - 210	18.3
IV	210 - 240	19.3
V	240 - 270	21.7
VI	270 - 300	N/A
VII	> 300	N/A

In table 9.1-2 the relative yields are given. They represent the relative amount of that fraction obtained during the distillation of the oil. For the fractions VI and VII, this was not analysed (denoted by N/A).

9.2 Stability testing and heat capacity measurements

As the coal oil and its fractions had already been distilled, it was to be expected that the fractions and the oil would be sufficiently stable. Recalling from the experiments of the Exxon oil, there was found no evidence in the DSC (differential scanning calorimetry) measurements that the oil was not thermally stable over the range of temperatures of interest for vapour pressure measurements.

Therefore, the experimental procedure was shortened after verification of the oil. The stability measurements were combined with the heat capacity measurements. The results from these heat capacity measurements, calibrated against sapphire (NIST), are shown in table 9.2-1 for all fractions.

Table 9.2-1 : Heat capacity measurements of the Point of Ayr oil (C_P in J g^{-1})

Fraction	I	II	III	IV	V	VI	VII	Oil
Boiling range (C)	< 150	150-180	180-210	210-240	240-270	270-300	> 300	
T/K								
303.15	2.25	2.44	2.16	1.91	2.00	2.18	1.84	2.45
313.15	2.37	2.52	2.20	1.97	2.05	2.19	1.90	2.53
323.15	2.43	2.55	2.24	2.02	2.09	2.22	1.98	2.57
333.15	2.46	2.56	2.26	2.03	2.11	2.22	2.06	2.60
343.15	2.50	2.59	2.30	2.06	2.14	2.25	2.15	2.64
353.15	2.56	2.65	2.35	2.12	2.19	2.31	2.16	2.68
363.15	2.63	2.71	2.42	2.17	2.25	2.39	2.18	2.74
373.15	2.72	2.79	2.49	2.22	2.30	2.46	2.24	2.81
383.15	2.79	2.84	2.55	2.28	2.36	2.54	2.28	2.87
393.15	2.85	2.89	2.60	2.32	2.39	2.59	2.34	2.93
403.15	2.90	2.95	2.66	2.36	2.44	2.65	2.38	2.98
413.15	2.97	3.00	2.70	2.42	2.49	2.70	2.43	3.04
423.15	3.04	3.06	2.76	2.49	2.55	2.77	2.47	3.09
433.15			2.81	2.53	2.60	2.82	2.53	3.14
443.15			2.88	2.59	2.64	2.87	2.57	3.20
453.15			2.94	2.63	2.69	2.90	2.62	3.25
463.15				2.67	2.73	2.97	2.66	
473.15					2.80	3.05	2.73	
483.15					2.84	3.10	2.76	
493.15						3.15	2.80	
503.15						3.20	2.84	
513.15						3.25	2.88	

The results for the fractions I (< 150 C), II (150-180 C), and III (180-210 C) are shown in figure 9.2-1. The heat capacity measurement of the oil is also plotted in figure 9.2-1. These results are plotted in the figures 9.2-2 and 9.2-3 for reference too.

The results for the fractions I-III indicate that there are no problems in stability. The C_P-curves show however, that there are some minor energy effects as a function of the temperature. A repetition of the C_P-measurement with the same sample container and the same sample indicated, that the effects are reproducible and reversible.

Similar results were also obtained for the Exxon oil, that was discussed in the previous chapter.

The heat capacity of the oil (expressed in J g^{-1} K^{-1}) is greater than that of the fractions. The heat capacity of fraction I is smaller than that of fraction II (at the same temperature), whereas the heat capacity of fraction III (expressed in J g^{-1} K^{-1}) is smaller than both the oil and the fractions I and II.

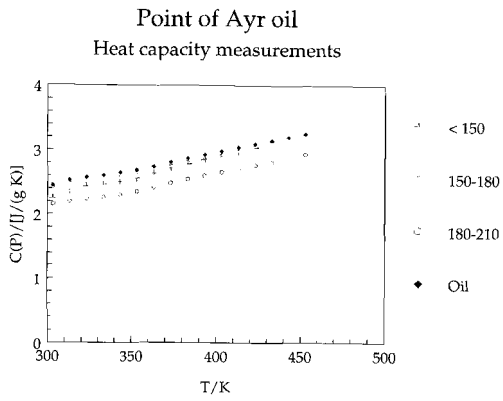

Figure 9.2-1 : Stability and heat capacity measurements of Point of Ayr oil, fractions I-III

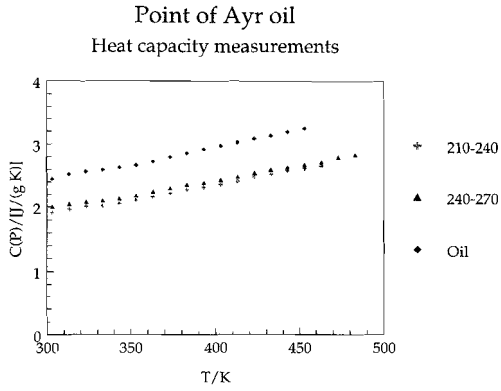

Figure 9.2-2 : Stability and heat capacity measurements of Point of Ayr oil, fractions IV and V

If the heat capacity would have been expressed in J $mole^{-1}$ K^{-1} rather than in J g^{-1} K^{-1}, then it is likely that the order of heat capacity (for a given temperature) would be in ascending order : I < II < III < Oil. The average molar weight of hydrocarbon fluids is an exponential function of the normal boiling point in first approximation [123].

The results for the fractions IV and V are shown in figure 9.2-3. The heat capacity of the fractions IV and V (expressed in J g^{-1} K^{-1}) are very close. However, taking into account that the molar weight increases exponentially with the boiling point temperature, there is a considerable difference if C_P is expressed in J $mole^{-1}$ K^{-1}.

The heat capacity measurements of the heaviest fractions (VI and VII) are shown in figure 9.2-3. The results of both fraction VI (270-300 C) and fraction VII (> 300 C) are show more small energy effects than those of figure 9.2-2. The material proved to be sufficiently stable for vapour pressure measurements and further characterisation, as these effects could be reproduced with the same sample. The effects visible are reversible and likely to occur during vapour pressure measurements as well.

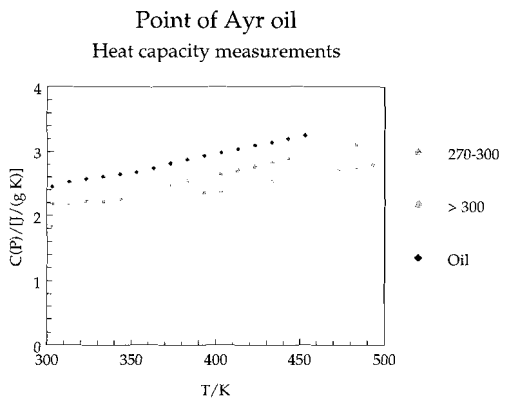

Figure 9.2-3 : Stability and heat capacity measurements of Point of Ayr oil, fractions VI and VII

9.3 Vapour pressure measurements

The main objective of the vapour pressure measurements was to obtain the best estimate for the saturation vapour pressure of the oil (or fraction) at a given temperature. In chapter 9, the development of a suitable measurement procedure was described. The protocol for the fractions of the Point of Ayr oil was as follows. The vapour pressure was measured three times as a function of the temperature. Between measurement runs #1 and #2, and between runs #2 and #3, the sample container was pumped off for a short time. If the results between runs #2 and #3 did not differ more than experimental error, the average of both runs was accepted as the vapour pressure at saturation for the mixture.

The results for the vapour pressure measurements obtained by this procedure are shown in table 9.3-1. In all cases, the vapour pressure could be measured with 3 runs. In all cases the resulting vapour pressures from the first run were significantly greater than those of runs #2 and #3.

Table 9.3-1 : Vapour pressure measurements Point of Ayr fractionated oil

Fraction	I	II	III	IV	V	VI	VII	Oil
Boiling range (C)	< 150	150-180	180-210	210-240	240-270	270-300	> 300	
T/K	P/Pa	P/Pa	P/Pa	P/Pa	P/Pa	P/Pa	P/Pa	P/Pa
320.70	8600	1450	400	250	175	120	100	11000
325.80	10700	1820	520	330	230	165	125	13000
330.83	13700	2340	730	435	290	200	150	15750
335.60	17000	2865	980	555	370	265	200	19000
340.90	23200	3480	1280	695	450	320	250	23000
345.90	27200	4670	1640	865	570	400	310	27900
351.00	33500	5780	2060	1075	700	500	380	33300
356.05	40600	7000	2530	1250	800	570	440	40500
361.10	46700	8080	3060	1555	1000	710	550	48700
366.15	55000	9560	3700	1900	1220	870	670	60000
371.20	65000	11300	4360	2300	1480	1050	800	69100
376.24	75500	13200	5160	2700	1700	1210	930	80200
381.30	88000	15400	6160	3300	2100	1500	1150	89000

The results for fractions I (< 150 C), II (150-180 C), and III (180-210 C) are shown in figure 9.3-1. The results of the oil are plotted as reference. The vapour pressure results of fraction I and the oil match pretty well.

From the results in table 9.3-1, it can be seen that the vapour pressure of the oil is even higher than that of the lightest fraction at low temperatures. This is probably due to the experimental procedure. The sample container was filled under nitrogen atmosphere, in order to prevent oxidation of the oil (or one of the fractions). The oil will contain nitrogen, that is mainly responsible for the higher vapour pressure of the mixture during the first run. The nitrogen is removed by pumping off the sample between run #1 and run#2. During the experiments of with the Exxon oil, it turned out that pumping off prior to the first run did not lead to satisfactory results in the second and third run.

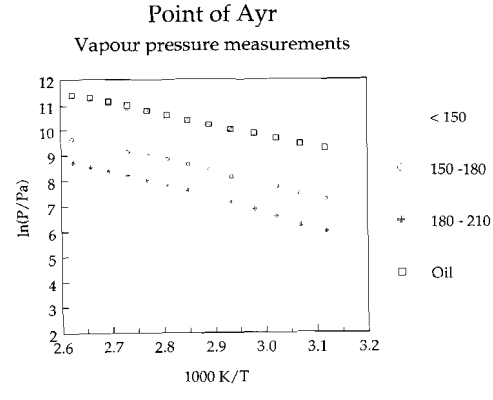

Figure 9.3-1 : Vapour pressure measurements of the Point of Air oil and the fractions I, II, and III

During evacuating the sample, it is inevitable that some of the lighter components are partially removed from the mixture. From the theory and the results of model mixtures (see chapters 7 and 8 of this work), it is known that the composition of the vapour depends on that of the liquid phase. As a result, the loss of light hydrocarbon species from the mixture may be less for the oil than for the lightest fraction.

When comparing the results of the figures 9.3-1 through 9.3-3 with the results on a selected group of pure substances, there is another difference. The vapour pressure curves as a function of the temperature are more linear for the pure substances than they are for the fractions and oil from Point of Ayr.

Except for the behaviour for fraction I, the other fractions show a regular behaviour in a sense, that the vapour pressure at a given temperature decreases as a function of the fraction number (boiling range), as is to be expected.

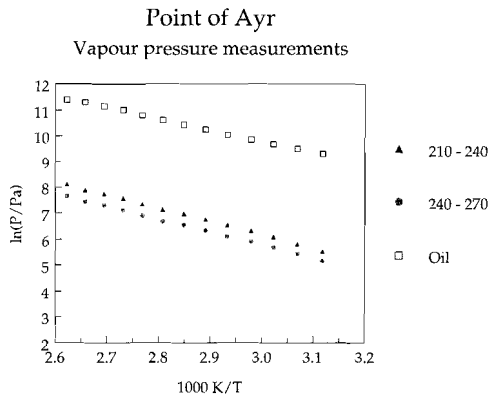

Figure 9.3-2 : Vapour pressure measurements of the Point of Air oil and the fractions IV and V

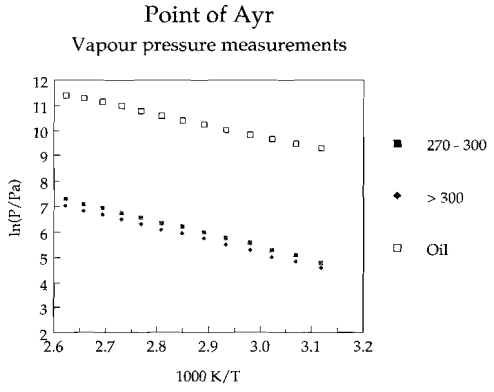

Figure 9.3-3 : Vapour pressure measurements of the Point of Air oil and the fractions VI and VII

9.4 Characterisation of the fractions

The elemental composition has been determined at the laboratory of RWTÜV Anlagentechnik GmbH in Essen (Germany). The carbon, nitrogen, and hydrogen contents have been determined by means of an element analyser of Perkin Elmer 2400. The oxygen content is determined with a modified CS-tube oven (Ströhlein) equipped with a CO-NDIR detector from UNOR. For these determinations, Acetanilide p.A. (Merck) was used as measurement standard.

The chlorine and sulphur contents were determined in accordance with DIN 51577-1 (total chlorine content) and DIN 51400-2 (total sulphur content) respectively. A sample was combusted at a temperature of 1000 C in a flow of oxygen. The detection followed from ion chromatography (IC), type DIONEX IC 2000. Synthetic chloride and sulphate solutions, prepared from standard solutions from Merck, were used for the quantitative determination of the two elements. The results from elemental analysis are shown in table 9.4-1.

Table 9.4-1 : Elemental analysis (weight %)

Fraction Boiling range	I < 150	II 150-180	III 180-210	IV 210-240	V 240-270	VI 270-300	Oil
Oxygen	0.39	1.1	0.57	0.28	0.12	0.15	0.33
Carbon	87.3	87.7	89.1	89.6	89.6	89.6	89.1
Hydrogen	12.3	11.1	10.2	10.1	10.2	10.2	10.6
Sulphur	< 0.01	0.03	0.02	0.01	0.01	0.03	0.02
Chlorine	< 0.02	< 0.02	< 0.02	0.05	0.05	< 0.02	< 0.02
Nitrogen	< 0.1	0.1	0.1	< 0.1	< 0.1	< 0.1	< 0.1

From the results in table 9.4-1, it can be seen that during liquefaction of the coal, sulphur, chlorine, nitrogen, and oxygen are effectively removed. From the elemental composition of the coal, the oxygen content (by difference) can be computed. The oxygen content for a Point of Ayr coal, that served as feedstock for the liquefier, is about 5.6 weight %. The oxygen content is reduced in the coal oil to 0.33 weight %. It can be seen that the oxygen content is not equal for all fractions. The fractions II (150-180 C) and III (180-210 C) contain more oxygen than the other fractions.

The sulphur content of the coal is 1.8 weight %, whereas in the coal liquids its contents are reduced to concentration levels of 0.03 weight % or lower. The same holds for chlorine content, that drops from 0.2 weight % in the feedstock, to 0.05 weight % or lower and for nitrogen.

The hydrogen content is increased from 4.8 weight % in the coal to between 10-12 weight % in the coal oil. The carbon content also increased, but there is another reason for this increase. The coal contains 1.5 weight % inherent moisture and 13.5 weight % ash. Ash is present in coal as mineral matter. The contents of ash and mineral matter are obviously related to one another, but the relationship is not straightforward. Ash is a product of the oxidation of the mineral matter during combustion. However, for an ash content of 13.5 weight %, a coal must contain a considerable amount of mineral matter. This mineral matter is removed during liquefaction, so the mass balance of the results of the oil and its fraction "misses" 13.5 weight % ash (or its equivalent in mineral matter).

The second characterisation of the oils is determination of the major species found by means of GC/MS-analysis (light hydrocarbons) and HPLC (polycyclic aromatic hydrocarbons). The results are shown in tables 9.4-2 (GC/MS) and 9.4-3 (HPLC) respectively.

The gas chromatographic analyses were performed on a GC/FID (FID = flame ionisation detector) (Hewlett-Packard HP-5890), with a Ultral 2, 25 m capillary column

(Hewlett-Packard), with a film thickness of 0.3 μm and a inner diameter of 0.2 mm. The measurement was carried out with toluene-D_8 (Merck) as standard.

The light halogenated hydrocarbons have been determined on a GC/ECD (ECD = electric conductivity detector) (Siemens SiChromat 1), equipped with a capillary column DB 624, 30 meter in length, 1.8 μm film thickness and an inner diameter of 0.325 mm.

For the determination of polycyclic aromatic hydrocarbons (PAHs), a high performance liquid chromatography (HPLC) system (Hewlett-Packard HP 1090) equipped with both a DAD and FCD 1046A. The column is from Vydac, type 201 TP 54, with C18 as column packing. A range of measurement standards has been used: naphthalene (Dr. Ehrenstorfer, certified 99.9%), acenaphthylene (Dr. Ehrenstorfer, 95%), fluorene (Dr. Ehrenstorfer, 99%), phenanthrene (preparation), anthracene (FLUKA, puriss.), fluoranthrene (BCR), pyrene (Dr. Ehrenstorfer, certified 99.3%), benz(a)anthracene (FLUKA, puriss.), chrysene (Dr. Ehrenstorfer, certified 97.9%), benzo(b)fluoranthrene (BCR), benzo(k)fluoranthrene (BCR), benzo(a)pyrene (FLUKA, pract.), dibenz(a,h)anthracene (FLUKA, puriss.), benzo(g,h,i)perylene (BCR), and indeno(1,2,3-c,d)pyrene (BCR).

The contents of trichloromethane (chloroform) are not due to an analytical error, but they are likely to come from a contamination of the oil by glassware that contained traces of chloroform. Chloroform is commonly used as solvent for cleaning glassware. It was reported [122] that during fractionation of the oil no chloroform was used for cleaning glassware or other purposes. So it may be assumed that the contamination by chloroform was not present in the samples used for the heat capacity and vapour pressure measurements.

The last item in table 9.4-2 are not only n-alkanes. It is not possible that coal liquids contain these concentration levels of unbranched aliphatic hydrocarbons. The item (n-Alkane C_9-C_{25}) is more likely the fraction of saturated substances. Many of these substances will be cycloalkanes, that are formed from reducing aromatic rings. However, this does not account completely for the increase in the content of alkanes in the fluid. The contents of aromatic carbon and aromatic hydrogen in the liquid, as determined from NMR-spectroscopy (table 9.6-1), do not differ too much between the fractions. The aromaticity of the lightest fraction is lower than that of the other fractions. The item may also include all other species not detected by GC/MS as well. This explains also the increase of this content with increasing boiling range. For the fractions III through VI, this content is between 950 and 980 g/kg, or in weight % between 95-98%.

Table 9.4-2 : GC/MS Analysis

Component	Unit	I < 150	II 150-180	III 180-210	IV 210-240	V 240-270	VI 270-300	Oil
Dichloromethane	mg/kg	< 0.1	< 0.1	< 0.1	< 0.1	< 0.1	< 0.1	< 0.1
Trichloromethane	mg/kg	4.8	0.99	0.43	594	777	262	6.5
1,1,1-Trichloroethane	mg/kg	< 0.1	< 0.1	< 0.1	< 0.1	< 0.1	< 0.1	< 0.1
Tetrachloromethane	mg/kg	< 0.1	< 0.1	< 0.1	< 0.1	< 0.1	< 0.1	< 0.1
Trichloroethene	mg/kg	< 0.1	< 0.1	< 0.1	< 0.1	< 0.1	< 0.1	< 0.1
Tetrachloroethene	mg/kg	< 0.1	< 0.1	< 0.1	< 0.1	< 0.1	< 0.1	< 0.1
Benzene	mg/kg	190000	220	5	< 5	< 5	< 5	26000
Toluene	mg/kg	180000	180	< 5	< 5	< 5	< 5	11700
Ethylbenzene	mg/kg	47000	7600	< 5	< 5	< 5	< 5	3300
o+m+p-Xylene	mg/kg	118000	16500	33	< 5	< 5	< 5	6610
1,2,3-Trimethylbenzene	mg/kg	820	4400	1000	< 5	< 5	< 5	590
1,2,4-Trimethylbenzene	mg/kg	8300	27000	2100	< 5	< 5	< 5	3000
1,3,5-Trimethylbenzene	mg/kg	3500	6700	340	< 5	< 5	< 5	790
1,2,3,5-Tetramethylbenzene	mg/kg	135	2400	1300	1000	< 5	< 5	4840
Pyridine	mg/kg	1700	10	< 5	< 5	< 5	< 5	15
Isopropylbenzene	mg/kg	5600	500	200	< 5	< 5	< 5	560
n-Alkane C_9-C_{25}	g/kg	400	700	950	950	950	980	690

Table 9.4-3 : PAH Analysis

Component	Unit	I < 150 C	II 150-180 C	III 180-210 C	IV 210-240 C	V 240-270 C	VI 270-300 C	VII Oil
Naphthalene	mg/kg	25.4	2250	34300	26000	1010	482	12240
Acenaphthylene	mg/kg	< 1	< 10	< 10	< 10	71.4	332	< 10
Acenaphthene	mg/kg	< 1	65.5	< 10	212	4790	2740	1630
Fluorene	mg/kg	< 1	< 10	< 10	588	2840	8620	1900
Phenanthrene	mg/kg	1.2	17.4	< 10	199	2750	22740	3620
Anthracene	mg/kg	1.1	1.2	< 10	< 10	10.5	144	23.6
Fluoranthene	mg/kg	< 1	3.8	< 10	< 10	19.9	131	135
Pyrene	mg/kg	1	2.9	< 10	< 10	< 10	342	930
Benzo(a)anthracene	mg/kg	0.4	< 10	< 10	< 10	21.2	< 10	29.4
Chrysene	mg/kg	0.1	< 10	< 10	< 10	51	< 10	15.3
Benzo(b)fluoranthene	mg/kg	0.8	< 10	< 10	< 10	< 10	< 10	11.6
Benzo(k)fluoranthene	mg/kg	1.5	< 10	< 10	< 10	< 10	< 10	5.9
Benzo(a)pyrene	mg/kg	1.6	< 10	< 10	< 10	< 10	< 10	7
Dibenzo(a,h)anthracene	mg/kg	0.7	< 10	< 10	< 10	< 10	< 10	19.5
Benzo(g,h,i)perylene	mg/kg	< 1	< 10	< 10	< 10	< 10	< 10	125
Indeno(1,2,3-c,d)pyrene	mg/kg	< 1	< 10	< 10	< 10	< 10	< 10	16.4
Total PAH (EPA)	g/kg	0.03	2.34	34.3	27	11.6	35.5	20.7

In fraction I (< 150 C), the dominant components are benzene (19 weight %), toluene (18 weight %), ethyl benzene (4.7 weight %), and xylenes (11.8 weight %). In addition to these components, some trimethyl benzenes, isopropyl benzene and tetramethyl benzene is found. Pyridine is also found in a concentration level of 0.17 weight %. From the PAH-analysis for this fraction it becomes clear apart from some naphthalene, the contents of other PAHs are low or below the determination limit.

The results for fraction II show a decrease of the contents for the light aromatic hydrocarbons, such as benzene and toluene. The tri- and tetramethyl benzenes, the concentration levels increase when compared to fraction I. The PAH-analysis shows an increase in naphthalene, acenaphthene, fluorene, phenanthrene among several others. The total PAH-content according to EPA increases.

The results for the heavier fractions are in agreement with the trends observed for fractions I and II. The contents of light aromatic species decrease rapidly (table 9.4-2) with increasing fraction number (boiling range). The contents of PAHs are less easily explained. Many substances have been measured, but most of them are below the determination limit. This may be a result from the fact, that may PAHs are not present in their usual form, but will contain short side-chains (methyl, ethyl, methoxy, carbonyl, etc.). If one wants to quantify these substituted PAHs, one has to extend the list with reference materials in order to do so. Another problem is that misinterpretations become more likely, because several different PAHs will have about the same retention time.

The reported concentration levels for benzo(a)anthracene and chrysene in the fractions 240-270 C and 270-300 C are likely to be due to such an misinterpretation [122]. These substances have considerably higher boiling points than the fractions, so probably other PAHs with the same retention time have been detected.

9.5 IR spectroscopy

The infrared (IR) spectra have been measured with a FT-IR spectrofotometer (Nicolet, 205 FT-IR). The measurements were carried out by RWTÜV in Essen (D).

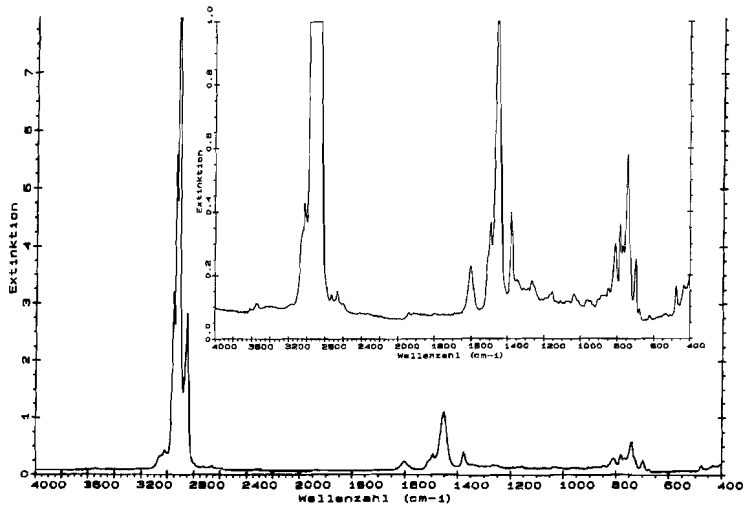

Figure 9.5-1 : IR-spectrum of Point of Ayr oil

Figure 9.5-1 shows the IR-spectrum of the Point of Ayr oil. The spectrum is typical for a fluid mixture consisting of almost only hydrocarbons. However, in the detail spectrum (upper right corner of figure 9.5-1) some other functional groups can be seen. If amine or hydroxyl is present, extinction peaks around 3500-3600 cm^{-1} (alcohol) or 3300-3500 cm^{-1} (amine) should be visible. The N-H and O-H stretch vibrations are medium to strong, so if these groups are present, they should be visible.

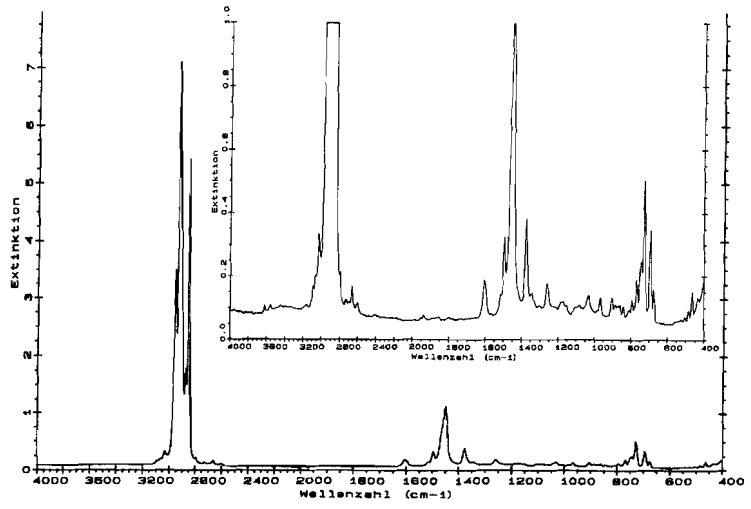

Figure 9.5-2 : IR-spectrum of Point of Ayr oil, fraction < 150 C

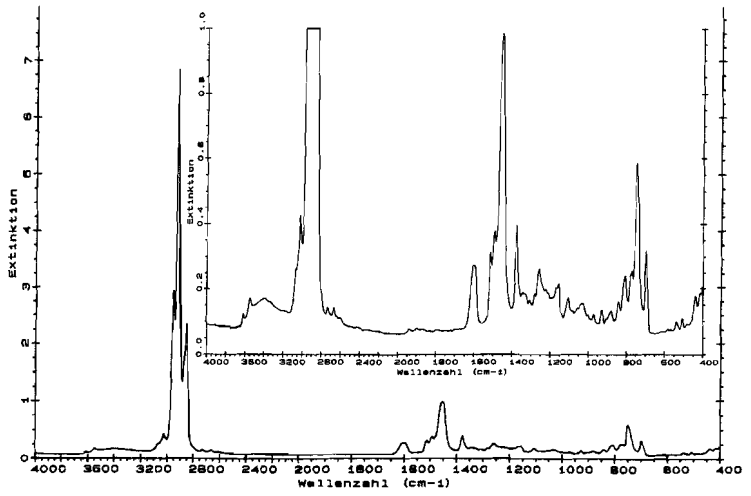

Figure 9.5-3 : IR-spectrum of Point of Ayr oil, fraction 150-180 C

Figure 9.5-1 indicates, that there is some hydroxyl and amine present in the oil. The peaks are however very small, so the concentration levels will be very low. This is in agreement with the elemental analysis, where very low oxygen and nitrogen contents were obtained.

C-H stretch vibrations are found around 3000 cm^{-1} for aromatic hydrogen, and between 2800-2900 for aliphatic hydrogen. The spectrum shows a large peak with several shoulders. The intensity of the C-H stretch vibrations is strong (alkyl-H) to medium (aromatic H). If carbonyl groups are present, then at about 1700 cm^{-1}, a peak should be present (C=O stretch vibration). No such peak is found in the spectrum of the oil. The peak at 1600 cm^{-1} is likely to be a bend vibration of C_{ar}-H. The peak at about 1500 cm^{-1} is due to aromatic C=C (stretching and deformation of the aromatic ring), because no olefinic carbon is present.

The spectrum of fraction II (figure 9.5-3, 150-180 C) confirms the higher oxygen and nitrogen content. At 3600, 3500, and 3400 peaks are present, likely to be due to hydroxyl and amine. As there is no peak around 1700 cm^{-1}, no carbonyl groups are detected.

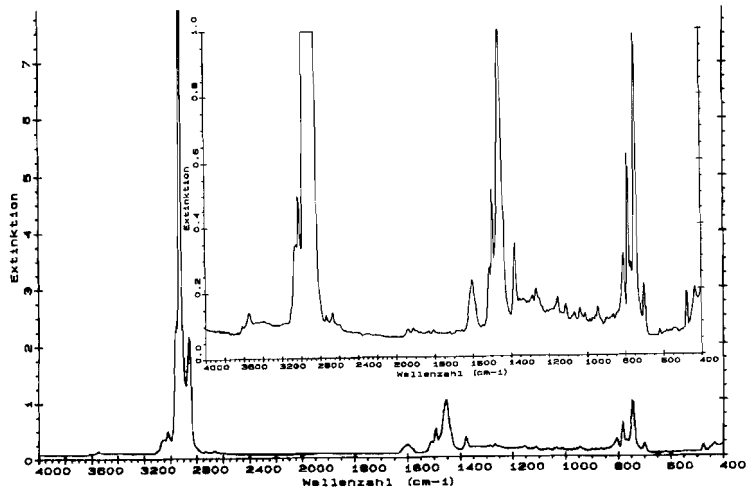

Figure 9.5-4 : IR-spectrum of Point of Ayr oil, fraction 180-210 C

The spectrum of the fraction 180-210 C shows also some small peaks at about 3550-3600 cm^{-1}, indicating hydroxyl groups. The contents are low however, as the intensity of these groups in an IR-spectrum is usually high.

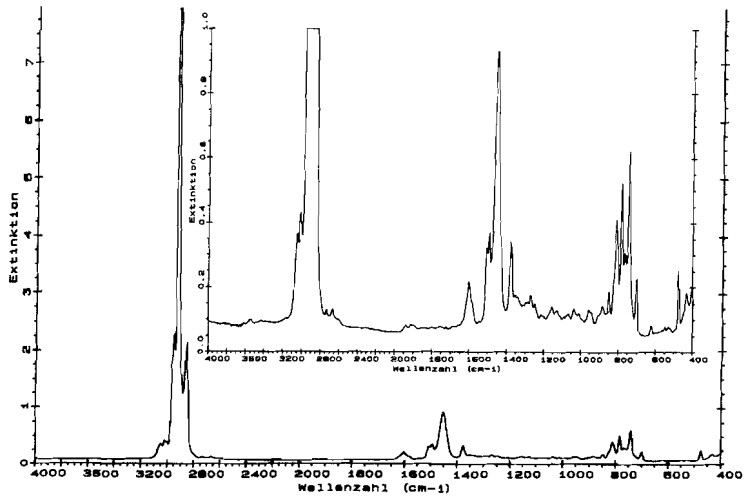

Figure 9.5-5 : IR-spectrum of Point of Ayr oil, fraction 210-240 C

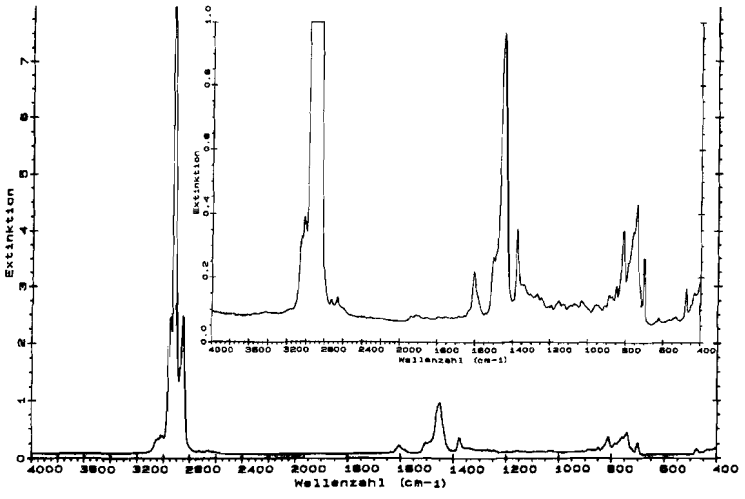

Figure 9.5-6 : IR-spectrum of Point of Ayr oil, fraction 240-270 C

The spectra of the fractions 210-240 C, 240-270 C, and 270-300 C (figures 9.5-5 through 9.5-7) indicate that the concentration levels of oxygen and nitrogen containing groups are very low.

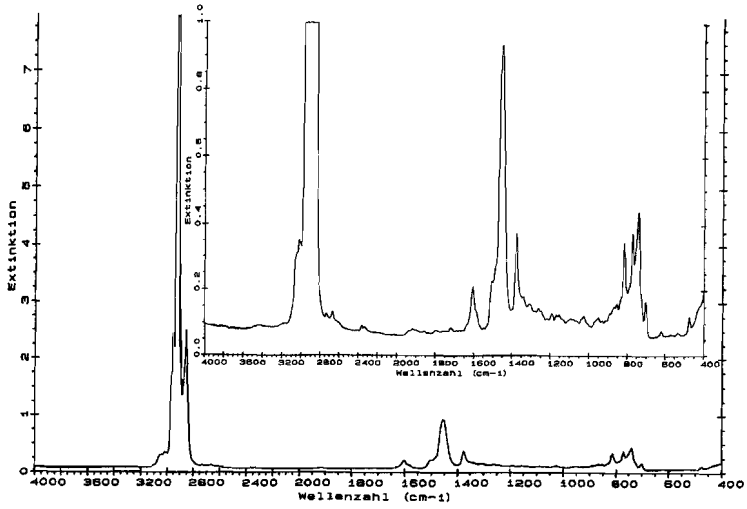

Figure 9.5-7 : IR-spectrum of Point of Ayr oil, fraction 270-300 C

Summarising, from the data presented so far it can be derived that little nitrogen and oxygen are present in the coal liquids. In those fractions where some oxygen and nitrogen was found in elemental analysis, it appears that most of these elements are present in the form of hydroxyl- and amine-groups respectively.

9.6 NMR spectroscopy

The ^{1}H- and ^{13}C-NMR spectroscopy was carried out by RWTÜV in Essen (D). The spectra were recorded on a Varian 300 MHz NMR spectrophotometer. The samples were diluted with a deuterated solvent. From the spectra, the following structural information was obtained (table 9.6-1).

Table 9.6-1 : Results from ^{1}H- and ^{13}C-NMR (contents in mol %)

Element	I < 150	II 150-180	III 180-210	IV 210-240	V 240-270	VI 270-300	Oil
H(aromatic)	7.7	12.2	16.4	16.7	13.6	12.7	13.6
H(saturated)	92.3	87.8	83.6	83.3	86.7	87.3	86.4
C(aromatic)	21	35.1	41.9	44.2	39.4	40.4	39.6
C(aromatic, alkyl)	4.1	5.3	3.8	4.8	6.9	6.9	4.3
C(alkyl)	79	64.9	58.1	55.8	60.6	59.6	60.4

Except for the lightest fraction, the ratio saturated hydrogen over aromatic hydrogen is about constant. The majority of the hydrogen is saturated, which is in agreement with the results from GC/MS and HPLC (section 9.4).

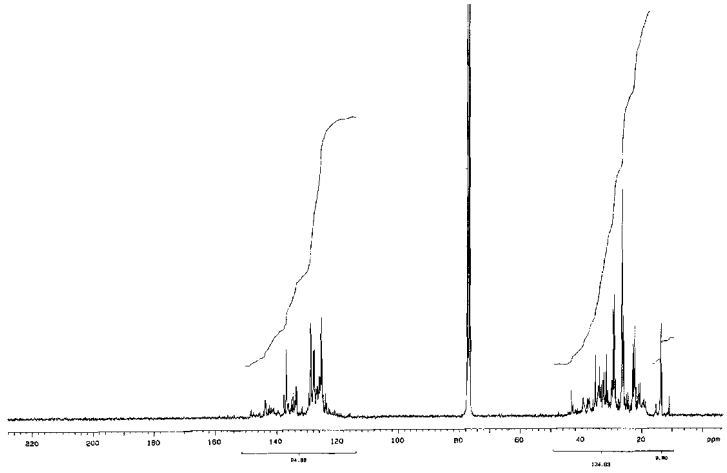

Figure 9.6-1 : ^{13}C-NMR spectrum of Point of Ayr oil

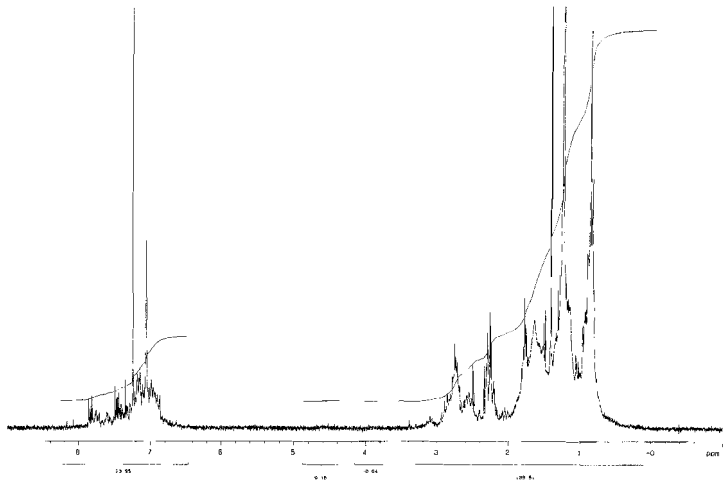

Figure 9.6-2 : ^{1}H-NMR spectrum of Point of Ayr oil

Figure 9.6-2 shows the proton NMR spectrum of the Point of Ayr oil. The spectra of the fractions show great similarity and have been included in appendix VI. From the proton NMR-spectrum, two groups of hydrogen atoms can be identified quantitatively, in fact aromatic hydrogen (left group of peaks in the spectrum) and aliphatic hydrogen (right group of peaks). In his work, Alexander [126] identifies additionally hydrogen bonded to an aliphatic carbon atom that in turn is bonded to an aromatic carbon (H_α), hydrogen bonded to a terminal aliphatic carbon (H_γ), and non-α, non-γ hydrogen (H_β).

The chemical shifts versus tetramethyl silane (TMS) are respectively 6.0-9.0 (H_{aro}), 1.7-4.0 (H_α), 0.9-1.7 (H_β), and 0.5-0.9 (H_γ). In this study, only H_{aro} and H_{ali} (sum of other hydrogen atoms) have been identified. In a personal communication [125], it was explained that for many key-substances, the ranges for H_α, H_β, and H_γ overlap, so it is theoretically not justified to use the classification as applied by Alexander et.al. [126,129].

9.7 Molecular weight determinations

The fractions and the oil were investigated by means of size exclusion chromatography (SEC) only, because the contents of volatile species were too high to perform MALDI-MS. The experimental procedure was adopted from the experiments with the Exxon oil (see section 8.9).

The results of SEC are given in figures 9.7-1 through 9.7-6. The graphs on the left-hand side present the complete spectrum from SEC. The graphs on the right hand side give a detail of the peaks in the spectrum. Figures 9.7-1 through 9.7-3 show the spectra of the oil, as well as fractions I-III. Fractions IV-VII are shown in figures 9.7-4

through 9.7-6. The figures have been grouped on two pages in order to visualise the differences between the UV-detection at wavelengths 270 nm, 300 nm, and 350 nm.

Figures 9.7-1 and 9.7-4 show that there is no material seen at the exclusion limit (short retention time). The graphs on the right hand show that the peak at about 22 min. decreases in intensity with increasing boiling range of the fraction. One would expect exact the opposite to happen: the heavier the fraction, the greater the peak(s) at lower retention time(s).

Figure 9.7-3 and 9.7-6 show that some material has a molar weight that exceeds the exclusion limit. This material is apparently visible only at 350 nm. At 300 nm (figures 9.7-2 and 9.7-5), only traces are visible.

Again, from SEC it was not possible to calculate molar weights from these results. However, from GC-MS/HPLC analysis, with the results of SEC as backup, it was possible to estimate the molar weights. The following estimates can be obtained (table 9.7-1).

Table 9.7-1 : MW estimates Pint of Ayr oil and fractions [127]

Fraction	Boiling range (C)	Molar weight (g/mol)
I	< 150	100
II	150-180	110
III	180-210	120
IV	210-240	130
V	240-270	155
VI	270-300	170
Oil		120

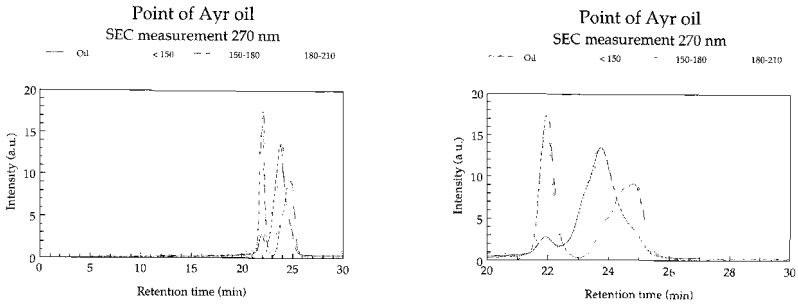

Figure 9.7-1 : Results of SEC for Point of Ayr oil and fractions I-III at 270 nm

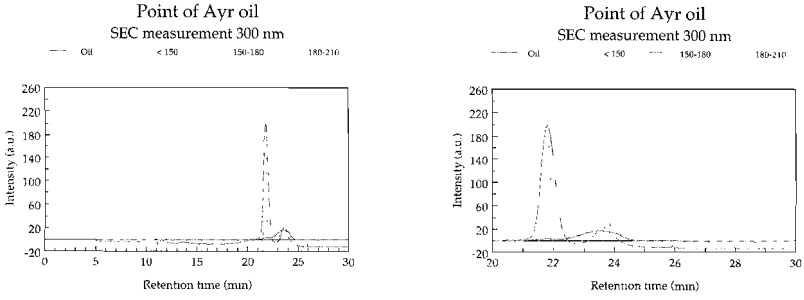

Figure 9.7-2 : Results of SEC for Point of Ayr oil and fractions I-III at 300 nm

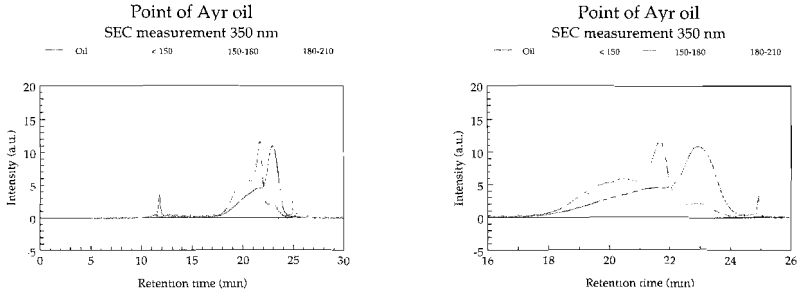

Figure 9.7-3 : Results of SEC for Point of Ayr oil and fractions I-III at 300 nm

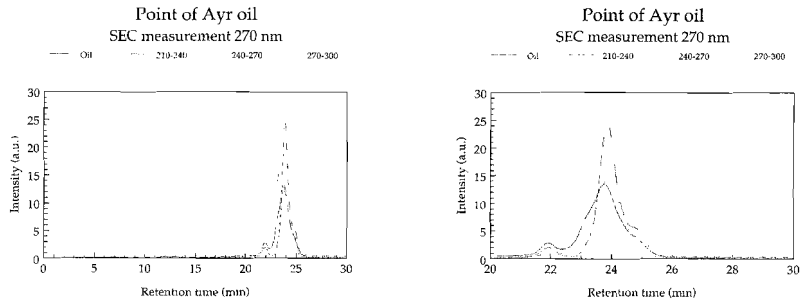

Figure 9.7-4 : Results of SEC for Point of Ayr oil and fractions IV-VII at 270 nm

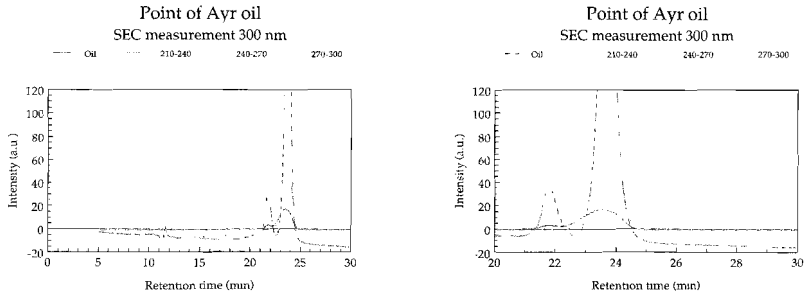

Figure 9.7-5 : Results of SEC for Point of Ayr oil and fractions IV-VII at 300 nm

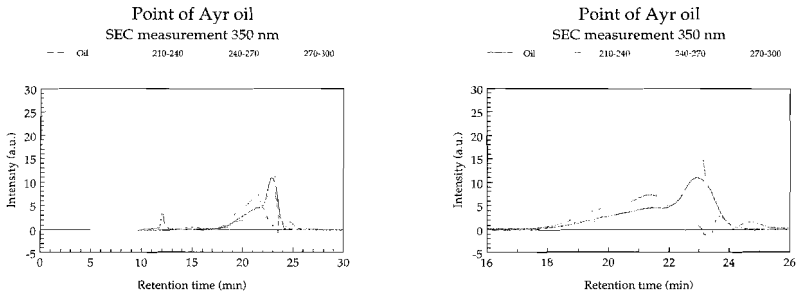

Figure 9.7-6 : Results of SEC for Point of Ayr oil and fractions IV-VII at 270 nm

9.8 Concluding remarks

The results presented in this chapter and the previous one indicate the effort necessary for obtaining a complete thermodynamic characterisation. A part of the programme is not necessary if a suitable equation of state has been established. Then

only the spectroscopic characterisations remain, including a molar weight determination.

From the techniques used here, it may be concluded that they are not as easy to implement and use as more commonly used techniques such as vapour pressure osmometry. However, the techniques used here will perform better on very heavy fractions. SEC appears to be sensitive to the polarity of the fluid being eluted. The technique can be improved considerably if good measurement standards with different average molecular weight, and a ranges of polarities are available. The results of the Point of Ayr oil indicate that good results are possible, but that the interpretation is problematic as no measurement standards are available with similar properties.

10. MODELLING OF ILL-DEFINED MIXTURES

10.1 Principles

Recalling from chapter 1 of this work, the general thought of the modelling of ill-defined mixtures is as follows. Rather than knowing the composition of the components of the mixture, one is able to determine relative concentration levels of structure fragments. These fragments 'contribute' to the properties of the mixture. This idea has been developed for group estimation procedures, such as were used for the estimation of the boiling point and the critical point properties. In chapter 6 of this work, the application of these methods has been demonstrated.

If for the critical pressure (P_{cr}) and for the critical temperature (T_{cr}) exist group contribution methods that predict these properties with reasonable accuracy, it may be expected that for the coefficients of an equation of state, such a method can be developed too. For the Soave-Redlich-Kwong equations of state, such a group contribution method has been developed. This method was applied for pure substances.

Many equations of state define one or more cross-coefficients in their mixing rules in order to improve the capacity of the model in modelling and predicting of the properties of these systems. These empirical cross-coefficients are of special importance in systems where the differences in chemical nature and size of the molecules are large. For a mixture with a large number of components, it is impossible to determine these cross-coefficients. From the modelling work in this study as well as from several publications [4,128] it follows that these empirical cross-coefficients k_{ij} are usually small, and can often be neglected without compromising too much on the level of accuracy of the model.

This fact forms the basis for a further generalisation of the equation of state in order to link the coefficients of the model to properties that can readily be obtained from common characterisation techniques. These techniques include infrared spectroscopy, ^{1}H- and ^{13}C-NMR spectroscopy, elemental composition, and molecular weight distribution analysis, as has been demonstrated in chapters 9 and 10. These techniques supply the following information

- contents of carbon, hydrogen, oxygen, sulphur, nitrogen, and chlorine
- relative contents of aromatic carbon, aliphatic carbon, aromatic hydrogen, aliphatic hydrogen, etc.
- average molecular weight
- contents of various oxygen and nitrogen containing functional groups

Obviously, these parameters can also be obtained for pure substances too. However, rather than performing measurements, the structural information can be derived directly from the molecular structure. In two papers, Alexander et. al. [126,129] demonstrate this method for the Soave-Redlich-Kwong equations of state. It was noted by the authors, that the relatively poor performance of the results on oil fractions was due to the poor representation of mixtures in general by the (simplified) Soave-Redlich-Kwong equations of state. The Cubic Chain-of-Rotators equations of state is

a better basis for modelling work on mixtures, as even for representing the vapour pressure as a function of the temperature, good estimates for the liquid and vapour densities are an requirement.

The method used by Alexander et.al. [126,129] was also used in this work. However, it has been reported [130] that although the regression of the coefficients of the Cubic Chain-of-Rotators equation of state was quite successful, the predictive performance of the model was poor. The explanation for this is found in the mathematical form of the equation of state. Recalling from section 4.4, the equation of state reads as

$$P = \frac{RT(1+0.77b/v)}{v-0.42b} + c^R \frac{0.055RTb/v}{v-0.42b} - \frac{a}{v(v+c)} - \frac{bd}{v(v+c)(v-0.42b)} \qquad 10.1\text{-}1$$

The first and second term on the right-hand side of equation 10.1-1 account for the repulsive forces, whereas the third and fourth term account for the attractive forces. Especially when looking at liquids, the pressure P is computed from a difference of two big numbers.

The regression method based on the coefficients in 10.1-1 does not work, due to the fact that with the new coefficients the values of both the attractive and the repulsive terms are somewhat different. However, this change is not equal for both terms. Due to the fact that the pressure is the difference of these two big values, it is very sensitive for this (relatively) small changes in the values of the terms. As a result, the predicted pressure is of poor quality.

10.2 Correlations for pure substances

In order to obtain a new set of variables, the pure substance porperties T_{cr}, P_{cr}, and ω have been fitted to selected hydrocarbon functional groups. This method has two advantages over regression of the coefficients of the Cubic Chain-of-Rotators equation of state, in fact

1. a reduction in the regression effort;
2. maintenance of the consistency of the equation of state.

The work started with the establishment of a database holding critical properties and acentric factors of hydrocarbons.

For a selected group of hydrocarbons, the dependency of the critical coefficients on the number of carbon atoms was evaluated. Based on the similarities between the coefficients of the SRK and CCOR, it was more or less to be expected that the coefficients of the CCOR could be expressed with similar functions as was done for the SRK. The group of hydrocarbons contained the n-alkanes up to $C_{19}H_{40}$ (nonadecane), several branched alkanes and cycloalkanes in the range C_5-C_{10}. Furthermore, some alkyl-substituted benzenes were added. The database thus compiled contained 81 substances. Critical data were taken from the tables of the Texas Research Centre (TRC) [62]. Acentric factors were taken from Reid [90] and Smith and Srivastava [65].

For the n-alkanes, the critical temperature as a function of the number of carbon atoms is shown in figure 10.2-1. The developers of estimation method for the critical pint usually use the ratio between the critical point temperature and boiling point [61,62] as basis for the group contribution method. However, for a regression of the critical point temperature it is undesirable to have to rely on the boiling point. As a result, the regression has been developed from the data plotted in figure 10.2-1 directly.

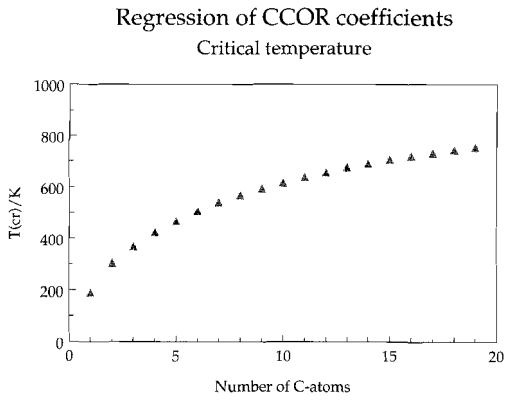

Figure 10.2-1 : Critical temperature versus number of carbon atoms for n-alkanes

For the critical pressure however, the estimation of its value is related to the molar weight [61,62]. This parameter is required any way, so the regression can be limited to the parameter G_P, that is a function of the critical pressure and molecular weight

$$G_P = \sqrt{\frac{MW}{P_{cr}}} \qquad 10.2\text{-}1$$

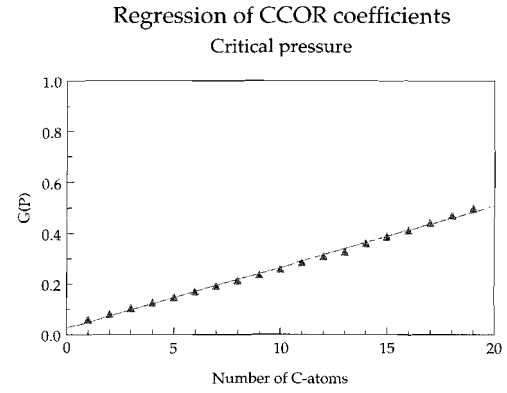

Figure 10.2-2 : G_P as a function of the number of carbon atoms for n-alkanes

The third parameter required for the computation of the coefficients of the equation of state is the acentric factor. Figure 10.2-3 shows the acentric factor as a function of the number of carbon atoms for n-alkanes. The regression line plotted is a quadratic curve.

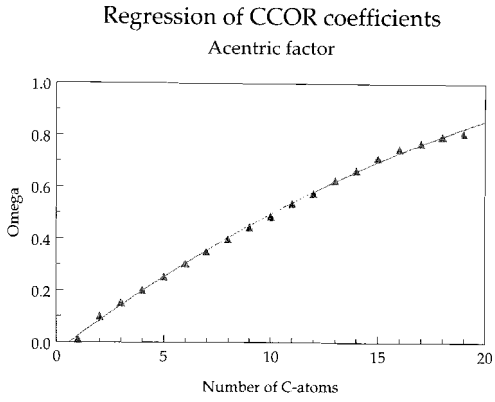

Figure 10.2-3 : Acentric factor as a function of the number of carbon atoms for n-alkanes

10.3 Correlation results

The three pure substance properties T_{cr}, P_{cr}, and ω have been fitted to a selected set of atoms in functional groups. Based on the analytical chemical experiments, for hydrocarbons the following variables have been defined

C_{al} (average) number of aliphatic carbon atoms per molecule

C_{ar} (average) number of aromatic carbon atoms per molecule[1]

$C_{ar,al}$ (average) number of aromatic carbon atoms that are alkyl-substituted per molecule

C_{tot} (average) number of all carbon atoms in a molecule (= $C_{al} + C_{ar} + C_{ar,al}$)

H_{al} (average) number of hydrogen atoms, bound to an aliphatic carbon atom

H_{ar} (average) number of hydrogen atoms, bound to an aromatic carbon atom

The selection of these variables follows from the data obtained from ^{1}H- and ^{13}C-NMR spectroscopy, as was explained in chapters 8 and 9. In the work of Alexander et.al. [126,129], a more elaborate set of variables was used, based on a separation of aliphatic hydrogen. This seems to be justified, as there is a serious overlap between the peaks of these types of hydrogen in different molecules in ^{1}H-NMR spectra [125].

[1] Excluding carbon atoms that are alkyl substituted

The first parameter fitted was T_{cr}. A database of hydrocarbons was set up and used for the regression. The regression function for T_{cr} reads as

$$T_{cr} = \alpha_1 + \frac{\alpha_2}{\sqrt{C_{tot}}} + \alpha_3 H_{al} + \alpha_4 H_{ar} + \frac{\alpha_5 H_{al} + \alpha_6 H_{ar}}{C_{tot}} + \alpha_7 \left(C_{ar} + C_{ar,al} \right) \qquad 10.3\text{-}1$$

Figure 10.3-1 shows the regression results. The regression results for T_{cr} are good. The coefficients α_I are given in table 10.3-1 at the end of this chapter. The coefficients have been obtained by fitting equation 10.3-1 to the reference values.

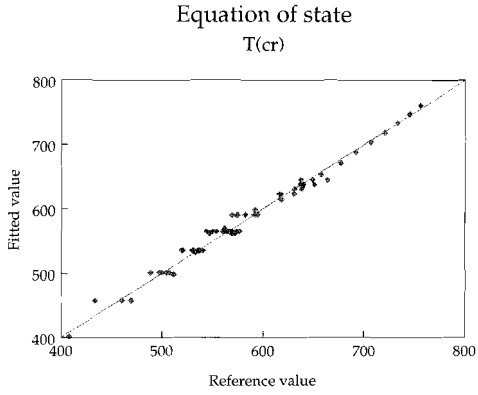

Figure 10.3-1 : Correlation results for coefficient T_{cr}

The second parameter fitted was critical pressure. For the regression, the parameter G_P as defined by equation 10.2-1. The regression of this parameter provided a simpler function. The only difference is that the parameter G_P has to be converted afterwards to a critical pressure.

The regression function reads as

$$G_P = \alpha_1 C_{al} + \alpha_2 C_{ar} + \alpha_3 C_{ar,al} + \alpha_4 \qquad 10.3\text{-}2$$

The regression results are plotted in figure 10.3-2. Rather than plotting the parameter G_P, the critical pressure has been plotted. In the minimisation process, the target function (equation 10.3-2) was minimised in two steps. First, the values for α_I were determined that minimised the difference between the predicted and experimental values of G_P. Then, in a second step the values of the coefficients were optimised in order to minimise the difference between predicted and experimental critical pressure. The regression as a single step process proved to be unsuccessful.

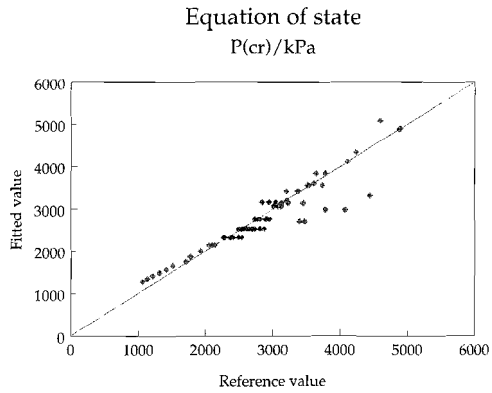

Figure 10.3-2 : Correlation results for critical pressure

The fitting results are generally speaking good, except for a small number of substances. In appendix VIII, the regression results are tabulated per substance. Especially the modelling of the alkane isomers gives some problems. These problems cannot be resolved with this set of variables.

The calculation follows from equation 10.2-1. The critical pressure obtained is in kPa.

The third parameter is the acentric factor. Little information was available about the behaviour of this parameter as a function of the number of carbon atoms. During the regression process, the following function was obtained

$$\omega = \alpha_1 C_{al} + \alpha_2 C_{al}^2 + \alpha_3 \left(C_{ar} + C_{ar,al}\right)^2 + \alpha_4 C_{ar} + \alpha_5 C_{ar,al} + \alpha_6 H_{al}^2 + \alpha_7 H_{ar}^2 + \alpha_8 \qquad 10.3\text{-}3$$

The regression results for the acentric factor are shown in figure 10.3-3. The results for the acentric factor are not too good. It should be noted however, that the influence of the acentric factor on the performance of the equation of state is somewhat smaller than that of critical pressure and critical temperature.

The values between 0.2 and 0.4 show considerable scattering. This scattering is a result from the selection of the set of variables, and cannot be resolved.

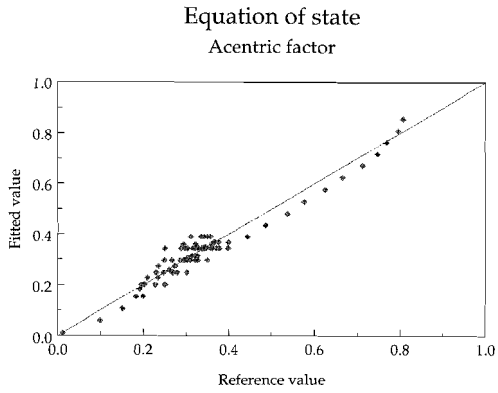

Figure 10.3-3 : Regression results for acentric factor

The coefficients for equations 10.3-1 through 10.3-3 are given in table 10.3-1.

Table 10.3-1 : Coefficients for the equations 10.3-1 through 10.3-12

Coeff.	α_1	α_2	α_3	α_4	α_5	α_6	α_7	α_8
T_{cr}	1007.406	-684.955	4.201066	2.999799	-122.344	-175.31	0.026036	
G_P	0.022342	0.015411	0.016299	0.033814				
ω	0.044761	-0.00157	0.006305	0.015054	0.000389	0.000381	-0.00211	-0.03828

The values for critical pressure, critical temperature, and acentric factor can be used for the calculation of the coefficients of the equation of state. In section 4.4, the equations for the Cubic Chain-of-Rotators equation of state are given.

10.4 Calculations with the new equation of state

For a selected group of hydrocarbons, the new equation of state was tested. The results are shown in table 10.4-1.

Table 10.4-1 : Performance of the CCOR and modified equation of state on selected heavy aromatic substances

Substance	This work		CCOR	
	AAD (%)	Bias (%)	AAD (%)	Bias (%)
benzene	11.47	11.47	0.89	-0.75
toluene	11.75	11.75	2.18	1.25
1,2-dimethylbenzene	5.53	-5.53	4.36	4.36
1,3-dimethylbenzene	10.35	10.35	3.93	3.93
1,4-dimethylbenzene	13.45	13.45	4.52	4.52
naphthalene	14.18	5.31	12.11	-12.11
1-methylnaphthalene	32.57	-19.28	19.34	-19.34
2-methylnaphthalene	27.05	-11.44	25.29	-25.29
1-ethylnaphthalene	24.33	21.80	36.16	-36.16
2-ethylnaphthalene	28.00	26.52	48.30	-48.30
tetralin	59.39	-59.39	9.51	-9.18
1,8-dimethylnaphthalene	19.90	-10.48	49.53	-49.53
2,3-dimethylnaphthalene	6.65	-0.35	43.41	-43.41
2,6-dimethylnaphthalene	16.66	16.66	41.92	-41.92
2,7-dimethylnaphthalene	27.58	27.58	40.09	-40.09
indan	9.99	-9.99	17.25	-17.25
1,1-dimethylindan	40.44	40.44	26.51	-26.51
4,6-dimethylindan	20.38	-20.38	14.81	10.06
4,7-dimethylindan	31.72	-31.72	14.06	8.26
1,1,4,6-tetramethylindan	45.89	45.89	27.55	21.73
1,1,4,7-tetramethylindan	31.90	31.90	22.47	19.12

From table 10.4-1, it can be seen that the values of the new equation of state are slightly worse when compared to the CCOR. This is partly due to the fact that the new equation of state does not make difference between isomers, such as the dimethylbenzenes and dimethylnaphthalenes.

A substance that gives unexpectedly poor results is tetralin. When comparing the results of tetralin with indan (two fused rings, an aromatic 6-ring and an aliphatic 5-ring), it is remarkable that indan gives significantly better results.

From the results it may be expected that the model will provide reasonable results when modelling ill-defined mixtures.

10.5 Modelling of ill-defined mixtures

The experimental data from the suite of Point of Ayr samples have been taken for the evaluation of the model performance. Based on the elemental composition (table 9.4-1) and the ^{1}H-NMR and ^{13}C-NMR data (table 9.6-1), the following elemental composition of the samples can be obtained (table 10.5-1).

The samples contained small amounts of hetero-atoms, that have been left out in the calculations. The weight percentages for carbon and hydrogen have been normalised to 100 %, and then with use of the molecular weights (table 9.7-1), the stoichiometric coefficients have been calculated. Table 10.5-1 shows the experimental data (columns 2-4) and the stoichiometric coefficients.

Table 10.5-1 : Elemental composition and stoichiometric coefficients of Point of Ayr samples

Fraction	C (w-%)	H (w-%)	MW (g/mol)	C_{al}	C_{ar}	$C_{ar,al}$	H_{al}	H_{ar}
I	87.3	12.3	100	5.77	1.23	0.30	11.31	0.94
II	87.7	11.1	110	5.28	2.42	0.43	10.77	1.50
III	89.1	10.2	120	5.21	3.42	0.34	10.22	2.01
IV	89.6	10.1	130	5.43	3.83	0.47	10.88	2.18
V	89.6	10.2	155	7.02	3.77	0.80	13.58	2.14
VI	89.6	10.2	170	7.57	4.26	0.88	15.05	2.19
Oil	89.1	10.6	120	5.39	3.15	0.38	10.94	1.72

With these input parameters, the model as presented in section 10.3 can be used. The results for the fractions I through IV are shown in table 10.5-2.

Table 10.5-2 : Experimental and calculated vapour pressures for the fractions I-IV of the Point of Ayr oil

Fraction	I		II		III		IV	
Boiling range (C)	< 150		150-180		180-210		210-240	
T/K	P/Pa (exp.)	P/Pa (calc.)	P/Pa (exp.)	P/Pa (calc.)	P/Pa (exp.)	P/Pa (calc.)	P/Pa (exp.)	P/Pa (calc.)
320.70	8600	7981	1450	3140	400	1153	250	530
325.80	10700	9901	1820	3994	520	1508	330	710
330.83	13700	12153	2340	5020	730	1946	435	936
335.60	17000	14660	2865	6188	980	2458	555	1207
340.90	23200	17928	3480	7742	1280	3155	695	1583
345.90	27200	21532	4670	9493	1640	3960	865	2025
351.00	33500	25793	5780	11605	2060	4952	1075	2581
356.05	40600	30659	7000	14062	2530	6132	1250	3254
361.10	46700	36239	8080	17239	3060	7537	1555	4069
366.15	55000	42606	9560	20261	3700	9201	1900	5051
371.20	65000	49837	11300	24106	4360	11158	2300	6223
376.24	75500	57996	13200	28513	5160	13441	2700	7611
381.30	88000	67220	15400	33571	6160	16107	3300	9255

The results for fraction I are good at low temperatures, and get slightly worse with increasing temperature. For fraction II, there is an overestimation of the vapour pressure of about 100%. This may be due to the estimated average molecular weight. Recalling from chapter 9, it was not possible derive a molecular weight directly from the SEC-measurements. Based on the GC/MS and HPLC data, an estimate of the molecular weight could be made.

For fraction III, the situation is even worse. There is an overestimation of the vapour pressure of more than a factor 2. For fraction IV, similar results are obtained, except that the vapour pressure difference increases (relatively) with increasing temperature.

The results for the fractions V, VI, and the oil are given in table 10.5-3.

Table 10.5-3 : Experimental and calculated vapour pressures for the fractions V, VI and the oil of Point of Ayr

Fraction	V		VI		Oil	
Boiling range (C)	240-270		270-300			
T/K	P/Pa		P/Pa		P/Pa	
320.70	175	96	120	27	11000	1275
325.80	230	135	165	41	13000	1664
330.83	290	187	200	59	15750	2143
335.60	370	251	265	82	19000	2699
340.90	450	345	320	117	23000	3457
345.90	570	460	400	161	27900	4329
351.00	700	610	500	220	33300	5402
356.05	800	798	570	297	40500	6674
361.10	1000	1030	710	396	48700	8188
366.15	1220	1329	870	523	60000	9976
371.20	1480	1694	1050	684	69100	12075
376.24	1700	2138	1210	886	80200	14520
381.30	2100	2682	1500	1138	89000	17370

The results of fraction V show that the estimate for the molecular weight is good. The model provides an underestimation of the vapour pressure at low temperatures and an overestimation at high temperatures. For fraction VI, the estimator for the molecular weight is probably less good: over the full range there is an underestimation of the vapour pressure.

The results of the oil show a serious underestimation of the vapour pressure. This result is not too surprising, taking into account that the vapour pressure is mainly determined by the lightest fraction. As the molecular weight of the oil is higher on average than that of the lightest fraction, the predicted vapour pressures will be lower. As a result, it can be assumed that the model is not very well suitable for unfractionated oils. In these oils, the average molecular weight is not a suitable parameter for the prediction of the vapour pressure.

11. CONCLUSIONS

11.1 Introduction

The main objective of this work was the establishment of a model, capable of predicting the temperature-pressure relationship of fluids obtained from coal. The model development can be visualised as follows (figure 11.1-1)

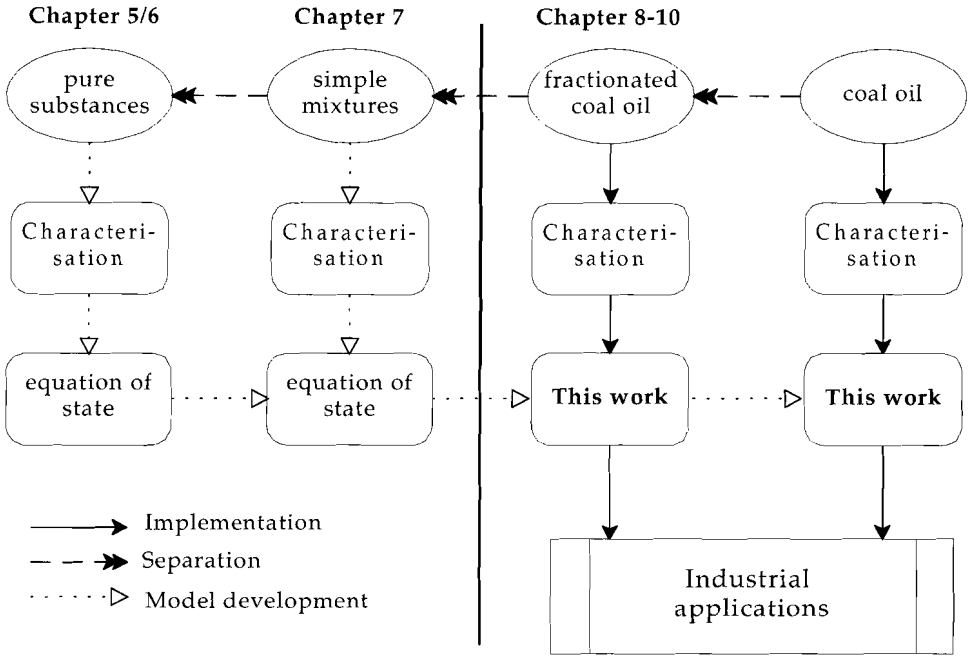

Figure 11.1-1 : Summary of the model development

In chapters 5 and 6, experimental and modelling work on pure substances has been presented. This work is to be regarded as complementary to existing work in this field. The next step in the model development is chapter 7, where binary mixtures were investigated. This investigation had to answer the question, whether the model is capable of dealing with simple mixtures without the need for empirical corrections. Chapters 8-10 cover the model development for ill-defined mixtures.

This model development included the verification of the stability of the samples, the fine-tuning of the experimental procedure of the measurement of the vapour pressure as a function of the temperature, as well as the characterisation of the fluids and the regression of the coefficients of the equation of state to concentration levels of structure fragments. The characterisation of the fluids is outlined in figure 11.1-2.

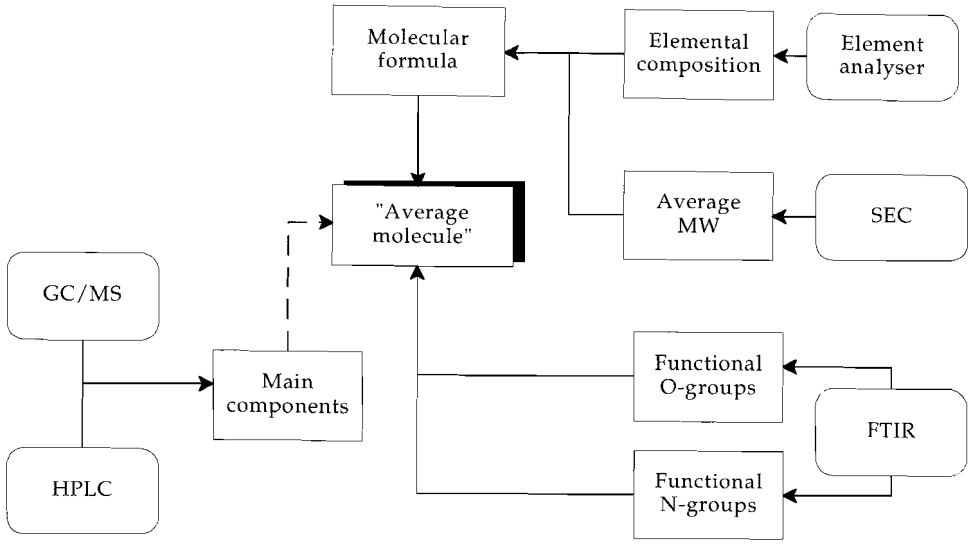

Figure 11.1-2 : Thermodynamic characterisation of coal fluids

The main objective of this characterisation is to obtain the properties of what may be called the "average molecule". The generalisations made during the regression of the coefficients of the equation of state to structure properties depend on this concept. The average molecule is an artificial species that incorporates the average properties of the fluids. In order to obtain the properties of this molecule, a range analytical chemical techniques is required.

With elemental analysis, a molecular formula can be obtained in the form $C_kH_lO_mN_nS_pCl_q$. The coefficients k..q follow from the average molecular weight, that can be obtained from for example size exclusion chromatography (SEC). It should be noted that the coefficients k..q of the average molecular formula will not be whole numbers. An equimolar mixture of benzene (C_6H_6) and phenol (C_6H_5OH) for instance will lead to a formula of $C_6H_6O_{0.5}$.

FTIR (Fourier transformed infrared spectroscopy) is capable of identifying various functional groups. A calibration in the form of a standard addition procedure is required to obtain quantitative concentration levels [126,129]. It is important to note, that the characterisation results obtained from both oils indicate very low concentration levels for oxygen and nitrogen. The need for identification of different types of oxygen and nitrogen is given only if these elements are present in relatively large amounts, and if it may be expected that they occur in different functional groups. The impact of a carbonylic oxygen (>C=O) on the thermodynamic properties differs widely from an alcoholic oxygen (-OH).

The characterisation of a fluid by GC/MS (gas chromatography/mass spectrometry) and/or HPLC (high performance liquid chromatography) provides additional information that can be of assistance in interpreting the results of other techniques. An example of this is the estimation of the average molecular size by means of the results from GC/MS and HPLC, with SEC as backup. A problem with both GC/MS and HPLC in this particular application is that these methods are not capable of

identifying all components in the mixture. A further problem is that identification often takes place on retention times. In the experiments on the Point of Ayr oil it was suspected that a misinterpretation of the data was made.

11.2 Work on simple systems

The Van Laar equation of state has proved to contain some mathematical imperfections. As a result, the equation of state is not capable of covering the whole range of possible values for temperature, density, and pressure. On the limited ranges of temperature however, the model provides reasonable results. The Cubic Chain-of-Rotators equation of state, that has a similar shape as Van Laar's equation of state, does not have these imperfections.

In this work, vapour pressure measurements were carried out on the following substituted naphthalenes: 1-methyl naphthalene , 2-methylnaphthalene , 1-ethylnaphthalene , 2-ethylnaphthalene , tetralin , 2-methoxynaphthalene , 2-naphthol, naphthalene-2-carboxylic acid , and 2-naphthaldehyde in the temperature range 40 C to about 150 C. Regressions of vapour pressure data showed that the experimental results obtained are in good agreement with data reported earlier.

The correlation of pure substance data of a selected group of heavy substances relevant to coal liquids to the Cubic Chain-of-Rotators equation of state was not too successful. The group of substances contained many dicyclic substances, such as naphthalenes, tetralin, and indans. All substances are representative for substances found in coal liquids. The reason for this behaviour of the CCOR is most likely the dimerisation that takes place. This hypothesis is supported by the fact, that the correlation results for the alkylnaphthalenes are hardly better than those of the naphthols, from which it is known that at least the hydroxyl groups allow dimerisation. As a consequence, the CCOR should be modified in order to improve its capabilities in modelling heavy aromatic fluids. This modification should take dimerisation equilibria into account. Several examples of approaches, especially in the field of alcohols and phenols exist in literature.

Two binary systems were investigated: toluene - 1-ethylnaphthalene and toluene - 2-methoxynaphthalene. The systems are representative for coal oils, but not for fractionated oils. This conclusion is supported by the great asymmetry observed in correlating the mixtures and the GC-MS and HPLC analysis on the coal liquids and coal liquid fractions. There is a good agreement between the K-factors and the vapour phase composition of the two systems between the Soave-Redlich-Kwong equation of state (SRK) and the CCOR.

The results on the binary mixtures show the limitations of the model being developed. With increasing asymmetry, the performance of the model will decrease even further. This feature has been illustrated by several authors that worked on the Cubic Chain-of-Rotators equation of state, by introducing empirical corrections. So, apart from the question whether the "average molecule" represents the fluid, there is also a limitation in the model: if the components in the mixture differ very widely in nature, then the performance of the model decreases and my become unsatisfactory.

11.3 Work on oils

The thermal stability of the (distilled) oils obtained in this project was sufficient for all other experiments. The vapour pressure measurements on the Exxon oil indicate, that with a properly designed experimental procedure, vapour pressure data may be obtained that approximate the real vapour pressure of a coal oil very nicely. However, a certain loss of volatiles, observed as a drop in vapour pressure at the same temperature with increasing run number, is inevitable.

The molecular weight determinations with both MALDI-MS (matrix-assisted laser-desorption ionisation mass spectrometry) and SEC (size exclusion chromatography) proved to be complicated. The Exxon oil was probably a mixture with a very wide variety in molecular weights, resulting in great difficulties in determining them. The average obtained for this oil is not only questionable from an experimental point of view: the range of molecular weights is that large (from below 1000 to over 200 000 u), that an average may be of little value to describe the complete fluid.

The molecular weight determinations of Point of Ayr oil and its fractions indicate that reasonable results with SEC with respect to molecular weight estimation can be obtained. However, problems arose due to differences in polarity of the samples. Finally SEC was used as "backup" and estimates were generated from GC-MS and HPLC data.

The development of an equation of state, based on the CCOR was quite successful. Previous work had shown that regression of structural fragments to the coefficients of the equation of state did not result in a consistent model. Regression of the critical temperature, critical pressure, and acentric factor proved to solve the problems. With the resulting equations, it is possible to convert any equation of state that uses T_{cr}, P_{cr}, and ω as input parameters into a model capable of predicting the vapour pressure as a function of temperature for ill-defined mixtures.

From the calculations with the new model, it could be concluded that the model is very sensitive with respect of the estimation of the molecular weight. For most of the fractions, the results are good, taking into account the performance of the model on pure substances. The modelling capacity for oils is less good, due to the fact that for mixtures containing a wide range of components, the vapour pressure is determined by the lightest components only. In that case, the average molecular weight is not a useful parameter. This observation is supported by the results on the binary mixtures as well as the results of fraction I and the oil from Point of Ayr.

The model development that resulted in an equation of state capable of predicting the temperature-pressure relationship for ill-defined mixtures was successful. The performance of the resulting model depends on two important factors: the input variables selected and the accuracy and representativity of the average molecular weight estimate.

12. LITERATURE

[1] Bender F., Erdöl und Kohle 34 (1981), 155

[2] Tromp P.J.J., "Coal pyrolysis. Basic phenomena relevant to conversion processes", Thesis, 1987

[3] Laar J.J. van, "Die Zustandsgleichung von Gasen und Flüssigkeiten mit besonderere Berücksichtigung der Veränderlichkeit der Werte von *a* and *b*, des kritischen Zustandes und der Theorie der Dampfspannungskurven", Leopold Voss Verlag, Leipzig (D) 1924

[4] Guo T.M., Kim H., Lin H.M., Chao K.C., "Cubic chain-of-rotators equation of state for polar fluids", Fluid Phase Equilibria **24** (1985), pp 43-61

[5] Lin H.M., Kim H., Guo T.M., Chao K.C., "Cubic chain-of-rotators equation of state and VLE calculations", Fluid Phase Equilibria **13** (1983), pp 143-152

[6] Kim H., Lin H.-M., Chao K.-C., "Cubic chain-of-rotators equation of state", Ind. Eng. Chem. Fundamentals **25** (1986), pp 75-84

[7] Veen A.M.H. van der, "Theromdynamic properties of coal fluids", Draft Final Report ECSC 7220/EC-602, European Centre for Coal Specimens SBN, Eygelshoven (NL), September 1992

[8] Fermont W.J.J., Joziasse J., Nater K.A., Veen A.M.H. van der, "Chemical and petrographical characterisation of representative samples of vitrinite and exinite concentrates", Fuel Proc. Techn. **36** (1993), pp 33-39

[9] Fermont W.J.J., Joziasse J., Nater K.A., Veen A.M.H. van der, "Analytical procedures for large-scale preparation of maceral concentrates", Fuel Proc. Techn. **36** (1993), pp 41-46

[10] Shinn J.H., Fuel **63** (1984), 1187 (from [2])

[11] Wilhelm A., Prausnitz J.M., "Vapour pressures and saturated liquid volumes for heavy fossil fuel fractions from a preturbed hard-chain equation of state", Fuel 1985, **64**, 501-508

[12] Collin P.J., Gilbert T.D., Philp R.P., Wilson M.A., "Structures of the distillates obtained from hydrogenation and pyrolysis of Liddell coal", Fuel, 1983, **62**, 450-458

[13] Nomura M., Yoshida T. Philp P., Gilbert T., "Structural study of hexane-soluble products from hydroliquefaction of three Yallourn brown coal lithotypes over molten salt catalysts", Fuel, 1985, **64**, 108-113

[14] Miyake M., Sakashita H., Nomura M., Kikkiwa S., "Catalytic activities of binary molten salts composed of $ZnCl_2$ and metal chlorides for hydrocracking of phenanthrene", Fuel, 1982, **61**, 124-128

[15] Farnum S.A., Farnum B.W., Bitzan E.F, Willson W.G., Baker G.G., "Coal liqueafction solvents. 1.Methods of separation: characterization by chromatography and pestrometry", Fuel, 1983, **62**, 799-805

[16] Kwon K.C., "Comparison of anthracene and phenanthrene in coal liquefaction", Fuel, 1985, **64**, 747-753

[17] Stock L.M., Duran J.E., Huang C., Srinivas V.R., Willis R.S., "Aspects of donor solvent coal dissolution reactions. Effects of organosulphur compounds on hydrogen transfer, decomposition of 1,3-diphenylpropane and liquefaction of Illinois coals", Fuel, 1985, 754-760

[18] McPherson W.P., Foster N.R., Okada K., Hastings D.W., Collin P.J., "Donor interactions of 1-methylindan in coal liquefaction", Fuel, 1985, **64**, 761-766

[19] Jones D.G., Rottendorf H., Wilson M.A., Collin F.J., "Hydrogenation of Liddell coal. Yields and mean chemical structures of the products", Fuel, 1980, **59**, 19-26

[20] Ouchi K., Chicade T., Itoh H., "Pressure and temperature effect on the mean chemical structure of coal hydrogenolysis product", Fuel, 1979, **58**, 37-42

[21] Owen J., "Conversion and uses of liquid fuels from coal", Fuel, 1981, **60**, 755-761

[22] Yoshimoto I., Itoh H., Makabe M., Ouichi K., "Pressure and temperature effects on the hydrogenation of coal-derived asphaltenes", Fuel, 1984, **63**, 978-983

[23] Gun S.R. et.al., "A mechanistic study of hydrogenation of coal. 1/2.", Fuel, 1979, **58**, 171-182

[24] Mondragon F., Itoh H., Ouchi K., "Coal liquefaction by in-situ hydrogen generation. 1. Zinc-water-coal reaction", Fuel, 1984, **63**, 968-972

[25] Mondragon F., Ouchi K., "Coal liquefaction by in-situ hydrogen generation. 1. Zinc-water model compound reactions", Fuel, 1984, **63**, 973-977

[26] Yarzab R.F., Given P.H., Spachman W., Davis A., "Dependence of coal liquefaction behaviour on coal characteristics. 4. Cluster analyses for characteristics of 104 coals", Fuel, 1980, **59**, 81-92

[27] Gray D., Barrass G., Jezko J. , "South African coal and their behaviour during liquefaction", ACS Symp. Ser. 1980, **139**, 35-51

[28] Kelvin N.V.P., "Hydroliquefaction of Australian coals", Div. Fuel, Chem. 1979, **24**, 177-184

[29] Gray D., Barrass G., Jezko J. Kershaw J.R., "Relations between hydroliquefaction behaviour and the organic properties of a variety of South African coals", Fuel, 1980, **59**, 146-150

[30] Baldwin R.M., Durfee S.L., Voorhees K.J., "Correlation of coal liquefaction reactivity with coal properties", Div. Fuel Chem. 1983, **28**, 1-7.

[31] Parkash S., Carson D., Ignasiak B., "Petrographic composition and liquefaction behaviour of North Dakota and Texas lignites", Fuel, 1983, **62**, 627-631

[32] Cronauer D.D. et.al., "Liquefaction of partially dried and oxidized coals. 3. Liquefaction results", Fuel, 1984, **63**, 71-77

[33] Ouchi K., Maeda Y., Itoh H., Makabe M., "Effect of air oxidation on coal hydrogenation", Fuel, 1984, **63**, 35-38

[34] Ouchi K. et.al., "Effect of blending on liquefaction of coals", Fuel, 1984, **63**, 78-83

[35] Okutani T. Yokoyama S., Machawa Y., "Viscosity changes in coal paste during hydrogenation", Fuel, 1984, **63**, 164-168

[36] Singh C.P.P. et.al., "Liquefaction of Coal by SRC-II Process. Part I: A New Kinetic Model", Canadian Journal of Chemical Engineering 1982, **60**, 248-260

[37] Singh C.P.P. et.al., "Liquefaction of Coal by SRC-II Process. Part II: Simulation of an SRC-II recycle system", Canadian Journal of Chemical Engineering, **60**, 261-271 1982

[38] Singh C.P.P. et.al., "Liquefaction of Coal by SRC-II Process. Part IV: Steady-state thermal behaviour of the reactor", Canadian Journal of Chemical Engineering, **60**, 831-841 1982

[39] Singh C.P.P. et.al., "Liquefaction of Coal by SRC-II Process. Part V: Dynamic thermal behaviour of the reactor", Canadian Journal of Chemical Engineering, **60**, 842-852 1982

[40] Deluzarche A. et.al., "Mecanisme des reactions Fischer-Tropsch en catalyse heterogene", Bull. Soc. Chim. Fr. 1982, **9-10**, 329-336

[41] Taylor P.D., Wojciechowski B.W., "A Quantitative Theoretical Treatment of the Fischer Tropsch Synthesis", Canadian Journal of Chem. Engineering 1983, **61**, 98-102

[42] Kuhlmann E.J., Jung D.Y., Guptill R.P., Dyke C.A., Zang H.K., "Coal liquefaction using a hydrogenated creosote oil solvent. H-atom transfer from hydrogen donor components in the solvent", Fuel, 1985, **64**, 1552-1557

[43] Petrakis L., Grandy D.W., Jones G.L., King B.A., "Free radicals in coal and coal conversion. 10. Kinetics and reaction pathways in hydroliquefaction", Fuel, 1983, **62**, 681-689

[44] Petrakis L., Grandy D.W., Jones G.L., "Free radicals in coal and coal conversions. 9. Statistical correlative models of the effect of process variables on hydroliquefaction products", Fuel, 1983, **62**, 671-680

[45] Petrakis L., Grandy D.W., Jones G.L., "Free radicals in coal and coal conversion. 8. Experimental determination of conversion in hydroliquefaction", Fuel, 1983, **62**, 665-670

[46] Petrakis L., Grandy D.W., Jones G.L., "Free radicals in coal and coal conversions. 7. An in-deth experimental investigation and statistical correlative model of effects of residence time, temperature and solvents", Fuel, 1982, **61**, 21-28

[47] Petrakis L., Grandy D.W., "Free radicals in coal and coal conversions. 6. Effects of liquefaction process variables on the in situ observation of free radicals", Fuel, 1981, **60**, 1017-1021

[48] Petrakis L., Grandy D.W., Jones G.L., "Free radicals in coal and coal conversions. 5. methodology for the in situ investigation of free radicals in coal depolymerization under SRC-II preheater/reactor conditions", Fuel, 1981, **60**, 1013-1016

[49] Benjamin B.M., Douglas E.C., Mesmer S., "Hydrogen transfer properties of some coal process recycle solvents (1)", Div. Fuel Chem. 1982, **27**, 1-5

[50] Poutsma M.L., "Thermolysis of partial coal structures: Bibenzyl and Naphthols", Div. Pet. Chem. 1980, **25**, 30-35

[51] Wilson M.A., Vassallo A.M., Collin M.J., "Deuterium as a tracer in coal liquefaction. Part 2. Non-catalytic studies", Fuel Processing Technology 1984, 8, 213-229

[52] Birkofer L., Pauly W., "Gaschromatografische und massenspektroskopische Untersuchung von Kohleextrakten", Brennstoff Chemie 1969, **50**, 376-382

[53] Parees D.M., Kamzelski A.Z., "Characterization of Coal-Derived Liquids Using Fused Silica Capillary Column GC-MS", J. Chrom. Science 1982, **20**, 441-448

[54] Burchill P., Herod A.A., Pritchard E., "Estimation of basic nitrogen compounds in some coal liquefaction products", Journal of Chromatography, 1982, **246**, 271-295

[55] Boduszynski M.M., Hurtubise R.J., Allen T.W., Silver H.F, "Compositions of distillate recycle solvents derived from direct coal liquefaction in the SRC-I process", Fuel, 1985, **64**, 242-254

[56] Inoue K., Yokoyama S., Sanada Y., "Chemical structure of coal-derived oil. Structural changes of each compound type with severity of hydrogenation", Fuel, 1982, **61**, 245-249

[57] Seshadri K.S., Young D.C., Cronauer D.C., "Characterization of coal liquids by 13C.n.m.r. and FT-i.r. spectroscopy - factions of oils of SRC-I and asphaltenes and preasphaltenes of SRC-I and SRC-II", Fuel, 1985, **65**, 22-28

[58] Chung K.E., Anderson L.L., Wiser W.H., "New procedure for molecular-weight determination by vapour phase osmometry", Fuel, 1979, **58**, 847-852

[59] Collins C.J., Triolo R., Lietzke M.H., "Do molecuar weight determinations of coal-derived materials give meaningful answers?", Fuel, 1984, **63**, 1202-1205

[60] Chao J., Lin C.T., Chung T.H., "Vapor pressure of coal chemicals", J. Phys. Chem. Ref. Data **12** (1983), pp 1033-1063

[61] Reid R.C., Prausnitz J.M., Poling B.E., "The properties of liquids and gases", 4th edition, McGraw-Hill, New York 1988, section 2.2

[62] Somayajulu G.R., "Estimation procedures for critical constants", J. Chem. Eng. Data **34** (1989), pp 106-120

[63] Reid R.C., Prausnitz J.M., Poling B.E., "The properties of liquids and gases", 4th edition, McGraw-Hill, New York 1988, chapter 7

[64] Dechema, "European Coal Database II", Final report, Frankfurt 1986.

[65] Smith B.D., Srivastava R., "Thermodynamic data for pure compounds", Physical sciences data 25, Elsevier, Amsterdam 1986

[66] Clarke E.C.G, Glew D.N., Trans. Faraday Soc. **62** (1966), 539

[67] Press W.H., Flannery B.P., Teukolsky S.A., Vetterling W.T., "Numerical Recipes. The art of scientific computation", Cambridge University Press, Cambridge 1986, chapter 14

[68] Cox E.R., Ind. Eng. Chem. **28** (1936), 613 (from: Steele W.V., Chirico R.D., "Thermodynamics and the hydrodexoygenation of 2,3-benzofuran", Topical Report, Department of Energy, NIPER-457, February 1990)

[69] Wagner W., "New vapour pressure measurements for argon and nitrogen and a new method for establishing rational vapour pressure equations", Cryogenics **21** (1953), pp 470-482

[70] Stull D.R., "Vapor pressure of pure substances - organic compounds", Ind. Eng. Chem. **39** (1947), pp 517-540

[71] Pitzer K.S., "The volumetric and thermodynamic properties of fluids. I. Theoretical basis and virial coefficients", J. Am. Chem. Soc. **77** (1955), pp 3427-3433

[72] Pitzer K.S., Lippmann D.Z., Curl Jr. R.F., Huggins C.M., Petersen D.E., "The volumetric and thermodynamic properties of fluids. II. Compressibility factor, vapor pressure and entropy of vaporization", J. Am. Chem. Soc. **77** (1955), pp 3433-3440

[73] Twu C.H., Coon J.E., Cunningham J.R., "A generalized vapor pressure equation for heavy hydrocarbons", Fluid Phase Equilibria **96** (1994), pp 19-31

[74] Prausnitz J.M., Lichtenthaler R.N., Gomez de Azevedo E., "Molecular thermodynamics of fluid phase equilibria", Second edition, Prentice-Hall Inc., Englewood Cliffs, N.J., 1986, chapter 3

[75] Beattie J.A., Stockmayer, (Taylor H.S., Glasstone S. eds.), "Treatise on physical chemistry", D. van Nostrand Company, Princeton, N.J., 1942, chapter 2

[76] Beattie J.A., (Rossini F.D. ed.), "Thermodynamics and physics of matter", Princeton University Press, Princeton, N.J., 1955, chapter 3, part C

[77] Waals J.D. van der, Thesis, Leiden 1873

[78] Redlich O., Kwong J.N.S., "On the thermodynamics of solutions. V. An equation of state. Fugacities of gaseous solutions", Chemical Review **44** (1949), 233-243

[79] Soave G., "Equilibrium constants from a modified Redlich-Kwong equation of state", Chemical Eng. Sci. **27** (1972), pp 1197-1203

[80] Graboski M.S., Daubert T.E., "A modified soave equation of state for phase equilibrium calculations. 1. Hydrocarbon systems", Ind. Eng. Chem. Process Des. Dev. **17** (1978), pp 443-448

[81] Soave G.S., "Application of the Redlich-Kwong-Soave equation of state to solid-liquid equilibria calculations", Chem. Eng. Science **34** (1979), pp 225-229

[82] Peng D.-Y., Robinson D.B., "A new two-constant euqation of state", Ind. Eng. Chem. Fundamentals **15** (1976), pp 59-64

[83] Chien C.H., Greenkorn R.A., Chao K.C., "Chain-of-Rotators equation of state", AIChE Journal **29** (1983), pp 560-571

[84] Carnahan N.F., Starling K.E., "Equation of state for nonattracting rigid spheres", Journal of Chemical Physics **51** (1969), pp 635-636

[85] Barker J.A., Henderson D., "Theories of liquids", Ann. Rev. Phys. Chem. 23 (1972) **23** (1972), pp 439-484

[86] Han S.J., Lin H.M., Chao K.C., "Vapor-liquid equilibrium of molecular fluid mixtures by equations of state", Chemical Engineering Science 43 (1988) **43** (1988), pp 2327-2367

[87] Lin H.-M., Lee M.-J., "Calculation of excess enthalpies with the CCOR equation of state", Fluid Phase Equilibria **100** (1994), 139-151

[88] Press W.H., Flannery B.P., Teukolsky S.A., Vetterling W.T., "Numerical Recipes. The art of scientific computation", Cambridge University Press, Cambridge 1986, section 9.5

[89] Press W.H., Flannery B.P., Teukolsky S.A., Vetterling W.T., "Numerical Recipes. The art of scientific computation", Cambridge University Press, Cambridge 1986, section 4.3

[90] Reid R.C., Prausnitz J.M., Poling B.E., "The properties of liquids and gases", 4th edition, McGraw-Hill, New York 1988, chapter 3

[91] Kruif C.G., Kuipers T., Miltenbrug J.C. van, Schaake R.C.F., Stevens G., "The vapour pressure of solid and liquid naphthalene", J. Chem. Thermodynamics **13** (1981), pp 1081-1086

[92] Stephenson R.M., Malanowski S., "Handbook of the thermodynamics of organic compounds", Elsevier, New York 1988

[93] Wieczorek S.A., Kobayashi R., "Vapor-pressure measurements of 1-methylnaphthalene, 2-methylnaphthalene, and 9,10-dihydrophenanthrene at elevated temperatures", J. Chem. Eng. Data **26** (1981), pp 8-11

[94] Macknick A.B., Prausnitz J.M., "Vapor pressures of high-molecular-weight hydrocarbons", J. Chem. Eng. Data **24** (1979), pp 175-178

[95] Vargaftik N.B., "Tables on the thermophysical properties of liquids and gases in normal and dissociated states", J. Wiley and Sons, New York 1975

[96] Boublik T., Fried V., Hala E., "The vapour pressures of pure substances. Selected values of the temperature dependence of the vapour pressures of some pure substances in the normal and low pressure region", Physical sciences data 10, Elsevier, Amsterdam 1973

[97] Goodwin R.D., "Benzene thermophysical properties from 279 K to 900 K at pressures to 1000 bar", J. Phys. Chem. Ref. Data **17** (1988), pp 1541-1636

[98] Goodwin R.D., "Toluene thermophysical properties from 178 K to 800 K at pressures to 1000 bar", J. Phys. Chem. Ref. Data **18** (1989), pp 1565-1636

[99] Nasir P., Hwang S., Kobauashi R., "Development of an apparatus to measure vapor pressure at high temperatures and its application to three higher-boiling compounds", J. Chem. Eng. Data **25** (1980), pp 298-301

[100] Kara M., Sung S., Klinzing G.E., Chiang S.H., "Tetralin vapour pressure at elevated temperatures", Fuel **60** (1981), pp 633-634

[101] Osborn A.G., Douslin D.R., "Vapor pressures and derived enthalpies of vaporization for some condensed ring hydrocarbons", J. Chem. Eng. Data **20** (1975), pp 229-231

[102] Osborn A.G., Scott D.W., "Vapor-pressure and enthalpy of vaporization of indan and five methyl-substituted indans", J. Chem. Thermodynamics **10** (1978), pp 619-628

[103] Aly G., Ashour I., "A modified perturbed hard-sphere equation of state", Fluid Phase Equilibria **101** (1994), pp 137-156

[104] Anderko A., "Phase equilibria in aqueous systems from an equation of state based on the chemical approach", Fluid Phase Equilibria **65** (1991), pp 89-110

[105] Anderko A., "Equation-of-state methods for the modelling of phase equilibria", Fluid Phase Equilibria **61** (1990), pp 145-225

[106] Reid R.C., Prausnitz J.M., Poling B.E., "The properties of liquids and gases", 4th edition, McGraw-Hill, New York 1988, chapter 8

[107] Barker J.A., "Determination of activity coefficients from total pressure measurements", Austr. J. Chem. **6** (1953), pp 207-210

[108] Abbott M.M., Ness H.C. van, "An extension of Barker's method for reduction of VLE data", Fluid Phase Equilibria **1** (1977), pp 3-11

[109] Hermsen R.W., Prausnitz J.M., "Thermodynamic properties of the benzene and cyclopentane system", Chem. Eng. Science **18** (1963), pp 485-494

[110] Ness H.C. van, Byer S.M., Gibbs R.E., "Vapor-liquid equilibrium: Part I. An appraisal of data reduction methods", AIChE Journal **19** (1973), pp 238-244

[111] Abbott M.M., Ness H.C. van, "Vapor-liquid equilibrium: Part III. Data reduction with precise expressions for G^E", AIChE Journal **21** (1975), pp 62-71

[112] Redlich O., Kister A.T., "Thermodynamics of non-electrolyte solutions. x-y-t-relations in a binary system", Ind. Eng. Chem. **40** (1948), pp 341-345

[113] Redlich O., Kister A.T., "Thermodynamics of nonl-electrolyte solutions. Algebraic representation of thermodynamic properties and the classification of solutions", Ind. Eng. Chem. **40** (1948), pp 345-348

[114] Prausnitz J.M., Lichtenthaler R.N., Gomez de Azevedo E., "Molecular thermodynamics of fluid phase equilibria", Second edition, Prentice-Hall Inc., Englewood Cliffs, N.J., 1986, chapter 7

[115] Tsonopoulos C., "An empirical correlation of second virial coefficients", AiCHE Journal **20** (1974), pp 263-272

[116] Tsonopoulos C., "Second virial coefficients of polar haloalkanes", AIChE Journal **21** (1975), pp 827-829

[117] Tsonopoulos C., "Second virial coefficients of water pollutants", AIChE Journal **24** (1978), pp 1112-1115

[118] Wendeler H., "Berechnungsethoden und Programmpaket zur thermodynamischen Auslegung von verfahrenstechnischen Prozessen", Technische Universität Berlin, Thesis, 1984

[119] Boublik T., "Hard sphere equation of state", J. Chem. Phys. **53** (1971), pp 471-472

[120] Mansoori G.A., Carnahan N.F., Starling K.E., Leland Jr. J.W., "Equilibrium thermodynamic properties of hard spheres", J. Chem. Phys. **54** (1971), pp 1523-1525

[121] Dohrn R., Prausnitz J.M., "A simple perturbation term for the Carnahan-Starling equation of state", Fluid Phase Equilibria **61** (1990), pp 53-69

[122] Moore S.A., personal communication

[123] Münster J.B., "Das Phasengleichgewichtsverhalten von Kohleölen und Kohleölkomponenten", VDI Verlag, Reihe 3 - Verfahrenstechnik, Düsseldorf 1988, pp 24-25

[124] Kandiyoti R., Herod A.A., personal communication

[125] Kunze A., personal communication

[126] Alexander G.L., Creagh A.L., Prausnitz J.M., "Phase equilibira for high-boiling fossil fuels destillates. 1. Characterization", Ind. Eng. Fundamentals 24 (1985) **24** (1985), pp 301-310

[127] Herod A.A., personal communication

[128] Schreiber D.R., Pitzer K.S., "Equation of state in the acentric factor system", Fluid Phase Equilibria **46** (1989), pp 113-130

[129] Alexander G.L., Schwarz B.J., Prausnitz J.M., "Phase equilibria for high-boiling fossil-fuel distillates. 2. Correlation of equation-of-state constants with characterization data for phase-equilibrium calculations", Ind. Eng. Chem. Fundamentals 24 (1985) **24** (1985), pp 311-315

[130] Veen A.M.H. van der, Broos A.J.M., "Thermodynamic basis for coal liquefaction modelling", Draft final report ECSC 7220/EC-603, Nederlands Meetinstituut, Eygelshoven, December 1996

I. LIST OF SYMBOLS

I.1 General

A	Helmholtz free energy
G	Gibbs free energy
H	Enthalpy
T	Temperature
P	Pressure
U	Energy
V	Volume
x	mole fraction (in liquid)
y	mole fraction (in vapour)
φ	fugacity coefficient
γ	activity coefficient
μ	chemical potential
ω	acentric factor

I.2 Equation of state

a	coefficient of an equation of state (attraction term)
b	co-volume coefficient
c	third coefficient of an equation of state
d	fourth coefficient of an equation of state

I.3 Vapour pressure correlations

A	first coefficient
B	second coefficient
C	third coefficient
D	fourth coefficient
E	fifth coefficients

I.4 Subscripts

calc	calculated property
exp	experimental property
cr	critical property
i	component number (in mixtures)
j	component number (in mixtures)
r	reduced property, property divided by critical propery
ref	reference

II. LIST OF ACRONYMS AND ABBREVIATIONS

II.1 General

DSC	Differential scanning calorimetry
FTIR	Fourier transformed infrared spectroscopy
GC	Gas chromatography
GC/MS	Gas chromatography/mass spectrometry
IR	Infrared spectroscopy
MS	Mass spectrometry
MALDI-MS	matrix-assisted laser-desorption ionisation mass spectrometry
NMR	Nuclear magnetic resonance spectroscopy
SEC	Size exclusion chromatography

II.2 Equations of state

CCOR	Cubic chain-of-rotators equation of state
COR	Chain-of-rotators equation of state
CS	Carnahan-Starling hard spheres equation of state
EOS	equation of state
PR	Peng-Robinson equation of state
RK	Redlich-Kwong equation of state
SRK	Soave-Redlich-Kwong equation of state
VdW	Van der Waals equation of state

II.3 Computer applications

The acronyms used for computer applications in this work are described in Annex C, first section C.1.

III. SOFTWARE DEVELOPMENT

III.1 Introduction and overview

Thermodynamic calculations are often very complicated and require specific input parameters. Modelling work without the support of a database containing (at least) key pure substance properties is not possible. In many calculations, as shown in chapters 3, 4, and 7, for example, require substance-specific information. In calculations using equations of state, the input is often limited to three parameters, critical pressure, critical temperature, and acentric factor.

In order to support the calculations, a simple database system has been developed with several applications. The following applications have been implemented

1. **CoDaMS II**; the central application of the system; its main objective is to shell the other applications of the system
2. **TDEdit**; the database editor; this application allows to search data, to modify data, and to generate reports from the database system
3. **LitRef**; database editor for the table containing literature references
4. **JL**; implementation of the Joback-Lydersen critical point estimation method
5. **TRC**; implementation of the TRC[1]-method for the estimation of the critical properties
6. **AcFactor**; the name of this application was dedicated to the acentric factor; in addition to have the capability of calculating this property, the application allows to fit vapour pressure data to a variety of empirical vapour pressure equations[2]
7. **VdW III**; this application models pure substance data and calculates the VLE-properties of pure fluids by means of a variety of equations of state, such as the Van der Waals equation of state, the Soave-Redlich-Kwong equation of state, and the Cubic Chain-of-Rotators equation of state
8. **VLEFit**; this part of the system models binary mixtures; it contains both data reduction methods such as Barker's method and equations of state[3]

All applications have been written in Turbo Pascal 6.0, later in Borland Pascal 7.0 [1]. The user interfaces of all applications have the same appearance, since Turbo Vision, an object-oriented toolbox has been used. Calculations were performed on an Intel 80386-based PC[4]-system equipped with a 100 Mb harddisk, 4 MB RAM, running under MS-DOS 4.0.

The main objective of this annex is to provide an overview over the application structure. It is not the substitute of the programmers' description of the system, but an extensive extract from it.

---

[1] Texas Research Centre
[2] See also chapter 3 for details
[3] See also chapter 7 for details
[4] Personal Computer

III.2 Turbo Vision and object oriented programming

The design and development of software was a tool for achieving the objectives of the research programme. The structuring of Turbo Vision allows to create applications that are transparent and easy to maintain. The structure of Turbo Vision is document elsewhere [1] and is illustrated in the next section.

III.3 Application framework

The application framework of the database and computational software has been developed with Turbo Vision (TV). Turbo Vision is an object-oriented toolbox for the design of an user interface. The desktop has a similar appearance as the Windows-environment, but simpler. The interface is a text-based interface.

The use of OOP (object-oriented programming) saves resources, both in the implementation phase as well as in the phase that software is used and maintained. The applications share several libraries, and the parts that are specific to an application are structured in such a way, that the structure of the applications is kept as similar as possible.

The use of OOP was not limited to the application structure. Many calculation algorithms have been embedded in an object, in order to speed up the development process. Especially the implementation of different, but in nature similar models can be done with OOP in a very efficient manner. An example of such an implementation is given in the next section.

All application have been derived from the object TApplication, that defines most basic behaviour for Turbo Vision applications (TVAs). In order to customise the application object, a new object type must be derived. This descendant of the TApplication object is called TVisionApp. It reads as follows (for AcFactor):

```
TYPE TVisionApp = OBJECT(TApplication)
                  ProgName,ProgVer,ProgPurp,ProgDate,CopyRight : PString;
                  Clock : PClockView;
                  Heap  : PHeapView;
                  Filename : PathStr;
                  DataAvail,CritPtAvail : BOOLEAN;
                  PROCEDURE InitStatusLine; Virtual;
                  PROCEDURE InitMenuBar; Virtual;
                  PROCEDURE InitGlobals;
                  PROCEDURE AboutBox;
                  PROCEDURE StartupBox;
                  PROCEDURE DOSShell;
                  PROCEDURE Tile;
                  PROCEDURE Cascade;
                  PROCEDURE Mouse;
                  PROCEDURE ChangeDir;
                  PROCEDURE OutOfMemory; VIRTUAL;
                  PROCEDURE Calculator;
                  PROCEDURE Colors;
                  FUNCTION GetPalette : PPalette; Virtual;
                  CONSTRUCTOR Init;
                  DESTRUCTOR Done; Virtual;
                  PROCEDURE Idle; Virtual;
                  PROCEDURE HandleEvent(VAR Event:TEvent); Virtual;
                  PROCEDURE MLFit;
```

```
END;
```

The object contains several fields with program defaults (ProgName, ProgVer, etc.), printer configuration (LPTPort, LPTType, LPTMode) and fields for indication of the system time and the amount of available memory. The program defaults are declared as constants

```
CONST sProgName   = 'AcFactor
      sProgPurp   = 'Fitting of Vapour Pressure Data';
      sProgVer    = '2.00';
      sProgDate   = '25 April 1994';
      sCopyRight  = '(c) S. Broos & A. van der Veen';
```

These strings appear in the "about"-box and in the message box at start-up of the program. Most of the methods of the TVisionApp object are directly called from the menu. The routine TVisionApp.Init is called once at start-up of ther program. It contains the initialization code for a proper set-up of the application framework.

The main program is very short

```
VAR TV : TVisionApp;

BEGIN
  TV.Init;
  TV.Run;
  TV.Done;
END.
```

First, a (global) variable of the type TVisionApp is created. In object oriented programming (OOP), TV is called an *instance* of the object TVisionApp. It is a good practice to use the following name conventions for objects:

Name	instance of an object
TName	type-declaration of the object
PName	pointer-type of the object

These conventions are used throughout Turbo Vision. The main program first initializes the program (TV.Init), then executes the program (TV.Run) and then terminates the program (TV.Done). The execution is carried out by TV.Run, which is identical to TApplication.Run.

The initialization of the program is carried out by the Init method. The init method of the TVisionApp object of AcFactor reads as

```
CONSTRUCTOR TVisionApp.Init;
VAR R : TRect;
  BEGIN
    RegisterObjects;
    RegisterViews;
    RegisterMenus;
    RegisterDialogs;
```

```
    RegisterApp;
    TApplication.Init;
    DataAvail := False;
    CritPtAvail := False;
    Filename := '';
    InitGlobals;
    { Initialization of Clock and Heap views : }
    GetExtent(R);
    R.A.X := R.B.X - 9;
    R.B.Y := R.A.Y + 1;
    Clock := New(PClockView,Init(R));
    Insert(Clock);
    GetExtent(R);
    Dec(R.B.X);
    R.A.X := R.B.X - 9;
    R.A.Y := R.B.Y - 1;
    Heap := New(PHeapView,Init(R));
    Insert(Heap);
    ProgName  := NewStr(sProgName);
    ProgPurp  := NewStr(sProgPurp);
    ProgVer   := NewStr(sProgVer);
    ProgDate  := NewStr(sProgDate);
    CopyRight := NewStr(sCopyRight);
    StartUpBox;

DBClrMode(M_EXPNDHANDLE+M_HALTONERROR+M_DISPLAYINFO+M_WITHDELETED+M_SEARCHE
XACT);
    DBSetMode(M_FLDREPLACES+M_BEEPONERROR+M_SHOWMESSAGE);
    DBInit;
    OpenDBF;
  END;
```

In order to allow the storage of the program configuration and the contents on the desktop (screen), the objects involved are registered. After registering the file viewer (RegisterFViewer), the clock is installed. This installation proceeds as follows. First, the coordinates of the desktop are got (GetExtent). The the coordinates of the record of type TRect are modified in such a way, that the clock appears in the menu bar, at the right side of the screen. Then the field Clock is initialized (this field is an instance of the type ClockView!) and inserted in the desktop. The initialization of the counter for the amount of free memory (HeapView) proceeds likewise. This counter is located at the right-most side of the status line.

After that, the fields ProgName, ProgPurp, ProgVer, ProgDate, and CopyRight are initialized, followed by a call to StartupBox, which displays this information. The initialization is completed after initialization of the editor and the clipboard, and the dBASE Engine.

The initialization of the status line and the menu bar are carried out by the method TApplication.Init. Since TVisionApp overwrites the virtual methods InitStatusLine and InitMenuBar, these methods are used rather than those of the TApplication object. This principle is known as *late binding*: the memory addresses of the methods are linked at run time rather than at compile time. The status line of TApplication has one entry: "Alt-X Exit". The status line of AcFactor is initialized as follows

```
PROCEDURE TVisionApp.InitStatusLine;
VAR R : TRect;
  BEGIN
    R.Assign(0,24,80,25);
```

```
    StatusLine := New(PStatusLine,Init(R,
      NewStatusDef(0,0,
        NewStatusKey('~Alt-X~ Exit',kbAltX,cmQuit,
        NewStatusKey('~F1~ Help',kbF1,cmHelp,
        NewStatusKey('~F10~ Menu',kbF10,cmMenu,
        NIL))),
      NIL)));
  END;
```

The option F10 activates the menu bar. After implementing the help system, the option F1-Help will be added as well.

The initialization of the menu bar is carried out by reading the menu from disk. The menu bar is read from the file ACFACTOR.MNU:

```
PROCEDURE TVisionApp.InitMenuBar;
VAR MenuStream : TDosStream;
  BEGIN
    MenuStream.Init('ACFACTOR.MNU',stOpenRead);
    MenuBar := PMenuBar(MenuStream.Get);
    MenuStream.Done;
  END;
```

The initialization of the global variables in AcFactor is carried out by a separate method, in fact InitGlobals. The reason for not including the initialization in the Init method (see above) is quite obvious: every time a new set of data is imported into AcFactor, the global variables should be set to their start-up defaults.

```
PROCEDURE TVisionApp.InitGlobals;
  BEGIN
    { Initialization of globals : }
    FillChar(WorkX,SizeOf(WorkX),0);
    FillChar(WorkY,SizeOf(WorkY),0);
    FillChar(VapRec,SizeOf(VapRec),0);
    FillChar(WorkSig,SizeOf(WorkSig),0);
    FillChar(ListA,SizeOf(ListA),0);
    FillChar(Covar,SizeOf(Covar),0);
    FillChar(Coeff,SizeOf(Coeff),0);
    FillChar(VapRec,SizeOf(VapRec),0);
    WorkN := 0; ResT := 0.0;
    Tcr := 0.0; Pcr := 0.0;
    Omega := 0.0;
    VapRec.ModelNo := 0; { Vapres2 }
  END;
```

The routine which processes menu commands (and all other types of "events") is called HandleEvent.

```
PROCEDURE TVisionApp.HandleEvent(VAR Event:TEvent);
  BEGIN
    TApplication.HandleEvent(Event);
    CASE Event.What OF
      evCommand : BEGIN
        CASE Event.Command OF
          cmAbout :
            AboutBox;
          cmCalculator :
            Calculator;
          cmChangeDir :
            ChangeDir;
          cmDOSShell :
            DOSShell;
```

```
        cmSetParam :
          DlgSetIsotherm(VapRec);
        cmImportData :
          WorkN := GetVapRec(VapRec,WorkX,WorkY);
        cmAppend :
          DlgArrayAppend(WorkX,WorkY,WorkN);
        cmModify :
          DlgArrayModify(WorkX,WorkY,WorkN);
        cmDelete :
          DlgArrayDelete(WorkX,WorkY,WorkN);
        cmEraseT :
          BEGIN
            FillChar(WorkX,SizeOf(WorkX),0);
            MessageBox(^C'Array "Temperatures" has been cleared.',NIL,
              mfInformation+mfOKButton);
          END;
        cmEraseP :
          BEGIN
            FillChar(WorkY,SizeOf(WorkY),0);
            MessageBox(^C'Array "Pressures" has been cleared.',NIL,
              mfInformation+mfOKButton);
          END;
        cmLinConvT :
          DlgArrayLin(WorkX,WorkN);
        cmLinConvP :
          DlgArrayLin(WorkY,WorkN);
        cmRecConvT :
          DlgArrayRec(WorkX,WorkN);
        cmRecConvP :
          DlgArrayRec(WorkY,WorkN);
        cmCalcAcF :
          CalcAcFactor(VapRec,Coeff);
        cmMLFit :
          MLFit;
        cmChModel :
          ChooseModel;
        cmSetMLParam :
          SetMLParam(Alamda00,Alamda01,MaxITest);
        cmResults :
          TotResult(VapRec);
      ELSE
        Exit;
      END; { CASE }
      ClearEvent(Event);
    END;
  END; { CASE }
END; { TVisionApp.HandleEvent }
```

The method TVisionApp.HandleEvent first calls its ancestor. This ancestor manages all other events than (menu) commands. If a menu option was selected, this option is processed (CASE-statement). At the end of the routine, the Event-field is cleared. Otherwise, an endless loop would be created!

The HandleEvent routine is called by the Run method of TApplication. In fact, the Run method is nothing else than an "endless" loop which processes commands, until the cmQuit command is given. In that case, the process is terminated and the program ends. The termination procedure (destructor method) has been discussed earlier this section.

The routine for closing down the program resembles the constructor TVision-App.Init. It is shown below.

```
DESTRUCTOR TVisionApp.Done;
  BEGIN
    DBTblCloseAll;
    DBExit;              { Deactivate dPAC ... }
    IF CopyRight<>NIL THEN DisposeStr(CopyRight);
    IF ProgDate<>NIL THEN DisposeStr(ProgDate);
    IF ProgVer<>NIL THEN DisposeStr(ProgVer);
    IF ProgPurp<>NIL THEN DisposeStr(ProgPurp);
    IF ProgName<>NIL THEN DisposeStr(ProgName);
    TApplication.Done;
  END;
```

The routine first closes all open files of the dBASE Engine, and it deallocates the memory used by the Engine (DBExit). Then the fields with program information are deallocated. Finally, the destructor TApplication.Done is called. This routine follows just the opposite direction for deallocations. The reason, that for instance the clock and het heap viewer do not need to be deallocated is, that they have been inserted into the desktop, and that they are deallocated when deallocating the application. All connected pointers are then checked.

III.4 Database

The database consists of a single main table (CODAMS2.DBF), and two tables containing vapour pressure data. The table TP_EQ.DBF contains only a subset of the fields present in TPV_EQ.DBF.

Table 4-1 : Structure of CODAMS2.DBF

Field	Field Name	Type	Width	Dec	
1	NAME	Character	100		Name of substance
2	TRIVNAME	Character	100		Trivial name
3	ABCNAME	Character	100		Alphabetical name
4	CODE	Character	6		code (primary key)
5	CAS	Character	11		chemical abstract sequence number
6	FORMULA	Character	25		molecular formula
7	MW	Numeric	8	3	molar weight
8	MP	Numeric	8	3	melting point
9	NBP	Numeric	8	3	normal boiling point
10	TPTEMP	Numeric	8	3	triple point temperature
11	TPPRES	Numeric	8	3	triple point pressure
12	PCR	Numeric	8	2	critical pressure
13	PCR_STATE	Character	1		status field P_{cr}
14	VCR	Numeric	8	3	critical volume
15	VCR_STATE	Character	1		status field V_{cr}
16	TCR	Numeric	8	3	critical temperature
17	TCR_STATE	Character	1		status field T_{cr}
18	OMEGA	Numeric	7	4	acentric factor
19	DIPOLE	Numeric	8	4	dipole moment (Debye)
20	GYRATION	Numeric	8	4	radius of gyration (A)
21	ZRA	Numeric	7	4	Rackett compressibility

Field	Field Name	Type	Width	Dec	
22	CRDATE	Date	8		date of creation of record
23	UPDATE	Date	8		date of last revision
24	H_FORM	Numeric	8	3	enthalpy of formation
25	H_STATE	Character	1		
26	S_FORM	Numeric	8	3	entropy of formation
27	S_STATE	Character	1		
28	CP0	Numeric	8	3	heat capacity
29	CP_STATE	Character	1		
30	LIT_CR	Numeric	5		reference critical data
31	LIT_ANT	Numeric	5		reference Antoine coefficients
32	LIT_VP	Numeric	5		reference vapour pressure data
33	RDL_A	Numeric	10	3	Riedel coefficient A
34	RDL_B	Numeric	10	3	Riedel coefficient B
35	RDL_C	Numeric	10	3	Riedel coefficient C
36	RDL_D	Numeric	10	3	Riedel coefficient D
37	RDL_TMIN	Numeric	8	3	Riedel min. temperature
38	RDL_TMAX	Numeric	8	3	Riedel max. temperature
39	VPR_A	Numeric	15	3	Vapres-2 coefficient A
40	VPR_B	Numeric	15	3	Vapres-2 coefficient B
41	VPR_C	Numeric	15	8	Vapres-2 coefficient C
42	VPR_D	Numeric	15	8	Vapres-2 coefficient D
43	VPR_E	Numeric	15	5	Vapres-2 coefficient E
44	VPR_TMIN	Numeric	8	3	
45	VPR_TMAX	Numeric	8	3	
46	CLG_A	Numeric	15	3	Clarke-Glew coefficient A
47	CLG_B	Numeric	15	3	Clarke-Glew coefficient B
48	CLG_C	Numeric	15	5	Clarke-Glew coefficient C
49	CLG_TMIN	Numeric	8	3	
50	CLG_TMAX	Numeric	8	3	
51	WNR_A	Numeric	8	3	Wagner coefficient A
52	WNR_B	Numeric	8	3	Wagner coefficient B
53	WNR_C	Numeric	8	3	Wagner coefficient C
54	WNR_D	Numeric	8	3	Wagner coefficient D
55	WNR_TYPE	Numeric	1		Wagner type (1, 2 or 3)
56	WNR_TMIN	Numeric	8	3	
57	WNR_TMAX	Numeric	8	3	
58	ANT_A	Numeric	10	3	Antoine coefficient A
59	ANT_B	Numeric	10	3	Antoine coefficient B
60	ANT_C	Numeric	8	3	Antoine coefficient C
61	ANT_TMIN	Numeric	8	3	
62	ANT_TMAX	Numeric	8	3	
63	COX_A	Numeric	8	3	Cox coefficient A
64	COX_B	Numeric	8	3	Cox coefficient B
65	COX_C	Numeric	8	3	Cox coefficient C
66	COX_TMIN	Numeric	8	3	
67	COX_TMAX	Numeric	8	3	

The status fields in the structure serve the purpose of categorising the origin of the data (experimental, estimation method, correlation, etc.).

Table 4-2 : Structure of TP_EQ.DBF

Field	Field Name	Type	Width	Dec
1	CODE	Character	6	
2	T	Numeric	19	5
3	P	Numeric	19	5
4	DTYPE	Character	1	

For most of the substances, the structure of TP_EQ.DBF was sufficient to hold all temperature dependent pure substance data. For the substances covered by the programme of NBS, it was not. For all substances, where more than only vapour pressure data was available, the structure below was used (table 4-3). Both TP_EQ.DBF and TPV_EQ.DBF implement a one to many relationship with CODAMS2.DBF. This relationship was maintained by the software.

Table 4-3 : Structure of TPV_EQ.DBF

Field	Field Name	Type	Width	Dec
1	CODE	Character	6	
2	T	Numeric	8	3
3	P	Numeric	14	5
4	VLIQ	Numeric	8	3
5	ZGAS	Numeric	8	3
6	ULIQ	Numeric	7	1
7	UGAS	Numeric	7	1
8	HLIQ	Numeric	7	1
9	HGAS	Numeric	7	1
10	SLIQ	Numeric	7	2
11	SGAS	Numeric	7	2
12	CVLIQ	Numeric	7	2
13	CVGAS	Numeric	7	2
14	CPLIQ	Numeric	7	2
15	CPGAS	Numeric	7	2
16	SND_LIQ	Numeric	7	1
17	SND_GAS	Numeric	7	1
18	VISC_LIQ	Numeric	7	2
19	VISC_GAS	Numeric	7	2
20	DTYPE	Character	1	

[1] Borland International, "Turbo Vision programming guide", Borland Pascal 7.0, Scotts Valley 1992

IV. LEAST SQUARES FITTING

IV.1 Principles

In this section and the next ones, least squares fitting is discussed as a method for obtaining the best possible coefficients of the model for a given set of measurements. In addition to obtaining these coefficients, there are two other items which should be considered while selecting a method. The coefficients on their own are not very valuable, if one does not know their uncertainties. This point is very important for discussing the reliability of the model. Further, a parameter should be computed which tells whether it is likely to have found a good model (with the appropriate values of the coefficients) or not.

For these reasons, *chi-square* fitting has been chosen to perform these tasks. Chi-square (χ^2) is a statistical defined parameter, which is defined as follows

$$\chi^2 = \sum_{i=1}^{n} \left\{ \frac{y_i - y(x_i;a)}{\sigma_i} \right\}^2 \qquad 1\text{-}1$$

where n is the number of data points, $y(x_i;a)$ is the by the model predicted value for the measured value y_i, a is the set of m coefficients, and σ_i is the random error in y_i. The division by σ_i of each term in the sum is very important: the sum is now dimensionless. The probability density of χ^2 at its minimum can be calculated analytically. This calculation is subject of section IV.4. The difference y_i-$y(x_i;a)$ will be written as Δy_i in the following.

For the models outlined in the previous chapter, χ^2 can be defined as follows

$$\chi^2 = \sum_{i=1}^{n} \left\{ \frac{P_i - P(T_i; A, B, C, \ldots)}{\sigma_i} \right\}^2 \qquad 1\text{-}2$$

The array a has been replaced by the coefficients A, B, C, etceteras, as used in the models of chapter 3. To use this definition of χ^2, the model used should calculate P itself, or P_r ($=P/P_{cr}$). If a linear relationship between the coefficients and the value predicted by the model is desired, then the equation should be linearised. The definition of χ^2 remains the same, but instead of P_i in most cases $\ln P_i$ is used (obviously, the value of σ_i should be recalculated).

The value of χ^2 should be minimised. Since χ^2 may be very complex (depending on the model), it may happen that there are more minima. Now the problem to be solved is therefore: find the absolute minimum. But, in general, it is practically impossible to figure out whether a minimum of χ^2 is absolute or relative. In the following, it is assumed the minimum being absolute. For the minimised value of χ^2, each of the derivatives of χ^2 with respect to the coefficients M a_j should be 0. This means that for every j from 1 to M the following equation holds [2]

$$0 = \sum_{i=1}^{N} \frac{\Delta y_i}{\sigma_i^2} \frac{\partial y(x_i; \ldots a_j \ldots)}{\partial a_j} \qquad 1\text{-}3$$

In general this is a set of M non-linear equations. There are various methods to solve this set of equations. One of them, the Marquardt-Levenberg method will be described later on in this chapter. In special cases, the set of equations can be solved in a single step. An example of such a special case is when the model is linear in its coefficients. In this case, the set of linear equations can be solved directly. This method will be discussed in the next section. When the model is non-linear, an iterative procedure is needed. In those cases, AcFactor solves the minimisation problem with the aid of a set of subroutines which implement the Marquardt-Levenberg method. This method is described in section IV.3.

IV.2 General Linear Least Squares

In the following, the way of solving the minimisation problem as defined in the previous section will be described in a rather formal way. Whenever illustrative, the Vapres-2 equation will be used as an example of the implementation of the general linear least squares (GLS) in AcFactor.

Each linear model can be written as follows

$$y_i = \sum_{k=1}^{M} a_k X_k(x_i) \qquad 2\text{-}1$$

where $X_k(x_i)$ is some function of $x_i$only. From this equation, χ^2 can be defined as follows:

$$\chi^2 = \sum_{i=1}^{N} \left\{ \frac{y_i - \sum_{k=1}^{M} a_k X_k(x_i)}{\sigma_i} \right\}^2 \qquad 2\text{-}2$$

If σ_i is not known, then it may be set to unity for all points.

Now a matrix A, called the *design matrix of the fitting problem*, can be defined. This matrix has dimensions N by M and its elements A_{ij} are defined as follows:

$$A_{ij} = X_j(x_i) \qquad 2\text{-}3$$

In general, A has more rows than columns (N≥M), since there should be more data points than coefficients in the model. The columns of this matrix contain the basis functions, which are in the case of the Vapres-2 equation 1, 1/T, T, T^2 and ln T. A vector b of length N can also be defined

$$b_i = \frac{y_i}{\sigma_i} \qquad 2\text{-}4$$

The minimum of χ^2 is reached when the derivative of χ^2 with respect to all M coefficients a_k is 0 [2]

$$0 = \sum_{i=1}^{N} \frac{1}{\sigma_i^2} \left\{ y_i - \sum_{j=1}^{M} a_j X_j(x_i) \right\} X_k(x_i) \qquad 2\text{-}5$$

After a few rearrangements the following matrix equation results [2]

$$[\alpha] \bullet a = [\beta] \qquad 2\text{-}6$$

which can be expressed in the matrix A and its transpose A^T

$$\{A^T \bullet A\} \bullet a = A^T \bullet b \qquad 2\text{-}7$$

The matrix α, which is the product of AA^T, is closely related to the covariance matrix. It may be derived that the relationship between the matrix α and the covariance matrix C is as follows

$$[\alpha] = C^{-1} \qquad 2\text{-}8$$

This means that the variance of the fitted coefficients a_j is equal to the matrix elements C_{jj}. The coefficients above and below the diagonal provide the covariances between all pairs of coefficients in the model. These variances and covariances may be used in further statistical treatment of the data.

In AcFactor, two methods have been implemented to solve the linear equations. The first way used to solve this problem is Gauss-Jordan elimination. In some cases, the set of equations is almost singular. In those cases, singular value decomposition (SVD) can be used to solve the set of equations. This method works even with singular matrices, but in that case the answer of the routine is not the desired one. (In fact, there is a large set of solutions.) However, in almost all cases Gauss-Jordan elimination will do the job. The matrix solver should be able to calculate the inverse of the matrix [α]. The Gauss-Jordan routine always calculates the inverse matrix, and the SVD method returns three matrices, which can be multiplied to obtain the inverse of [α]. Other matrix solving routines could be used as well, but they have to calculate the inverse of [α].

IV.3 Non-linear Least Squares: Marquardt-Levenberg method

Non-linear models need more mathematical and computational effort to obtain the coefficients of the model for which χ^2 is minimised. For non-linear models, an iterative calculation procedure is needed to improve step by step the coefficients. Iterative calculations have three important problems to deal with: first, find a set of starting estimates. Second, find an initial step size which is as large as possible, but not so large that the calculation routine shoots far over the target. And finally, one has to find a stopping criterion.

The stopping criterion for iterative least squares method follows from mathematical statistics. Since a change in χ^2 much less than 1 is never significant, the calculation can be terminated if χ^2 did not change significantly the last two (or more) steps. This means that a comparison should have to take place of the last value of χ^2 with the next last value, to calculate the difference [2].

The problem of the step size is difficult to solve in general. Fortunately, the Marquardt-Levenberg minimisation method provides a mechanism which is able control

this size itself. It is determined by a parameter, which becomes greater after each successful step and becomes smaller after a failure. A failure occurs when χ^2 increases if the new estimates for the coefficients are accepted. In those cases, the new estimates are not accepted and the only effect of the step is a change in step size. The problem of the initial step size remains unsolved. The Marquardt-Levenberg method provides some values of the initial step size and for the change in it which should satisfy in general. To find the appropriate choices for a given fitting problem is often question of "trial and error".

The third problem to deal with is the starting estimates of the coefficients. The solution of this problem depends on the kind of model in use. Almost all models presented in chapter 2 can be linearized. The linear form of a model can be used to calculate the starting estimates of the non-linear least squares fitting method by using the method described in the previous section. These estimates may be that good that a few iterations are needed to obtain the values of the coefficients which minimise χ^2 in case of the non-linear model.

The Marquardt-Levenberg method works as follows. Sufficiently close to the minimum, the χ^2 can be well approximated by a quadratic form [2]

$$\chi^2(a) \approx C - d \bullet a + \frac{1}{2} a \bullet D \bullet a \qquad 3\text{-}1$$

where c is some constant, d is an M-vector and D is an M by M matrix. If this approximation is good, then the coefficients a at the minimum can be calculated in one single step

$$a_{\min} = a_{cur} + D^{-1} \bullet \left[-\nabla \chi^2 (a_{cur}) \right] \qquad 3\text{-}2$$

If the approximation is poor, the only thing that can be done is take a step in the right direction

$$a_{next} = a_{cur} - \text{constant} \bullet \nabla \chi^2 (a_{cur}) \qquad 3\text{-}3$$

where the constant is small enough not to exhaust the downhill direction. This equation is a steepest descent formula. For the implementation of a fitting method which uses these two equations to step to the minimum, the calculation of the gradient of χ^2 is needed.

Using the same definition for χ^2 as in the previous sections, the gradient of χ^2, $\nabla\chi^2(a)$ can be calculated as follows. Each of the M partial derivatives with respect to the coefficients a_k has the form

$$\frac{\partial \chi^2}{\partial a_k} = -2 \sum_{i=1}^{N} \frac{\Delta y_i}{\sigma_i^2} \frac{\partial y(x_i;a)}{\partial a_k} \qquad 3\text{-}4$$

Taking an additional partial derivative yields

$$\frac{\partial^2 \chi^2}{\partial a_k \partial a_l} = 2 \sum_{i=1}^{N} \frac{1}{\sigma_i^2} \left\{ \frac{\partial y(x_i;a)}{\partial a_k} \frac{\partial y(x_i;a)}{\partial a_l} - \Delta y_i \frac{\partial^2 y(x_i;a)}{\partial a_k \partial a_l} \right\} \qquad 3\text{-}5$$

The factors 2 can be removed by defining

$$\beta_k \equiv -\frac{1}{2}\frac{\partial \chi^2}{\partial a_k} \qquad 3\text{-}6$$

$$\alpha_{kl} \equiv \frac{1}{2}\frac{\partial^2 \chi^2}{\partial a_k \partial a_l}$$

The matrix [α] is equal to 1/2•D. The equation to obtain a_{min} can now be written as a set of linear equations

$$\sum_{l=1}^{M} \alpha_{kl}\delta a_l = \beta_k \qquad 3\text{-}7$$

where δa_l are the increments to the current values of a. The steepest descent formula, which provides a_{next}, translates to

$$\delta a_l = \text{constant} \bullet \beta_l \qquad 3\text{-}8$$

which is a steepest descent equation.

The components of the Hessian matrix [α] depend both on the first and the second derivatives of χ^2. These second derivatives are very small if the model tends to be linear. Another reason why the term with the second derivatives could be neglected is that the difference y_i-$y(x_i;a)$ tends to cancel out when the summation over N points is taken. For a successful model should therefore this term in equation 3-5 be very small. As a result, α_{kl} can be defined as

$$\alpha_{kl} = \sum_{i=1}^{N} \frac{1}{\sigma_i^2}\left\{\frac{\partial y(x_i;a)}{\partial a_k}\frac{\partial y(x_i;a)}{\partial a_l}\right\} \qquad 3\text{-}9$$

This approximation does not affect the values a for which χ^2 reaches its minimum. It only affects the iterative route to be followed by the method. The criterion of the minimum is namely that β_k=0 for each k at the χ^2 minimum.

Now the Marquardt-Levenberg mechanism to find the minimum will be explained. There are two insights of Mr. Marquardt which form the principles of this method. In the first place, the constant in the steepest descent formula (3-9) should be considered. The value of this constant is very important to the process: its success or failure depends on it. Marquardt figured out that the following substitution for the constant should be performed

$$\delta a_l = \frac{1}{\lambda \alpha_{ll}}\beta_l \qquad 3\text{-}10$$

where λ is some non-dimensional constant. It may be derived that this equation is consistent with the units of each of the parameters al. The second insight refers to the matrix [α]. By combining its definition and the use of , a new matrix [α'] may be calculated

$$\alpha'_{jj} = \alpha_{jj}(1+\lambda) \qquad 3\text{-}11$$

$$\alpha'_{jk} = \alpha_{jk} \qquad 3\text{-}12$$

and a new linear set of equations results

$$\sum_{i=1}^{M} \alpha'_{kl}\, \delta a_l = \beta_k \qquad 3\text{-}13$$

When λ is very large, the matrix $[\alpha']$ is forced into being diagonal dominant, so equation (3-7) goes over into equation (3-8). The recommended procedure is now as follows [2]

- Compute $\chi^2(a)$.
- Pick a value for λ, say $\lambda = 0.001$.
- ($\surd$) Solve the set of linear equations for δa and evaluate $\chi^2(a+\delta a)$.
- If χ^2 has increased, increase λ by a factor (10 for example) and return to ($\surd$).
- If χ^2 has decreased, decrease λ by the same factor, update a (accept the new solution), and return to ($\surd$)

A criterion for the termination of this process has already been given. The process as outlined here is implemented in AcFactor. For calculating the matrix solution, the Gauss-Jordan elimination is used. For the minimum value of χ^2, the inverse of $[\alpha]$ is the covariance matrix C.

The full calculation process in AcFactor falls also in two parts. First, a linearized form of the vapour pressure equation is used to obtain the first estimates. If the user has chosen the nonlinear fitting option, the Marquardt-Levenberg method (ML) is performed to improve the results of the linear least squares method (GLS).

IV.4 Statistical Error Analysis

As outlined in the previous sections, the calculation routines in AcFactor are able to calculate the standard deviations in the coefficients. Unfortunately, the uncertainties in the coefficients tell nothing about the quality of the fit. For this purpose, the value of χ^2 at the minimum is needed, which is also calculated by the fitting routines. Depending on the number of degrees of freedom, one may calculate the chance of finding a value for χ^2 that is lower than the value in the current minimum. It is clear that this chance should be small for a good fit. Before the calculation procedure is shown, a few remarks about χ^2 should be made.

The value of χ^2 depends on the difference between the observed and the calculated values of the dependent variable (in our case the vapour pressure or some expression in it) and it depends on the random error of measurement. In many cases, the values of i are known or can be estimated. Whenever these random errors are not known or cannot be estimated, one can set them to unity and get the results from the fitting routine. For the calculations to be performed, the approximate values of i must be known or estimated, and in the following it is assumed so. If the random error is overestimated, χ^2 becomes too small and if the errors are underestimated, χ^2 becomes too large for a good fit. The user of the program should be aware of this problem, and be suspicious about the value of the chance Q (defined shortly) if one is not sure about the random error in the measurement.

The parameter Q can be calculated using the incomplete gamma function. This function has as input the value of χ^2 and the number of degrees of freedom, which is

equal to N-M (N = number of points, M = number of coefficients). Q is the probability that χ^2 should exceed a particular value of χ^2 by chance. If Q is very small for a particular set of data, then the apparent discrepancies are unlikely to be chance fluctuations. Much more probably either (1) the model is wrong -this can be statistically rejected-, (2) the random error σ_i is really larger than stated. There is a third reason why Q could be small: the errors may not be distributed normally.

The value of Q for a good model and a good fit should be larger than 10^{-3}. For a truely wrong model, Q can be as small as 10^{-18}. If the value of χ^2 is nearly unity, the fit is too good to be true. Often, this means the errors being overestimated. When the values of i are made smaller, Q decreases to a "normal" value.

The computation of Q will be shown shortly. Q is the symbol for the incomplete gamma function, which is closely related to the gamma function itself. The incomplete gamma function is the probability density function of χ^2. The gamma function, $\Gamma(a)$ is defined as follows [2]

$$\Gamma(a) = \int_0^\infty y^{\alpha-1} e^{-y} dy \qquad 4\text{-}1$$

It has been proved $\Gamma(a)$ being positive for $\alpha>0$. If $\alpha=1$, clearly

$$\Gamma(1) = \int_0^\infty e^{-y} dy \qquad 4\text{-}2$$

If $\alpha>1$, an integration by parts shows that

$$\Gamma(\alpha) = (\alpha-1)\int_0^\infty y^{\alpha-2} e^{-y} dy = (\alpha-1)\Gamma(\alpha-1) \qquad 4\text{-}3$$

Accordingly, if α is a positive integer and $\alpha>1$,

$$\Gamma(\alpha) = (\alpha-1)! \qquad 4\text{-}4$$

This equation implicates that the Γ-function for any positive integer is nothing else than the faculty of that integer minus 1. For computations, this fact is very important: it reduces the computational effort considerably.

The gamma distribution function can be derived as follows. In the definition of $\Gamma(a)$, y can be substituted by x/β, where $\beta>0$

$$\Gamma(\alpha) = \int_0^\infty \left(\frac{x}{\beta}\right)^{\alpha-1} e^{-\frac{x}{\beta}} \frac{1}{\beta} dx \qquad 4\text{-}5$$

or

$$1 = \int_0^\infty \left(\frac{x^{\alpha-1}}{\Gamma(\alpha)\beta^\alpha}\right) e^{-\frac{x}{\beta}} dx \qquad 4\text{-}6$$

Since $\alpha>0$, $\beta>0$, and $\Gamma(\alpha)>0$, a function f can be defined as follows

$$f(x) = \frac{1}{\Gamma(\alpha)\beta^\alpha} x^{\alpha-1} e^{-\frac{x}{\beta}} \qquad 4\text{-}7$$

where $0<x<\infty$ and

$$f(x) = 0 \qquad \text{4-8}$$

elsewhere. This function is the probability density function of the gamma distribution.

The incomplete gamma function $P(\alpha,x)$ is defined as follows

$$P(\alpha,x) = \frac{1}{\Gamma(\alpha)} \int_0^x e^{-t} t^{\alpha-1} dt \qquad \text{4-9}$$

which is closely related to the probability density function of the gamma distribution. P is defined for $\alpha>1$. The integral part can be denoted as $\gamma(\alpha,x)$. P has limiting values $P(\alpha,0)=0$ and $P(\alpha,\infty)=1$. Since Q is the complement of P, it is defined as follows

$$Q(\alpha,x) = \frac{\Gamma(\alpha,x)}{\Gamma(\alpha)} = \frac{1}{\Gamma(\alpha)} \int_x^\infty e^{-t} t^{\alpha-1} dt \qquad \text{4-10}$$

and has limiting values $Q(\alpha,0)=1$ and $Q(\alpha,\infty)=0$.

For $\gamma(\alpha,x)$ there is a series development, which makes it easier to evaluate the function

$$\gamma(\alpha,x) = e^{-x} x^{\alpha} \sum_{k=0}^{\infty} \frac{\Gamma(\alpha)}{\Gamma(\alpha+1+k)} x^k \qquad \text{4-11}$$

which can be terminated if the contribution of the last term is no longer significant. Each new value of $\Gamma(\alpha+1+k)$ can be calculated using its previous value.

The chance Q after a least squares fit can be calculated by substituting (N-M)/2 for α and $\chi^2/2$ for x. It can easily be seen that if the value of χ^2 increases, Q decreases (at constant α). For a given model and a given set of data, α is fixed, since both M and N are fixed.

[2] Press W.H., Flannery B.P., Teukolsky S.A., Vetterling W.T., "Numerical Recipes. The art of scientific computation", Cambridge University Press, Cambridge 1986

V. ESTIMATION METHODS FOR THE CRITICAL POINT

V.1 Introduction

For many heavy aromatic hydrocarbons, the critical point data (critical temperature, critical pressure, and critical volume) are not known. For some substances, they cannot even be measured, because under the conditions at the critical point, the substances are not stable. However, the critical point has not only physical significance, but it is also of mathematical interest. One could imagine that even if the critical point cannot be determined experimentally, it exists in the sense that the VLE-area can be extrapolated to a point, where the difference between vapour and liquid phases vanish.

The estimation procedures for the critical point serve a two-fold objective. Apart from substances, where no experimental critical data are available, the procedures enable the estimation of the critical point properties of a substance, that cannot exist physically under these conditions. These estimates can be used in equations of state for the calculation of the coefficients, and the calculation of the acentric factor.

V.2 Joback-Lydersen method

The Joback-Lydersen method is based on the method originally proposed by Lydersen in 1955. The method is based on three empirical formulae, which require the normal boiling point (for T_{cr}), the number of atoms in the molecule (n_A, for P_{cr}), and group contributions for P_{cr}, T_{cr}, V_{cr} T_m (melting point), and T_b (normal boiling point). The group contributions are tabulated in table 2-1.

Table 2-1 : Joback group contributions for critical properties, the normal boiling point and the freezing point

Group	ΔT_{cr}	ΔP_{cr}	ΔV_{cr}	ΔT_b	ΔT_m
-CH3	0.0141	-0.0012	65	23.58	-5.10
>CH2	0.0189	0.0000	56	22.88	11.27
>CH-	0.0164	0.0020	41	21.74	12.64
>C<	0.0067	0.0043	27	18.25	46.43
=CH2	0.0113	-0.0028	56	18.18	-4.32
=CH-	0.0129	-0.0006	46	24.96	8.73
=C<	0.0117	0.0011	38	24.14	11.14
=C=	0.0026	0.0028	36	26.15	17.78
≡CH	0.0027	-0.0008	46	9.20	-11.18
≡C-	0.0020	0.0016	37	27.38	64.32
-CH2- (ring)	0.0100	0.0025	48	27.15	7.75
>CH- (ring)	0.0122	0.0004	38	21.78	19.88
>C< (ring)	0.0042	0.0061	27	21.32	60.15
=CH- (ring)	0.0082	0.0011	41	26.73	8.13
=C< (ring)	0.0143	0.0008	32	31.01	37.02

Group	ΔT_{cr}	ΔP_{cr}	ΔV_{cr}	ΔT_b	ΔT_m
-F	0.0111	-0.0057	27	-0.03	-15.78
-Cl	0.0105	-0.0049	58	38.13	13.55
-Br	0.0133	0.0057	71	66.86	43.43
-I	0.0068	-0.0034	97	93.84	41.69
-OH (alcohol)	0.0741	0.0112	28	92.88	44.45
-OH (phenol)	0.0240	0.0184	-25	76.34	82.83
-O-	0.0168	0.0015	18	22.42	22.23
-O- (ring)	0.0098	0.0048	13	31.22	23.05
>C=O	0.0380	0.0031	62	76.75	61.20
>C=O (ring)	0.0284	0.0028	55	94.97	75.97
-CHO (aldehyde)	0.0379	0.0030	82	72.24	36.90
-COOH (acid)	0.0791	0.0077	89	169.09	155.50
-COO- (ester)	0.0481	0.0005	82	81.10	53.60
=O	0.0143	0.0101	36	-10.50	2.08
-NH2	0.0243	0.0109	38	73.23	66.89
>NH	0.0295	0.0077	35	50.17	52.66
>NH (ring)	0.0130	0.0114	29	52.82	101.51
>N-	0.0169	0.0074	9	11.74	48.84
-N=	0.0255	-0.0099	0	74.60	0.00
-N= (ring)	0.0085	0.0076	34	57.55	68.40
-CN	0.0496	-0.0101	91	125.66	59.89
$-NO_2$	0.0437	0.0064	91	152.54	127.24
-SH	0.0031	0.0084	63	63.56	20.09
-S-	0.0119	0.0049	54	68.78	34.40
-S- (ring)	0.0019	0.0051	38	52.10	79.93

The values at the critical point can be calculated by means of the following relationships:

$$T_{cr} = T_b\left[0.584 + 0.965\sum \Delta T_{cr} - \left(\sum \Delta T_{cr}\right)^2\right]^{-1} \qquad 2\text{-}1$$

$$P_{cr} = \left[0.113 + 0.0032 n_A - \sum \Delta P_{cr}\right]^{-2} \qquad 2\text{-}2$$

$$V_{cr} = 17.5 + \sum \Delta V_{cr} \qquad 2\text{-}3$$

The units of the critical point properties are Kelvin, bar, and ml/mole respectively. The calculation of $\Sigma\Delta T_{cr}$, $\Sigma\Delta P_{cr}$, and $\Sigma\Delta V_{cr}$ is very easy. First, the organic molecule has to be split up in fragments, according to table 2-1. This can be illustrated best by some examples.

The most simple group of hydrocarbons are the n-alkanes. Example 1 lists the groups appearing in the n-butane molecule. Summation of the group contributions and substituting them in the equations above yields the desired estimates for the critical point. In the next chapter, the results of this calculation are shown.

Example 1 : n-Butane

Compound	Butane $CH_3CH_2CH_2CH_3$				
Group	Frequency	ΔP_{cr}	ΔT_{cr}	ΔV_{cr}	n_A
CH3-	2	-0.0024	0.0282	130	8
CH2< (chain)	2	0	0.0378	112	6
<MI>Totals :		-0.0024	0.0660	242	14

More complex hydrocarbons, such as benzene, are also covered by the method. With a little fantasy, benzene can be regarded as being cyclohexatriene. Cyclohexatriene consists of 6 =CH- groups in a ring. This group is also listed in table 2-1. For substituted benzenes, the method works as follows. For each substitution at the ring, a =CH- (ring) group must be replaced by a =C< (ring) group. Now the substituents can be added. In example 2, this is shown for 1,3,5-trimethylbenzene.

Summation of the group contributions yields again the desired estimates. From the list of example 2, it may be concluded that the method does not distinguish between different substitutions at the benzene ring. It follows 1,2,4-trimethylbenzene has the same estimates as 1,3,5-trimethylbenzene. In the next chapter, the influence of the substitution on the critical properties will be investigated by the estimation of the critical properties of some substituted benzenes: xylenes (three isomers), methylphenols (three isomers) and xylenols (five isomers).

Example 2 : 1,3,5-Trimethylbenzene

Compound	1,3,5-Trimethylbenzene				
Group	Frequency	ΔP_{cr}	ΔT_{cr}	ΔV_{cr}	n_A
CH3-	3	-0.0036	0.0423	195	12
-CH= (ring)	3	0.0012	0.0366	114	6
=C< (ring)	3	0.0024	0.0429	96	3
<MI>Totals:		-0.0072	0.1218	405	21

In addition to the estimation of the critical point properties, the Joback-Lydersen method is capable in predicting the normal boiling point and the melting point of a pure compound as well. Table 2-1 lists also the increments for these estimations. The equations for the melting and the boiling point read as follows

$$T_b = 198 + \sum \Delta T_b \qquad 2\text{-}4$$

$$T_m = 122 + \sum \Delta T_m \qquad 2\text{-}5$$

The accuracy of the predictions of these equations is considerably lower than those of the critical point estimation formulae.

V.3 TRC-method

The Joback-Lydersen method for the estimation of the critical properties of pure organic compounds shows some insensitivity with respect of isomers, especially those related to aromatic hydrocarbons. This lack is the major reason for implementing a second estimation procedure. This method has been developed at the Thermodynamics Research Centre of the Texas A&M University (TRC).

The method from TRC has been developed from the methods of Lydersen, Ambrose, and Kreglewski. These methods are all similar to the Joback-Lydersen method. The method from TRC has some advantages however. First of all, ortho-, meta-, and para- substitutions are recognized by the method. Second, interactions between halogen atoms and between halogen atoms and hydrogen atoms (all non-bonded) are covered. Finally, the number of compounds has been extended. Many inorganic compounds can be treated as well.

The most obvious reason for implementing the method from TRC (the computer application has been called TRC too) is the better performance on substituted aromates. Since aromatic compounds form the basic components in coal fluids, and this application has been developed within the framework of a study into the thermodynamical properties of coal fluids, it is very important have an accurate estimation procedure, in order to have starting estimates for the critical point, when no or no reliable data are available.

Just as the Joback-Lydersen method, the TRC method uses some simple expressions in order to calculate the critical estimates from the group contributions. The expressions read as follows

$$F_t = a_t + b_t N_t \qquad 3\text{-}1$$

or alternatively

$$F_t = a_t + b_t N_t - b_t^2 N_t^2 \qquad 3\text{-}2$$

where

$$F_t = \frac{T_b}{T_{cr}} \qquad 3\text{-}3$$

where T_b is the boiling point temperature. For the critical pressure and volume, the expressions for G_p and G_V are similar to equation 3-1

$$G_p = a_p + b_p N_p \qquad 3\text{-}4$$

and

$$G_v = a_v + b_v N_v \qquad 3\text{-}5$$

Expression 3-5 yields the critical volume directly ($V_{cr} = G_v$), whereas the critical pressure is obtained via

$$P_{cr} = \frac{M}{G_p^2} \qquad 3\text{-}6$$

where M is the moelcular weight. In the equations appear the property N with subscripts t, p, v respectively. For each of the properties N_i, the following expression holds

$$N_i = \sum n_i \qquad 3\text{-}7$$

where n_i is a group index from table 2-2. The coefficients appearing in the equations 3-1, 3-2, 3-4, and 3-5 are given in table 3-1.

Table 3-1 : Values of the coefficients a_i and b_i

Equation	a_i	b_i
2-1	0.567	0.020
2-2	0.567	0.020
2-4	0.339	0.226
2-5	40.00	55.00

In table 3-2, the values for the group indices n_i are given.

Table 3-2 : Group contributions relative to the -CH_3 group for the TRC method

No.	Group	n_t	n_p	n_v
1	-CH_3	1.000	1.000	1.000
2	>CH_2	1.000	1.000	1.000
3	>CH-	0.849	1.079	0.970
4	>C<	0.494	1.104	0.987
5	C-C-C-C (gauche)	-0.197	-0.133	-0.086
6	-CH_2- (ring)	0.640	0.805	0.809
7	>CH- (ring)	0.640	0.805	0.809
8	>C< (ring)	0.420	0.805	0.809
9	>CH- (fused ring)	0.250	0.625	0.809
10	=CH_2	0.900	0.900	0.820
11	=CH-	0.800	0.800	0.780
12	=C<	0.800	0.800	0.780
13	=C=	0.400	0.600	0.400
14	trans alkene	-0.200	-0.150	0.000
15	=CH- (ring)	0.542	0.681	0.672
16	=C< (ring)	0.542	0.681	0.653
17	=C< (fused ring)	0.250	0.460	0.653
18	CH	1.180	0.690	0.653
19	C-	0.680	0.540	0.635
20	phenyl substitution	-1.000	-1.000	0.000
21	iso-Propyl	2.849	3.079	2.970
22	iso-Butyl	3.849	4.079	3.970
23	sec-Butyl	3.652	3.946	3.884
24	tert-Butyl	3.494	4.104	3.987
25	iso-Pentyl	4.652	4.946	4.884

No.	Group	n_t	n_p	n_v
26	neo-Pentyl	4.494	5.104	4.987
27	cyclobutyl	2.560	3.220	3.236
28	cyclopentyl	3.200	4.025	4.045
29	cyclohexyl	3.840	4.830	4.854
30	phenyl	3.252	4.086	4.032
31	naphthyl	4.836	6.368	6.682
32	vinyl	1.700	1.700	1.600
33	allyl	2.600	2.600	2.560
34	-OH (water)	0.870	-0.236	0.290
35	-OH (methanol)	4.000	0.284	0.290
36	-OH (ethanol)	4.670	0.360	0.290
37	-OH (propanol)	4.080	0.280	0.290
38	-OH (butanol)	3.490	0.200	0.290
39	-OH (pentanol)	2.900	0.120	0.290
40	-OH (hexanol)	2.310	0.040	0.290
41	-OH (heptanol)	1.720	-0.040	0.290
42	-OH (octanol)	1.130	-0.120	0.290
43	-OH (phenols)	1.530	-0.100	-0.014
44	-OH and X (ortho)	-0.340	-0.100	0.000
45	X and Y (ortho)	-0.100	-0.100	0.000
46	X and Y (meta)	0.200	0.100	0.000
47	C-C-C-OH (gauche)	-0.500	0.000	0.000
48	-O- (non-ring)	0.870	0.710	0.363
49	-O- (ring)	0.800	0.710	0.363
50	>CO (non-ring)	2.300	1.250	1.070
51	-C-C-C=O	-0.500	0.000	0.000
52	>C=O (ring)	3.300	1.540	1.100
53	-CHO	2.800	1.250	1.070
54	-C-C-CHO	-0.500	0.000	0.000
56	-CHO (aromatic)	1.250	1.100	1.070
56	-COOH	4.000	2.000	1.360
57	-C-C-COOH	0.400	0.000	0.000
58	-COO- (formates)	2.100	2.080	1.433
59	-COO-	2.100	2.080	1.433
60	-COO- (aromatic)	2.200	2.080	1.433
61	-CO-O-CO-	8.200	3.035	2.503
62	=O	1.000	0.660	0.290
63	-NH2	1.700	0.420	0.580
64	-NH-	1.500	0.420	0.580
65	-NH- (ring)	1.000	0.260	0.580
66	>N- (non-ring)	0.600	0.800	0.580
67	$-NH_2$ (aromatic)	1.500	0.280	0.580
68	>NH (aromatic)	1.500	0.280	0.580
69	>N- (aromatic)	1.500	0.500	0.580

No.	Group	n_t	n_p	n_v
70	>N- (ring)	0.050	0.260	0.580
71	=N- (general)	0.542	0.355	0.580
72	N^V	-0.400	0.040	0.580
73	-CN	3.000	1.580	1.450
74	-CN (aromatic)	1.800	1.330	1.450
75	$-NO_2$	2.700	2.000	1.420
76	$-CONH_2$	4.000	1.670	1.650
77	$-ONH_2$	2.600	1.130	0.943
78	N	1.250	1.260	0.900
79	HN (non-bonded)	2.000	-0.135	0.000
80	-SH	0.650	1.200	1.000
81	-S- (non-ring)	0.760	1.200	1.000
82	-S- (ring)	0.460	1.130	0.570
83	=S	0.260	1.200	1.000
84	S^{IV}	0.400	1.200	1.000
85	S^{VI}	0.800	0.800	1.000
86	-F (aliphatic)	0.688	1.072	0.230
87	-Cl (aliphatic)	0.570	1.409	0.820
88	-Br (aliphatic)	0.570	2.800	1.150
89	-I (aliphatic)	0.570	4.068	1.620
90	-F (aromatic)	0.572	0.827	0.230
91	-Cl (aromatic)	0.642	1.400	0.820
92	-Br (aromatic)	0.642	2.800	1.150
93	-I (aromatic)	0.642	4.086	1.620
94	HF (non-bonded)	0.230	-0.130	0.000
95	HCl (non-bonded)	0.093	-0.040	0.000
96	HBr (non-bonded)	0.040	0.000	0.000
97	HI (non-bonded)	0.040	0.000	0.000
98	FCl (non-bonded)	0.070	0.000	0.000
99	FBr (non-bonded)	-0.300	0.000	0.000
100	FI (non-bonded)	-0.030	0.000	0.000
101	ClBr (non-bonded)	-0.300	0.000	0.000
102	ClI (non-bonded)	-0.050	0.000	0.000
103	BrI (non-bonded)	-0.050	0.000	0.000
104	FC (non-bonded)	-0.230	-0.180	0.000
105	FC (non-bonded, in ring and alkenes)	-0.120	-0.140	-0.035
106	$-CF_3$ (normal)	3.064	4.216	1.690
107	$-CF_3$ (per)	2.604	3.856	1.690
108	$-CHF_2$ (normal)	2.836	2.884	1.460
109	$-CHF_2$ (per)	2.836	2.524	1.460
110	$-CH_2F$ (normal)	2.184	1.812	1.230
111	$>CF_2$ (normal)	2.376	3.144	1.460
112	$>CF_2$ (per)	1.456	2.424	1.460

No.	Group	n_t	n_p	n_v
113	>CF- (normal)	1.688	2.072	1.230
114	>CF- (per)	0.998	1.532	1.230
115	-CF_2- (ring, per)	1.546	2.389	1.199
116	-CHF- (ring, per)	1.328	1.467	0.969
117	>CF- (ring, per)	-0.400	1.417	0.969
118	=CF_2 (normal)	2.276	3.044	1.269
119	=CF_2 (per)	2.036	2.764	1.199
120	=CHF (per)	1.698	1.702	1.015
121	=CF- (per)	1.138	1.522	1.015
122	=CCl_2 (per)	1.800	3.438	2.390
123	=CHCl (per)	1.443	2.129	1.605
124	=CFCl (per)	1.988	3.101	1.800
125	=CF- (ring, per)	1.095	1.508	0.902
126	-CF_2Cl (normal)	3.086	4.553	2.280
127	-CF_2Cl (per)	2.626	4.193	2.280
128	-$CFCl_2$ (normal)	2.968	4.890	2.870
129	-$CFCl_2$ (per)	2.508	4.530	2.870
130	-CF_2Br (normal)	2.886	5.944	2.610
131	-CF_2Br (per)	2.426	5.584	2.610
132	-CRClBr (per)	2.378	5.921	2.610
133	-CCl_3 (normal)	2.710	5.227	3.460
134	-CCl_3 (per)	2.250	4.867	3.460
135	-$CHCl_2$	2.326	3.738	2.640
136	-CH_2Cl	1.756	2.329	1.820
137	-CH_2Br	1.650	3.800	2.150
138	-$CHBr_2$	2.220	6.600	3.300
139	-CH_2I	1.650	5.068	2.620
140	Se^{II}	0.400	2.700	1.500
141	Te^{II}	0.400	2.700	1.500
142	Si^{IV}	1.500	2.400	2.100
143	-$OSi(CH_3)_2$	3.600	5.110	4.463
144	-$OSiEt_2$	2.800	7.110	6.463
145	>Si< (ring)	0.800	2.400	2.100
146	C-C-Si-O	-0.900	0.000	0.000
147	Ge^{IV}	2.000	3.200	2.000
148	Sn^{IV}	2.000	4.500	2.400
149	Ti^{IV}	1.200	1.800	2.100
150	Zr^{IV}	14.000	1.800	2.200
151	Hf^{IV}	20.000	3.600	2.200
152	V^{III}	1.700	1.800	2.200
153	Nb^{V}	2.000	1.800	2.200
154	Ta^{V}	2.000	3.500	2.400
155	Mo^{VI}	0.500	2.000	2.900
156	W^{VI}	0.500	3.900	2.000

No.	Group	n_t	n_p	n_v
157	Hg^{II}	0.250	3.600	0.800
158	B^{III}	1.500	2.000	1.200
159	Al^{III}	6.000	4.000	1.500
159	Ga^{III}	5.000	4.000	1.500
160	P^{III}	1.000	1.700	1.600
161	P^{V}	0.750	1.700	1.600
163	As^{III}	1.000	1.500	1.400
172	Sb^{III}	0.750	1.500	1.800
173	Bi^{III}	0.500	1.500	1.500
174	U^{VI}	0.500	4.200	2.400
175	Re^{VI}	0.500	4.200	2.500
176	Os^{VIII}	0.500	4.200	2.500
177	-D	0.100	0.050	0.000
178	$Xe^{IV,VI}$	0.900	2.000	1.500
179	-H (part. ionic)	3.000	0.125	0.220

In comparison with the Joback-Lydersen method, several elements and steric corrections have been added. For several inorganic compounds, it is now possible to estimate the critical properties. In organic molecules, several interactions between groups play a role, such as the gauche-conformation, the interaction between halogen atoms and hydrogen or other halogen atoms, and the ortho and meta substitutions at the benzene ring. All these interactions have their influences on the critical point (see also the discussion of the Joback-Lydersen method), and therefore they should be taken into account.

VI. NMR-SPECTRA POINT OF AYR OIL

VI.1 Introduction

In this annex, the spectra of the fractions of the Point of Ayr oil are given. The spectra differ not to much from one another, so they are given here for the sake of completeness only.

VI.2 Spectra ^{13}C-NMR

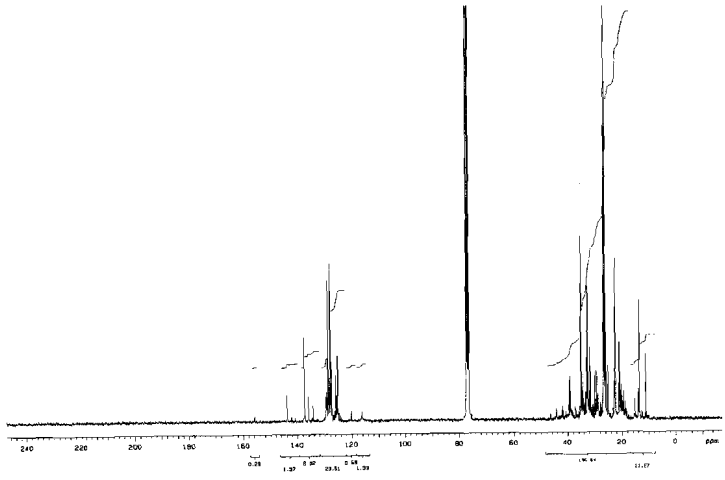

Figure 2-1 : ^{13}C-NMR spectrum of Point of Ayr oil, fraction < 150 C

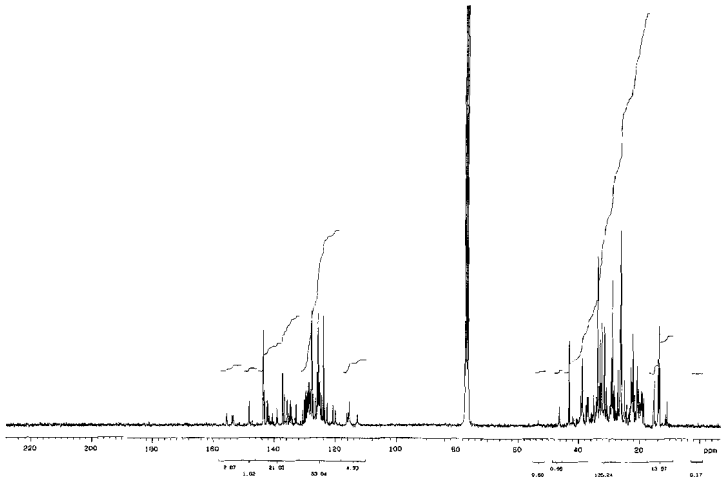

Figure 2-2 : ^{13}C-NMR spectrum of Point of Ayr oil, fraction 150-180 C

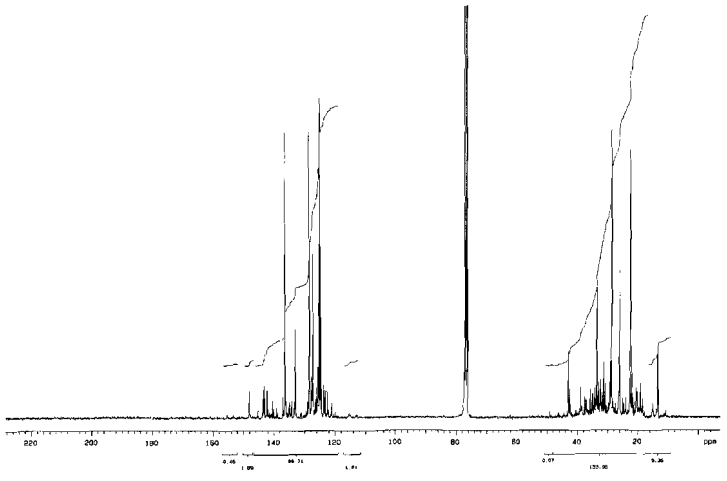

Figure 2-3 : ^{13}C-NMR spectrum of Point of Ayr oil, fraction 180-210 C

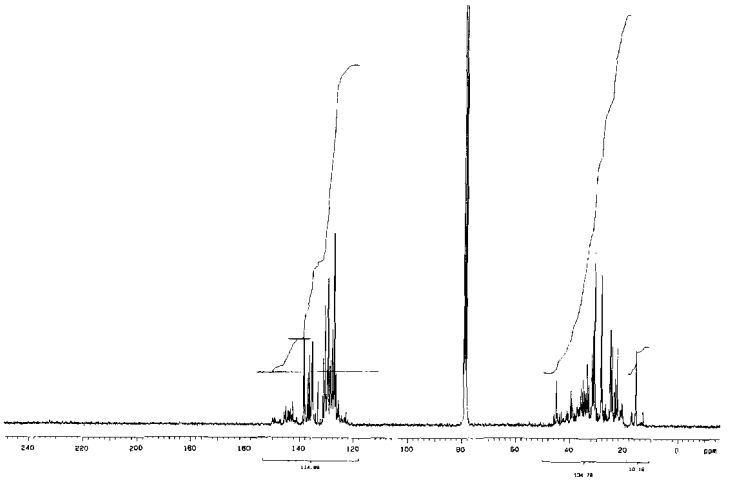

Figure 2-4 : ^{13}C-NMR spectrum of Point of Ayr oil, fraction 210-240 C

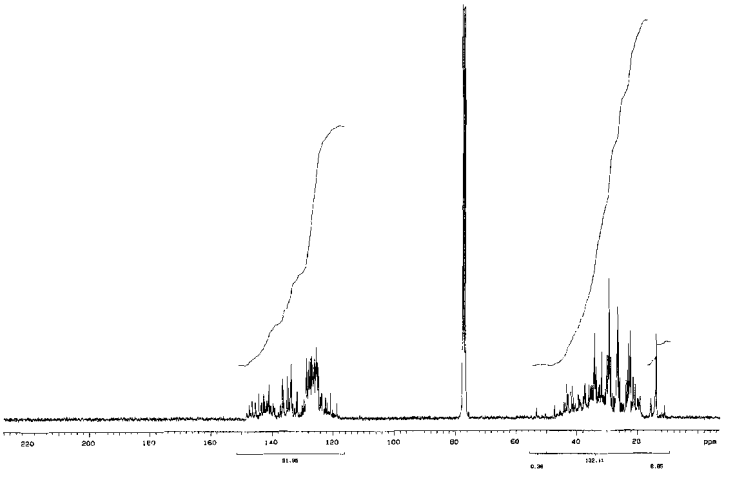

Figure 2-5 : ^{13}C-NMR spectrum of Point of Ayr oil, fraction 240-270 C

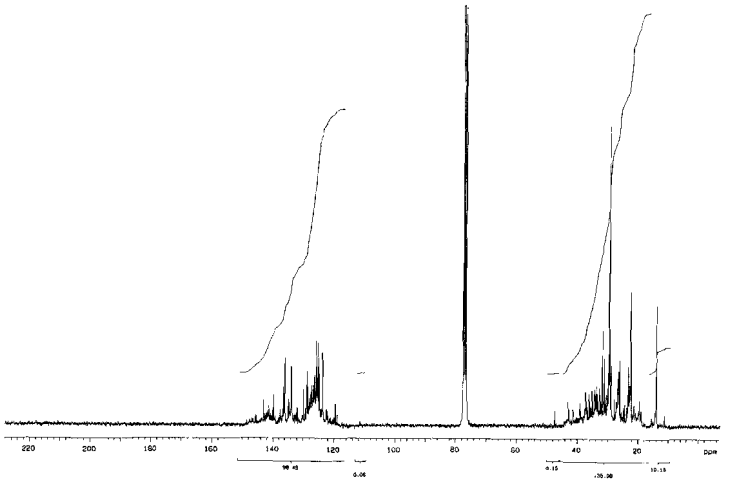

Figure 2-6 : ^{13}C-NMR spectrum of Point of Ayr oil, fraction 270-300 C

VI.3 ^{1}H-NMR spectra

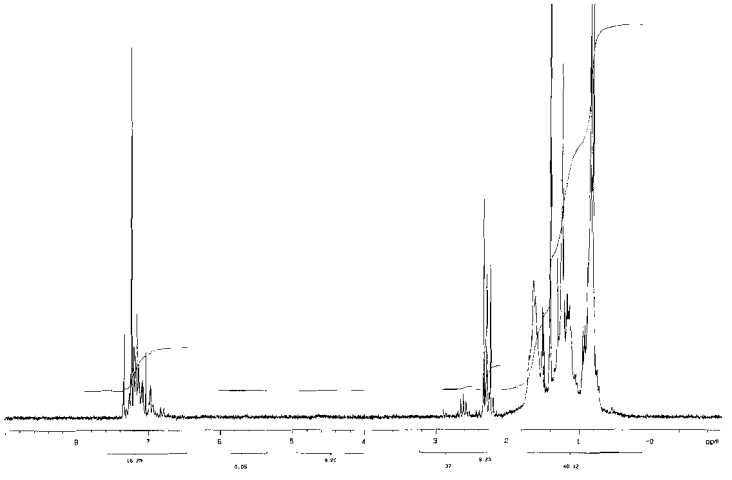

Figure 3-1 : ^{1}H-NMR spectrum of Point of Ayr oil, fraction < 150 C

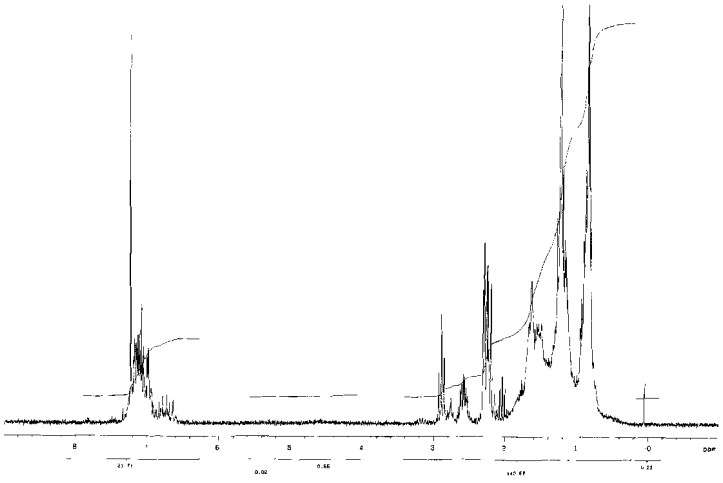

Figure 3-2 : ^{1}H-NMR spectrum of Point of Ayr oil, fraction 150-180 C

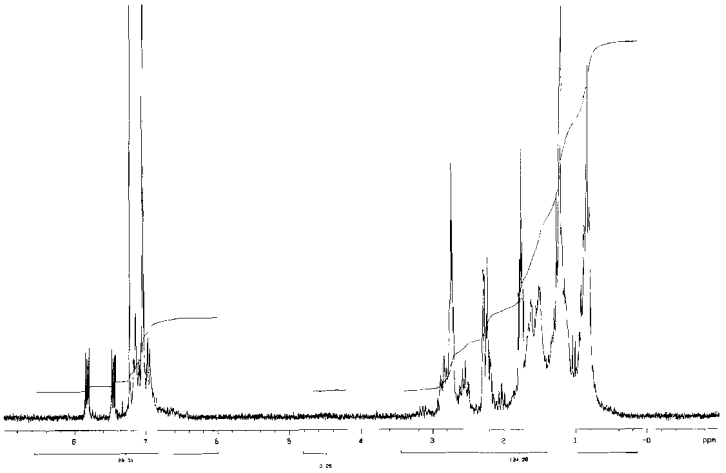

Figure 3-3 : ^{1}H-NMR spectrum of Point of Ayr oil, fraction 180-210 C

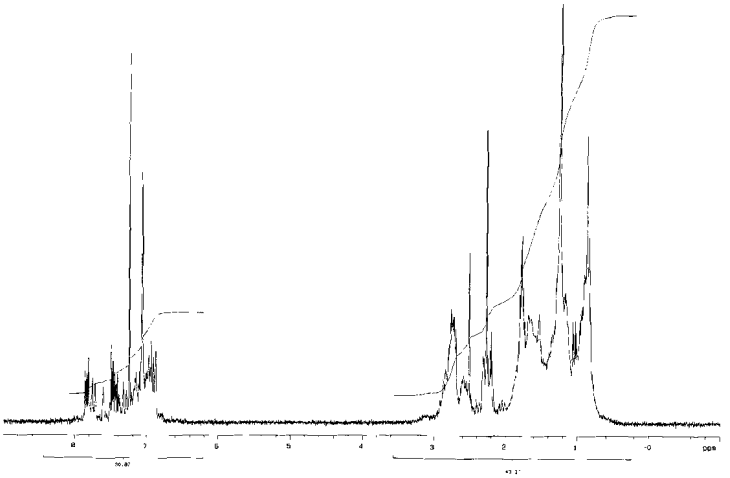

Figure 3-4 : ^{1}H-NMR spectrum of Point of Ayr oil, fraction 210-240 C

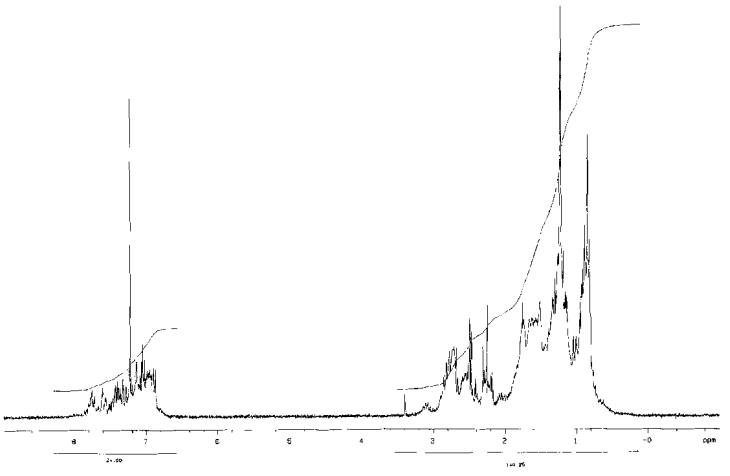

Figure 3-5 : ^{1}H-NMR spectrum of Point of Ayr oil, fraction 240-270 C

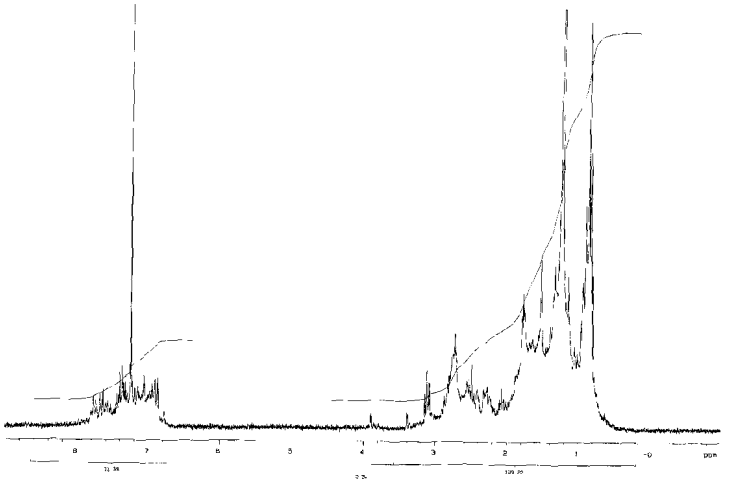

Figure 3-6 : ^{1}H-NMR spectrum of Point of Ayr oil, fraction 270-300 C

VII. CALCULATED RESULTS OF BINARY MIXTURES

This annex compiles the calculated K-factors and vapour pressures from the Soave-Redlich-Kwong and the Cubic Chain-of-Rotators equations of state.

VII.1 System Toluene - 1-Ethylnaphthalene (SRK)

Table 1-1 : Toluene - 1-Ethyl naphthalene (SRK) at T = 320 K

T (K)	x	y	K	P_{exp} (Pa)	P_{calc} (Pa)	P_{exp}-P_{calc} (Pa)	AAD
320	0.16	0.9839	6.149	1610	1773	-163	0.101
320	0.41	0.9955	2.428	4640	4507	133	0.029
320	0.51	0.997	1.955	5420	5601	-181	0.033
320	0.71	0.9987	1.407	6520	7775	-1255	0.192

Table 1-2 : Toluene - 1-Ethyl naphthalene (SRK) at T = 325 K

T (K)	x	y	K	P_{exp} (Pa)	P_{calc} (Pa)	P_{exp}-P_{calc} (Pa)	AAD
325	0.16	0.9818	6.136	1910	2199	-289	0.151
325	0.41	0.9949	2.427	5570	5581	-11	0.002
325	0.51	0.9966	1.954	6510	6934	-424	0.065
325	0.71	0.9985	1.406	8040	9624	-1584	0.197

Table 1-3 : Toluene - 1-Ethyl naphthalene (SRK) at T = 330 K

T (K)	x	y	K	P_{exp} (Pa)	P_{calc} (Pa)	P_{exp}-P_{calc} (Pa)	AAD
330	0.16	0.9794	6.121	2255	2706	-451	0.200
330	0.41	0.9943	2.425	6650	6859	-209	0.031
330	0.51	0.9962	1.953	7780	8521	-741	0.095
330	0.71	0.9984	1.406	9860	11823	-1963	0.199

Table 1-4 : Toluene - 1-Ethyl naphthalene (SRK) at T = 335 K

T (K)	x	y	K	P_{exp} (Pa)	P_{calc} (Pa)	P_{exp}-P_{calc} (Pa)	AAD
335	0.16	0.9769	6.106	2650	3308	-658	0.248
335	0.41	0.9936	2.423	7910	8369	-459	0.058
335	0.51	0.9957	1.952	9250	10395	-1145	0.124
335	0.71	0.9982	1.406	12010	14420	-2410	0.201

Table 1-5 : Toluene - 1-Ethyl naphthalene (SRK) at T = 340 K

T (K)	x	y	K	P_{exp} (Pa)	P_{calc} (Pa)	P_{exp}-P_{calc} (Pa)	AAD
340	0.16	0.9742	6.089	3100	4015	-915	0.295
340	0.41	0.9928	2.421	9350	10142	-792	0.085
340	0.51	0.9952	1.951	10930	12594	-1664	0.152
340	0.71	0.9979	1.405	14545	17469	-2924	0.201

Table 1-6 : Toluene - 1-Ethyl naphthalene (SRK) at T = 345 K

T (K)	x	y	K	P_{exp} (Pa)	P_{calc} (Pa)	P_{exp}-P_{calc} (Pa)	AAD
345	0.16	0.9713	6.071	3600	4843	-1243	0.345
345	0.41	0.9919	2.419	11000	12211	-1211	0.110
345	0.51	0.9946	1.950	12865	15161	-2296	0.178
345	0.71	0.9977	1.405	17520	21024	-3504	0.200

Table 1-7 : Toluene - 1-Ethyl naphthalene (SRK) at T = 350 K

T (K)	x	y	K	P_{exp} (Pa)	P_{calc} (Pa)	P_{exp}-P_{calc} (Pa)	AAD
350	0.16	0.9682	6.051	4175	5806	-1631	0.391
350	0.41	0.991	2.417	12880	14611	-1731	0.134
350	0.51	0.994	1.949	15065	18137	-3072	0.204
350	0.71	0.9974	1.405	20990	25147	-4157	0.198

Table 1-8 : Toluene - 1-Ethyl naphthalene (SRK) at T = 355 K

T (K)	x	y	K	P_{exp} (Pa)	P_{calc} (Pa)	P_{exp}-P_{calc} (Pa)	AAD
355	0.16	0.9648	6.030	4820	6921	-2101	0.436
355	0.41	0.9901	2.415	15015	17379	-2364	0.157
355	0.51	0.9933	1.948	17565	21569	-4004	0.228
355	0.71	0.9971	1.404	25025	29901	-4876	0.195

Table 1-9 : Toluene - 1-Ethyl naphthalene (SRK) at T = 360 K

T (K)	x	y	K	P_{exp} (Pa)	P_{calc} (Pa)	P_{exp}-P_{calc} (Pa)	AAD
360	0.16	0.9612	6.008	5540	8204	-2664	0.481
360	0.41	0.989	2.412	17430	20556	-3126	0.179
360	0.51	0.9926	1.946	20330	25506	-5176	0.255
360	0.71	0.9968	1.404	29685	35354	-5669	0.191

Table 1-10 : Toluene - 1-Ethyl naphthalene (SRK) at T = 365 K

T (K)	x	y	K	P_{exp} (Pa)	P_{calc} (Pa)	P_{exp}-P_{calc} (Pa)	AAD
365	0.16	0.9574	5.984	6345	9675	-3330	0.525
365	0.41	0.9879	2.410	20150	24183	-4033	0.200
365	0.51	0.9918	1.945	23580	30000	-6420	0.272
365	0.71	0.9965	1.404	35050	41577	-6527	0.186

Table 1-11 : Toluene - 1-Ethyl naphthalene (SRK) at T = 370 K

T (K)	x	y	K	P_{exp} (Pa)	P_{calc} (Pa)	P_{exp}-P_{calc} (Pa)	AAD
370	0.16	0.9533	5.958	7240	11351	-4111	0.568
370	0.41	0.9867	2.407	23205	28304	-5099	0.220
370	0.51	0.991	1.943	27155	35105	-7950	0.293
370	0.71	0.9961	1.403	41200	48646	-7446	0.181

Table 1-12 : Toluene - 1-Ethyl naphthalene (SRK) at T = 375 K

T (K)	x	y	K	P_{exp} (Pa)	P_{calc} (Pa)	P_{exp}-P_{calc} (Pa)	AAD
375	0.16	0.949	5.931	8230	13255	-5025	0.611
375	0.41	0.9854	2.403	26620	32965	-6345	0.238
375	0.51	0.9901	1.941	31160	40877	-9717	0.312
375	0.71	0.9957	1.402	48220	56637	-8417	0.175

Table 1-13 : Toluene - 1-Ethyl naphthalene (SRK) at T = 380 K

T (K)	x	y	K	P_{exp} (Pa)	P_{calc} (Pa)	P_{exp}-P_{calc} (Pa)	AAD
380	0.16	0.9445	5.903	9325	15408	-6083	0.652
380	0.41	0.984	2.400	30340	38214	-7874	0.260
380	0.51	0.9892	1.940	35620	47375	-11755	0.330
380	0.71	0.9953	1.402	56200	65634	-9434	0.168

VII.2 System Toluene - 1-Ethylnaphthalene (CCOR)

Table 2-1 : Toluene - 1-Ethyl naphthalene (CCOR) at T = 320 K

T (K)	x	y	K	P_{exp} (Pa)	P_{calc} (Pa)	P_{exp}-P_{calc} (Pa)	AAD
320	0.16	0.9904	6.190	1610	2386	-776	0.482
320	0.41	0.9969	2.431	4640	5456	-816	0.176
320	0.51	0.9977	1.956	5420	6472	-1052	0.194
320	0.71	0.9987	1.407	6520	8173	-1653	0.254

Table 2-2 : Toluene - 1-Ethyl naphthalene (CCOR) at T = 325 K

T (K)	x	y	K	P_{exp} (Pa)	P_{calc} (Pa)	P_{exp}-P_{calc} (Pa)	AAD
325	0.16	0.9889	6.181	1910	2941	-1031	0.540
325	0.41	0.9964	2.430	5570	6733	-1163	0.209
325	0.51	0.9974	1.956	6510	7993	-1483	0.228
325	0.71	0.9985	1.406	8040	10116	-2076	0.258

Table 2-3 : Toluene - 1-Ethyl naphthalene (CCOR) at T = 330 K

T (K)	x	y	K	P_{exp} (Pa)	P_{calc} (Pa)	P_{exp}-P_{calc} (Pa)	AAD
330	0.16	0.9872	6.170	2255	3599	-1344	0.596
330	0.41	0.9958	2.429	6650	8244	-1594	0.240
330	0.51	0.997	1.955	7780	9796	-2016	0.259
330	0.71	0.9983	1.406	9860	12423	-2563	0.260

Table 2-4 : Toluene - 1-Ethyl naphthalene (CCOR) at T = 335 K

T (K)	x	y	K	P_{exp} (Pa)	P_{calc} (Pa)	P_{exp}-P_{calc} (Pa)	AAD
335	0.16	0.9853	6.158	2650	4370	-1720	0.649
335	0.41	0.9952	2.427	7910	10020	-2110	0.267
335	0.51	0.9965	1.954	9250	11917	-2667	0.288
335	0.71	0.9981	1.406	12010	15144	-3134	0.261

Table 2-5 : Toluene - 1-Ethyl naphthalene (CCOR) at T = 340 K

T (K)	x	y	K	P_{exp} (Pa)	P_{calc} (Pa)	P_{exp}-P_{calc} (Pa)	AAD
340	0.16	0.9833	6.146	3100	5271	-2171	0.700
340	0.41	0.9945	2.426	9350	12095	-2745	0.294
340	0.51	0.996	1.953	10930	14397	-3467	0.317
340	0.71	0.9978	1.405	14545	18332	-3787	0.260

Table 2-6 : Toluene - 1-Ethyl naphthalene (CCOR) at T = 345 K

T (K)	x	y	K	P_{exp} (Pa)	P_{calc} (Pa)	P_{exp}-P_{calc} (Pa)	AAD
345	0.16	0.981	6.131	3600	6317	-2717	0.755
345	0.41	0.9938	2.424	11000	14502	-3502	0.318
345	0.51	0.9955	1.952	12865	17277	-4412	0.343
345	0.71	0.9975	1.405	17520	22045	-4525	0.258

Table 2-7 : Toluene - 1-Ethyl naphthalene (CCOR) at T = 350 K

T (K)	x	y	K	P_{exp} (Pa)	P_{calc} (Pa)	P_{exp}-P_{calc} (Pa)	AAD
350	0.16	0.9785	6.116	4175	7522	-3347	0.802
350	0.41	0.993	2.422	12880	17280	-4400	0.342
350	0.51	0.9949	1.951	15065	20603	-5538	0.368
350	0.71	0.9972	1.405	20990	26342	-5352	0.255

Table 2-8 : Toluene - 1-Ethyl naphthalene (CCOR) at T = 355 K

T (K)	x	y	K	P_{exp} (Pa)	P_{calc} (Pa)	P_{exp}-P_{calc} (Pa)	AAD
355	0.16	0.9758	6.099	4820	8905	-4085	0.848
355	0.41	0.9921	2.420	15015	20465	-5450	0.363
355	0.51	0.9942	1.949	17565	24421	-6856	0.390
355	0.71	0.9969	1.404	25025	31289	-6264	0.250

Table 2-9 : Toluene - 1-Ethyl naphthalene (CCOR) at T = 360 K

T (K)	x	y	K	P_{exp} (Pa)	P_{calc} (Pa)	P_{exp}-P_{calc} (Pa)	AAD
360	0.16	0.9728	6.080	5540	10483	-4943	0.892
360	0.41	0.9911	2.417	17430	24100	-6670	0.383
360	0.51	0.9935	1.948	20330	28783	-8453	0.416
360	0.71	0.9965	1.404	29685	36953	-7268	0.245

Table 2-10 : Toluene - 1-Ethyl naphthalene (CCOR) at T = 365 K

T (K)	x	y	K	P_{exp} (Pa)	P_{calc} (Pa)	P_{exp}-P_{calc} (Pa)	AAD
365	0.16	0.9696	6.060	6345	12275	-5930	0.935
365	0.41	0.99	2.415	20150	28227	-8077	0.401
365	0.51	0.9927	1.946	23580	33739	-10159	0.431
365	0.71	0.9961	1.403	35050	43406	-8356	0.238

Table 2-11 : Toluene - 1-Ethyl naphthalene (CCOR) at T = 370 K

T (K)	x	y	K	P_{exp} (Pa)	P_{calc} (Pa)	P_{exp}-P_{calc} (Pa)	AAD
370	0.16	0.9661	6.038	7240	14301	-7061	0.975
370	0.41	0.9888	2.412	23205	32889	-9684	0.417
370	0.51	0.9919	1.945	27155	39344	-12189	0.449
370	0.71	0.9956	1.402	41200	50722	-9522	0.231

Table 2-12 : Toluene - 1-Ethyl naphthalene (CCOR) at T = 375 K

T (K)	x	y	K	P_{exp} (Pa)	P_{calc} (Pa)	P_{exp}-P_{calc} (Pa)	AAD
375	0.16	0.9624	6.015	8230	16582	-8352	1.015
375	0.41	0.9875	2.409	26620	38132	-11512	0.432
375	0.51	0.9909	1.943	31160	45653	-14493	0.465
375	0.71	0.9952	1.402	48220	58978	-10758	0.223

Table 2-13 : Toluene - 1-Ethyl naphthalene (CCOR) at T = 380 K

T (K)	x	y	K	P_{exp} (Pa)	P_{calc} (Pa)	P_{exp}-P_{calc} (Pa)	AAD
380	0.16	0.9584	5.990	9325	19137	-9812	1.052
380	0.41	0.9862	2.405	30340	44003	-13663	0.450
380	0.51	0.9899	1.941	35620	52724	-17104	0.480
380	0.71	0.9946	1.401	56200	68256	-12056	0.215

VII.3 System Toluene - 2-Methoxynaphthalene (SRK)

Table 3-1 : Toluene - 2-Methoxy naphthalene (SRK) at T = 310 K

T (K)	x	y	K	P_{exp} (Pa)	P_{calc} (Pa)	P_{exp}-P_{calc} (Pa)	AAD
310	0.18	0.9963	5.535	1500	1308	192	0.128
310	0.39	0.9987	2.561	3660	2811	849	0.232
310	0.52	0.9992	1.922	4640	3721	919	0.198
310	0.67	0.9996	1.492	6320	4743	1577	0.250
310	0.89	0.9999	1.123	6450	6201	249	0.039

Table 3-2 : Toluene - 2-Methoxy naphthalene (SRK) at T = 315 K

T (K)	x	y	K	P_{exp} (Pa)	P_{calc} (Pa)	P_{exp}-P_{calc} (Pa)	AAD
315	0.18	0.9956	5.531	1790	1646	144	0.080
315	0.39	0.9985	2.560	4390	3538	852	0.194
315	0.52	0.9991	1.921	5550	4682	868	0.156
315	0.67	0.9995	1.492	7580	5967	1613	0.213
315	0.89	0.9999	1.123	7920	7801	119	0.015

Table 3-3 : Toluene - 2-Methoxy naphthalene (SRK) at T = 320 K

T (K)	x	y	K	P_{exp} (Pa)	P_{calc} (Pa)	P_{exp}-P_{calc} (Pa)	AAD
320	0.18	0.9949	5.527	2110	2055	55	0.026
320	0.39	0.9982	2.559	5200	4414	786	0.151
320	0.52	0.9989	1.921	6600	5842	758	0.115
320	0.67	0.9994	1.492	9040	7445	1595	0.176
320	0.89	0.9998	1.123	9700	9732	-32	0.003

Table 3-4 : Toluene - 2-Methoxy naphthalene (SRK) at T = 325 K

T (K)	x	y	K	P_{exp} (Pa)	P_{calc} (Pa)	P_{exp}-P_{calc} (Pa)	AAD
325	0.18	0.994	5.522	2500	2546	-46	0.018
325	0.39	0.9979	2.559	6200	5465	735	0.119
325	0.52	0.9988	1.921	7800	7231	569	0.073
325	0.67	0.9993	1.491	10700	9214	1486	0.139
325	0.89	0.9998	1.123	11800	12045	-245	0.021

Table 3-5 : Toluene - 2-Methoxy naphthalene (SRK) at T = 330 K

T (K)	x	y	K	P_{exp} (Pa)	P_{calc} (Pa)	P_{exp}-P_{calc} (Pa)	AAD
330	0.18	0.9931	5.517	2930	3130	-200	0.068
330	0.39	0.9976	2.558	7320	6715	605	0.083
330	0.52	0.9986	1.920	9170	8883	287	0.031
330	0.67	0.9992	1.491	12650	11318	1332	0.105
330	0.89	0.9998	1.123	14300	14796	-496	0.035

Table 3-6 : Toluene - 2-Methoxy naphthalene (SRK) at T = 335 K

T (K)	x	y	K	P_{exp} (Pa)	P_{calc} (Pa)	P_{exp}-P_{calc} (Pa)	AAD
335	0.18	0.9921	5.512	3420	3821	-401	0.117
335	0.39	0.9972	2.557	8600	8191	409	0.048
335	0.52	0.9983	1.920	10750	10834	-84	0.008
335	0.67	0.9991	1.491	14850	13803	1047	0.071
335	0.89	0.9998	1.123	17200	18045	-845	0.049

Table 3-7 : Toluene - 2-Methoxy naphthalene (SRK) at T = 340 K

T (K)	x	y	K	P_{exp} (Pa)	P_{calc} (Pa)	P_{exp}-P_{calc} (Pa)	AAD
340	0.18	0.9909	5.505	4000	4632	-632	0.158
340	0.39	0.9968	2.556	10000	9923	77	0.008
340	0.52	0.9981	1.919	12500	13123	-623	0.050
340	0.67	0.999	1.491	17350	16719	631	0.036
340	0.89	0.9997	1.123	20600	21858	-1258	0.061

Table 3-8 : Toluene - 2-Methoxy naphthalene (SRK) at T = 345 K

T (K)	x	y	K	P_{exp} (Pa)	P_{calc} (Pa)	P_{exp}-P_{calc} (Pa)	AAD
345	0.18	0.9896	5.498	4600	5580	-980	0.213
345	0.39	0.9964	2.555	11700	11943	-243	0.021
345	0.52	0.9978	1.919	14500	15793	-1293	0.089
345	0.67	0.9988	1.491	20200	20119	81	0.004
345	0.89	0.9997	1.123	24500	26306	-1806	0.074

Table 3-9 : Toluene - 2-Methoxy naphthalene (SRK) at T = 350 K

T (K)	x	y	K	P_{exp} (Pa)	P_{calc} (Pa)	P_{exp}-P_{calc} (Pa)	AAD
350	0.18	0.9882	5.490	5300	6679	-1379	0.260
350	0.39	0.9959	2.554	13500	14285	-785	0.058
350	0.52	0.9975	1.918	16800	18888	-2088	0.124
350	0.67	0.9986	1.490	23400	24061	-661	0.028
350	0.89	0.9996	1.123	29000	31463	-2463	0.085

Table 3-10 : Toluene - 2-Methoxy naphthalene (SRK) at T = 355 K

T (K)	x	y	K	P_{exp} (Pa)	P_{calc} (Pa)	P_{exp}-P_{calc} (Pa)	AAD
355	0.18	0.9867	5.482	6100	7949	-1849	0.303
355	0.39	0.9953	2.552	15600	16986	-1386	0.089
355	0.52	0.9972	1.918	19300	22456	-3156	0.164
355	0.67	0.9985	1.490	27000	28605	-1605	0.059
355	0.89	0.9996	1.123	34200	37410	-3210	0.094

Table 3-11 : Toluene - 2-Methoxy naphthalene (SRK) at T = 360 K

T (K)	x	y	K	P_{exp} (Pa)	P_{calc} (Pa)	P_{exp}-P_{calc} (Pa)	AAD
360	0.18	0.985	5.472	7000	9406	-2406	0.344
360	0.39	0.9947	2.551	18000	20083	-2083	0.116
360	0.52	0.9968	1.917	22100	26548	-4448	0.201
360	0.67	0.9983	1.490	31000	33817	-2817	0.091
360	0.89	0.9995	1.123	40100	44232	-4132	0.103

Table 3-12 : Toluene - 2-Methoxy naphthalene (SRK) at T = 365 K

T (K)	x	y	K	P_{exp} (Pa)	P_{calc} (Pa)	P_{exp}-P_{calc} (Pa)	AAD
365	0.18	0.9831	5.462	7930	11072	-3142	0.396
365	0.39	0.994	2.549	20500	23617	-3117	0.152
365	0.52	0.9964	1.916	25300	31216	-5916	0.234
365	0.67	0.998	1.490	35500	39763	-4263	0.120
365	0.89	0.9995	1.123	46900	52019	-5119	0.109

Table 3-13 : Toluene - 2-Methoxy naphthalene (SRK) at T = 370 K

T (K)	x	y	K	P_{exp} (Pa)	P_{calc} (Pa)	P_{exp}-P_{calc} (Pa)	AAD
370	0.18	0.9811	5.451	9000	12966	-3966	0.441
370	0.39	0.9933	2.547	23400	27629	-4229	0.181
370	0.52	0.996	1.915	28800	36516	-7716	0.268
370	0.67	0.9978	1.489	40500	46515	-6015	0.149
370	0.89	0.9994	1.123	54500	60865	-6365	0.117

Table 3-14 : Toluene - 2-Methoxy naphthalene (SRK) at T = 375 K

T (K)	x	y	K	P_{exp} (Pa)	P_{calc} (Pa)	P_{exp}-P_{calc} (Pa)	AAD
	0.18	375	5.439	10200	15111	-4911	0.481
375	0.39	0.9925	2.545	26600	32164	-5564	0.209
375	0.52	0.9955	1.914	32600	42506	-9906	0.304
375	0.67	0.9975	1.489	46000	54147	-8147	0.177
375	0.89	0.9993	1.123	63200	70869	-7669	0.121

Table 3-15 : Toluene - 2-Methoxy naphthalene (SRK) at T = 380 K

T (K)	x	y	K	P_{exp} (Pa)	P_{calc} (Pa)	P_{exp}-P_{calc} (Pa)	AAD
380	0.18	0.9766	5.426	11500	17528	-6028	0.524
380	0.39	0.9917	2.543	30100	37268	-7168	0.238
380	0.52	0.995	1.913	36900	49245	-12345	0.335
380	0.67	0.9972	1.488	52000	62737	-10737	0.206
380	0.89	0.9992	1.123	73000	82134	-9134	0.125

Table 3-16 : Toluene - 2-Methoxy naphthalene (SRK) at T = 385 K

T (K)	x	y	K	P_{exp} (Pa)	P_{calc} (Pa)	P_{exp}-P_{calc} (Pa)	AAD
385	0.18	0.9741	5.412	21900	20242	1658	0.076
385	0.39	0.9907	2.540	34000	42987	-8987	0.264
385	0.52	0.9944	1.912	41500	56798	-15298	0.369
385	0.67	0.9969	1.488	58800	72363	-13563	0.231
385	0.89	0.9992	1.123	83900	94768	-10868	0.130

VII.4 System Toluene - 2-Methoxynaphthalene (CCOR)

Table 4-1 : Toluene - 2-Methoxy naphthalene (CCOR) at T = 310 K

T (K)	x	y	K	P_{exp} (Pa)	P_{calc} (Pa)	P_{exp}-P_{calc} (Pa)	AAD
310	0.18	0.998	5.544	1500	1719	-219	0.146
310	0.39	0.9992	2.562	3660	3362	298	0.081
310	0.52	0.9995	1.922	4640	4193	447	0.096
310	0.67	0.9996	1.492	6320	4995	1325	0.210
310	0.89	0.9999	1.123	6450	5998	452	0.070

Table 4-2 : Toluene - 2-Methoxy naphthalene (CCOR) at T = 315 K

T (K)	x	y	K	P_{exp} (Pa)	P_{calc} (Pa)	P_{exp}-P_{calc} (Pa)	AAD
315	0.18	0.9975	5.542	1790	2155	-365	0.204
315	0.39	0.999	2.562	4390	4220	170	0.039
315	0.52	0.9993	1.922	5550	5268	282	0.051
315	0.67	0.9996	1.492	7580	6286	1294	0.171
315	0.89	0.9998	1.123	7920	7563	357	0.045

Table 4-3 : Toluene - 2-Methoxy naphthalene (CCOR) at T = 320 K

T (K)	x	y	K	P_{exp} (Pa)	P_{calc} (Pa)	P_{exp}-P_{calc} (Pa)	AAD
320	0.18	0.997	5.539	2110	2678	-568	0.269
320	0.39	0.9988	2.561	5200	5251	-51	0.010
320	0.52	0.9992	1.922	6600	6563	37	0.006
320	0.67	0.9995	1.492	9040	7842	1198	0.133
320	0.89	0.9998	1.123	9700	9455	245	0.025

Table 4-4 : Toluene - 2-Methoxy naphthalene (CCOR) at T = 325 K

T (K)	x	y	K	P_{exp} (Pa)	P_{calc} (Pa)	P_{exp}-P_{calc} (Pa)	AAD
325	0.18	0.9965	5.536	2500	3301	-801	0.320
325	0.39	0.9986	2.561	6200	6481	-281	0.045
325	0.52	0.9991	1.921	7800	8109	-309	0.040
325	0.67	0.9994	1.492	10700	9703	997	0.093
325	0.89	0.9998	1.123	11800	11722	78	0.007

Table 4-5 : Toluene - 2-Methoxy naphthalene (CCOR) at T = 330 K

T (K)	x	y	K	P_{exp} (Pa)	P_{calc} (Pa)	P_{exp}-P_{calc} (Pa)	AAD
330	0.18	0.9958	5.532	2930	4037	-1107	0.378
330	0.39	0.9983	2.560	7320	7936	-616	0.084
330	0.52	0.9989	1.921	9170	9940	-770	0.084
330	0.67	0.9993	1.491	12650	11912	738	0.058
330	0.89	0.9997	1.123	14300	14422	-122	0.009

Table 4-6 : Toluene - 2-Methoxy naphthalene (CCOR) at T = 335 K

T (K)	x	y	K	P_{exp} (Pa)	P_{calc} (Pa)	P_{exp}-P_{calc} (Pa)	AAD
335	0.18	0.9951	5.528	3420	4900	-1480	0.433
335	0.39	0.998	2.559	8600	9646	-1046	0.122
335	0.52	0.9987	1.921	10750	12096	-1346	0.125
335	0.67	0.9992	1.491	14850	14517	333	0.022
335	0.89	0.9997	1.123	17200	17612	-412	0.024

Table 4-7 : Toluene - 2-Methoxy naphthalene (CCOR) at T = 340 K

T (K)	x	y	K	P_{exp} (Pa)	P_{calc} (Pa)	P_{exp}-P_{calc} (Pa)	AAD
340	0.18	0.9942	5.523	4000	5907	-1907	0.477
340	0.39	0.9977	2.558	10000	11643	-1643	0.164
340	0.52	0.9985	1.920	12500	14616	-2116	0.169
340	0.67	0.999	1.491	17350	17568	-218	0.013
340	0.89	0.9996	1.123	20600	21359	-759	0.037

Table 4-8 : Toluene - 2-Methoxy naphthalene (CCOR) at T = 345 K

T (K)	x	y	K	P_{exp} (Pa)	P_{calc} (Pa)	P_{exp}-P_{calc} (Pa)	AAD
345	0.18	0.9932	5.518	4600	7074	-2474	0.538
345	0.39	0.9973	2.557	11700	13959	-2259	0.193
345	0.52	0.9982	1.920	14500	17544	-3044	0.210
345	0.67	0.9988	1.491	20200	21118	-918	0.045
345	0.89	0.9996	1.123	24500	25731	-1231	0.050

Table 4-9 : Toluene - 2-Methoxy naphthalene (CCOR) at T = 350 K

T (K)	x	y	K	P_{exp} (Pa)	P_{calc} (Pa)	P_{exp}-P_{calc} (Pa)	AAD
350	0.18	0.9921	5.512	5300	8417	-3117	0.588
350	0.39	0.9969	2.556	13500	16629	-3129	0.232
350	0.52	0.9979	1.919	16800	20924	-4124	0.245
350	0.67	0.9987	1.491	23400	25225	-1825	0.078
350	0.89	0.9995	1.123	29000	30802	-1802	0.062

Table 4-10 : Toluene - 2-Methoxy naphthalene (CCOR) at T = 355 K

T (K)	x	y	K	P_{exp} (Pa)	P_{calc} (Pa)	P_{exp}-P_{calc} (Pa)	AAD
355	0.18	0.9909	5.505	6100	9955	-3855	0.632
355	0.39	0.9964	2.555	15600	19690	-4090	0.262
355	0.52	0.9976	1.918	19300	24805	-5505	0.285
355	0.67	0.9985	1.490	27000	29950	-2950	0.109
355	0.89	0.9994	1.123	34200	36653	-2453	0.072

Table 4-11 : Toluene - 2-Methoxy naphthalene (CCOR) at T = 360 K

T (K)	x	y	K	P_{exp} (Pa)	P_{calc} (Pa)	P_{exp}-P_{calc} (Pa)	AAD
360	0.18	0.9895	5.497	7000	11707	-4707	0.672
360	0.39	0.9958	2.553	18000	23181	-5181	0.288
360	0.52	0.9972	1.918	22100	29237	-7137	0.323
360	0.67	0.9982	1.490	31000	35357	-4357	0.141
360	0.89	0.9993	1.123	40100	43367	-3267	0.081

Table 4-12 : Toluene - 2-Methoxy naphthalene (CCOR) at T = 365 K

T (K)	x	y	K	P_{exp} (Pa)	P_{calc} (Pa)	P_{exp}-P_{calc} (Pa)	AAD
365	0.18	0.988	5.489	7930	13692	-5762	0.727
365	0.39	0.9952	2.552	20500	27141	-6641	0.324
365	0.52	0.9968	1.917	25300	34272	-8972	0.355
365	0.67	0.998	1.490	35500	41511	-6011	0.169
365	0.89	0.9992	1.123	46900	51032	-4132	0.088

Table 4-13 : Toluene - 2-Methoxy naphthalene (CCOR) at T = 370 K

T (K)	x	y	K	P_{exp} (Pa)	P_{calc} (Pa)	P_{exp}-P_{calc} (Pa)	AAD
370	0.18	0.9863	5.479	9000	15931	-6931	0.770
370	0.39	0.9945	2.550	23400	31612	-8212	0.351
370	0.52	0.9964	1.916	28800	39965	-11165	0.388
370	0.67	0.9977	1.489	40500	48484	-7984	0.197
370	0.89	0.9991	1.123	54500	59743	-5243	0.096

Table 4-14 : Toluene - 2-Methoxy naphthalene (CCOR) at T = 375 K

T (K)	x	y	K	P_{exp} (Pa)	P_{calc} (Pa)	P_{exp}-P_{calc} (Pa)	AAD
375	0.18	0.9845	5.469	10200	18444	-8244	0.808
375	0.39	0.9938	2.548	26600	36636	-10036	0.377
375	0.52	0.9958	1.915	32600	46372	-13772	0.422
375	0.67	0.9974	1.489	46000	56347	-10347	0.225
375	0.89	0.999	1.122	63200	69597	-6397	0.101

Table 4-15 : Toluene - 2-Methoxy naphthalene (CCOR) at T = 380 K

T (K)	x	y	K	P_{exp} (Pa)	P_{calc} (Pa)	P_{exp}-P_{calc} (Pa)	AAD
380	0.18	0.9824	5.458	11500	21253	-9753	0.848
380	0.39	0.9929	2.546	30100	42257	-12157	0.404
380	0.52	0.9953	1.914	36900	53551	-16651	0.451
380	0.67	0.997	1.488	52000	65175	-13175	0.253
380	0.89	0.9989	1.122	73000	80696	-7696	0.105

Table 4-16 : Toluene - 2-Methoxy naphthalene (CCOR) at T = 385 K

T (K)	x	y	K	P_{exp} (Pa)	P_{calc} (Pa)	P_{exp}-P_{calc} (Pa)	AAD
385	0.18	0.9802	5.446	21900	24380	-2480	0.113
385	0.39	0.992	2.544	34000	48518	-14518	0.427
385	0.52	0.9947	1.913	41500	61561	-20061	0.483
385	0.67	0.9966	1.487	58800	75047	-16247	0.276
385	0.89	0.9987	1.122	83900	93147	-9247	0.110

VIII. CORRELATION RESULTS COEFFICIENTS EQUATION OF STATE

VIII.1 Introduction

This appendix contains the reference and fitted values for the coefficients of the Cubic Chain-of-Rotators equation of state. The column with "(calc.)" lists the values from the regression. The column "Relative AAD" lists the relative difference between reference and fitted value.

VIII.2 Results

Table 2-1 : Regression results for T_{cr}

Substance	T_{cr}	T_{cr} (calc.)	Relative AAD
Pentane	469.69	457.87	0.025
Hexane	507.50	501.12	0.013
Heptane	540.30	536.09	0.008
Octane	568.83	565.58	0.006
Nonane	594.64	591.23	0.006
Decane	617.90	614.07	0.006
Undecane	639.00	634.78	0.007
Dodecane	658.20	653.83	0.007
Tridecane	677.15	671.55	0.008
Tetradecane	691.90	688.21	0.005
Pentadecane	706.80	703.99	0.004
Hexadecane	720.60	719.02	0.002
Heptadecane	733.30	733.44	0.000
Octadecane	745.20	747.32	0.003
Nonadecane	756.20	760.74	0.006
Cyclopentane	511.61	498.41	0.026
Methylcyclopentane	532.79	533.50	0.001
Ethylcyclopentane	569.50	562.65	0.012
1,1-Dimethylcyclopentane	547.00	562.65	0.029
Cyclohexane	533.50	533.50	0.000
Methylcyclohexane	572.19	562.65	0.017
2-Methylpropane	407.85	401.08	0.017
2,2,3,3-Tetramethylbutane	567.80	565.58	0.004
2,2,4-Trimethylpentane	543.90	565.58	0.040
3,3-Dimethylpentane	536.30	536.09	0.000
3-Ethylpentane	540.50	536.09	0.008
2,3-Dimethylpentane	537.30	536.09	0.002
2,4-Dimethylpentane	519.70	536.09	0.032
2,2-Dimethylpentane	520.40	536.09	0.030
2-Methylhexane	530.10	536.09	0.011
2,2-Dimethylpropane	433.75	457.87	0.056

Substance	T_{cr}	T_{cr} (calc.)	Relative AAD
2-Methylbutane	460.39	457.87	0.005
2-Methylheptane	559.64	565.58	0.011
3-Methylheptane	563.60	565.58	0.004
3-Methylhexane	535.26	536.09	0.002
2,2,3-Trimethylbutane	531.12	536.09	0.009
2,4,4-Trimethylhexane	582.20	591.23	0.016
2,2,3-trimethylhexane	591.30	591.23	0.000
2,2,4-trimethylhexane	574.20	591.23	0.030
2-Methylpentane	497.50	501.12	0.007
3-Methylpentane	504.40	501.12	0.007
2,2-Dimethylbutane	488.70	501.12	0.025
2,3-Dimethylbutane	499.90	501.12	0.002
4-Methylheptane	561.70	565.58	0.007
3-Ethylhexane	565.40	565.58	0.000
2,2-Dimethylhexane	549.80	565.58	0.029
2,3-Dimethylhexane	563.40	565.58	0.004
2,4-Dimethylhexane	553.50	565.58	0.022
2,5-Dimethylhexane	550.00	565.58	0.028
3,3-Dimethylhexane	562.00	565.58	0.006
3,4-Dimethylhexane	568.80	565.58	0.006
3-Ethyl-2-methylpentane	567.00	565.58	0.002
3-Ethyl-3-methylpentane	576.50	565.58	0.019
2,2,3-Trimethylpentane	563.40	565.58	0.004
2,3,3-Trimethylpentane	573.50	565.58	0.014
2,3,4-Trimethylpentane	566.30	565.58	0.001
2,2,5-Trimethylhexane	569.70	591.23	0.038
2,2,4,4-Tetramethylpentane	574.70	591.23	0.029
Benzene	562.16	570.62	0.015
Toluene	591.80	598.62	0.012
Ethylbenzene	617.20	615.37	0.003
1,2-Dimethylbenzene	630.33	623.19	0.011
1,3-Dimethylbenzene	617.05	623.19	0.010
1,4-Dimethylbenzene	616.23	623.19	0.011
Propylbenzene	638.20	631.10	0.011
Isopropylbenzene	631.10	631.10	0.000
1-Methyl-2-ethylbenzene	651.00	638.19	0.020
1-Methyl-3-ethylbenzene	637.00	638.19	0.002
1-Methyl-4-ethylbenzene	640.00	638.19	0.003
1,2,3-Trimethylbenzene	664.50	645.27	0.029
1,2,4-Trimethylbenzene	649.20	645.27	0.006
1,3,5-Trimethylbenzene	637.50	645.27	0.012

Table 2-2 : Regression results for P_{cr}

Substance	P_{cr}/kPa	P_{cr}/kPa (calc.)	Relative AAD
Methane	4599	5087	0.1062
Ethane	4880	4880	0.0000
Propane	4240	4337	0.0228
Butane	3784	3831	0.0123
Pentane	3365	3407	0.0125
Hexane	3012	3058	0.0154
Heptane	2736	2770	0.0123
Octane	2487	2529	0.0167
Nonane	2290	2325	0.0151
Decane	2100	2150	0.0240
Undecane	1930	2000	0.0362
Dodecane	1780	1869	0.0498
Tridecane	1720	1753	0.0195
Tetradecane	1520	1651	0.0865
Pentadecane	1420	1561	0.0990
Hexadecane	1320	1479	0.1205
Heptadecane	1220	1406	0.1521
Octadecane	1140	1339	0.1746
Nonadecane	1070	1278	0.1948
Cyclopentane	4443	3312	0.2546
Methylcyclopentane	3784	2987	0.2107
Ethylcyclopentane	3397	2714	0.2011
1,1-Dimethylcyclopentane	3400	2714	0.2018
Cyclohexane	4073	2987	0.2667
Methylcyclohexane	3471	2714	0.2181
2-Methylpropane	3640	3831	0.0524
2,2,3,3-Tetramethylbutane	2870	2529	0.1190
2,2,4-Trimethylpentane	2570	2529	0.0161
3,3-Dimethylpentane	2950	2770	0.0611
3-Ethylpentane	2891	2770	0.0419
2,3-Dimethylpentane	2911	2770	0.0485
2,4-Dimethylpentane	2740	2770	0.0109
2,2-Dimethylpentane	2773	2770	0.0012
2-Methylhexane	2733	2770	0.0134
2,2-Dimethylpropane	3199	3407	0.0650
2-Methylbutane	3381	3407	0.0077
2-Methylheptane	2484	2529	0.0179
3-Methylheptane	2550	2529	0.0084
3-Methylhexane	2813	2770	0.0154
2,2,3-Trimethylbutane	2953	2770	0.0621
2,4,4-Trimethylhexane	2410	2325	0.0354
2,2,3-trimethylhexane	2540	2325	0.0848
2,2,4-trimethylhexane	2370	2325	0.0191
2-Methylpentane	3010	3058	0.0160

Substance	P_{cr}/kPa	P_{cr}/kPa (calc.)	Relative AAD
3-Methylpentane	3120	3058	0.0198
2,2-Dimethylbutane	3080	3058	0.0071
2,3-Dimethylbutane	3130	3058	0.0229
4-Methylheptane	2540	2529	0.0045
3-Ethylhexane	2610	2529	0.0312
2,2-Dimethylhexane	2530	2529	0.0006
2,3-Dimethylhexane	2630	2529	0.0386
2,4-Dimethylhexane	2560	2529	0.0123
2,5-Dimethylhexane	2490	2529	0.0155
3,3-Dimethylhexane	2650	2529	0.0458
3,4-Dimethylhexane	2690	2529	0.0600
3-Ethyl-2-methylpentane	2700	2529	0.0635
3-Ethyl-3-methylpentane	2810	2529	0.1002
2,2,3-Trimethylpentane	2730	2529	0.0738
2,3,3-Trimethylpentane	2820	2529	0.1033
2,3,4-Trimethylpentane	2730	2529	0.0738
2,2,5-Trimethylhexane	2270	2325	0.0241
2,3,5-Trimethylhexane	2380	2325	0.0233
2,2,4,4-Tetramethylpentane	2490	2325	0.0664
2-Methylnonane	2050	2150	0.0490
3-Methylnonane	2140	2150	0.0048
5-Methylnonane	2140	2150	0.0048
2,4-Dimethyloctane	2100	2150	0.0240
Benzene	4898	4899	0.0001
Toluene	4106	4122	0.0039
Ethylbenzene	3606	3595	0.0031
1,2-Dimethylbenzene	3734	3558	0.0471
1,3-Dimethylbenzene	3536	3558	0.0062
1,4-Dimethylbenzene	3511	3558	0.0134
Propylbenzene	3200	3187	0.0040
Isopropylbenzene	3210	3187	0.0071
1-Methyl-2-ethylbenzene	3040	3158	0.0389
1-Methyl-3-ethylbenzene	2840	3158	0.1121
1-Methyl-4-ethylbenzene	2940	3158	0.0743
1,2,3-Trimethylbenzene	3450	3130	0.0928
1,2,4-Trimethylbenzene	3230	3130	0.0310
1,3,5-Trimethylbenzene	3130	3130	0.0001

Table 2-3 : Regression results for acentric factor

Substance	ω	ω (calc.)	Relative AAD
Methane	0.0110	0.0110	0.0017
Ethane	0.0990	0.0587	0.4071
Propane	0.1514	0.1063	0.2979
Butane	0.2000	0.1538	0.2310

Substance	ω	ω (calc.)	Relative AAD
Pentane	0.2506	0.2012	0.1971
Hexane	0.3018	0.2486	0.1764
Heptane	0.3497	0.2958	0.1541
Octane	0.3979	0.3430	0.1381
Nonane	0.4445	0.3900	0.1226
Decane	0.4872	0.4370	0.1030
Undecane	0.5377	0.4839	0.1001
Dodecane	0.5766	0.5307	0.0796
Tridecane	0.6251	0.5774	0.0763
Tetradecane	0.6661	0.6241	0.0631
Pentadecane	0.7128	0.6706	0.0592
Hexadecane	0.7483	0.7171	0.0417
Heptadecane	0.7700	0.7634	0.0085
Octadecane	0.7964	0.8097	0.0167
Nonadecane	0.8079	0.8559	0.0594
Cyclopentane	0.1928	0.1844	0.0434
Methylcyclopentane	0.2347	0.2287	0.0255
Ethylcyclopentane	0.2755	0.2729	0.0094
1,1-Dimethylcyclopentane	0.2730	0.2729	0.0003
Cyclohexane	0.2095	0.2287	0.0917
Methylcyclohexane	0.2353	0.2729	0.1598
2-Methylpropane	0.1836	0.1538	0.1623
2,2,3,3-Tetramethylbutane	0.2510	0.3430	0.3663
2,2,4-Trimethylpentane	0.3036	0.3430	0.1296
3,3-Dimethylpentane	0.2674	0.2958	0.1062
3-Ethylpentane	0.3103	0.2958	0.0467
2,3-Dimethylpentane	0.2942	0.2958	0.0054
2,4-Dimethylpentane	0.3016	0.2958	0.0192
2,2-Dimethylpentane	0.2864	0.2958	0.0328
2-Methylhexane	0.3281	0.2958	0.0985
2,2-Dimethylpropane	0.1961	0.2012	0.0261
2-Methylbutane	0.2278	0.2012	0.1167
2-Methylheptane	0.3777	0.3430	0.0920
3-Methylheptane	0.3701	0.3430	0.0734
3-Methylhexane	0.3217	0.2958	0.0805
2,2,3-Trimethylbutane	0.2500	0.2958	0.1832
2,4,4-Trimethylhexane	0.3421	0.3900	0.1401
2,2,3-trimethylhexane	0.3358	0.3900	0.1615
2,2,4-trimethylhexane	0.3498	0.3900	0.1150
2-Methylpentane	0.2787	0.2486	0.1082
3-Methylpentane	0.2692	0.2486	0.0767
2,2-Dimethylbutane	0.2305	0.2486	0.0783
2,3-Dimethylbutane	0.2480	0.2486	0.0022
4-Methylheptane	0.3708	0.3430	0.0751
3-Ethylhexane	0.3609	0.3430	0.0497
2,2-Dimethylhexane	0.3363	0.3430	0.0198
2,3-Dimethylhexane	0.3463	0.3430	0.0097

Substance	ω	ω (calc.)	Relative AAD
2,4-Dimethylhexane	0.3424	0.3430	0.0016
2,5-Dimethylhexane	0.3571	0.3430	0.0396
3,3-Dimethylhexane	0.3203	0.3430	0.0707
3,4-Dimethylhexane	0.3388	0.3430	0.0123
3-Ethyl-2-methylpentane	0.3294	0.3430	0.0411
3-Ethyl-3-methylpentane	0.3039	0.3430	0.1285
2,2,3-Trimethylpentane	0.2973	0.3430	0.1536
2,3,3-Trimethylpentane	0.2888	0.3430	0.1875
2,3,4-Trimethylpentane	0.3156	0.3430	0.0867
2,2,5-Trimethylhexane	0.3573	0.3900	0.0916
2,2,4,4-Tetramethylpentane	0.3118	0.3900	0.2509
Benzene	0.2029	0.2029	0.0000
Toluene	0.2607	0.2581	0.0099
Ethylbenzene	0.3035	0.3043	0.0026
1,2-Dimethylbenzene	0.3132	0.3128	0.0011
1,3-Dimethylbenzene	0.3263	0.3128	0.0412
1,4-Dimethylbenzene	0.3215	0.3128	0.0269
Propylbenzene	0.3440	0.3503	0.0184
Isopropylbenzene	0.3260	0.3503	0.0747
1-Methyl-2-ethylbenzene	0.2940	0.3604	0.2260
1-Methyl-3-ethylbenzene	0.3600	0.3604	0.0012
1-Methyl-4-ethylbenzene	0.3220	0.3604	0.1194
1,2,3-Trimethylbenzene	0.3660	0.3671	0.0029
1,2,4-Trimethylbenzene	0.3760	0.3671	0.0238
1,3,5-Trimethylbenzene	0.3990	0.3671	0.0801